An investigation of the rock mechanics aspects of a system of short face in-seam development for subsequent longwall retreat extraction

P. R. Sheorey (Prakash R.)

University of Newcastle upon Tyne

1976

An investigation of the rock mechanics aspects of a system of short face in-seam development for subsequent longwall retreat extraction

Synopsis

The research work undertaken in this study was sponsored by the National Coal Board and consists of an investigation into the rock mechanics feasibility of a method of in-seam development by short faces with a centre pack, creating two roadways for subsequent retreating.

An elastostatic solution by an approximate analysis has been given for this method of advancing for roof behaviour and to obtain pack load with face advance and the ribside abutment pressure distribution.

The elastostatic analysis for the short face advancing situation has been done for anhydrite (setting) and conventional (non-setting) packs.

A method is given for assessing the ribside abutment loading during subsequent retreating and loads in the goaf.

The floor loadings obtained during short face advancing and subsequent retreating have been used for a floor stress analysis and for predicting the post-failure viscoelastic floor heave during retreating.

Some anhydrite properties relevant to the analysis have also been investigated in the laboratory and a formula for estimating the in-situ strength of anhydrite packs has been given.

* * *

TO

*** ***

JYOT

AN INVESTIGATION OF THE ROCK MECHANICS ASPECTS OF A SYSTEM OF SHORT FACE IN-SEAM DEVELOPMENT FOR SUBSEQUENT LONGWALL RETREAT EXTRACTION

CONTENTS

* * *

ACKNOWLEDGEMENTS

I would like to express my sincere gratitude to Professor E.L.J. Potts for giving me the opportunity of visiting this country and working in his Department.

I also owe a debt of thanks to Dr. R.K. Dunham, Lecturer and my Supervisor, for his kind and timely help in all matters and his supervision.

I am grateful to the National Coal Board for financing the work in this Thesis.

My thanks are also due to:

Dr. Martin Thompson, then Senior Research Officer in the Department of Mining Engineering, for his useful hints in computing, of which I had little previous knowledge.

My postgraduate colleagues: Bruce Hebblewhite for the use of the face element technique, Ergin Arioglu, Warren Dudley, Dave Hodkin and Ussam Mirza, for their help in various matters, both technical and otherwise.

Bill Clasper, for anhydrite specimen preparation.

Mrs. Edna Gannie, for her efficient and accurate typing of the script, in spite of my illegible handwriting.

Rob Liddell and John Stanger for the offset-litho work.

* * *

List of Figures

Fig. No.	Title
	Chapter 5 (contd)
5.7	- Pack load variation with face advance at point A
5.8	- Pack load variation with face advance at point B
5.9	- Lateral considerations
5.10	- Pack load variation with face advance - Heading width 12 m
5.11	- Pack load variation with face advance - Heading width 14 m
5.12	- Pack load variation with face advance - Heading width 16 m
5.13	- Ultimate loading on pack and ribside - Heading width 12 m
5.14	- Ultimate loading on pack and ribside - - Heading width 14 m
5.15	- Ultimate loading on pack and ribside - Heading width 16 m

Fig. No.	Title
	Chapter 6 (contd)
6.4	- Ultimate loading on conventional pack and ribside - Heading width 14 m
6.5	- Ultimate loading on conventional pack and ribside - Heading width 16 m
6.6	- Variation of ultimate pack load with modulus of elasticity
6.7	- Variation of ribside abutment pressure with pack modulus of elasticity
6.8	- Ultimate bending moments and shear forces in the roof (conventional packs) - Heading width 12 m
6.9	- Ultimate bending moments and shear forces in the roof (conventional packs) - Heading width 14 m
6.10	- Ultimate bending moments and shear forces in the roof (conventional packs) - Heading width 16 m
6.11	- Maximum roadway tensile stress vs. pack modulus

Fig. No.	Title
	Chapter 7
7.1(a)	- Forces on a ribside element
7.1(b)	- Abutment pressure schematic
7.2	- Triaxial fracture strength of coal
7.3	- Mechanical model for ribside loading
7.4	- Abutment pressure distribution on the ribside - pack load 3000 kN/m^2, pack width 1.5 m
7.5	- Abutment pressure vs. pack load and width - Face length 183 m
7.6	- Variation of ribside abutment pressure with face length - pack load 3000 kN/m^2, Pack width 1.5 m
7.7	- Effect of pack load and width on the extent of ribside crushing - Face length 183 m
7.8	- Effect of face length on the extent of ribside crushing - Pack load 3000 kN/m^2, pack width 1.5 m

Fig. No.	Title
	Chapter 7 (contd)
7.20	- Elastostatic lift during retreating - effect of pack width - Face length 183 m, Pack load 3000 kN/m^2
7.21	- Elastostatic lift during retreating - effect of face length - Pack width 1.5 m, Pack load 3000 kN/m^2
7.22	- Safety factor contours during retreating - Pack width 1.5 m, Pack load 3000 kN/m^2
7.23	- Safety factor contours during retreating - Pack width 1.5 m, Pack load 7000 kN/m^2
7.24	- Safety factor contours during retreating - Pack width 6 m, Pack load 3000 kN/m^2
7.25	- Safety factor contours during retreating - Pack width 6 m, Pack load 7000 kN/m^2
7.26	- Safety factor contours during retreating - Pack width 3 m, Pack load 3000 kN/m^2
7.27	- Safety factor contours during retreating - Pack width 4.5 m, Pack load 3000 kN/m^2

* * *

List of mathematical notations

σ_x, σ_y	- Normal stresses along x- and y-axes
τ_{xy}	- shear stress
u,v	- displacements along x and y
E	- elastic modulus
μ	- Poisson's ratio
ρ	- unit depth pressure
k	- foundation modulus of an elastic support
q	- loading on a strata beam due to its own weight
D	- flexural rigidity of strata
M	- bending moment
Q	- shear force
A, B, C	- General notations for integration constants or arbitrary functions

$$F'(x) = \frac{dF(x)}{dx}, \quad F''(x) = \frac{d^2F(x)}{dx^2} \text{ etc.,}$$

$$F_I(x) = \int F(x)dx, \quad F_{II}(x) = \iint F(x)dxdx \text{ etc. for any function of x.}$$

t	- time
s	- Laplace transform parameter
S	- safety factor
σ	- normal stress
τ	- shear stress
ε	- strain
η	- modulus of viscosity

* * *

CHAPTER 1

Introduction

CHAPTER 1

INTRODUCTION

In recent years, interest has developed in dirtless mining as higher speeds of advance require minimisation of non-productive work like ripping a roadway and building wide dirt packs at the side of a longwall gateroad. Especially noteworthy is the case of crushed natural anhydrite as a roadside packing medium which was introduced in Germany with considerable success. According to German experience it had the following advantages:

(a) Much narrower packs could be built than before, anhydrite being stronger and stiffer; load acceptance is quicker.

(b) Prevention of leakage ventilation through waste could be effectively achieved.

(c) Faster rates of advance could be obtained.

(d) It could effectively fill gaps and cavities.

(e) Less shift outlay than for transporting and setting of chocks.

With dirtless mining comes 'in-seam' mining, eliminating roof ripping and the problem of dirt disposal, in conjunction with retreating systems of extraction. To make it economically more feasible, a method of initial development by advancing short faces, with a centre pack support to the wide

heading, has been proposed[1,2]. This would create two roadways on either side of the centre pack, which would be used subsequently as gateroads during retreating as in Fig. 2.8. This Thesis is devoted almost exclusively to an assessment of the feasibility of this method of working from the point of view of rock mechanics, with special reference to the use of anhydrite packs.

The four main structural elements of the short face advancing configuration, viz. nether roof strata, centre pack, ribside and floor, have been dealt with during both stages of working, advancing and subsequent retreating.

An analytical elastostatic solution has been given for the behaviour of the roof, pack load acceptance with face advance and ribside loading in short face advancing. This problem has been analysed using the theory of thick beams on elastic support for extreme fibre deflections, developing an approximate method for applying it to the present situation. A review of beam analysis is presented in Chapter 3 and Chapters 5 and 6 deal with the analysis of short face advancing for anhydrite and conventional non-setting packs respectively, comparing the effectiveness of the two kinds of pack when applied with this method.

Chapter 2 includes a literature survey of roadway stability vis-à-vis pack properties and behaviour with special attention to anhydrite and other setting pack materials.

A formula for estimating the strength of an anhydrite pack is given in Chapter 4, based on laboratory tests on anhydrite. Also included in this Chapter is a study of the material's setting property with time.

Chapter 7 shows how the short face method differs in respect of floor heave from ordinary advancing. The recently developed face element technique has been used for stress analysis of the floor for advancing and subsequent retreating. This is followed by a post-failure analysis and a viscoelastic analysis for obtaining the final floor heave picture. The starting point of the floor heave analysis was defining the ribside abutment pressure distribution. In the beginning of Chapter 7 a method to obtain the ribside abutment pressure, after ribside failure, is given. The influence of pack load and width and face length on floor heave in retreating has been considered.

General conclusions are presented in Chapter 8.

* * *

CHAPTER 2

Influence of roadside packs on stability of roadways and a concept of short face advancing with a centre pack

CHAPTER 2

Influence of roadside packs on stability of roadways and a concept of short face advancing with a centre pack

2.1 Introduction

Most of the coal in Britain is being extracted by the longwall advancing system. Considerable strata control research has been and is being carried out with reference to gateroad supports. Many references are available on the subject of supports within longwall roadways and at the roadside, but only the latter aspect of support of the roadside by means of packs is reviewed in this Chapter. At the end a brief description is given of a method of short face advancing with a centre pack support to create a pair of 'in-seam' roadways for subsequent retreat mining.

Until some years ago, roadside packs were generally formed from ripping dirt packed to a width of up to 10 m on one or either side of the road, depending upon the extracted seam height. Recently, however, building of lengthy dirt packs has become costly, mainly because workers have to be engaged in non-productive work. Dirt packs are also unable to cope with faster rates of advance. Retreat mining, which is slowly becoming more popular, and today's faster rates of advance, require a simple, inexpensive and effective support at the roadside. In the context of retreating, interest is developing in 'in-seam' mining, eliminating the problem of dirt disposal. Short face advancing with centre packs may be one of the methods for dirtless mining[1-3].

2.2 Roadway Stability

Modern longwall systems favour the positioning of gateroads near the ribside and such a position subjects the roadway to uneven or differential rock pressures on its two sides, as shown in Fig. 2.1. This happens because on one side support is offered by the pre-existing solid coal, while the other side can be supported by a pack only after a certain amount of convergence has occurred in the roof. This initial convergence later increases as the face moves, until it tapers off to a final value when the face is about 100 m away[3], this later increase causing pack compression and pack load. As will be seen later, the pack load is considerably smaller than the ribside abutment pressure and this causes the differential pressure distribution around the roadway. The bending of the roof strata down into the goaf causes pack settlement and some crushing of the ribside, shifting the abutment pressure deeper into the coal. Very high bending and shear stresses are generated in the roof near the roadway region causing fractures.

Jenkins *et al.*[4] worked on photoelastic models of a roadway adjacent to a ribside, incorporating layers of differing elastic moduli to represent coal, pack, roof and floor. Their findings indicate a beamlike behaviour of the nether strata giving rise to very high shear stresses at the lower corners of the roadway and a tensile stress at the central region of the floor. It would seem that not only is tensile failure of the floor possible, but shear failure may also be expected if the floor rock is weak enough. Large roof and abutment stresses were also seen to occur. Hobbs has carried out considerable work on roadway models made of sand-plaster mixtures, though not with special reference to packs[5].

FIG.2.1-DIFFERENTIAL LOADING ACROSS A GATEROAD

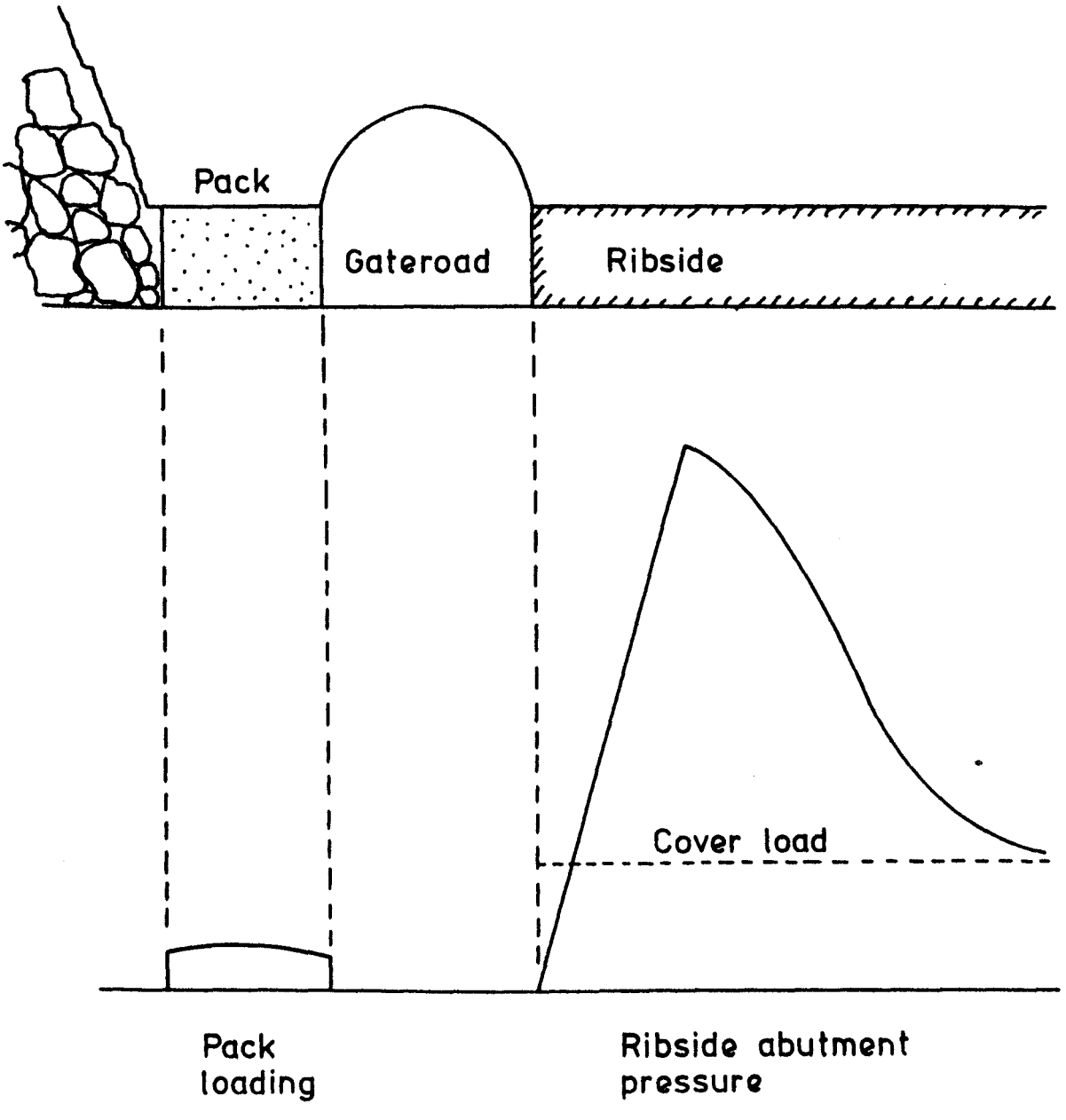

The differential pressure distribution can thus give rise to shear failure of the roof as well as floor failure and heaving, together with pack settlement, producing overall roadway closure.

2.3 Roadside Packs

It would thus appear advisable to reduce the differential nature of the pressure distribution for better stability of the roadway. This can be achieved in one of three ways:

(a) Erecting a pack at the ribside, shifting the abutment peak further.

(b) Slotting the ribside, leaving gummings in the slot to create a gradual pressure gradient and also shifting the abutment pressure away.

(c) Using a compact material for the goafside pack.

The advantage gained by using method (a) has been clearly shown by Jenkins et al.[4] on their photoelastic models. Breer[6] mentions three methods of roadside support currently being practised in Germany:

(a) No roadside pack for friable, easily cavable rock which breaks higher up.

(b) Yielding roadside support like wood chocks for soft surrounding rock capable of higher deflection.

(c) Compact packs (natural or synthetic anhydrite, Blitz-dammer quick-setting materials) for harder strata.

Spruth[7] has given several cases where no difference in the roadway condition resulted when roadside chocks were completely eliminated. Conducting tests on 50 equivalent material models, he concludes that complete elimination of roadside support is preferable in the cases of rocks caving in fine pieces rather than where thick strong beds fail to break off at the goaf edge and so remain hanging. As was natural, substantial economic savings could be achieved by removing roadside support.

Yielding roadside supports like wood chocks with or without dirt filling, stone or dirt packs were most commonly used until some years ago and are still prevalent. These materials are highly compressible even under quite low pressures and, in contrast to the ribside, are generally not sufficiently rigid to prevent large differential convergences across the roadway. They have to get compressed a great deal before they show substantial load acceptance. Their rigidity, however, would be somewhat increased by using stronger pack walls, building central pack walls, grading of the strength within the pack towards the roadway or using double packs. According to Jenkins et al.[4], the ultimate pack convergence may vary between 38% and 53% of its original height.

Farmer and Robertson[8] assume a soil mechanics convention for underground movement of fracture zones around a roadway. When both ribside packs are used, three zones of active pressure, radial shear and passive pressure develop about the rib edge, which is comparatively remote from the roadway. With increased rates of advance, the ribside pack is eliminated and the goafside pack is reduced in width. The zones of radial movement at the rib edge will now exist in the

roadway, reducing failure in the roof and floor. The situation can be improved by slotting the ribside or using a rigid pack to preserve a structurally sound rock around the roadway. Farmer and Robertson suggest the following properties desirable in a rigid pack material:

(a) Sufficient initial strength to support the roof at the face end,

(b) strength lower than that of the ribside during the waste caving period to prevent abutment stress concentration at the faceside,

(c) sufficient strength to support stresses induced in the roadside after equilibrium, and

(d) very low initial compressibility (about 5% strain).

It would thus seem more desirable to introduce more rigid packs to obtain a more even pressure distribution around roadways. Experiments at Holland Colliery (Germany) were initiated in 1964 to introduce crushed natural anhydrite as a pack material in order to reduce pack setting time, relieve gateroad haulage of the transport of wood and prevent leakages of ventilation through wastes[9]. This is a mined product prepared as a binder and was supplied to this colliery in a size range of 0-6 mm, with at least 30% fines under 0.2 mm. Chemically, anhydrite is Calcium Sulphate ($CaSO_4$) and, in combination with water and a suitable accelerator, becomes dihydrate ($CaSO_4.2H_2O$). The accelerator, which is 1 part potassium sulphate (K_2SO_4) and 1.8 parts ferrous sulphate ($FeSO_4.7H_2O$), greatly increases the speed of hydration and promotes the growth of crystals forming a strong compact mass. Because of its recent success in Germany, its

properties will be considered here, together with those of conventional and other substitute packing materials.

2.4 Properties of packing materials

Much work has been done in determining pack properties, to understand the effects a particular pack would produce in the roadway and also to achieve the 'ideal' packing condition at the roadside. The various types of packs or roadside support are as noted below:

(a) Wood chocks, with and without dirt filling.

(b) Dirt or stone packs.

(c) Aglite blocks and concrete slabs with wood.

(d) Crushed natural anhydrite.

(e) Synthetic anhydrite.

(f) 'Blitzdammer' quick-setting fillers.

(g) Pump packs.

(h) Bonded dirt.

These will be considered one by one.

2.4.1 Wood chocks with and without dirt filling

Whittaker and Titley[3] have given results of 23 compression tests on wood chocks, both open and stone filled. Open chocks showed an initial elastic compression at low loads which soon changed to a sort of plastic deformation until failure, resembling a Bingham substance. The rate of

compression decreased with respect to load as the blocks were squashed and effective contact area increased. The open half round chock was much weaker than the square chock during the initial loading stages. Fig. 2.2(a) shows a typical load-compression characteristic. It can be seen that open wood chocks possess a high degree of compressibility.

The effect of filling the chock with stone was not apparent until a load at which the rock had been sufficiently compacted. After this, however, the filled chock showed much better load bearing capacity with a marked increase in rigidity. Fig.2.2(a) indicates clearly the advantage gained in later stages of loading due to filling in that the filled chock compressed by 25 cm at 150 tonnes, whereas the open chock took only about 50 tonnes to produce the same compression. At higher loadings (up to 300 tonnes), most of the filled chock strength was due to the compacted rock, the wood merely serving as a lateral restraint.

2.4.2 Dirt or stone packs

Barraclough et al.[10] conducted compression tests on stone packs in the laboratory. The load-compression characteristic was seen to depend on pack construction, compactness and location of walls and the type of stone used. Packs built by two different teams but in the same manner exhibited very similar behaviour, indicating the reproducibility of the results. When fine river sand, 18% by volume, was used with stones, the pack compression increased from 9.2% to 10.3%. Fig. 2.2(b) gives a typical test

FIG. 2.2 - LOAD-YIELD CHARACTERISTICS

(a) Wood chock (after Whittaker & Titley)

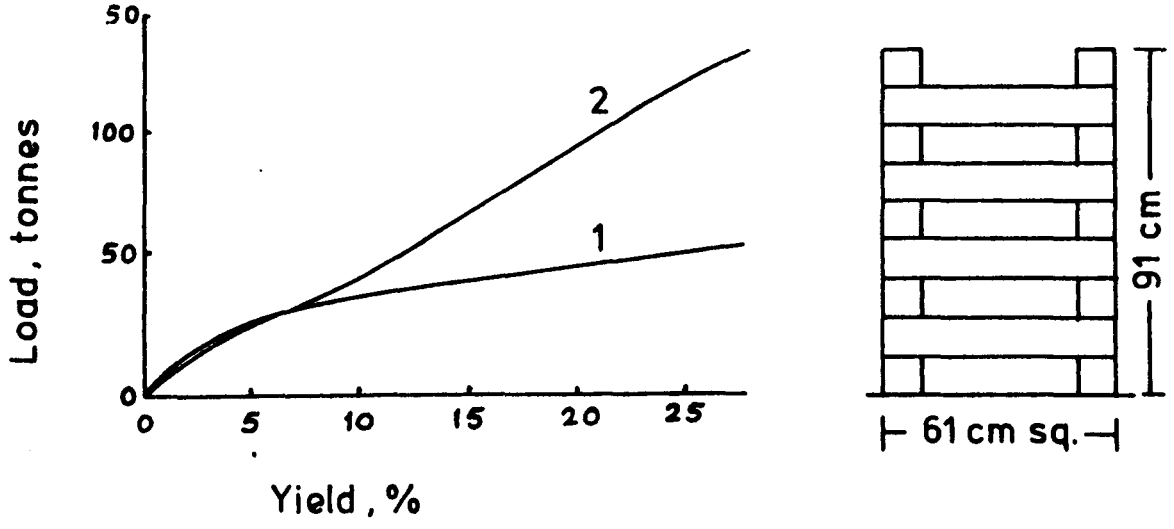

1 Open 2 Dirt-filled

(b) Stone pack (after Barraclough et al.)

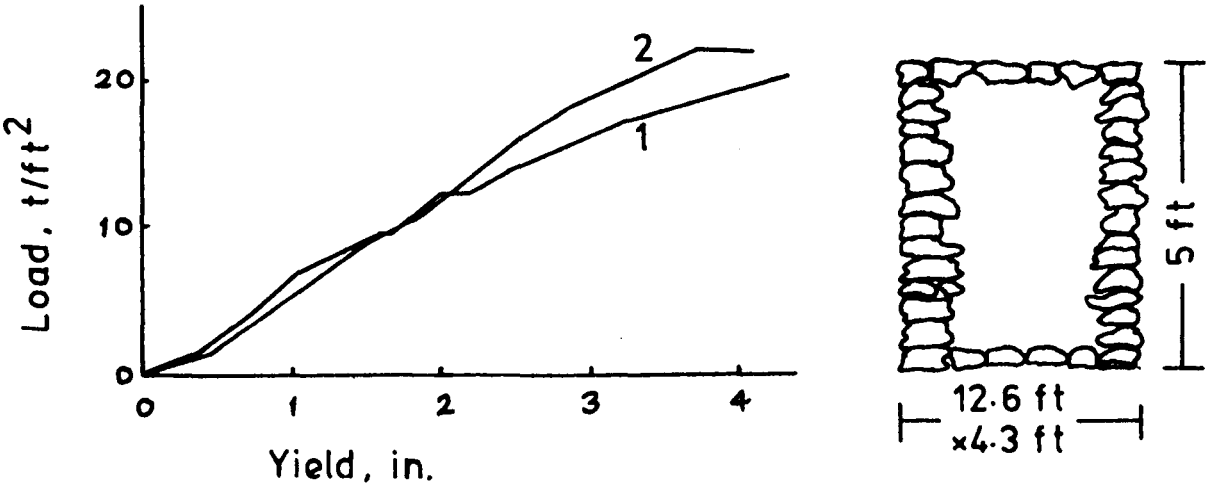

Built by teams 1 & 2

result showing two curves for two teams of builders. The behaviour of the packs is seen to be fairly linear. Also noticeable is the high degree of yield.

2.4.3 Aglite and concrete blocks

The building of lightweight concrete blocks in the pack area was first adopted at Daw Mill Colliery[11]. The main advantage of Aglite over dense concrete is its low density, which is important considering the handling problems involved. Aglite is a trade name for lightweight concrete made from sintered clay and shale, screened, graded and mixed with cement.

The technique in use is to build solid chocks (because of the poor shear strength) with the blocks in a continuous strip along the gateroad. These blocks have a compressive strength of 5500 kN/m^2 (800 psi). A comparison of the yield characteristic of Aglite with those of hard wood and soft wood[12] in Fig.2.3 shows Aglite to be far from ideal. Field experience shows that if the bearing strengths of the roof and floor exceed that of Aglite, the chock will yield slightly until failure load which depends greatly on the slenderness of the pack and the constraint offered by the gateroad supports. In thin seams, where a pack is more flat, the shear breaks developed do not weaken the major part of the bearing surface, and a high resistance will develop with little yield. In thick seams, however, the chock will disintegrate into a broken mass if the yield point is reached.

FIG. 2.3 - LOAD-YIELD CHARACTERISTIC OF AGLITE
(After Lewis)

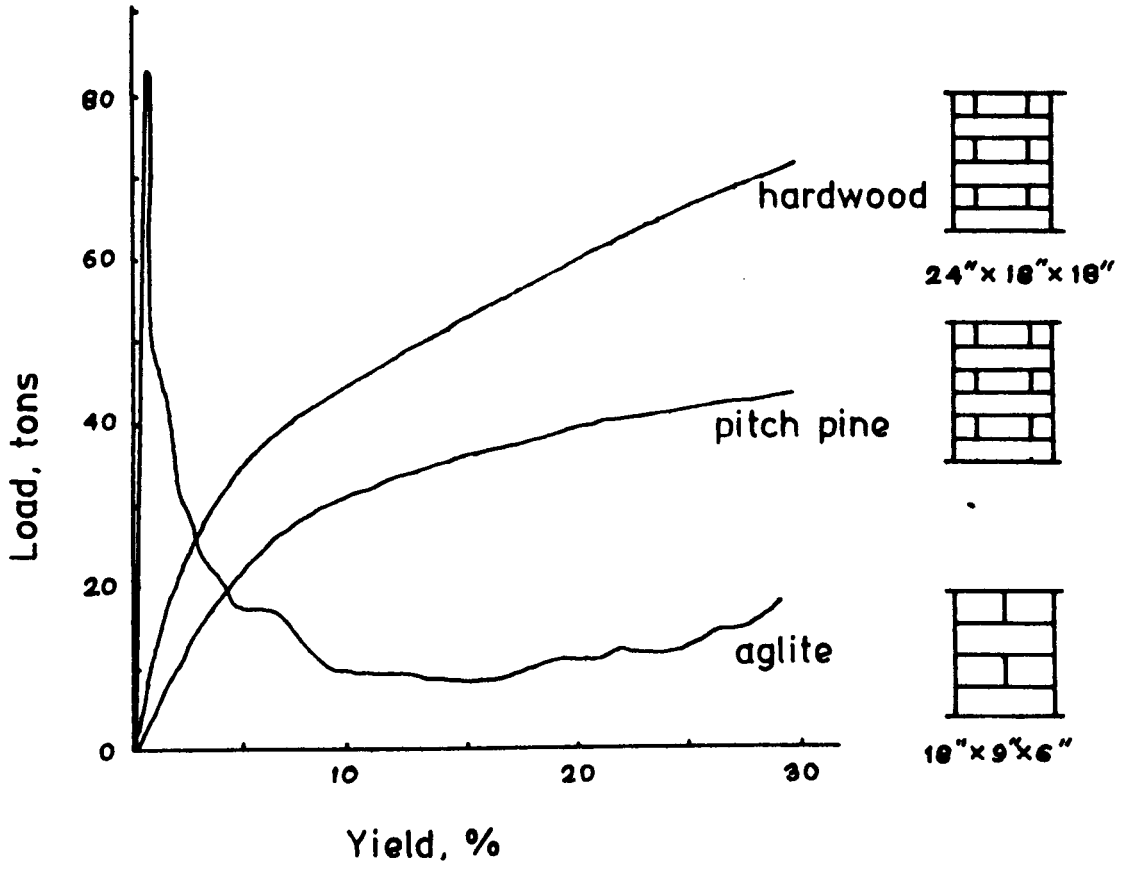

When the bearing strength of the roof and floor is not sufficiently high, penetration of the strata will occur before the chock fails and it will become an integral part of the roadway mass.

At the Dutch State Mine Emma[12] composite chocks of alternating layers of concrete slabs and hardwood boards were built at the roadside. These chocks were built approximately 3 ft from the roadside and the intervening space was filled with roadway rippings. Breaker props were erected on the other side. The purpose of the chocks was to induce breaks along the line of the chocks rather than over the edge of the solid roadside. It was found that the waste did not break at the line of chocks, especially when soft wood was used instead of hardwood.

2.4.4 Crushed natural anhydrite

Since its introduction in Holland Colliery in 1964, crushed natural anhydrite is being used considerably in German mines as a gateside packing material. The reasons which induced various collieries to use natural anhydrite, Blitzdammer quick setting fillers or synthetic anhydrite have been given as[13]:

(a) Less shift outlay than for the transport and setting of timber chocks.

(b) Increased pack resistance and better adaption to roadway supports.

(c) Supporting a road against a face in the process of starting up.

(d) Preventing ventilation air leaks.

(e) Fire prevention.

Genthe[9] has reported a fall in strength of anhydrite with an increasing water content like all hydraulically setting materials, the highest crushing strength being obtained at 8% water. The strength after 24 hours of setting at this value of moisture was 10300 kN/m^2 (105 kg/cm^2) and the lowest value of about 2000 kN/m^2 corresponded to 16% water.

Arioglu and Dunham[14] varied the water content from 6% to 16% and showed that the highest strength occurred at 8.5%, the strength falling on either side of this percentage. At values less than 8.5% sufficient water is not available for complete hydration. Like Genthe they have also reported a rise in strength with setting time at varying water contents and have given the following general equation for variation of strength s with time t:

$$s = \frac{At}{B + t}$$

in which A and B are empirical constants changing with water content. These findings are shown in Fig. 2.4.

Genthe[9] and Arioglu and Dunham[14] have also shown a marked fall in the strength value with a rise in temperature and humidity, indicating that anhydrite may not be of much benefit as a packing medium in hot and humid conditions. Sample cubes of anhydrite which were prepared and stored underground at a temperature of 21.5°C and 74% relative humidity only attained after

FIG. 2·4 - COMPRESSIVE STRENGTH OF ANHYDRITE
(After Arioglu & Dunham)

Compressive strength vs. water/anh. ratio

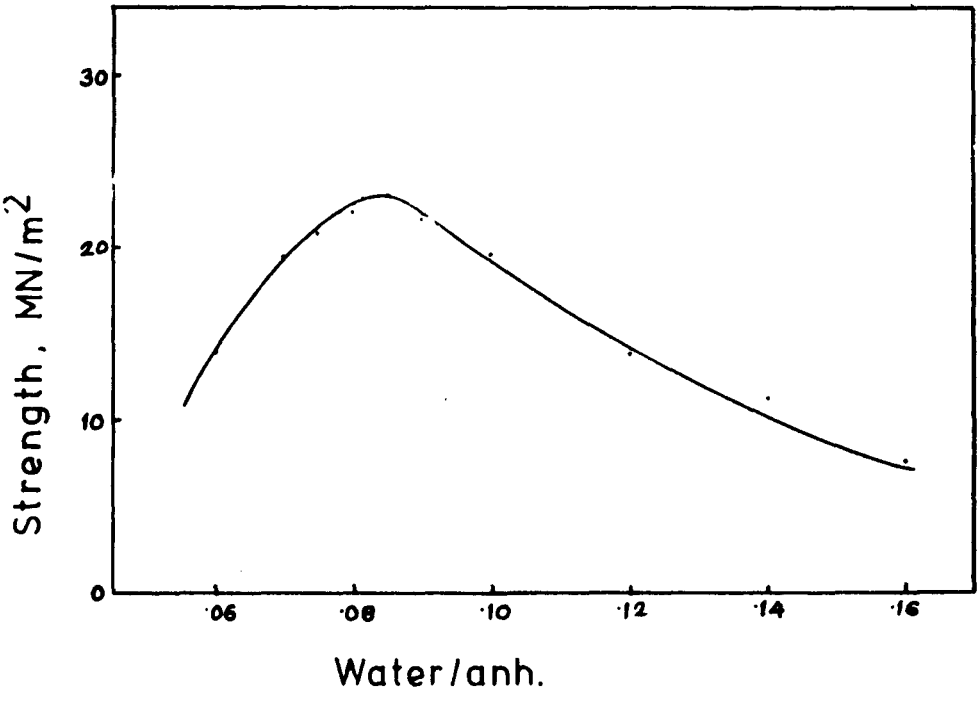

Compressive strength vs. setting time

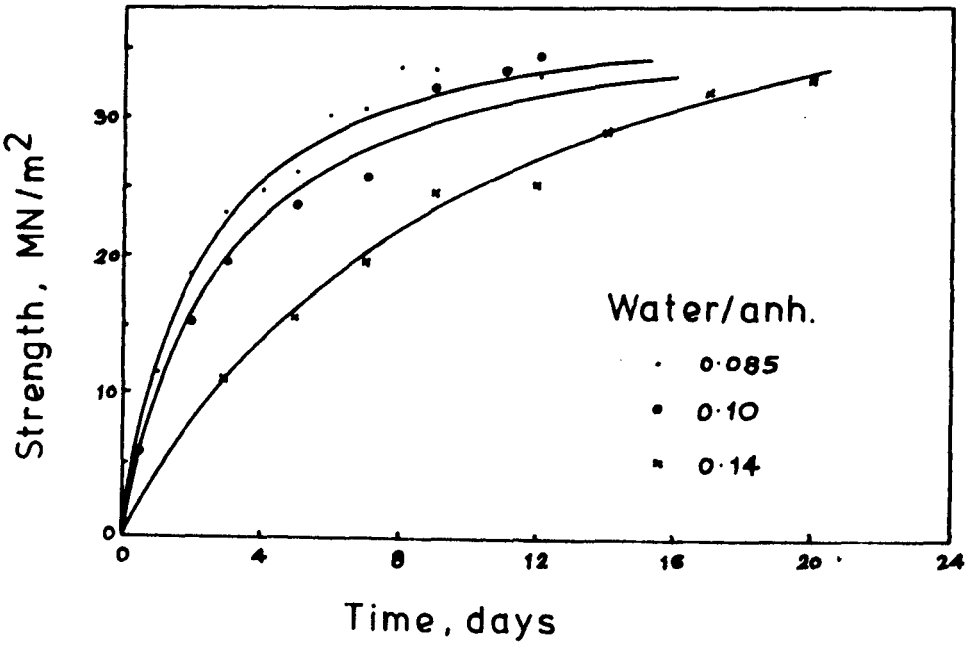

24 hours 10 - 50% of the crushing strength values which were registered at 22°C and 40% humidity[9]. Quick-setting fillers on the contrary increase in strength with a rise in temperature[9].

2.4.5 Hydro-mechanically stowed pack materials

Synthetic anhydrite, Blitzdammer quick-setting fillers and pump packs have so far been used hydro-mechanically. Synthetic anhydrite is obtained as a by-product in the manufacture of hydrofluoric acid and was successfully used as a pack medium in Germany in 1968 for the first time[9]. The Blitzdammer filler is produced by Elsa-Zement of Germany and consists of 54% cement clinker, 40% lime marl, and 1% calcium chloride and 5% Lepol furnace clinker. It has roughly the same strength as natural anhydrite but is much more fine-grained. Synthetic anhydrite also has a comparable strength but the water-solids ratio is 0.36 as compared to about 0.09 for natural anhydrite. This ratio is 0.40 for the quick-setting filler. The accelerator for synthetic anhydrite is the same ($FeSO_4$ and K_2SO_4) but the proportion is 1 : 1[9, 15].

Pump packing in Britain is currently practised by Thyssen and Cementation Run of mine coal/shale is transported over a vibrator screen (0.1 inch) and the undersize is sprayed with sodium bentonite to increase fluidity and later a solution of pack bind (quick-setting cement, citric acid and water) is added before being pumped into the pack area[16]. Properties of pump packs do not appear to be available.

2.4.6 Bonded Packs

Blades and Whittaker[17, 18] carried out compression tests on dirt packs

bonded with resinous cement, anhydrite, resins (polyester) and cement to improve load acceptance. The consolidated pack appears to provide a compromise characteristic between those of wood and cement blocks with a gradual decline in resistance after a fairly rapidly achieved ultimate bearing load. The test results are shown in Fig. 2.5. in comparison with wood chocks and dirt packs.

2.5 Load acceptance and behaviour of roadside packs

Underground pack load measurement is an important aspect of strata control in gate roadways. The nature of load acceptance of a pack with face advance indicates how well or how early the roadway receives protection from rock pressure. Pack behaviour depends on the following factors:

(a) Properties of the material used in constructing the pack.

(b) Number and location of packs near the roadway.

(c) Size and slenderness of the pack.

(d) Rate of advance.

(e) Other miscellaneous factors like strata and coal properties, face length, condition of the ribside, depth of the mine, etc.

Phillips and Walker[19] in their early work on packs, obtained underground experimental evidence to indicate that roadway closure could be

FIG.2.5 - LOAD-YIELD CHARACTERISTICS OF PACKS
(After Blades & Whittaker)

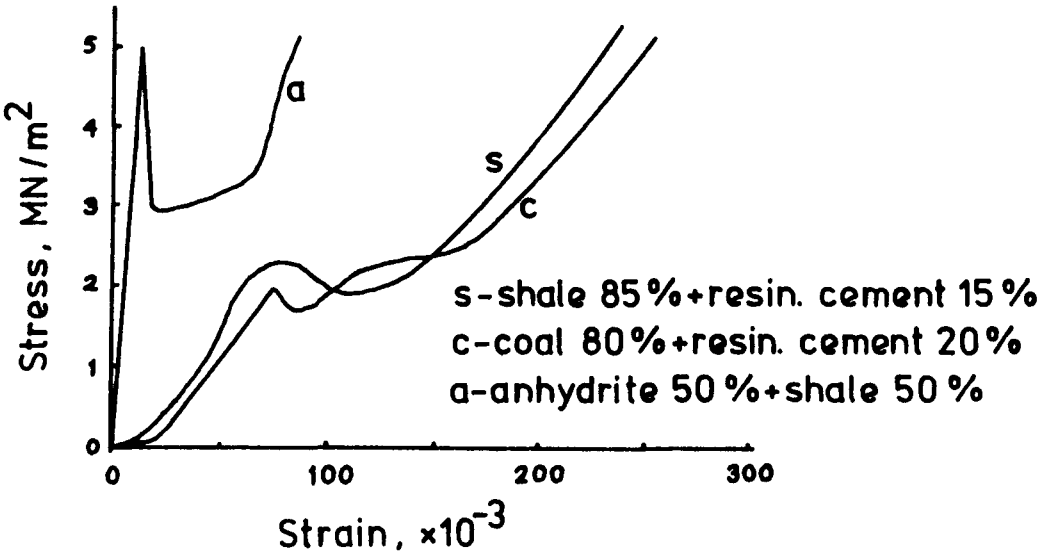

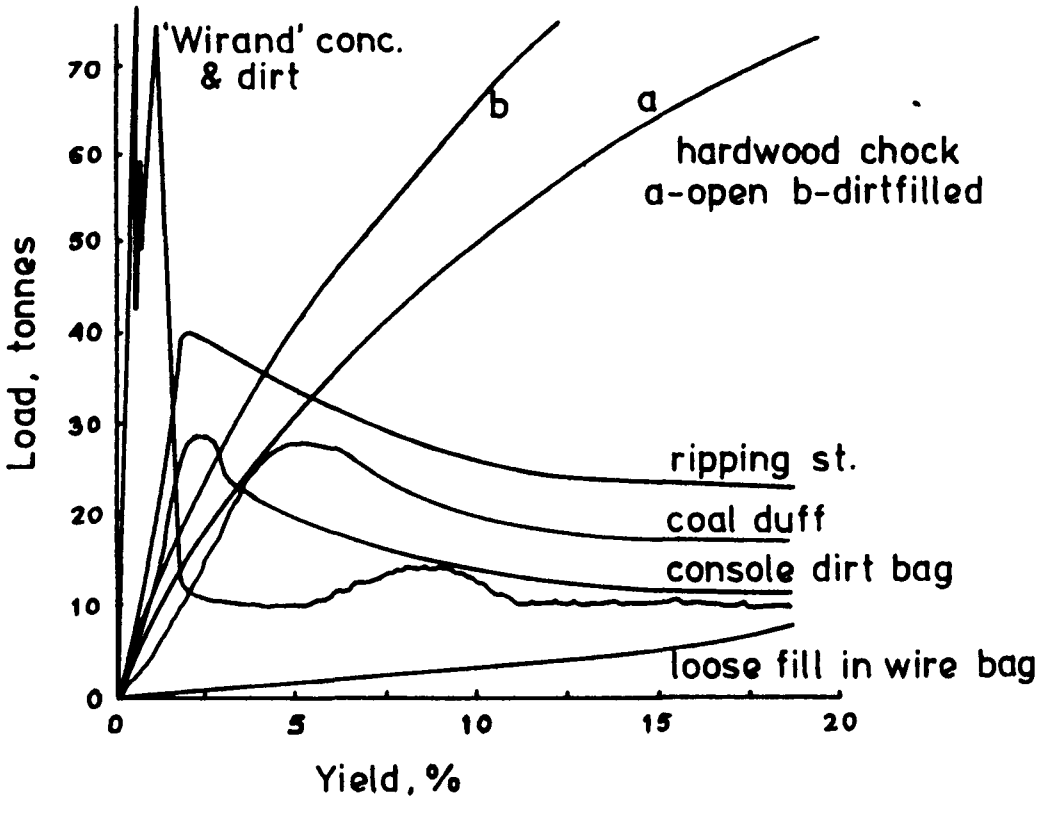

reduced if two dirt filled packs were used instead of one on either side of a middle gate. The total width of double packs was kept the same as the single pack.

Evans et al.[20] measured load by means of mechanical dynamometers in middle gate packs in two mines at different depths (1000 to 2000 ft.). The face lengths were 370 to 400 yds. (330 to 360 m) and the pack width 8 to 10 yards (7.2 to 9 m). They also measured pack convergence with a convergence recorder. In all cases the pack showed a peak load build up at about 150 to 200 ft. (45 to 60 m) from the face. The peak load was observed to be greater than the cover load which later dropped considerably and rose again to be steadied off to a value slightly greater than the cover load (see Fig.2.6(a)). The pack compression and lateral roadway closure in the meantime increased more or less smoothly.

Similar curves of pack load have been produced by Phillips[21] at 90 yds (81 m) and 900 yds (810 m) depths, the face length being 180 yds (162 m) and 218 yds (194 m) respectively. Fig.2.6(b) shows his results and indicates again the existence of a peak load value some distance from the face, which Phillips terms as the back abutment pressure. Curves 1 and 2 in this figure are for the 90-yd depth with load cells 2.5 and 7.5 ft inside the pack. The pack edge appears to carry much less load. Curve 3 is for the 900-yd depth.

In another investigation by Phillips and Jones[22] the peak load occurrence is confirmed giving support to the back abutment hypothesis. They also contend that if pack load observations are taken from the start

FIG.2.6 - DIRT PACK LOAD ACCEPTANCE

(a) After Evans et al.

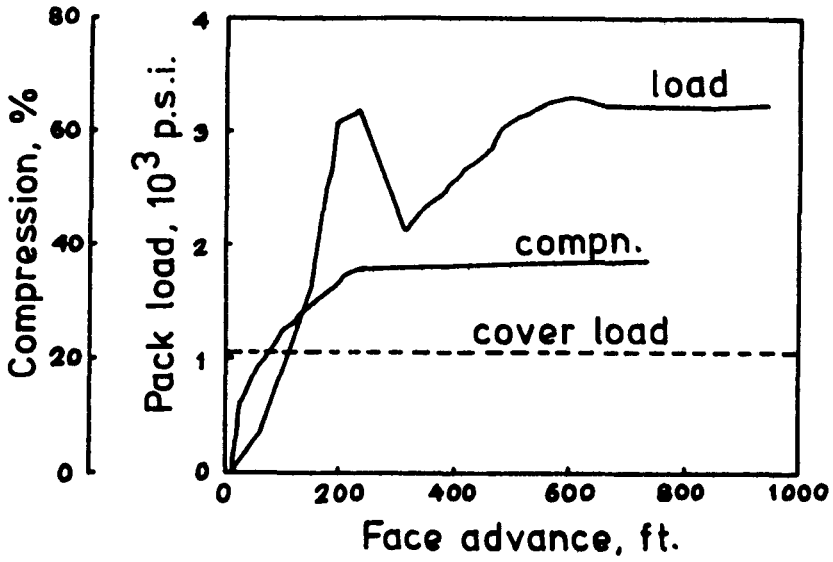

(b) After Phillips

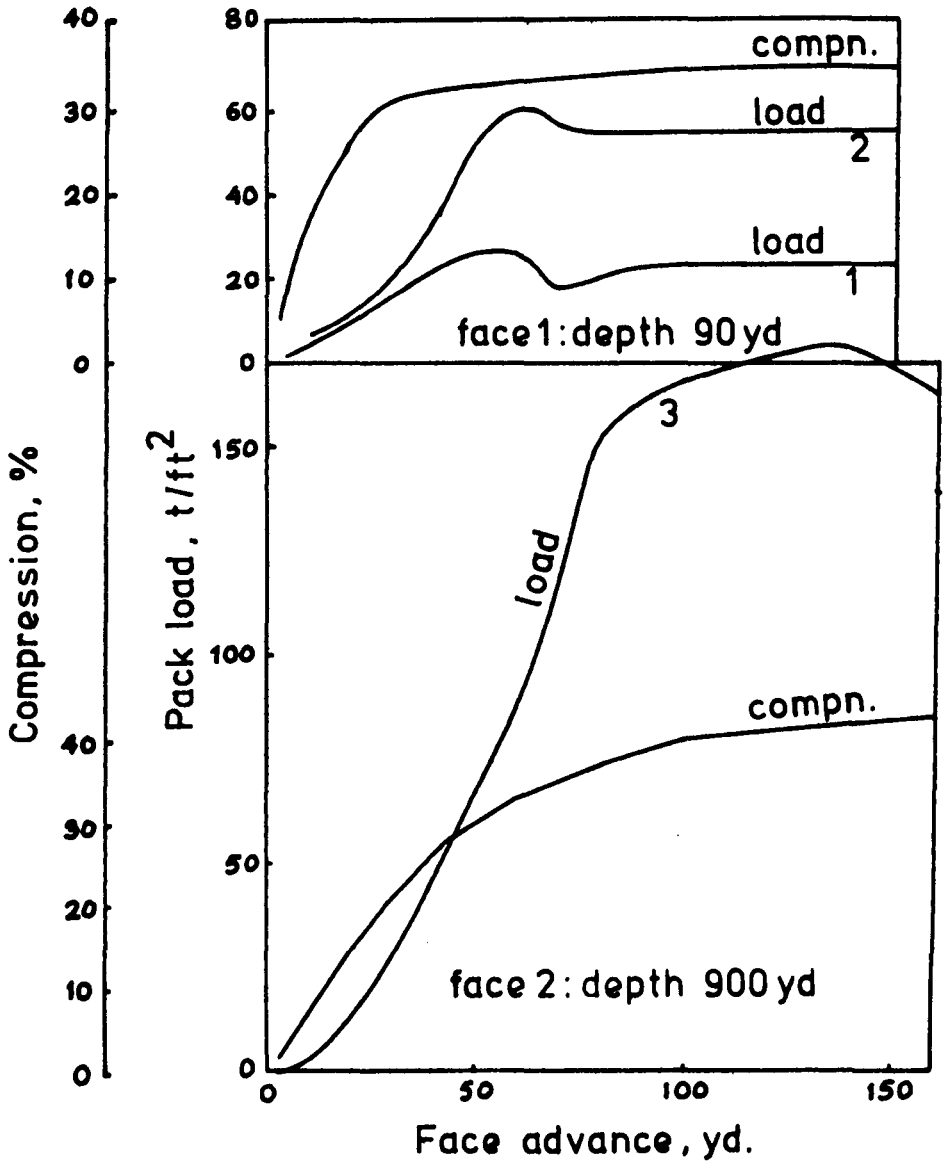

of a face, there is a limiting distance from the coal pillar from which an appreciable back abutment pressure is not developed.

Two other researchers later obtained pack load characteristics very much similar to those of Phillips and others. Winstanley[23] chose a very long face, 3000 ft (900 m), at a depth of 2100 ft (830m) for measuring pack load. His investigation gave a steady rise of pack load to greater than the depth pressure at 107 ft (32 m), a later fall and steadying off to the depth pressure. Price[24] went a step further and installed two load cells, one on the floor and the other in a dug-out in the floor (in-floor). The loading curve confirmed the observations of others for the on-floor location in that there was a load peak at about 60 ft (18 m) from the face. The in-floor location, however, produced surprising results in that there was no peak load build up and the load later steadied off to a value 67% greater than for the on-floor measurement.

Jacobi[25] installed Maihak pressure capsules in the pneumatically stowed goaf and could not observe any back abutment pressure even after 6 months of face advance. Similar observations have been reported by Creuels and Hermes[26] for a pneumatically stowed area. Jacobi disagrees with the back abutment hypothesis.

More recently load measurements were carried out in dirt packs by Thomas by means of a hydraulic pack dynamometer developed at the Mining Research Establishment[27]. He has criticised the earlier work of Evans et al.[20] that their observations were affected by the roadway since the dynamometer was installed too near the pack wall, even under it sometimes.

Thomas's measurements were taken near ribside roadways at Hucknall Colliery from which he concluded that

(a) the pressures measured are rarely more than 0.5 times the cover load,

(b) the pressures are usually limited by the flow of pack floor into the roadway or waste, and

(c) the proximity of a ribside causes loads on the ribside pack to be low.

No definite evidence of a back abutment pressure was obtained. Thomas is, however, silent about the work of other authors.

It can be seen that most investigations of pack load reviewed till now deal with dirt packs. Work was recently carried out by Genthe[9] to estimate loads on Blitzdammer packs in Germany. His findings, shown in Fig. 2.7(a), indicate again a peak load occurrence at about 25 m from the face. The maximum load that could be recorded was only 22.5 kg/cm^2 (2220 kN/m^2) in a gateroad located near the ribside. Surprisingly this is much lower than the figures from Limburg Coalfield, Germany of 42 kg/cm^2 (4120 kN/m^2) in the case of wood chocks and 63 kg/cm^2 (6180 kN/m^2) for packs of alternate oak planks and concrete blocks[13].

Investigations are being carried out by the Department of Mining Engineering of the University of Newcastle upon Tyne at Easington Colliery for assessing the behaviour of gate roads adjacent to ribsides using anhydrite

FIG. 2.7 - PACK LOAD ACCEPTANCE

(a) Blitzdammer filler (after Genthe)

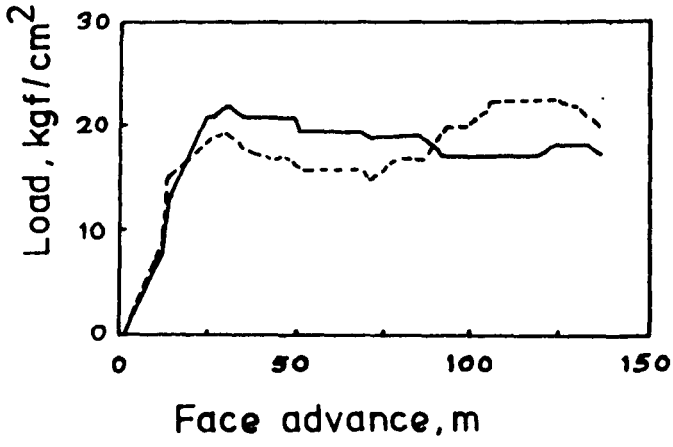

(b) Anhydrite (after Dudley)

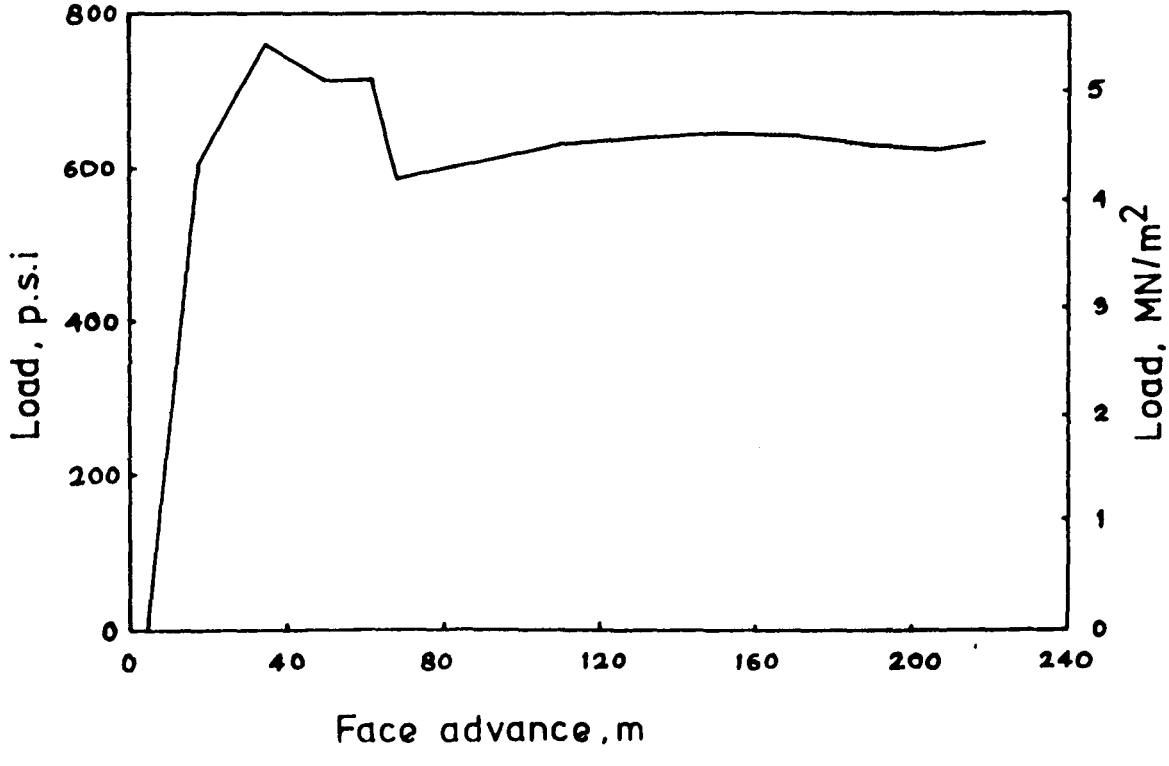

packs[28]. One panel in which pack load measurements have been carried out is 1800 ft (590 m) deep and has a face length of 200 yds (180 m). The pack is 1.5-m wide and exhibited a load acceptance characteristic which is similar in general to many others reviewed till now and also to Genthe's observation, as can be noticed from Fig. 2.7(b). The peak load reached was about 5300 kN/m^2 as compared to 2220 kN/m^2 reported by Genthe. The steady state load was about 4500 kN/m^2. The maximum load was attained at about 40m of face advance. The values of these loadings are more comparable with those reported from Limburg Coalfield of Germany for wood chocks and oak-and-concrete packs.

The loading characteristics in the earlier work of Phillips, Evans and others were obtained in dirt packs in the middle gate region. The face length was also considerable in most cases. It would thus seem natural that the ultimate pack load corresponded to the depth pressure. Packs at the side of roadways located adjacent to the solid ribside will not probably undergo the same load as middle gate packs because of the resistance offered by the ribside. The general shape of the load characteristic, consisting of a steady rise to a peak value, later fall and steadying off to a plateau value, appears to be the same for anhydrite packs as for dirt -filled middle gate packs. There is more evidence in favour of the pack undergoing back abutment pressure than against it. Hence the back abutment hypothesis may be regarded as sufficiently general and acceptable.

The pack load values and the consequent convergence variation against face advance as obtained by earlier workers on middle gates can hardly be

comparable with those observed for anhydrite since the latter have been obtained at roadways adjacent to a ribside. Thus a comparative picture is difficult to establish, unless observations are taken under similar conditions at roadways employing conventional and anhydrite packs. Anhydrite and other substitute hydraulically setting materials have, however, met with considerable success in Germany and seem to show obvious superiority in behaviour over other packs. A brief comparison based on field experience in Germany is made below.

2.6 Substitute packing materials and improvement in roadway stability

Genthe[9], Heinrich[13], and Lenge et al.[15] have reported in general about the improvement in roadway stability due to introduction of anhydrite (natural and synthetic) and quick-setting fillers.

According to Genthe, roadside packs of hydraulically setting materials can at the most be compressed by 0.5-1.5% of their initial height before breaking. They can obviously serve a better purpose in preventing the rock mass over the pack area and the roadway from breaking up as far as possible. Empirically speaking, Genthe contends, as a rule the condition of roadways with hydraulically setting packs is much better, in particular on account of the lack of convergence in the pack area, than in comparable roadways, while employing only 1-m wide packs in seam thicknesses of up to 1.5 m.

Heinrich[13] has collated the experience gained with roadway packs of hydraulically setting materials. Up to October 1970 roadway packs had been stowed in 17 German pits in 22 different seams (a total of 26 packs), 12 with

natural anhydrite, 8 with synthetic anhydrite and 6 with Blitzdammer filler. In most cases the seam thickness was greater than 1.4 m and the pack was 0.7 to 0.9 times thicker than the seams. This criterion for pack width was found to be generally satisfactory.

Hydraulically setting materials, besides having other obvious advantages, were early load bearing and rigid and attained considerable strengths quickly. They were, therefore, expected to give considerable success at the time of implementation in Germany. They have, of course, given notable success in some mines but they have also brought about no improvement in a few instances and in rare cases have worsened the roadway conditions.

The most successful cases of improvement in roadway conditions have been reported by Heinrich in three mines. In all these three cases the arched supports were usually placed below the roof, i.e. the roof was not ripped. In this circumstance the anhydrite pack is able to fill the cavity between the arch and the roof, which wood chocks cannot, and is obviously advantageous.

Heinrich has further recounted examples of success with rigid side packs at Auguste Victoria Colliery where the roadway stood with hardly any loss of cross-section and could be used a second time, at Walsum Colliery where the roadway supports have remained undeformed and at Matthias Stinnes Colliery in which the loss of cross-section has been reduced so much that it was possible to replace the 14-m^2 arches by 11-m^2 ones.

Three more cases have been mentioned where hydraulically-setting materials have been used as main packs with complete success.

Lenge et al.[15] have reported successful application of pneumatically stowed quick setting filler in pack construction at Heinrich Robert Colliery. Records kept by Steinkohlenbergbauverein show a slight distortion of the supports, which is not sufficient to be visible, and the elimination of the need for dinting. After the face had passed, 85% of the cross-section of the roadway remained, whereas in previous roadways in the same seam only about 65% of the original section had been preserved.

There have been cases, however, where hydraulically setting packs have shown little improvement or have even deteriorated the roadway further by causing additional floor heave[13]. The packs erected at Holland Colliery have shown no improvement over wood chocks as regards roadway behaviour. To a certain extent this caused rather more floor heaving, but there are no measurements available to support this.

In Zollverein Colliery a road supported by chocks was accompanied by a side pack. The road had been cut about 1.4 m into the floor. It was seen that the side of the road with a rigid pack flowed into the floor to a greater extent than when only wood chocks were used.

A 120-m long side pack was stowed in Hugo Colliery. A width of approximately 1.6 m was first selected for the 2-m thick seam. This brought about some improvement in the roof condition. When the width of the pack was reduced to 1 m (half the seam thickness), the side pack was partly

destroyed, there was a greater floor lift and the supports were deformed. This case shows that the width-height ratio may not be reduced to 0.5. The floor strength was 250 kg/cm^2 (2500 kN/m^2 approximately) and the pack pressure on the floor was so great as to cause floor penetration, upon pack width reduction. The deformation of the supports could be attributed to the fact that the pack was erected at a distance of 0.5 to 1 m behind them.

2.7 Advantages of hydraulically setting materials and their applicability

It would thus appear that packs built from hydraulically setting substitute materials like anhydrite have certain obvious advantages as compared to conventional packs, like wood chocks and stone packs. Economically, German experience shows that these packs are either superior to or the same as conventional packs. From the standpoint of strata control they have brought about considerable improvement in roadways of some German mines, judging by the case histories in 2.6, but in a few cases have caused no better roadway behaviour or even a further deterioration in terms of floor heave. The success with setting packs is thus not entirely unqualified. However, some other reasons, which are not rock mechanical, may sometimes seem more important, e.g. prevention of ventilation leakage from the goaf area. This has been the case at Holland Colliery where German engineers continued to use anhydrite packing in spite of the fact that it gave no better roadways than the wood chocks[13]. Another reason for its popularity in Germany is that it can cope with high speeds of face advance. Its advantages from the point of view of strata control are:

(a) It attains high strengths in short periods and it is not necessary to build wide packs.

(b) It is early load bearing, i.e. it accepts strata pressure earlier than conventional packs.

(c) It is comparatively rigid and causes less convergence in roadways.

(d) It can effectively fill gaps and cavities.

Hydraulically setting packs have, however, some limitations to their applicability:

(a) In seams with a weak floor liable to flow and fracture, packs of anhydrite or such materials may increase floor lift due to their rigidity, especially since such packs are narrow. In this connection, it is worthwhile investigating the effect of pack width on floor heave. According to German experience, pack widths should not be less than 0.75 times the seam thickness for overall stability. An increase in the width may alleviate floor heave to some extent, but of course, may mean higher costs. Sufficient measurements of pack load under similar conditions are not available, so it is difficult to say that anhydrite packs will create a higher pressure on the floor, and will, in fact, cause additional floor heave.

(b) The setting process of anhydrite slows down considerably with temperature (as opposed to Blitzdammer). Hence it may not be successful in hot, humid conditions.

2.8 Short face advancing with a centre pack

Having considered the advantages and limitations of anhydrite and other substitute pack materials, it is clear that they can serve a very useful purpose as roadside packs. In recent years, the building of wide stone packs has become costly and the price of wood is becoming higher. Retreat mining is becoming more popular and interest is developing in in-seam mining in conjunction with retreating.

Longwall retreating has, however, the disadvantage that it requires initial development by headings, which makes it largely unproductive and uneconomical during development. A method of developing by short-face wide headings with a centre pack of anhydrite or other setting materials was, therefore, thought of[1] and is currently under consideration in conjunction with pump packs in the Barnsley area[2]. This method of development and subsequent retreating is shown schematically in Fig.2.8. It consists of driving a pair of in-seam wide headings (12 to 16 m wide) with a centre pack of suitable width, creating two roadways on either side of the pack. These roadways can later be used as gate roads during retreating. Roadways will be supported in the usual manner while advancing. This method will have the advantage of productivity in the stage of development, as opposed to conventional developing for retreating.

Before implementation, however, it would be beneficial to consider the rock mechanical feasibility of the method and the work in the next Chapters is devoted almost exclusively to this method. The next Chapter

FIG.2·8 - SHORT FACE DEVELOPMENT WITH CENTRAL ANHYDRITE PACK & SUBSEQUENT RETREATING

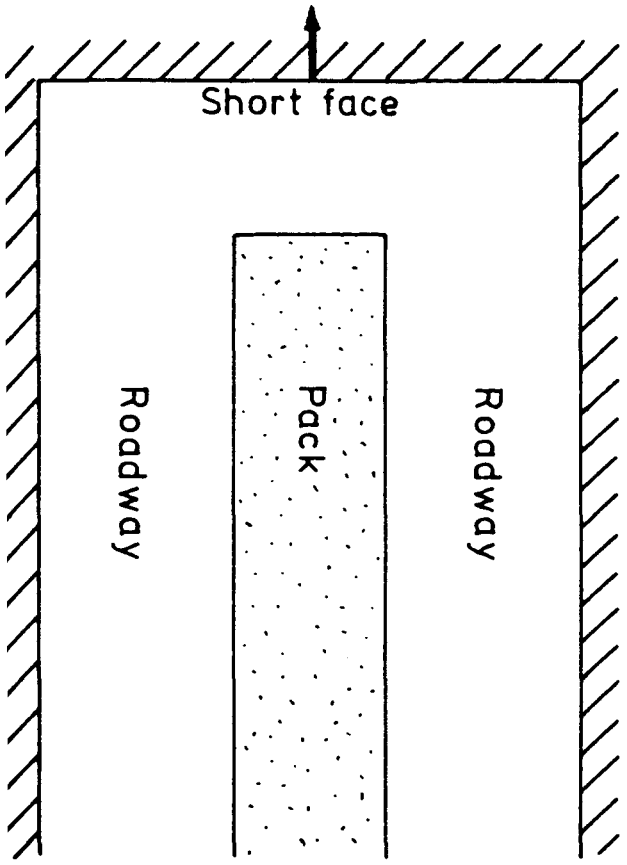

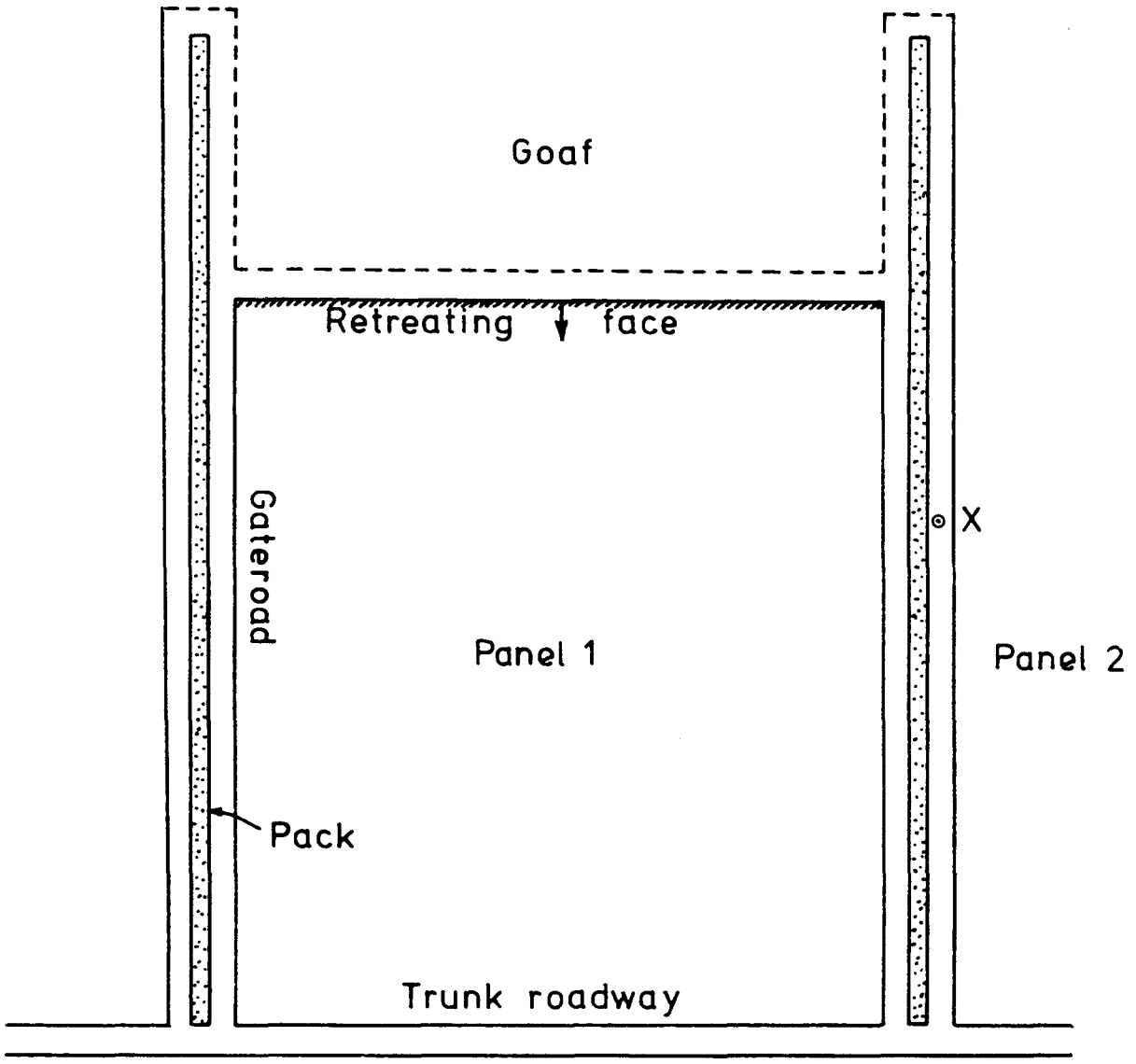

considers the beam theory in review, as a possible means of assessing the centre pack advancing method.

* * *

CHAPTER 3

The beam theory and its application to strata mechanical problems

CHAPTER 3

The Beam Theory and its application to Strata Mechanical Problems

Many instances of mining in stratified rock require estimation of roof behaviour. The classical pressure arch theory, with its pre-requisite of rather systematic bed separation in the roof, explained schematically rather than analytically or quantitatively the occurrence of abutment pressure on the ribside of a mine opening and also support load and subsidence. The theory is too well known to warrant a description here and this Chapter will consider the more realistic and later theory of beams in its various stages of development.

The beam theory regards the stratified rock in the roof as a beam which deflects downwards due to mining over openings, supports, pillars, etc. in some manner, causing convergence or load as the case may be. It must be made clear at the outset that the roof rock is infinite in two horizontal directions and hence should be considered as a plate rather than a beam. The differential equation for deflections w of a simple plate in a rectangular coordinate system (x,y) is

$$\frac{\partial^4 w}{\partial x^4} + 2\frac{\partial^4 w}{\partial x^2 \partial y^2} + \frac{\partial^4 w}{\partial y^4} = \frac{q}{D} \quad .$$

where q is the loading on the plate and D is its flexural rigidity. For any support configuration under the plate which is considered infinite in one direction y, the second and third terms on the left hand side of this

equation vanish and the first term becomes an ordinary derivative, leading to

$$\frac{\partial^4 w}{\partial x^4} = \frac{q}{D}$$

This latter equation then represents plane strain since the plate bends only along the x-axis[29] and is identical to a beam deflection equation except for the flexural rigidity D. Hence the term beam instead of plate is used in all plane strain analytical solutions to problems of strata deflection, as has been done throughout in this thesis.

3.1 Beams with rigid and elastic support

Until quite recently roof rock over an opening was likened to either a beam simply supported at its two ends by ribs or pillars, as the situation may be, or clamped rigidly at its ends between the main rockmass and the coal seam. The differential equation for beam deflection v is

$$D \frac{d^4 v}{dx^4} = q \qquad (3.1)$$

which has the general solution

$$v = \frac{q}{24 D} x^4 + A_1 x^2 + A_2$$

for a symmetrical rectangular opening with ribs on either side. According to these two beam models the following boundary conditions at the coal edge

are applied to the solution to obtain the integration constants A_1 and A_2 and so complete the solution:

Simply supported:	$v = 0 \ , \ \frac{d^2v}{dx^2} = 0$	(deflection and bending moment are zero)
Clamped:	$v = 0 \ , \ \frac{dv}{dx} = 0$	(deflection and slope are zero)

(3.2)

Both beam models, however, treat the roof as finite and completely disregard the behaviour of the roof over the coal and so give the following erroneous answers:

(a) With both models no abutment pressure exists over the coal edge.

(b) In the simply supported case the bending moment is zero at the coal edge and the clamped case produces sharp clamping moments at the coal edge, the bending moment being suddenly zero further inside over the coal.

(c) The coal seam produces perfect clamping or a simple unyielding point support preventing roof deflection at the coal edge, while in reality coal is softer than most rocks and hence cannot be expected to remain rigid while the roof strata deflect downward.

The deflections and moments are shown schematically in Fig. 3.1 for these two models.

FIG.3.1 - BENDING OF NETHER ROOF WITH RIGID AND YIELDING SEAM SUPPORT

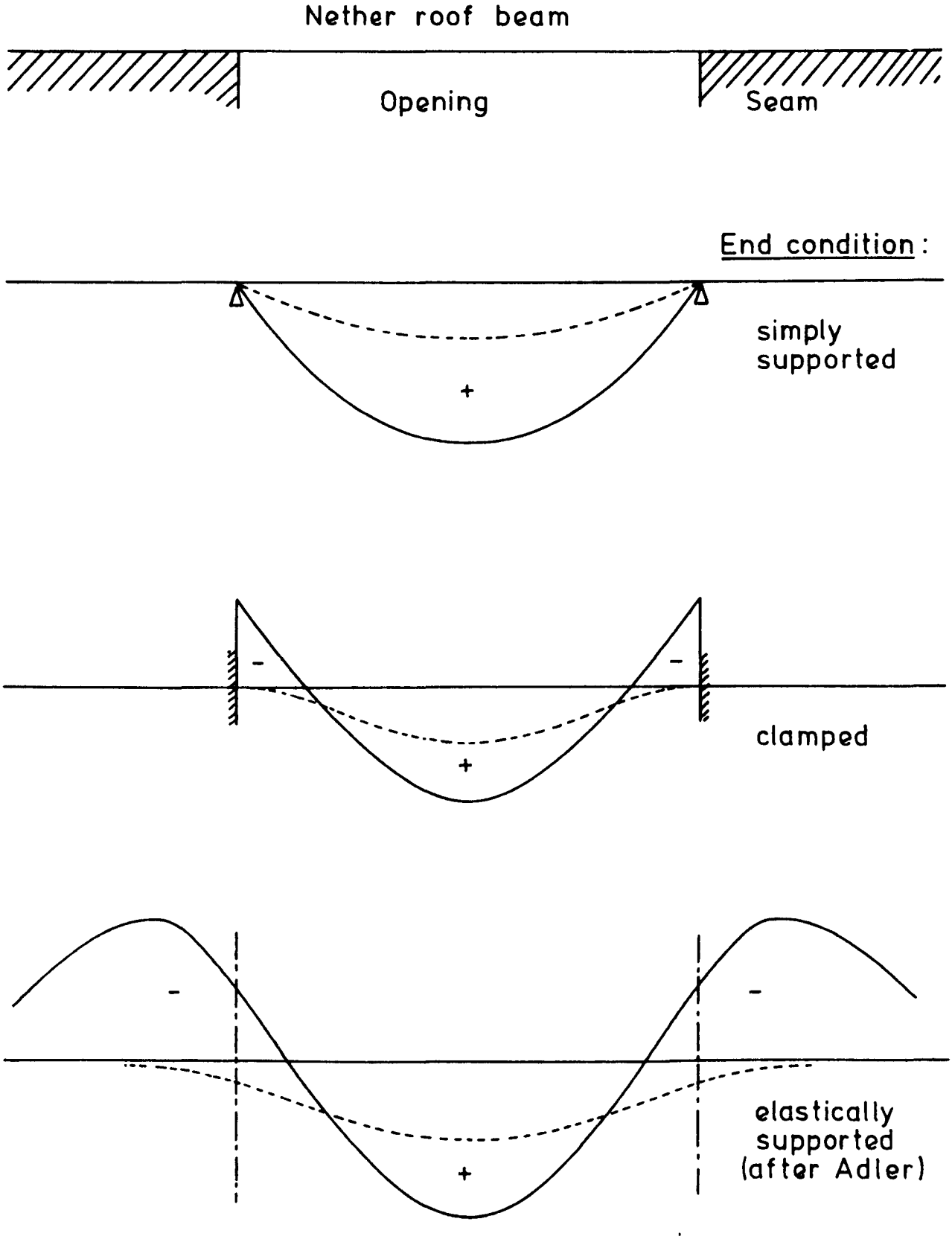

From the objections (a), (b) and (c) it can thus be seen that the seam will yield under the bending action of the roof and will give rise to deflections and bending moments at the coal edge in the beam and also further inside. Hetenyi[30] enumerates various examples of beams supported elastically by a continuous yielding 'foundation' and it is, perhaps, the first comprehensive work in the theory of beams on elastic foundations. Though his work is quite old, it was seldom seriously considered for application to mining in stratified rock until quite recently, when Tincelin and Sinou[31] showed, probably for the first time, how the theory could be applied to a practical mining situation. They used the method to estimate pillar loads in a panel of pillars with barriers on either side. Adler[32] used the theory to show mathematically how the nether roof behaves over an opening and also over the ribside and corroborated his results by models. The deflection and bending moment variation as per Adler is shown schematically in Fig. 3.1. A comparison with the simply supported and clamped cases in the same figure shows the significantly different distribution of bending moments and deflections, when the elasticity of the seam is taken into consideration. Large values of bending moments and deflections are seen to occur over the ribside.

When a transversely loaded beam is supported elastically, the deflection v at any point in the beam is equal to the compression produced in the supporting foundation, the upward reaction to the beam being proportional to the deflection v. Thus, if the transverse load on the beam is q, the differential equation for beam deflection in this case will be[30, 33].

$$D \frac{d^4 v}{dx^4} = q - kv \qquad (3.3)$$

where k is the foundation modulus, of which more will be said later in this Chapter. When Equ. (3.3) is applied to the ribside k becomes the foundation modulus of the seam. Considering again the symmetrical configuration of a rectangular opening with infinite ribs on either side, as done by Adler[32], for the unsupported opening region we again have Equ. (3.1) and for the ribside Eq. (3.3). From these the expressions for deflections in the two regions can be written down as

Opening:

$$v_1 = \frac{q}{24D} x^4 + A_1 x^2 + A_2$$

Ribside:

$$v_2 = \frac{q}{k} + e^{-\alpha x}\left(A_3 \cos \alpha x + A_4 \sin \alpha x \right)$$

the first expression satisfying the condition of symmetry and the second one at $x = \infty$, $v_2 = q/k$. When the second expression is multiplied through by k, the loading on the ribside is obtained as

$$k v_2 = q + k e^{-\alpha x}\left(A_3 \cos \alpha x + A_4 \sin \alpha x \right)$$

which will have the general shape shown in Fig. 3.1. The ribside loading thus shows an abutment peak stress at the edge which falls to the depth pressure q eventually. This abutment peak stress is likely to cause crushing of the ribside, reducing its support capacity and consequently shift the peak into the coal. This will be considered in greater detail in Chapter 7. The peak mentioned here is the prefracture peak. The

integration constants A_1 and A_2 can be determined from the continuity conditions at the coal edge:

$$\text{at } x = \frac{L}{2} \;, \left[\begin{array}{ll} v_1 = v_2 \;, & v_1' = v_2' \;, \\ v_1'' = v_2'' \;, & v_1''' = v_2''' \end{array} \right] \tag{3.4}$$

where L is the opening width. The conditions in words state that at the common boundary between the two regions - the coal edge - the deflections, slopes, bending moments and shear forces must be equal for continuity. These continuity conditions can, incidentally, be used for any two neighbouring regions. It can be seen that these boundary conditions are completely different from (3.2) and so is the procedure for determining deflections when the elasticity of the seam is accounted for.

3.2 Foundation Models

The foundation k in Equ. (3.3) is a measure of elasticity of the foundation, in this case, the seam. It is defined as[31]

$$k = \frac{E}{H(1-\mu^2)} \tag{3.5}$$

nearer the coal edge due to biaxial conditions and

$$k = \frac{E(1-\mu)}{H(1+\mu)(1-2\mu)}$$

deeper into the seam because of triaxial conditions of stress. E is the modulus of elasticity of the seam, μ is Poisson's ratio and H is the seam

thickness. For the usual values of μ for coal (0.2 or 0.25) the two expressions for k are not significantly different. Also the region of interest is nearer the opening usually and as such the first expression (3.5) will be used in future work.

The simplest representation of an elastic foundation has thus been provided in Equ. (3.5) by Winkler[30], who assumed the foundation as consisting of closely spaced independent linear springs. Kerr[34] has reviewed several alternative foundation models in order to incorporate interaction between springs. Some of them are noteworthy:

(a) Filonenko-Borodich Foundation: In this model the top ends of the springs are connected to a stretched membrane subjected to a constant elastic tension of some value. Thus the behaviour of the foundation depends on the value of the tension assumed.

(b) Pasternak Foundation: A shear interaction between spring elements is accomplished by connecting the ends of the springs to a beam (or plate) which consists of incompressible vertical elements and deforms only by shear.

(c) 'Generalised' Foundation: In this, it is assumed, in addition to the Winkler hypothesis, in which the pressure is proportional to deflection at each point, that also the moment is proportional to rotation. The second assumption is regarded by Kerr as quite arbitrary.

(d) Reissner Foundation: Reissner assumes that in-plane stresses throughout the foundation and the horizontal displacements of the contact surface between the beam and foundation are zero. This leads to the Pasternak foundation model again.

The usual approach in formulating deflection problems over such foundations is based on the inclusion of the foundation reaction into the differential equation for beam deflection. For example, when the reactions as per the Winkler model are included, we get Equ. (3.3). For the other foundation models the differential equations are more complicated. For simplicity the Winkler model will be used in subsequent work, as has been done by others[30-33, 35 - 38].

3.3 Thin and thick beams

In all that has been said till now, there is an implicit assumption that the beam is regarded as thin. If the distance between the supports of a beam is less than five times its thickness or depth it is considered to be a thick beam generally[36]. In most mining situations in stratified rock, the nether roof, or the strata up to the surface, has to be considered as thick. Any beam, thick or thin, undergoes deflections which are the sum total of the three kinds of deflections due to

(a) bending moments,

(b) shear forces, and

(c) vertical stress σ_y depending on the loading on the beam[39].

The last-mentioned deflections have not been included in any thick beam differential equation and in fact mention is rarely made of these deflections even in standard works on the subject of beams in strength of materials, presumably because they are not very significant. In a thin beam the only deflections of consequence are those due to bending moments. Equ. (3.3) is the thin beam differential equation and so gives deflections due to bending moments alone. The influence of shear force becomes more and more prominent as the beam becomes thicker. The total curvature produced in a thick beam is the sum of the curvatures due to bending moments and shear forces:

$$\frac{d^2v}{dx^2} = \frac{d^2v_m}{dx^2} + \frac{d^2v_s}{dx^2} \tag{3.6}$$

where v is the total vertical displacement at any point (x,y) in the beam and v_m and v_s are those due to the bending moment and shear force at the beam cross-section containing (x,y). When the beam is thin the second curvature term on the right is negligible, and we get Equ. (3.3) when the curvature is differentiated twice, multiplied by the flexural rigidity D and equated to the loading on the beam.

The curvature in a thin beam is directly proportional to the bending moment M according to the relation

$$\frac{d^2v}{dx^2} = -\frac{M}{D} \tag{3.7}$$

so it is simple enough to obtain the differential equation like (3.3) once the bending moments (or curvature) are known, as for a thin beam, but such an

expression for bending moments does not hold for thick beams (which will be seen later). So the derivation for a thick beam cannot proceed ahead from this point.

An exhaustive review of literature on thick beams has been made by the U.S. Army Engineers Waterways Experiment Station[40], but no case of thick beams on elastic foundations has been included, perhaps because of their field of interest in civil engineering. The first attempt at formulating a differential equation for thick beams supported elastically appears to be made by Tincelin and Sinou[31] for pillar load distribtuion in a panel, visualising the fact that pillar loads are governed by the distance between panel barriers or panel width since this will affect the deflection of strata in the panel. Their derivation is given briefly below:

The deflection v_s due to shear force is related to the shear force according to

$$\frac{dv_s}{dx} = \frac{3Q(1+\mu)}{Eh} \tag{3.8}$$

where E, μ are elastic constants of the strata and h is the strata beam thickness. Differentiating once,

$$\frac{d^2v_s}{dx^2} = \frac{3(1+\mu)}{Eh} \cdot \frac{dQ}{dx}$$

Now
$$\frac{dQ}{dx} = -D\frac{d^4v}{dx^4} = -(q-kv) \tag{3.9}$$

so
$$\frac{d^2v_s}{dx^2} = -\frac{3(1+\mu)}{Eh}(q-kv)$$

and using (3.6) and (3.7) we finally get

$$D\frac{d^4v}{dx^4} - \frac{3(1+\mu)kD}{Eh}\cdot\frac{d^2v}{dx^2} = q - kv \qquad (3.10)$$

which is a differential equation for deflection of a thick beam supported elastically. As has been pointed out in (41), Equ. (3.9) assumes the thin beam equation (3.3) again as valid for thick beams even though v are now the total deflections given by (3.6). It was doubtful whether Equ. (3.10) could, therefore, be regarded as acceptable.

3 3.1 The flexural rigidity of strata

The product of the moment of inertia of the beam cross-section and its modulus of elasticity is defined as its flexural rigidity. In the case of a plate, the term $(1-\mu^2)$ also occurs in the denominator. Thus in general for roof strata

$$D = \frac{Eh^3}{12(1-\mu^2)}$$

where h is strata beam thickness. Depending on the nature of the problem h may be the nether roof thickness or the depth from surface.

Mandel[42] proposed to define the strata as a series of thin beams loosely placed one over the other without friction, and so proposed the following expression for flexural rigidity:

$$D = \sum_{i=1}^{n}\frac{E_i h_i^3}{12(1-\mu_i^2)} = \sum_{i=1}^{n} D_i \qquad (3.11)$$

This is just a summation of the flexural rigidities of all the strata involved in the roof, the limit of summation n depending on the stratigraphy of the area concerned. This expression is valid only within regions so affected by workings as to loosen up and break cohesion between different rock beds.

Sometimes, however, it may be doubtful whether cohesion can be assumed to have broken as in the case of a panel of pillars where the rooms will affect the strata only locally leaving the rest intact up to the surface. Also in a longwall panel, strata can be expected to loosen up to a certain height only, depending on face length. Thus it may at times be necessary to determine the flexural rigidity assuming existence of a firm bond between different layers. The strata will then be a thick composite beam of several materials. It is known from elementary applied mechanics that the flexural rigidity of a composite beam whose cross-section consists of two layers of different materials (like wood riveted on steel) can be determined, if the cross-section is converted into an equivalent T-section of only one of the two materials such that

$$b_1 = b \frac{E_w}{E_s}$$

where E_w and E_s are the elastic moduli of the two materials, say wood and steel respectively. b is the original beam width and b_1 is the equivalent width of the wooden part when it is replaced by a steel flange (see Fig.3.2).

FIG. 3.2 - CONVERSION OF A COMPOSITE BEAM SECTION INTO AN EQUIVALENT ONE-MATERIAL SECTION

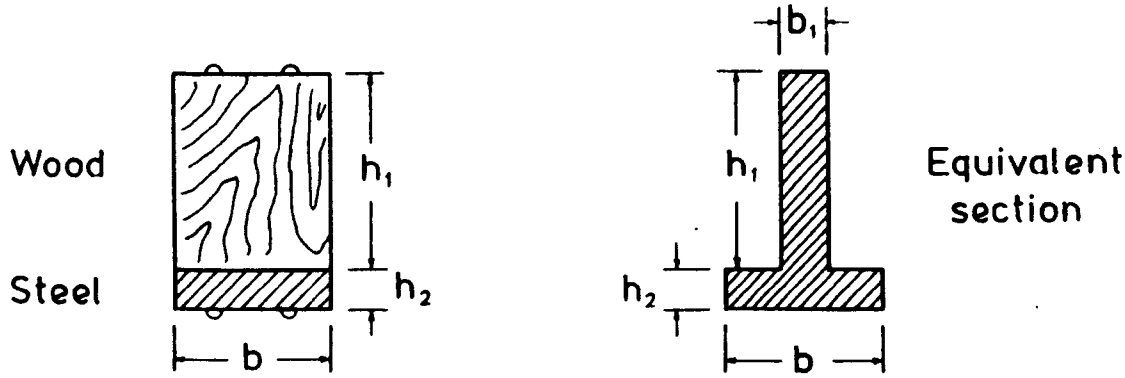

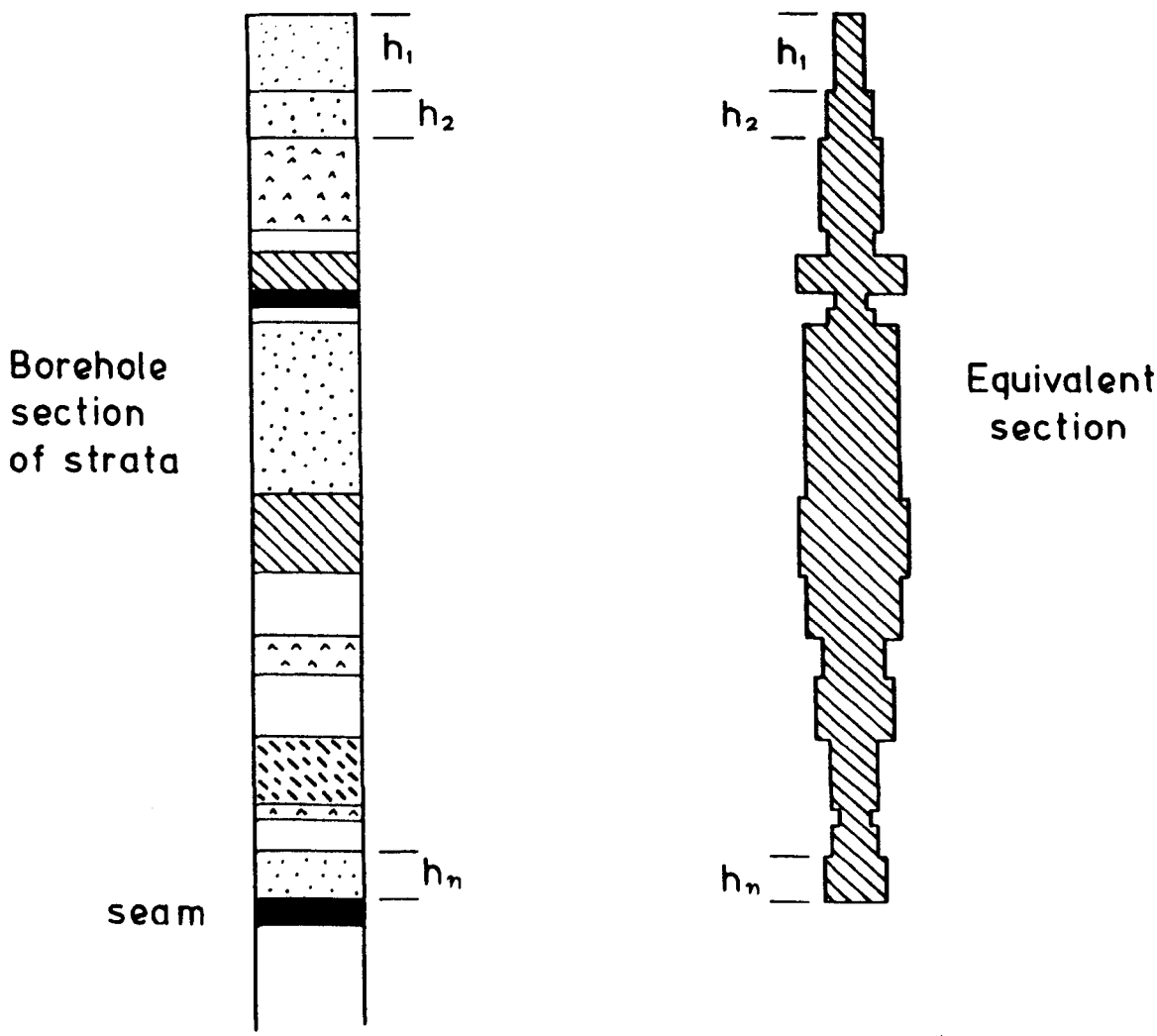

Proceeding along similar lines, a set of mine strata can be converted into an equivalent cross-section as shown in the same figure and the flexural rigidity can be shown to be given by[43]

$$D = \sum_{i=1}^{n} \frac{E_i h_i}{1-\mu_i^2} \left(\frac{h_i^2}{12} + s_i^2 \right) \tag{3.12}$$

where

$$s_i = \left(\frac{h_i}{2} + h_{i+1} + h_{i+2} + \cdots + h_n - \bar{y} \right)$$

$$\bar{y} = \frac{\sum_{i=1}^{n} \left(\frac{h_i}{2} + h_{i+1} + h_{i+2} + \cdots + h_n \right) \frac{E_i h_i}{1-\mu_i^2}}{\sum_{i=1}^{n} \frac{E_i h_i}{1-\mu_i^2}}$$

the terms $(1-\mu_i^2)$ occurring because of plate effect, the same as in Equ. (3.11).

For the same set of strata Equ. (3.12) gives a greater value of D than Equ. (3.11), i.e. loosened strata will deflect more than composite strata.

3.3.2 Middle-plane, average and bottom-fibre deflections

When the beam is considered thin, the vertical displacement v at any point (x,y) in the body of the beam does not change with y, i.e. the deflection of any horizontal fibre in the beam is identical to the one below or above it. This is because in the theory of pure bending beam cross sections remain plane during the process of bending. In thick

beams, however, the influence of shear stresses causes the cross-sections to be deformed laterally and the vertical displacement varies through the depth of the beam.

In a thick beam theory it is, therefore, essential to define the deflections in terms of which the beam differential equation is being formed. Though not mentioned explicitly, Tincelin and Sinou [31] formulated the thick beam differential equation (3.10) in terms of deflections in the middle plane of the beam. Reissner has given a theory of thick plates[44] in terms of deflections taken as an average over the plate depth, assuming a linear variation of the horizontal stress σ_x through the depth. Based on this theory, a thick beam equation was developed in terms of the average deflections[43]. The average deflections were defined by

$$v = \frac{3}{2h} \int_{-h/2}^{h/2} v_o \left(1 - \frac{4y^2}{h^2}\right) dy \tag{3.13}$$

where v_o are the deflections at any depth y and h is the beam depth. This definition was the direct result of the relations

$$\int_{-h/2}^{h/2} \tau_{xy} v_o \, dy = Q v$$

$$\tau_{xy} = \frac{3Q}{2h} \left(1 - \frac{4y^2}{h^2}\right) \tag{3.14}$$

where τ_{xy} is the shear stress and Q is the shear force. This analysis gave the following equations for deflections, bending moments and shear forces in an elastically supported thick beam

$$D \frac{d^4 v}{dx^4} + \frac{(2+\mu) h^2}{10(1-\mu^2)} \cdot \frac{d^2}{dx^2} (q - kv) = q - kv \qquad (3.15)$$

$$M = - D \frac{d^2 v}{dx^2} - \frac{(2+\mu) h^2}{10(1-\mu^2)} (q - kv) \qquad (3.16)$$

$$Q = \frac{dM}{dx}$$

Taking the case of a horizontal seam, the load on the beam q will be the uniform weight of the strata and, as such, independent of x. Equ.(3.15) then assumes a form somewhat similar to the one arrived at by Tincelin and Sinou, Equ. (3.10). The main difference between the two equations is the second order derivative of q, which appears in (3.15). This is not very important when q is a uniform load, but will make a considerable difference when it is a function of x, as it is on the parting between two contiguous workings[43].

A comparison between Equ. (3.7) of the thin beam theory and Equ.(3.16) shows that the expression for the bending moment gets changed so that an additional term is included in terms of the deflections. This is a correction term because the influence of shear force is considered.

Equ. (3.14) is for the distribution of shear stress across the beam depth and is parabolic, satisfying the conditions of zero shear stress most commonly employed in beam and plate theories:

$$(\tau_{xy})_{y = \pm h/2} = 0$$

This parabolic law of shear stress distribution, which is incorporated in the definition of the average deflections Equ. (3.13) is obtained as a direct result of the basic assumption in this thick beam theory of the linear variation of the horizontal stress σ_x with y. Filon[45] has shown that in a beam with point loads eccentrically applied on the top and bottom edges of the beam, the shear stress distribution across the beam section is not parabolic for small values of c/h, c being the distance between the two loads. Between c/h = 0.5 and ∞ the distribution is near-parabolic, or parabolic. This, in other words, means that only a small error is introduced by the assumption of a parabolic law of shear stress distribution (or a linear law for σ_x) in a thick beam, if the distance between supports is equal or greater than the beam depth. In fact, it will be noticed that Equ. (3.8) used by Tincelin and Sinou for their thick beam equation also assumes a parabolic shear stress distribution.

The two thick beam theories reviewed so far give differential equations for beam deflection in terms of middle-plane and average deflections. If the stability of the strata beam only were under consideration, these two kinds of deflection would serve the purpose well enough, but it can be visualised that the compressions produced in an elastic foundation are equal to the deflections at the surface of contact between the foundation and the thick beam. Hence an element of error is introduced in the equations in terms of middle-plane or average deflections in the case of thick beams supported elastically. In a thin beam these considerations are immaterial, since the deflections are assumed not to vary through the beam depth.

The derivation of a thick beam differential equation in terms of the lowest or bottom-fibre deflections is given below[46].

3.3.3 A thick beam differential equation in terms of bottom-fibre deflections

The thick beam theory of bottom-fibre deflections was developed originally for seam or pillar reactions to the roof, but is generally applicable to any elastic foundation, e.g. a pack. The derivation of the differential equation is given here in some detail (with some inevitable short cuts for brevity), because it is this method which has been used in subsequent Chapters on short face advancing with a centre pack. The basic assumption in the case of this derivation, as explained in previous theories, is the parabolic law of shear stress distribution (or a linear law of distribution of the horizontal stress σ_x) over the beam depth.

Fig. 3.3 shows an infinite beam on some elastic foundation, say a coal seam, in the coordinate system (x,y), y being taken positive downward. Then the two equations of equilibrium for a two-dimensional system

$$\frac{\partial \sigma_x}{\partial x} + \frac{\partial \tau_{xy}}{\partial y} = 0$$

$$\frac{\partial \sigma_y}{\partial y} + \frac{\partial \tau_{xy}}{\partial x} = 0$$

and the boundary conditions on the top and bottom edges of the beam

FIG.3.3 - SCHEMATIC OF A THICK BEAM ON A CONTINUOUS ELASTIC FOUNDATION

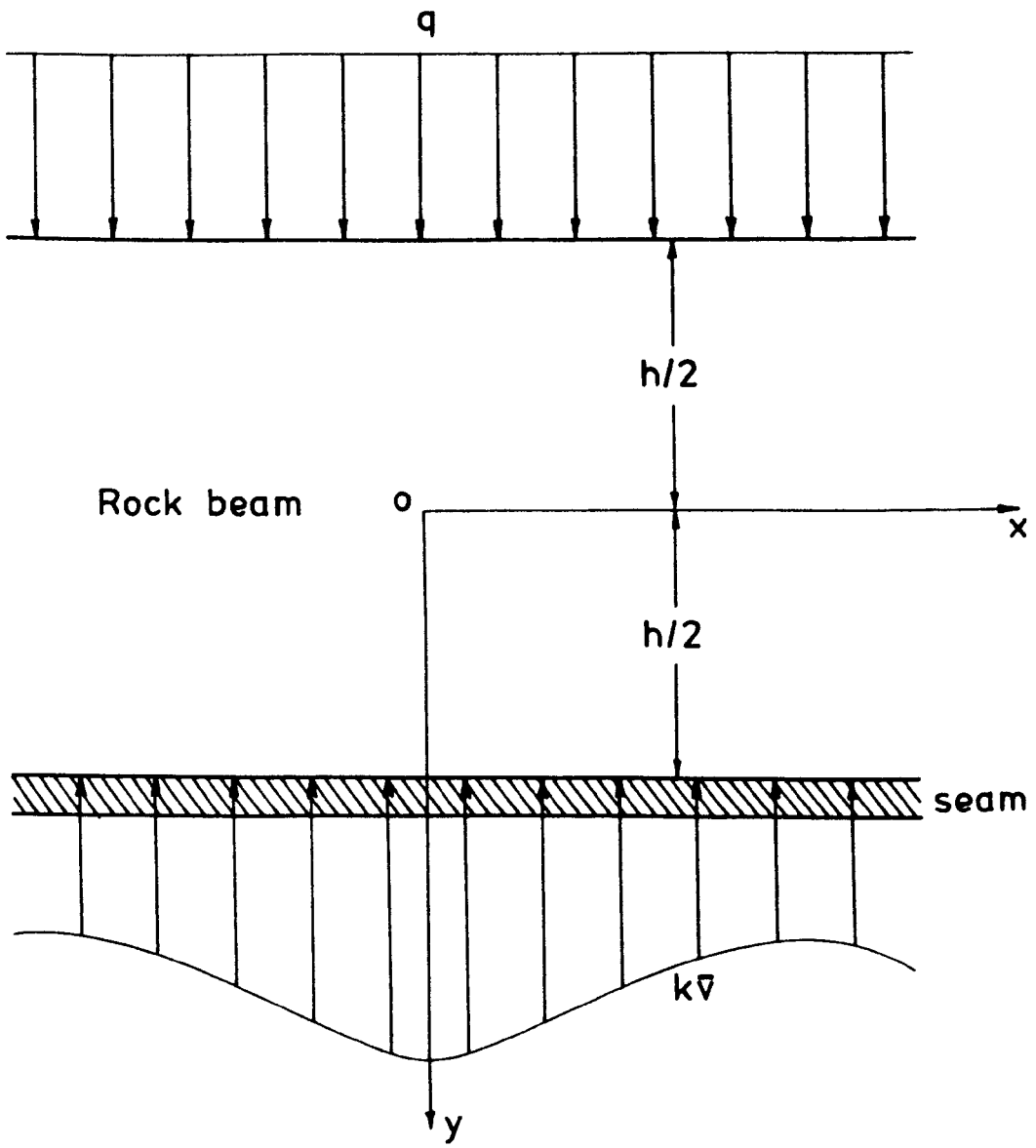

$$\left.\begin{aligned} &(\tau_{xy})_{y=\pm h/2} = 0 \\ &(\sigma_y)_{y=h/2} = -k\bar{v} \quad , \quad (\sigma_y)_{y=-h/2} = -q \end{aligned}\right] \tag{3.17}$$

are satisfield by the following expressions for the stresses σ_x, σ_y, τ_{xy} :

$$\left.\begin{aligned} \sigma_x &= f(x)\, y \\ \sigma_y &= -\frac{q+k\bar{v}}{2} + (q-k\bar{v})\left(\frac{3y}{2h} - \frac{2y^3}{h^3}\right) \\ \tau_{xy} &= \frac{1}{2} f'(x)\left(\frac{h^2}{4} - y^2\right) \end{aligned}\right] \tag{3.18}$$

These expressions are in accordance with the initial assumption of a parabolic shear stress distribution. Here $\bar{v}$ are the bottom-fibre deflections and the function f(x) is defined by

$$f''(x) = -\frac{12}{h^3}(q - k\bar{v}) \tag{3.19}$$

The rest of the symbols have the usual meanings.

Expressions for displacements u,v can be obtained if Equ. (3.18) are used in the displacement relations in plane strain

$$\frac{\partial u}{\partial x} = \frac{1}{E}\left[(1-\mu^2)\,\sigma_x - \mu(1+\mu)\,\sigma_y\right]$$

$$\frac{\partial v}{\partial y} = \frac{1}{E}\left[(1-\mu^2)\,\sigma_y - \mu(1+\mu)\,\sigma_x\right]$$

$$\frac{\partial u}{\partial y} + \frac{\partial v}{\partial x} = \frac{2(1+\mu)}{E}\,\tau_{xy}$$

Only the vertical displacements v are of interest and mentioned here:

$$v = -\frac{1-\mu^2}{E} f_{II}(x) + \frac{\mu(1+\mu)}{E}\left(q\frac{x^2}{2} - k\bar{v}_{II}\right)\left(\frac{3}{2h} - \frac{6y^2}{h^3}\right)$$

$$+ \frac{1+\mu}{E} f(x)\left(\frac{h^2}{4} - y^2\right) - B_1'(y)\,x + B_2(y)$$

where $B_1(y)$ and $B_2(y)$ are arbitrary functions of y only. From this $\bar{v}$ can be seen to be

$$\bar{v} = (v)_{y=h/2} = -\frac{1-\mu^2}{E} f_{II}(x) - B_1'\left(\frac{h}{2}\right)x + B_2\left(\frac{h}{2}\right)$$

Differentiating four times with respect to x and using Equ. (3.19)

$$D\frac{d^4\bar{v}}{dx^4} = q - k\bar{v} \qquad (3.20)$$

which is the differential equation for bottom-fibre deflections of a thick beam on an elastic foundation. It will be immediately seen that this equation is identical to the classical thin beam equation (3.3), the reason being

simply that when the usual condition of zero shear stress, given in Equ.(3.17), is applied to the top and bottom edges of a thick beam, the deflections of these edges become independent of shear stress. This means that the curvature due to shear force vanishes from the total curvature at these extreme edges, so that the bottom-fibre deflection depends on bending moments alone. The problem of a thick beam thus becomes more realistic due to Equ. (3.20), which has the advantage of being simpler to handle than previous more complicated equations.

3.4 Application of the beam theory in general to strata mechanics

The beam theory in general has been applied in the past to underground strata behaviour problems associated with pillar and seam loadings, and stability of mine openings, i.e. room and pillar mining. The reason is that this method of mining permits the use of such a method ofpre-failure analysis of the situation, while in longwall mining some sort of post-failure analysis is necessary after having understood the nature and extent of the goaf that is close by. Also the failure in the goaf is progressive as the longwall face moves, leaving some intact rock higher up and over the ribside, leaving a geometry which is largely unknown and also difficult to analyse.

The work of Tincelin and Sinou[31] has already been mentioned in the previous Sections, in connection with the thick beam theory. The thick beam equation (3.10) developed by them was subsequently used by Höfer and Menzel[35] for loading problems associated with rock salt pillars in thick rigid strata and they found by lateral deformation measurements carried out on pillars that Equ. (3.10) gave reasonable values of pillar load. In view

of the error pointed out in the derivation of this equation in 3.3, mention may be made that this Equ. (3.10) and the later developed Equ. (3.15)[43] are not significantly different for a uniform depth pressure, i.e. level single seams, as given in 3.3.2.

The thin beam theory has been applied in the past to obtain a comparative picture of loading on split pillars at the goaf edge during depillaring with caving, depending on the extent of splitting[37], also by Tincelin and Sinou in their work on pillar loads[31], by Adler[32] for the stability of a mine opening, as described earlier and by Salustowicz and Borecki[47, 48], for seam reactions and load on the stowed goaf.

Stephansson[36] used both the thin and thick beam theories in extensive investigations into the stability of a wide mine opening in horizontally bedded rock. He also used equations for deflection of multiple beams, simulating multilayered roofs and compared his results with experiments on plaster modelling in a centrifuge. When friction was used in his models between the seam and the roof, the results on the ribside did not agree completely with theory. This showed the approximation introduced due to the condition of zero shear stress on beam edges.

An application of the theory of bottom-fibre deflections has been given in (49) for estimating the stability of barrier pillars in a pyrite mine using the principle of strain energy.

The work on beams so far reviewed indicates that rock strata in most situations are to be treated as thick and it is also shown how the

theory of bottom-fibre deflections is somewhat more realistic than the other thick beam methods, though with inevitable approximations involved. This method has been used in the work described in subsequent Chapters on short face advancing with a centre pack and on floor heave analysis to obtain the loading on floors during retreating.

* * *

CHAPTER 4

Experimental work - elastic modulus of anhydrite and a pack strength formula

CHAPTER 4

Experimental work - Elastic modulus of anhydrite and a pack strength formula

4.1 Introduction

A roadside pack made of crushed natural anhydrite becomes increasingly stiffer with time because of the setting process and so, with face advance, develops increasing resistance to roof lowering. This property is peculiar to all setting packs as opposed to conventional packs like wood chocks or dirt packs. This fact has been taken into consideration in the next Chapter which deals with an elastic analysis of the short face advancing method using a centre pack of anhydrite. It was, therefore, necessary to determine the variation in the elastic modulus of anhydrite with setting time, especially since work on this aspect did not appear to be available.

All rocklike materials are subject to a fall in strength with an increase in the size of the specimen tested, because of the presence of macroscopic flaws. Pores, grain boundaries, cleat planes etc. fall under the category of flaws and initiate failure in a specimen under stress. The probability of failure under a particular stress value increases with the number of these flaws in the specimen or, in other words, there is a fall in strength with an increase in specimen volume. This is the weakest-link theory. Epstein[50] has given equations of strength considering several frequency distributions (Gaussian, skew, Weibull, rectangular) for the

strength of brittle materials. Grobelaar [51] has shown the applicability of this theory to several rock types and coal, when the frequency distribution is Gaussian or normal. Thus, according to the weakest-link theory, it could be visualised that anhydrite would reduce in strength with greater specimen size and a small specimen could lead to erroneous estimates of pack strength.

Also of interest with reference to anhydrite packs is the well-known effect of slenderness on the compressive strength of a specimen, slender specimens being weaker than flat ones. Since anhydrite packs could occur in various heights and widths, it was important that this influence be considered in estimating pack strength.

4.2 Experimental investigations

Crushed natural anhydrite was obtained from British Gypsum for the purpose of these experiments, in the size range of 0–6 mm with about 30% fines under 0.2 mm as per German standardisation[9]. A water-anhydrite ratio of 0.1 was used so that no tamping was necessary to produce a consistent specimen. The percentage accelerator used was 1% by weight of the anhydrite.

4.2.1 Influence of setting time on the elastic modulus of anhydrite

10-cm cubes of the anhydrite mix were cast into suitable wooden moulds. The moulds were gently hammered from the outside to settle the mix. No tamping was necessary. The setting period was varied from 1 day to 6 weeks as seen from Table 4.1. All specimens were prepared from the same bag of anhydrite.

TABLE 4.1

Variation of elastic modulus of anhydrite with setting time

Setting period, days	Elastic modulus, x 10^6/kN/m^2
1	1.73
3	3.20
7	4.92
14	6.50
28	7.53
42	8.15

TABLE 4.2

Influence of size and slenderness on compressive strength of anhydrite

Specimen cross-section, cm square	Specimen Height, cm	No. of specimens tested	Mean Strength kN/m^2	Standard Deviation, %
2.50	5.00	5	62,720	5.01
3.75	2.50	5	85,470	4.17
5.00	5.00	4	70,700	0.97
6.25	9.40	4	48,510	5.46
7.50	3.75	4	75,865	0.94
10.00	2.50	3	92,665	4.50
15.00	5.00	3	72,665	2.65

The prepared specimens, after the required setting period, were compressed uniaxially in a universal testing machine. Their deformation was measured simply by two dial gauges, one on either side of the specimen. Three replications were used for each setting period.

Fig. 4.1 to 4.6 show the stress-strain characteristics of anhydrite at the six setting periods. Each curve shows an initial non-linear deformation indicating closure of pores and squeezing of the cementitious matrix in the material. Then follows a fairly linear behaviour. The stress-strain curve is thus similar to that of sedimentary rocks. The tangent elastic modulus from the straight line part of the curve was determined for every replication graphically and a mean value was calculated for each setting time. The mean elastic moduli are given in Table 4.1 and their values against setting time are shown plotted in Fig.4.7. A best fit to the regression was obtained to give the following relation for the variation of the elastic modulus of anhydrite E with setting time t (in days):

$$E = \frac{7{\cdot}89\,t}{3{\cdot}65 + t} \times 10^6 \ \text{kN/m}^2 \qquad (4.1)$$

This equation is asymtotic to the plateau value of 7.89×10^6 kN/m^2 at $t = \infty$. The coefficent of correlation for this regression equation was 0.995 at the significance level of 0.1% and thus shows a high degree of correlation.

FIG.4.1 - STRESS-STRAIN CURVE OF ANHYDRITE AFTER 1 DAY (24 HOURS)

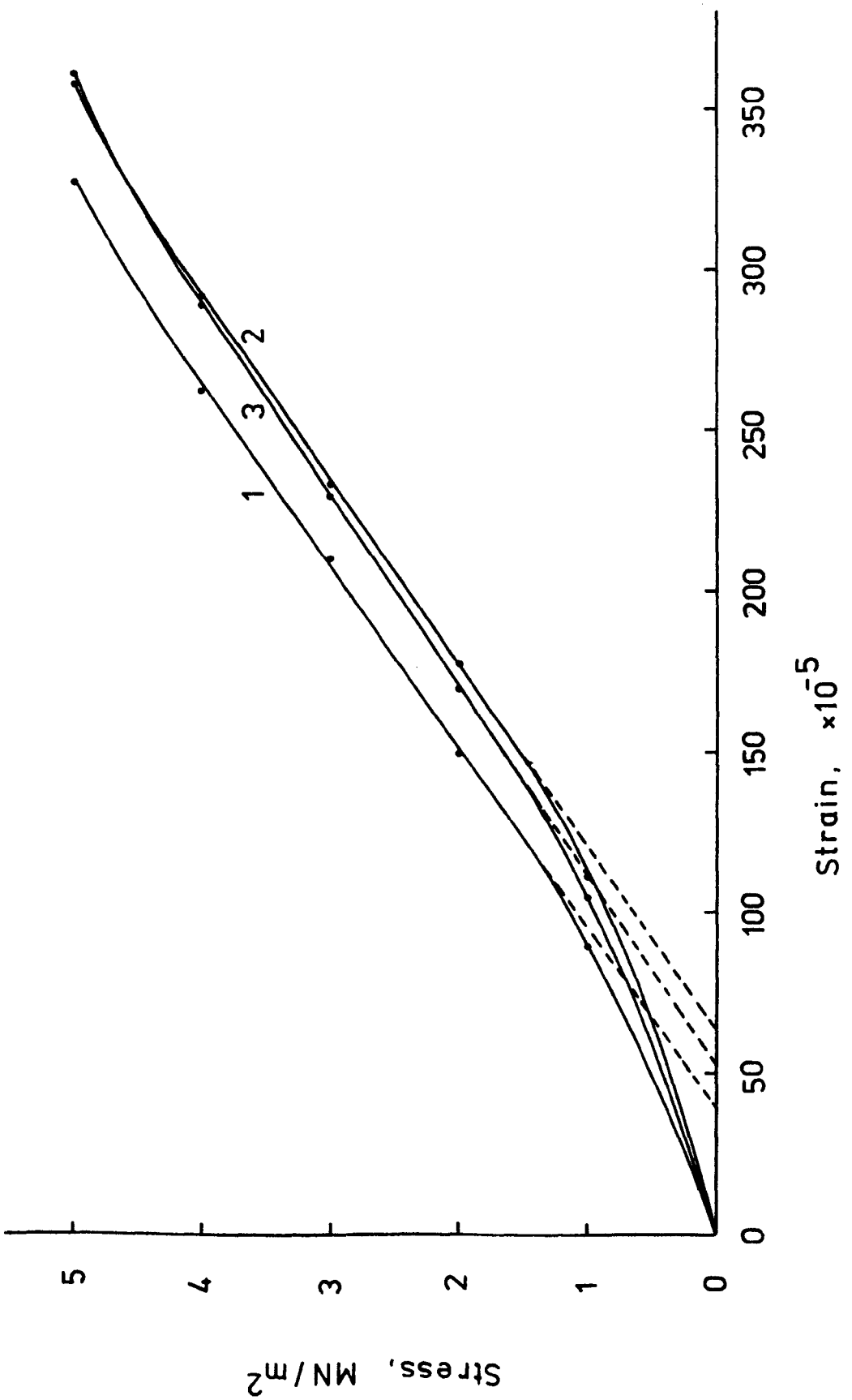

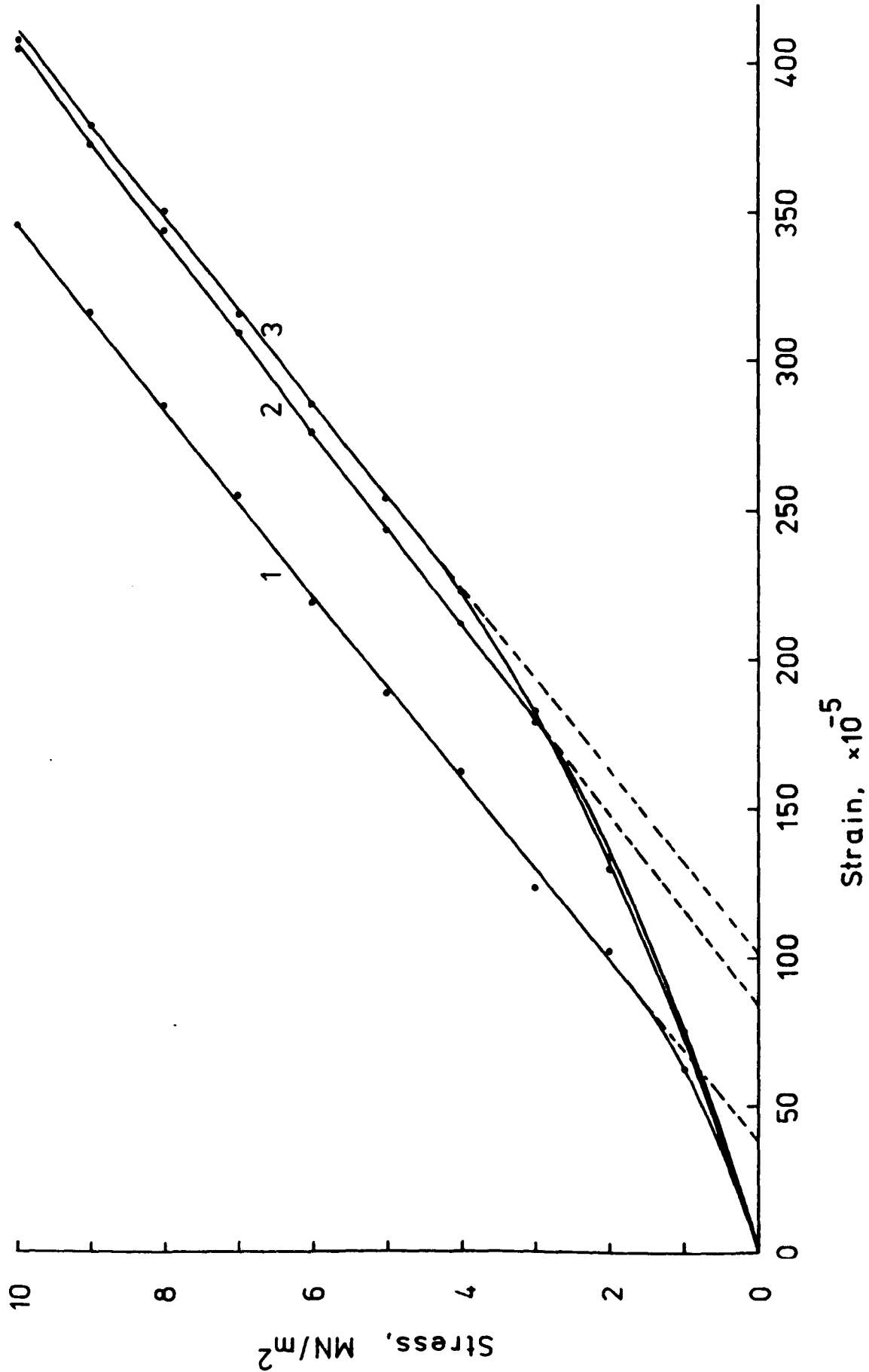

FIG.4.2-STRESS-STRAIN CURVE OF ANHYDRITE AFTER 3 DAYS (72 HOURS)

FIG.4.3 - STRESS-STRAIN CURVE OF ANHYDRITE AFTER 1 WEEK

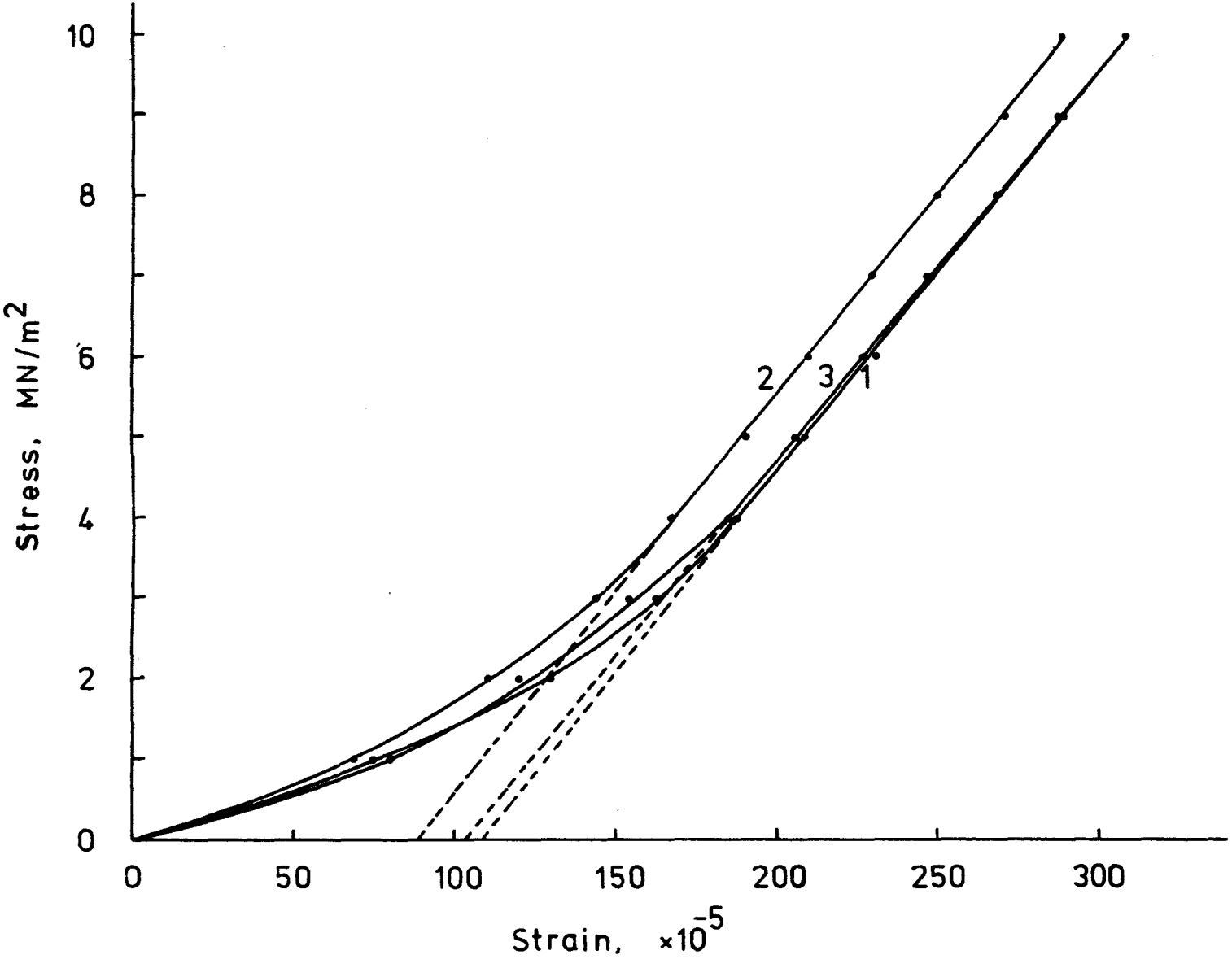

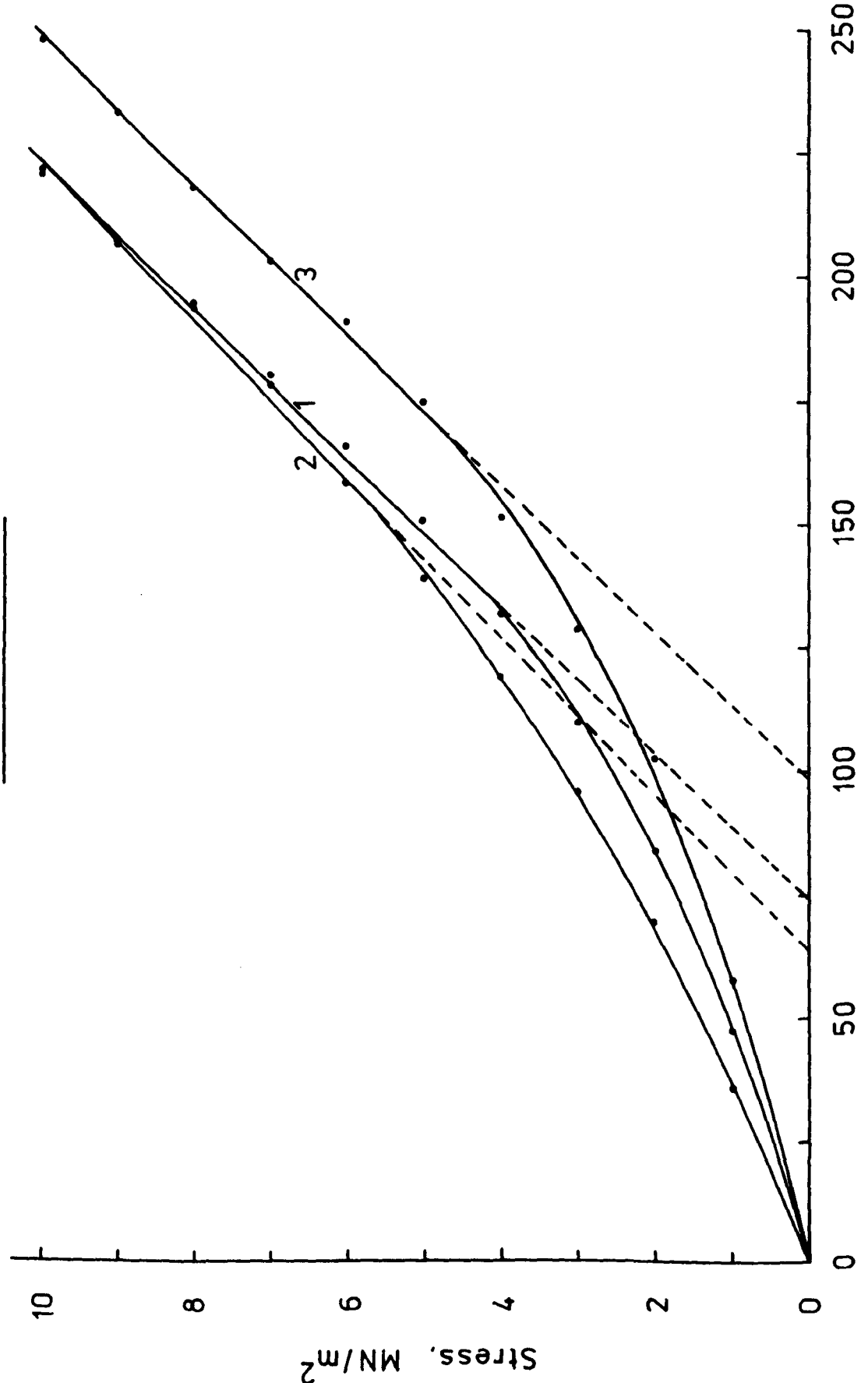

FIG.4.4 - STRESS-STRAIN CURVE OF ANHYDRITE AFTER 2 WEEKS

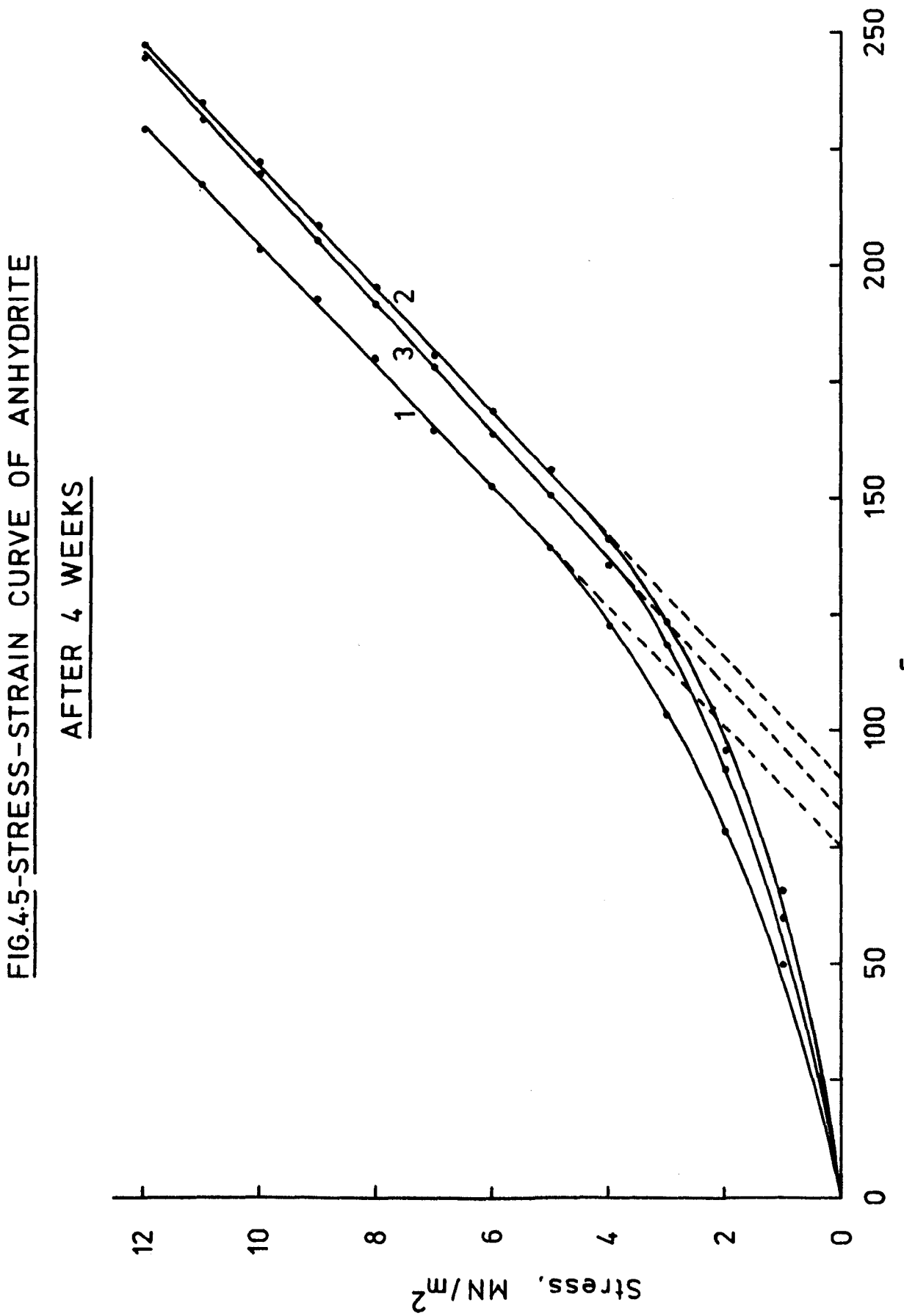

FIG.4.5-STRESS-STRAIN CURVE OF ANHYDRITE

AFTER 4 WEEKS

FIG.4.6-STRESS-STRAIN CURVE OF ANHYDRITE AFTER 6 WEEKS

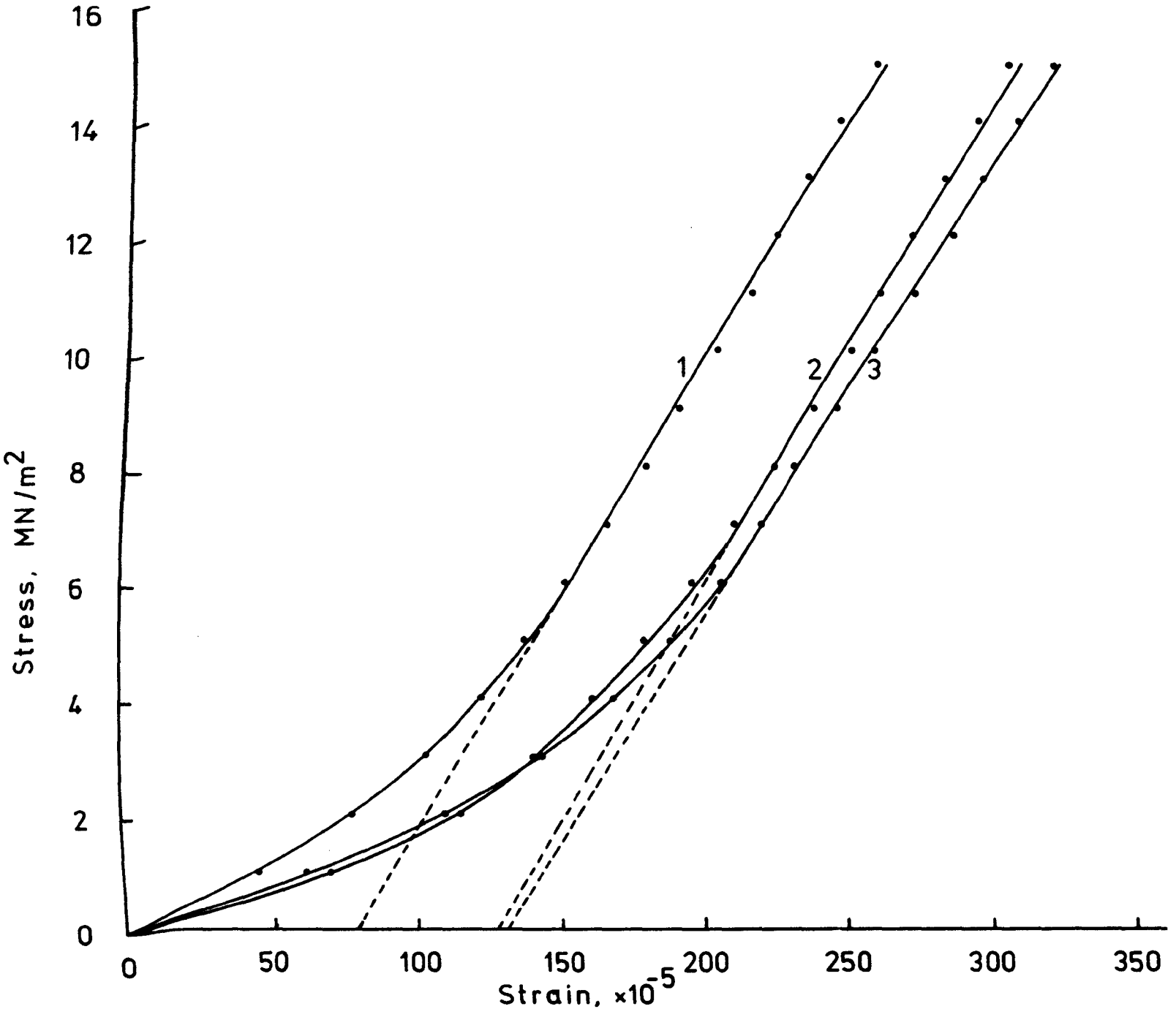

FIG.4·7-VARIATION IN VALUE OF MODULUS OF ELASTICITY OF ANHYDRITE WITH SETTING TIME

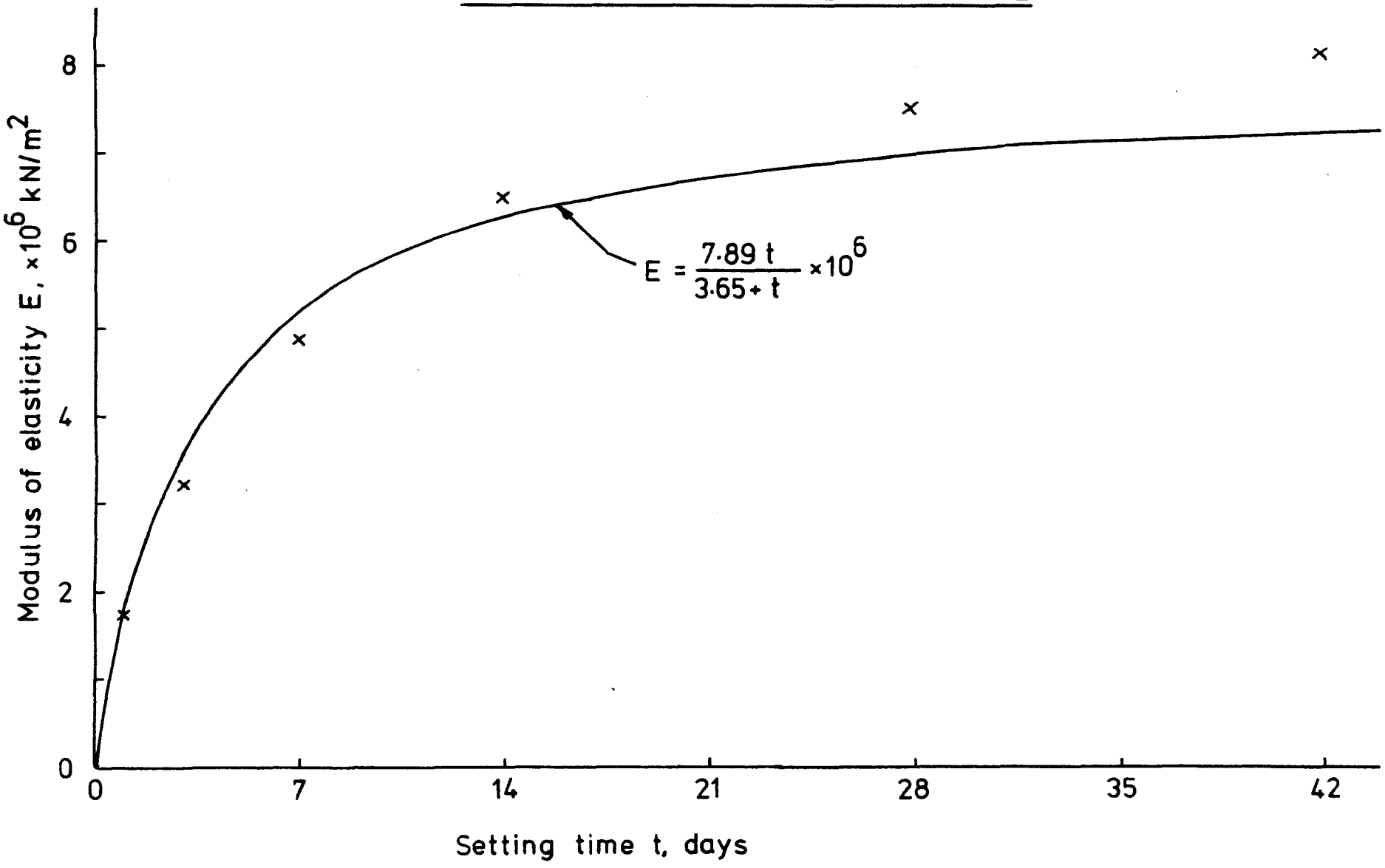

4.2.2 Effect of size and height of specimen on the crushing strength of anhydrite

In order to obtain a relation between crushing strength, size and slenderness it was necessary to carry out tests on specimens of varying sizes and width-height ratios. This was a three-variable experiment and a statistical design gave rise to a total of 28 tests having 7 sizes, from 2.5 cm to 15.0 cm. square, and width-height ratios from 0.5 to 4.0. For consistency and careful blocking, a 30-cm cube of anhydrite was cast and all 28 specimens were prepared from this single cube by cutting and grinding after 7 weeks of setting. A view of these specimens is given in Plate 4.1.

All specimens showed a docile failure under crushing. The dimensions of these specimens and the corresponding crushing strength values are given in Table 4.2. It may be noticed that the number of specimens tested (replications) for each size reduces from 5 to 3 as the specimen cross-section increases. This is in keeping with the corollary of the weakest-link theory that the percentage standard deviation falls with increasing specimen volume, which is found to be reasonably true in practice[50, 52]. A three-variable regression analysis gave the following equation for the strength of anhydrite:

$$S = 22025 \frac{w^{0.073}}{h^{0.439}} \quad kN/m^2 \qquad (4.2)$$

where S is the crushing strength of an anhydrite specimen of width w and height h m. The correlation coefficient was 0.99 at 0.1% significance level.

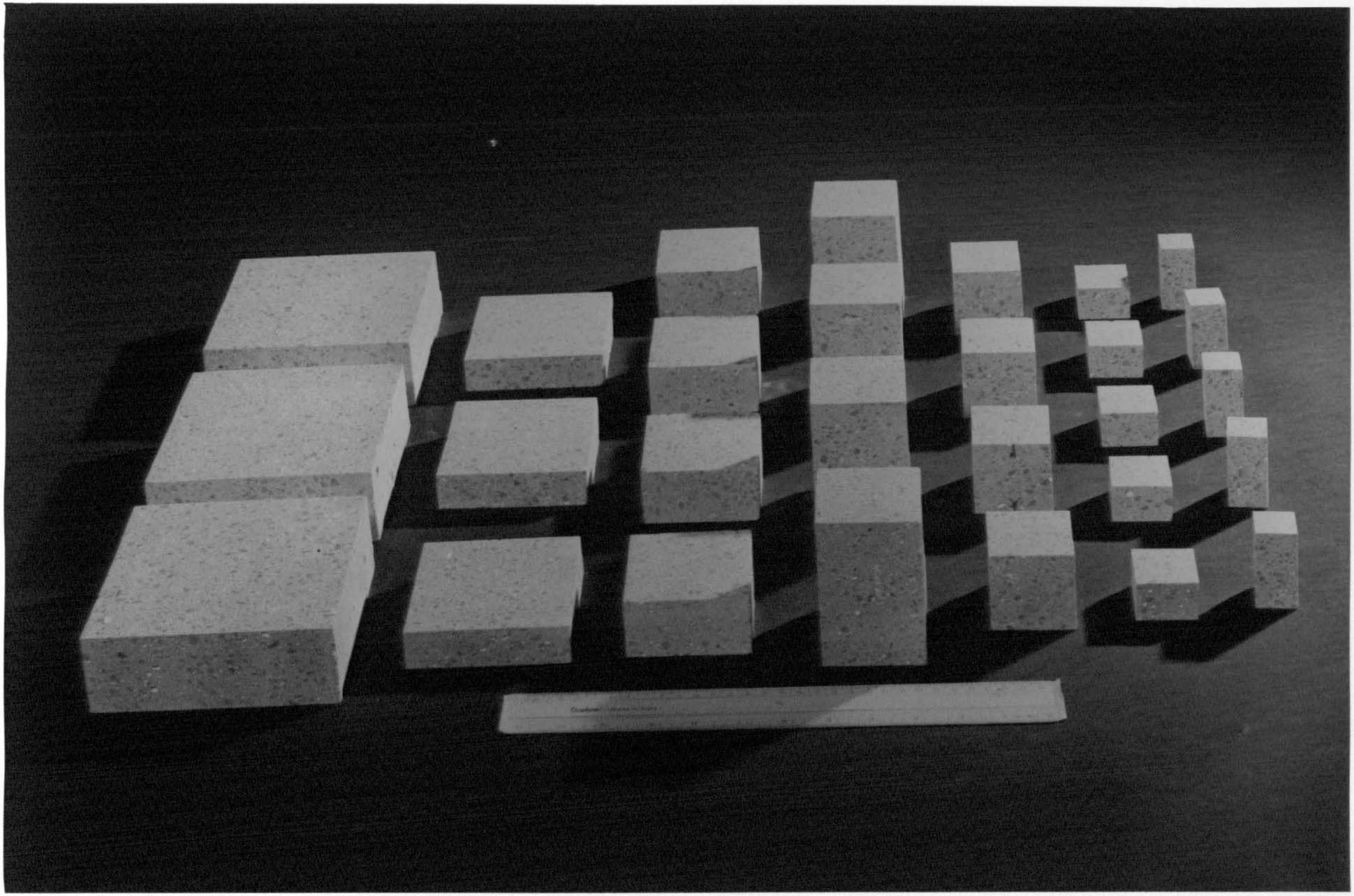

PLATE 4.1

Since Equ. (4.2) is in three variables it cannot be shown plotted on a graph. A graphic representation of only the influence of size on strength can be made according to the following reduced equation for cubes obtained from Eq. (4.2):

$$S = 22025\ w^{-0.366}$$

This gives the fall in strength with size of cubes of anhydrite, as shown in Fig. 4.8. It can be readily seen that the fall is significant. The strength of a 1-m cube is obtained as 22025 kN/m^2 so that the reduction in strength from, say, a 10-cm cube to a 1- m cube is more than 50%. Considering the usual order of pack size - a couple of metres - the fall in strength from a laboratory small sample is obvious.

Equ. (4.2) has the same general form as that for the strength of square coal pillars given by many investigators[52-56].

4.3 Pack strength formula

Equ. (4.2) thus affords a means of estimating the strength of an anhydrite pack of given dimensions. To use it in practice as a pack strength formula, however, it has to be modified to the form

$$S = 22025\ \frac{w^{0.073}}{h^{0.439}}\ F_1 \cdot F_2 \cdot F_3 \qquad (4.3)$$

where F_1 is a correction factor to incorporate the difference in the laboratory and in-situ strengths of anhydrite and is simply the ratio of the two. F_2 is a second factor to be used if the pack is less mature than

FIG.4·8-INFLUENCE OF SPECIMEN SIZE ON STRENGTH OF ANHYDRITE

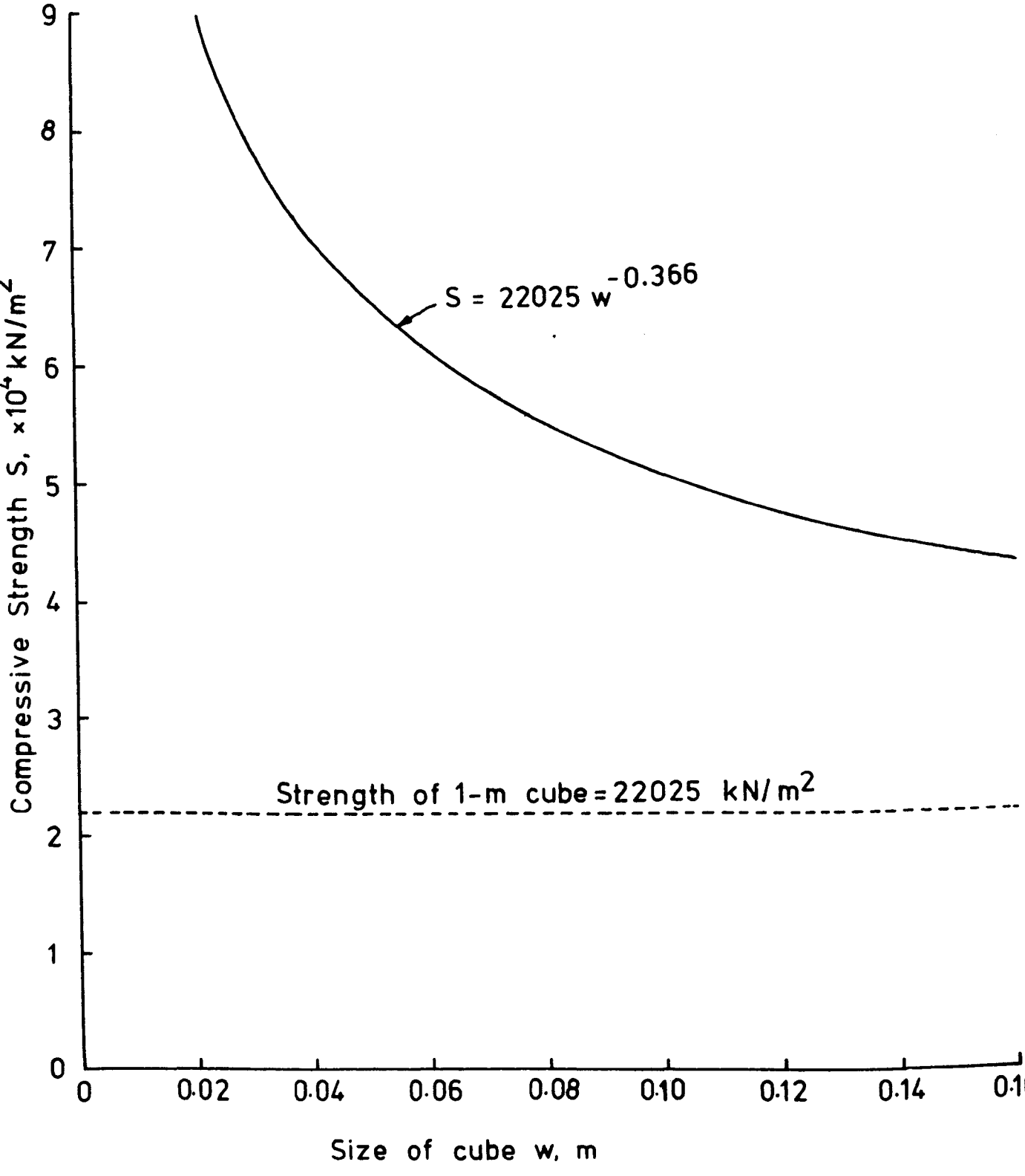

7 weeks, which is the setting period used for these tests. The correction factor F_3 is meant to include the strength increase due to biaxial effects underground.

F_1 is being determined in the laboratory by drawing core samples from Easington Colliery[57]. Tests so far have not been sufficient but there is an indication that F_1 may lie between 0.5 and 1.0 approximately.

The likelihood of a peak pressure on the pack after some face advance has been indicated by several workers (see Chapter 2). There is a good probability that the pack may not have set fully at this time. Knowing the distance at which the peak occurs and the rate of face advance, it is simple enough to estimate the strength of anhydrite at the time the peak occurs from the following equation[14]

$$S = \frac{39226\ t}{2.84 + t} \quad kN/m^2 \qquad (4.4)$$

The correction factor F_2 is then obtained as the ratio of the strength so calculated to the final strength (i.e. at 7 weeks), and is always less than1.0.

Past experience has indicated that there is a significant increase in the strength of rectangular specimens under compression, when the longer lateral dimension is increased[58]. In fact, the rise in strength is indefinite, showing that a specimen with infinite length would be virtually indestructible, if it is not too slender laterally. Thus a well consolidated long pack can be expected to be very strong, but experience with

anhydrite packs at Easington has shown that complete consolidation is not possible. Anhydrite remains fluffy and uncrystallised in pockets inside the pack, so that the lateral restraint along its length is only partly achieved. Hence the factor F_3 for biaxial restraint should, it is felt, be taken conservatively as 1.0. Equ. (4.3) then becomes

$$S = 22025 \frac{w^{0.073}}{h^{0.439}} F_1 \cdot F_2 \qquad (4.5)$$

It may be of interest to estimate the safety factor of the pack at Easington from Equ. (4.5). Taking the observed peak load of 5300 kN/m^2 (Fig.2.7(b)), F_1 = 0.75, w = h = 1.5 m, the safety factor of the pack can be estimated, if F_2 is obtained. The time of peak load can be taken as 14 days. From Equ. (4.4) we then get the strength value at this time and the ultimate value, and F_2, their ratio, is 0.83. Then using Equ. (4.5) the safety factor is found to be 2.28.

4.4 Conclusion

1. Anhydrite is found to exhibit a change in its modulus of elasticity with setting time, as given by Equ. (4.1), the plateau value being 7.89 x 10^6 kN/m^2 for the size range of the particles mentioned. This value is nearly reached after about 6 weeks. This equation will not be valid for other size ranges of particles.

2. The strength of anhydrite is found to be influenced significantly by the size and height of the specimen. The strength of a pack is, therefore, very much overestimated if

judged from only small samples tested in the laboratory. The fall in strength from a usual laboratory specimen to a large one comparable in size with a pack can be 50% or more.

3. Equ. (4.5), while accounting for the influence of size and height on strength, can be used for pack strength estimation.

* * *

CHAPTER 5

Short face advancing with a centre pack of anhydrite - theoretical estimation of pack loading with face advance and roof bending stresses

CHAPTER 5

Short face advancing with a centre pack of anhydrite - Theoretical estimation of pack loading with face advance and roof bending stresses

5.1 Introduction

Having considered in Chapter 3 the working of the method of short face advancing with centre pack support, the situation will be analysed elastically to estimate

(a) the load on the centre pack with face advance,

(b) the influence of the rate of advance on pack loading,

(c) bending moments and shear forces in the nether roof and the maximum tensile stress, and

(d) the abutment pressure on the ribside.

Then referring to Fig. 2.8 the short face is seen to commence from a trunk roadway. It has to be advanced to create a certain span before the first section of the pack can be erected. Pack placement is then subsequently established for each face advance, leaving sufficient working space at the face and also leaving two rectangular roadways on either side. The face thus advances stage by stage and brings the roof down further in each stage. The situation must, therefore, be analysed for each face movement.

The advance of the wide heading with a centre pack of anhydrite is shown along a longitudinal section in Fig. 5.1. Stage (1) is seen to consist

FIG.5.1-SCHEME SHOWING ROOF DEFLECTIONS ETC. ALONG THE SECTION OF HEADING

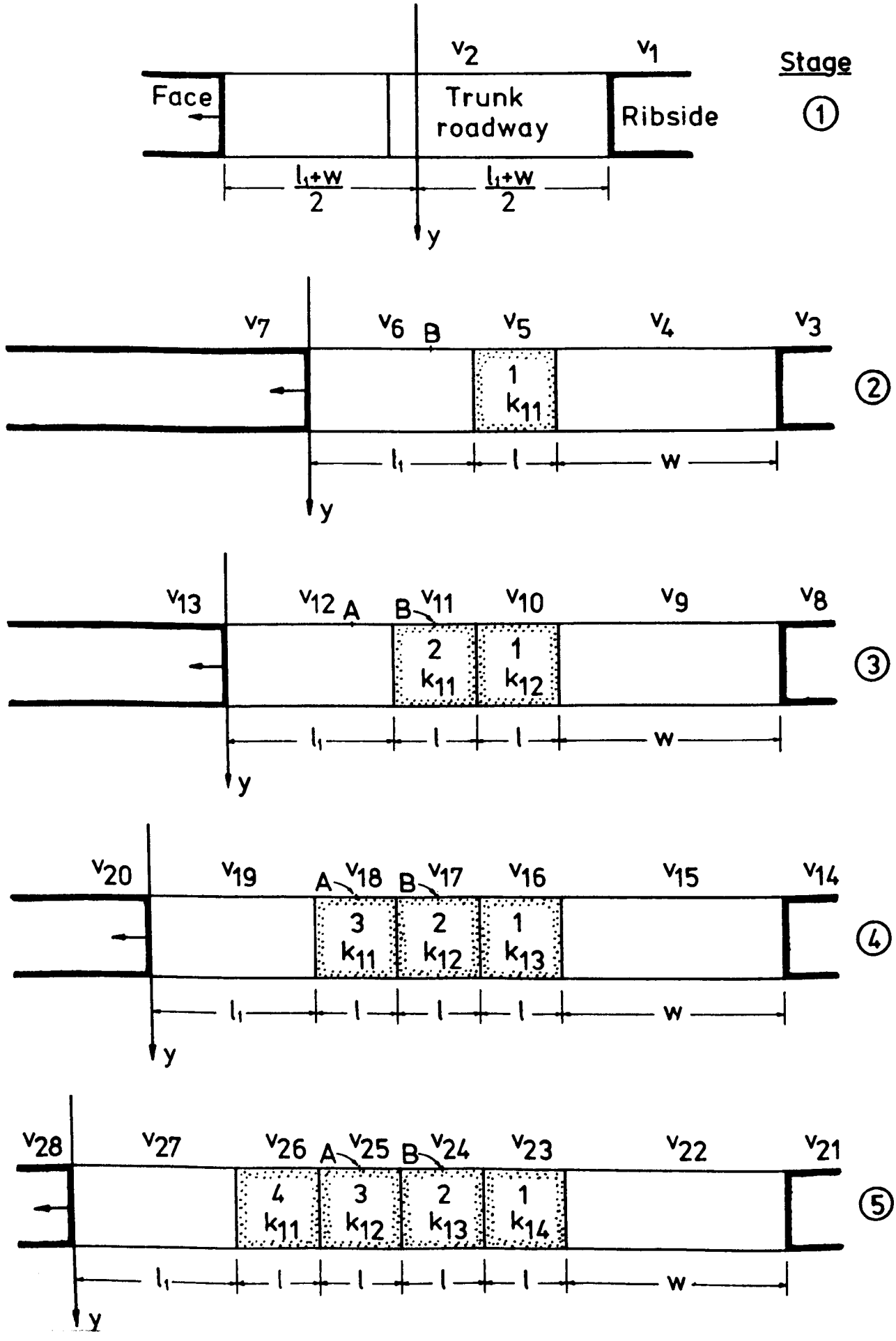

of the maximum pack-free advance of the short face and causes a certain amount of roof deflection. The first pack section is now erected and the face advanced further. This is stage (2) in which the roof deflects over the pack, causing pack compression. In stage (3) another pack section is erected adjacent to the first and the face is again advanced. This causes the roof to deflect over both pack sections.

It must here be remembered that during the setting process by crystallisation, anhydrite goes on changing its modulus of elasticity, and hence compressibility, with time, so that no two pack sections erected one after the other have the same compressibility. As seen in Chapter 4, the change in the modulus of elasticity with setting time is given by (see Ch. 4, Sec. 4 2.1)

$$E = \frac{7{\cdot}89\,t}{3{\cdot}65 + t} \times 10^6 \quad kN/m^2 \tag{5.1}$$

and the pack foundation modulus k_1, which defines its stiffness, is given by

$$k_1 = \frac{E}{H(1-\mu^2)} \tag{5.2}$$

where H is the pack height (see Ch. 3, Sec. 3.2). Then the foundation modulus of the first pack section is not the same as that of the second section at any stage of face advance under consideration. This will be true for any two adjacent pack sections.

Considering the stages of face advance once again, in stage (2) roof deflections over the pack occur due to face advance when the pack has a certain

instantaneous foundation modulus, say k_{11}, depending on the rate of advance. k_{11} can be estimated from Equ. (5.1) and (5.2), knowing the time required for face advancement since erection of the first pack section. In stage (3) another pack section is placed and the face advanced, causing further roof deflection over the first section, its foundation modulus having, in the meantime, increased to another value k_{12}, $k_{12} > k_{11}$. The second pack section erected in this stage, however, undergoes compression with its modulus being k_{11}.

This goes on as the short face advances, any one pack section achieving successively higher moduli, k_{11}, k_{12}, k_{13}, etc. with each advance. Thus, at any stage of advancement, each pack section is stiffer than the one succeeding it and softer than the one preceding it. In other words, the foundation modulus of a pack section is in a higher phase, the farther it is from the short face. This shows how an anhydrite pack becomes increasingly stiffer and hence more resistant to roof convergence as the face moves away.

5.2 An elastic analysis to obtain pack load acceptance, etc. - Longitudinal considerations

Presented here is an elastic solution in plane strain along the heading axis stage by stage for obtaining roof deflections. When the heading face advances by a distance greater than half the heading width, plane strain consideration along the heading axis can hardly be valid. The error due to this consideration will be minimised by (a) first considering that the heading is infinitely wide and obtaining the deflections of the roof along the heading axis (which will be rigorous enough) and then by (b) reducing the width of the

heading to a finite practical value using what can be termed as an equivalent loading method. This method will be explained as the derivation proceeds and its validity and limitations will be shown at the end.

The mathematical derivation will then consist of two main parts, longitudinal and lateral considerations.

A glance at Fig. 2.8 of Chapter 2 and Fig. 5.1 indicates the complicated nature of the problem. Not only is the problem really three-dimensional, but also has to be solved for each individual face advance until a sufficient number of stages to obtain the pack load acceptance characteristic. It was felt that numerical methods of stress analysis like the finite element method[59] would be somewhat cumbersome to use in the present situation. Also the later technique of face elements[60] would be equally unwieldy, especially since it was originally devised for single-material bodies under stress and since it loses its superiority over the former when several materials comprise a body. As has been explained, each pack section would have different properties which, in turn, would differ from those of the ribside and of the roof.

Analytically, a solution to the problem does not exist if we consider it three-dimensionally, treating the roof like a plate. In fact, very few analytical solutions exist in the theory of plates, especially on elastic support[61].

Due to the above considerations, it was decided to use the theory of beams and later try to minimise the errors due to two-dimensional considerations, primarily in the regions of interest, by devising a suitable method for lateral

considerations, giving an approximate solution. The particular theory of beams that has been employed in the derivation is that of the bottom-fibre (or extreme-fibre) deflections of a beam on elastic support[46], as explained in Chapter 3 (see Sec. 3.3.3). Pack load and ribside abutment loadings will be obtained once the nether roof deflections are known,as will be shown in the derivation.

5.2.1 The mechanical model for roof strata

When an opening is made in a stratified rock mass, experience has shown the formation of bed separation cavities between layers of rock. These cavities form up to a certain height in the roof of the opening and seldom beyond a height equal to the width of the opening. Any mine support erected in the opening has then to take only the weight thrown on it due to the deflection of this separated rock, the main rock mass being self-supporting (because of its rigidity) across the abutments which comprise the ribside.

The probable configurations resulting from cavity formation in the nether roof are shown in Fig. 5.2. With a single kind of stratified rock up to a considerable height in the immediate roof, there is a good probability that a single cavity develops, instead of multiple cavities, which travels upward as the opening is widened. Its height from the bottom of the roof is generally less than the width of the opening, as seen from equivalent material model studies[62]. Configuration (2) shown in Fig. 5.2 is thus more probable if a single kind of stratified rock exists in the roof below the limit of cavity formation (i.e. at least up to a height equal to the

FIG.5.2 - PROBABLE CONFIGURATIONS FOR BED SEPARATION IN THE NETHER ROOF

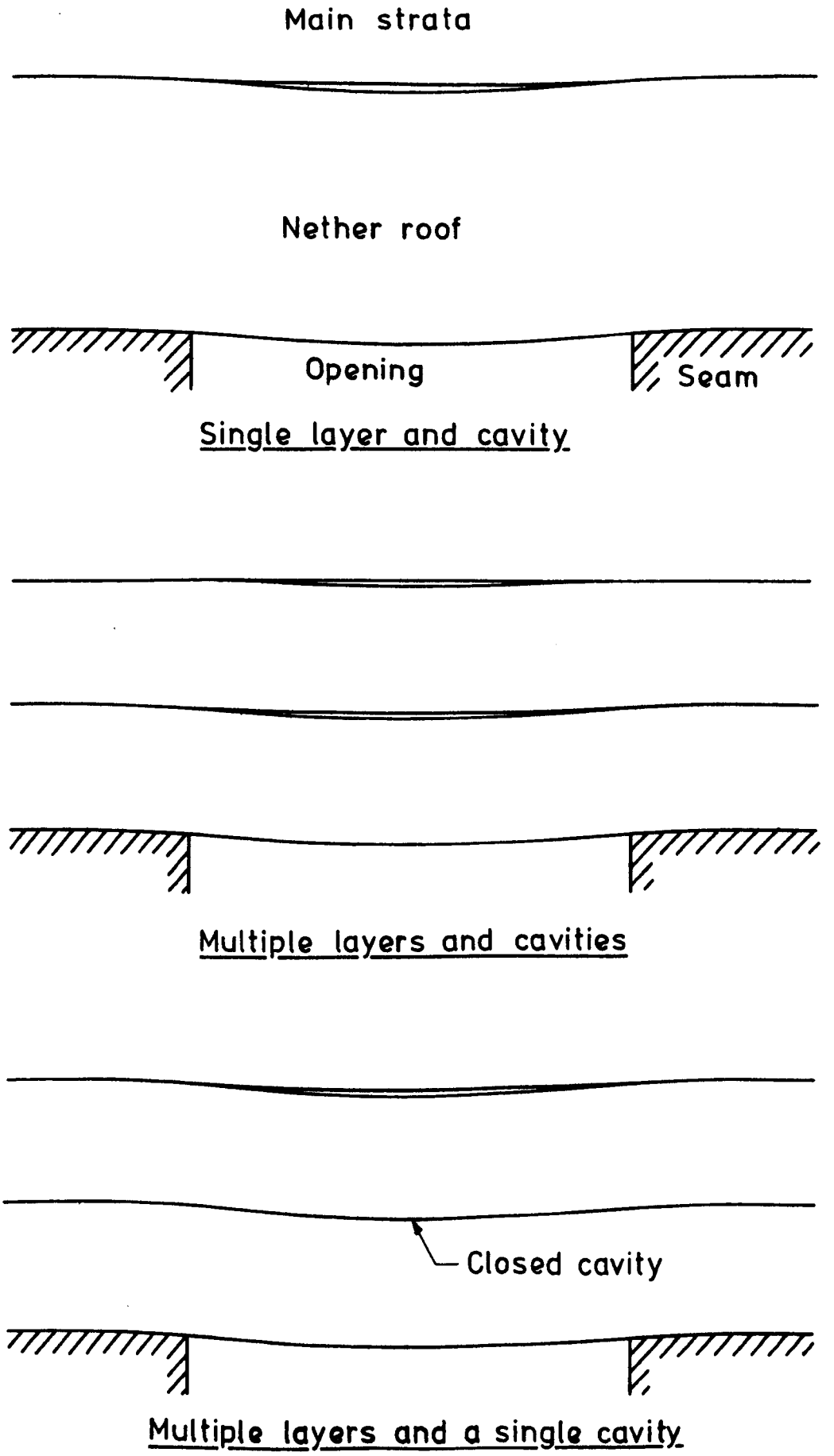

width of the opening). With a competent massive rock, it is also possible that no appreciable bed separation may occur before failure of the roof.

Since it was intended to apply this analysis to the High Main seam (E) at Dawdon Colliery, a borehole section of the nether strata from this mine is given in Fig. 5.3[63]. The mudstone in the immediate roof has been described as a medium-strength rock 10 m or more in thickness.

With these considerations the mechanical model shown in Fig. 5.4 has been chosen for stage (1). This model assumes the existence of a single separation cavity in the roof, the separated nether rock consisting of either (a) a thick composite beam of several layers, or (b) several layers, one above the other, with cohesion broken between them due to extraction.

The main rock mass is intact and self-supporting.

5.2.2 Assumptions used in the analysis

Besides the assumptions (given later) made for the numerical analysis of this method considering conditions at Dawdon Colliery, the following were used in the analytical part. Some of these assumptions refer to the thick beam theory of extreme fibre deflections.

(a) The horizontal stress σ_x is assumed to vary linearly through the depth of a beam. This is equivalent to assuming that the shear stress τ_{xy} varies parabolically.

FIG.5·3-TYPICAL SECTION OF HIGH MAIN SEAM (E) AT DAWDON COLLIERY

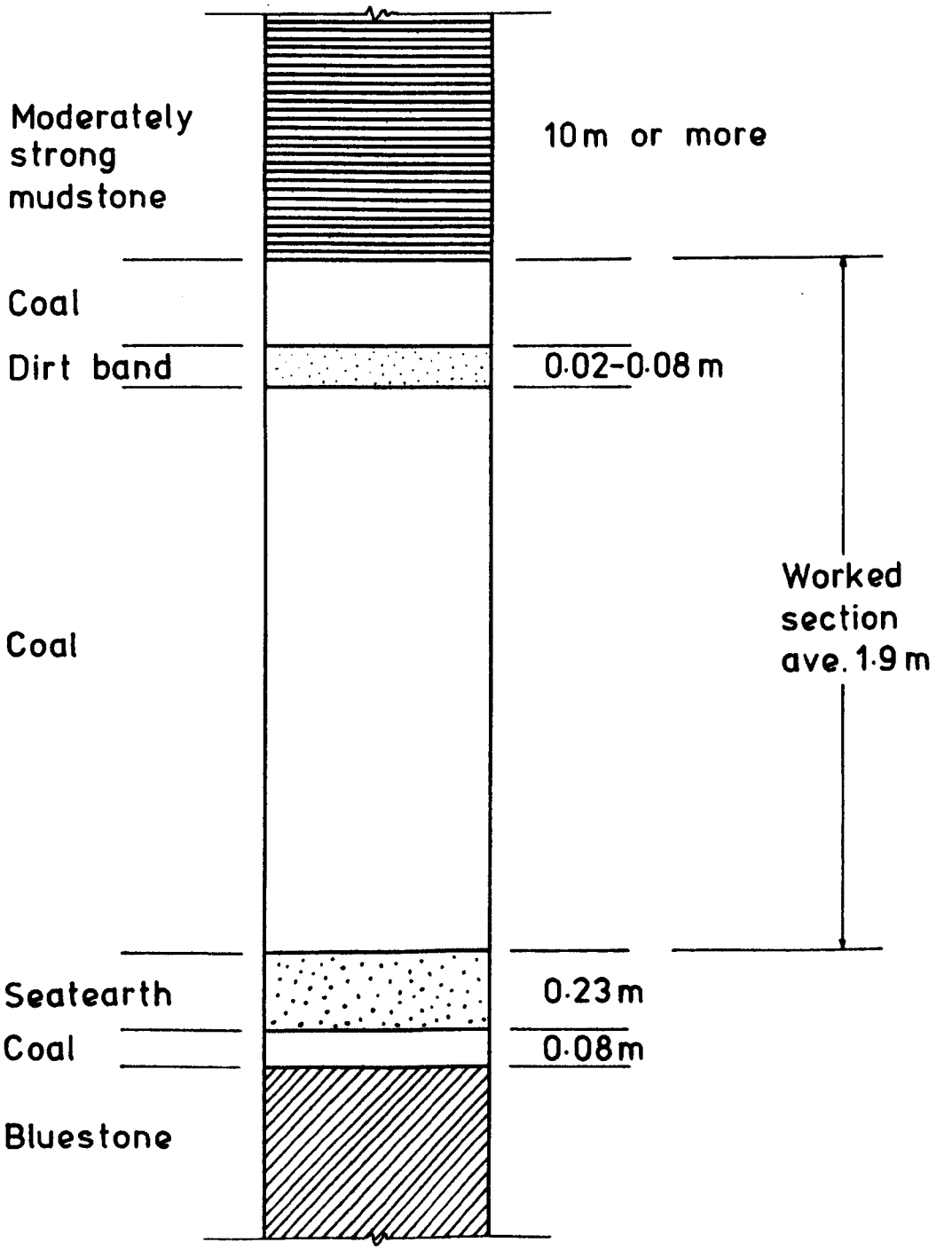

FIG.5.4-MECHANICAL MODEL FOR STAGE (1)
-SINGLE-BEAM NETHER ROOF

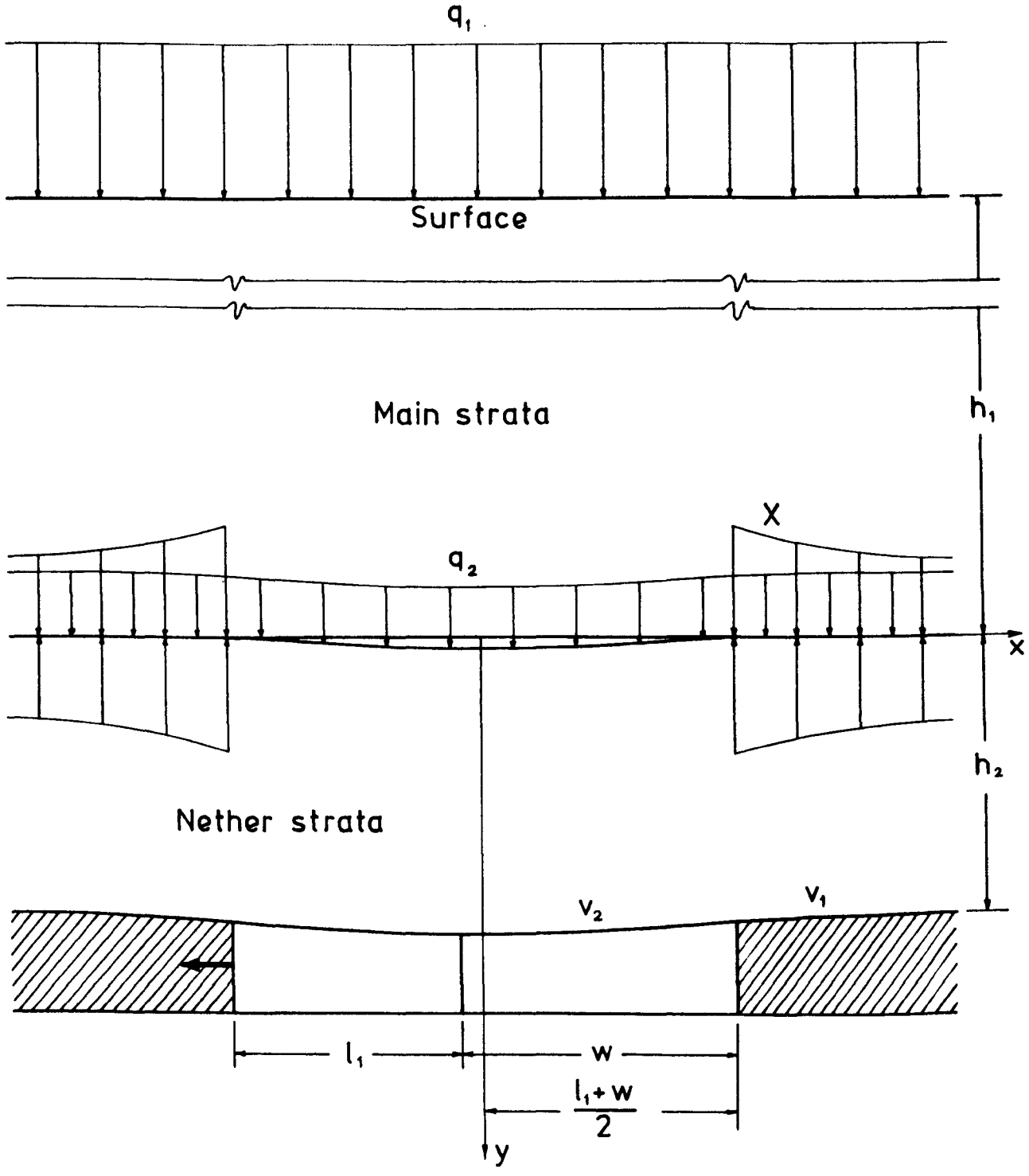

(b) There is no friction or cohesion between two adjacent beams or between a beam and its elastic foundation, i.e. the shear stress τ_{xy}, at contact planes is zero.

(c) The weight of a beam can be taken as an externally applied uniform loading on the top edge of a beam in addition to reactional normal stresses between beams, if any.

(d) The associated pack sections, rock and coal are assumed to behave linearly and isotropically with stress.

(e) Every pack section in any stage of advance is assumed to be erected with complete contact with the roof.

(f) Coal ribs and strata are theoretically infinite on either side of the short-face heading so that the roof becomes an infinite thick beam on elastic support. The analysis, therefore, considers that the lateral constraining stress σ_x is $\frac{\mu}{1-\mu}$ times the vertical stress σ_y at an infinite distance from the heading, μ being Poisson's ratio.

5.2.3 Beam analysis for the nether roof

The analysis has been carried out stage by stage from the initial stage (1) up to stage (7). From Fig.5.4 it is seen that the nether roof has separated from the main rock mass above, forming a single cavity. We then have a configuration which consists of a pack-free opening of width (ℓ_1 + w), the face having advanced to a distance ℓ_1, the trunk roadway

width being w. The nether roof is like a thick beam without support over the opening and supported elastically over the coal ribside. The main strata rest on the nether beam, sandwiching it between itself and the ribside, giving a two beam problem.

The various notations used in stage (1), shown in Fig. 5.4, have the following meanings:

h_1 = main strata thickness,

h_2 = nether strata thickness,

q_1 = uniform loading on the main strata beam representing its own weight,

q_2 = uniform loading on the nether roof beam due to its own weight,

$q_1 + q_2$ = total depth pressure at the working level,

X = reactions set up at the contact plane between the two beams over the ribside,

v_1, v_2 = deflections of the bottom fibre of the nether roof over the ribside and opening regions respectively.

Stage (1) has been analysed for two kinds of nether roof beams:

(a) as a thick single beam, cohesion between beds unbroken,

(b) as consisting of several beams of equal thickness, cohesion between them broken due to working.

The main strata have throughout been considered as a single thick composite beam.

The configuration is symmetrical about the y-axis in stage (1), the position of the rectangular coordinate axes being as indicated in Fig. 5.4. The y-axis is taken downward positive.

5.2.3.1 Stage (1): nether roof as a single thick beam

The situation in stage (1) will be analysed in parts for the main and nether strata beams over the ribside and over the opening.

Main strata: $\frac{\ell_1 + w}{2} < x < \infty$

In accordance with the theory of extreme fibre deflections, the horizontal stress σ_x can be assumed to vary linearly through the depth of the main strata beam in the coordinate system of Fig. 5.4 as

$$\sigma_x = F(x)\left(y + \frac{h_1}{2}\right) \tag{5.3}$$

where F(x) is an as yet unknown function of x only. Substituting Equ.(5.3) in the first of the equilibrium equations in plane strain:

$$\frac{\partial \sigma_x}{\partial x} + \frac{\partial \tau_{xy}}{\partial y} = 0$$

$$\frac{\partial \sigma_y}{\partial y} + \frac{\partial \tau_{xy}}{\partial x} = 0 \qquad (5.4)$$

we get the shear stress τ_{xy} as

$$\tau_{xy} = -\frac{1}{2} F'(x)\left(y^2 + h_1 y\right) + A_1(x)$$

where $A_1(x)$ is an arbitrary function of x only.

Applying the conditions

$$\left(\tau_{xy}\right)_{y=0} = \left(\tau_{xy}\right)_{y=h_1} = 0$$

on the upper and lower edges of the main strata, we find

$$A_1(x) = 0$$

and $$\tau_{xy} = -\frac{1}{2} F'(x)\left(y^2 + h_1 y\right) \qquad (5.5)$$

From this expression for τ_{xy} and the second of the equilibrium equations (5.4)

$$\sigma_y = \frac{1}{2} F''(x)\left(\frac{y^3}{3} + \frac{h_1 y^2}{2}\right) + A_2(x) \qquad (5.6)$$

From Fig. (5.4) the conditions in terms of the vertical normal stress σ_y on the two edges of the main strata are seen to be

$$(\sigma_y)_{y=0} = -X \quad , \quad (\sigma_y)_{y=-h_1} = -q_1$$

both X and q_1 being taken negative because they are compressive.

These conditions, when applied to (5.6) give

$$A_2(x) = 0 \quad , \quad F''(x) = -(q_1 - X)\frac{12}{h_1^3} \tag{5.7}$$

so that $$\sigma_y = -X - \frac{6}{h_1^3}(q_1 - X)\left(\frac{y^3}{3} + \frac{h_1 y^2}{2}\right) \tag{5.8}$$

Having determined $F''(x)$ in Equ. (5.7) the following are obtained by direct integration

$$F'(x) = -\left(q_1 x - X_I\right)\frac{12}{h_1^3} + A$$

$$F(x) = -\left(q_1\frac{x^2}{2} - X_{II}\right)\frac{12}{h_1^3} + Ax + B$$

where A = o to satisfy τ_{xy} = o on the edges and B depends on the beam end conditions.

The expressions for the three stresses (5.3), (5.5) and (5.8) become

$$\left.\begin{aligned} \sigma_x &= -\frac{12}{h_1^3}\left(q_1\frac{x^2}{2} - X_{II}\right)\left(y + \frac{h_1}{2}\right) + B\left(y + \frac{h_1}{2}\right) \\ \sigma_y &= -X - \frac{6}{h_1^3}(q_1 - X)\left(\frac{y^3}{3} + \frac{h_1 y^2}{2}\right) \end{aligned}\right\} \tag{5.9}$$

$$\tau_{xy} = \frac{6}{h_1^3}\left(q_1 x - X_I\right)\left(y^2 + h_1 y\right) \quad \Big]$$

The loading reactions X between the main and nether strata are still unknown but can be determined later from displacements taking place at the contact plane y = o.

The displacement relations in plane strain are

$$\left.\begin{aligned} \frac{\partial u}{\partial x} &= \frac{1}{E_1}\left[\left(1-\mu_1^2\right)\sigma_x - \mu_1\left(1+\mu_1\right)\sigma_y\right] \\ \frac{\partial v}{\partial y} &= \frac{1}{E_1}\left[\left(1-\mu_1^2\right)\sigma_y - \mu_1\left(1+\mu_1\right)\sigma_x\right] \\ \frac{\partial u}{\partial y} + \frac{\partial v}{\partial x} &= \frac{2\left(1+\mu_1\right)}{E_1}\tau_{xy} \end{aligned}\right\} \qquad (5.10)$$

E_1 and μ_1 being the elastic constants of the main rock strata. The second equation in (5.10) does not agree with the initial assumption of linear variation of σ_x with y as in Equ. (5.3)[46]. Also, only the first and third equations in (5.10) are sufficient to obtain an expression for the vertical displacements v . Then making use of only these two displacement relations and the stress equations (5.9), the horizontal and vertical displacements u and v can be written down as

$$u = -\frac{1-\mu_1^2}{E_1}\cdot\frac{12}{h_1^3}\left(q_1\frac{x^3}{6} - X_{III}\right)\left(y+\frac{h_1}{2}\right) + \frac{\mu_1(1+\mu_1)}{E_1}X_I + Bx\left(y+\frac{h_1}{2}\right)$$

$$+\frac{\mu_1(1+\mu_1)}{E_1}\cdot\frac{6}{h_1^3}\left(q_1 x - X_I\right)\left(\frac{y^3}{3}+\frac{h_1 y^2}{2}\right) + B_1(y)$$

$$v = \frac{1-\mu_1^2}{E_1}\cdot\frac{12}{h_1^3}\left(q_1\frac{x^4}{24} - X_{IV}\right) - B\frac{x^2}{2}$$

$$-\frac{\mu_1(1+\mu_1)}{E_1}\cdot\frac{6}{h_1^3}\left(q_1\frac{x^2}{2} - X_{II}\right)\left(y^2+h_1 y\right)$$

$$+\frac{1+\mu_1}{E_1}\cdot\frac{12}{h_1^3}\left(q_1\frac{x^2}{2} - X_{II}\right)\left(y^2+h_1 y\right) - B_1'(y)x + B_2(y)$$

where $B_1(y)$ and $B_2(y)$ are arbitrary functions of y only. The expression for v gives the vertical displacements at the contact plane between the beams as

$$(v)_{y=0} = \frac{1-\mu_1^2}{E_1}\cdot\frac{12}{h_1^3}\left(q_1\frac{x^4}{24} - X_{IV}\right) - B_1'(0)x + B_2(0) - B\frac{x^2}{2}$$

$$= \frac{1}{D_1}\left(q_1\frac{x^4}{24} - X_{IV}\right) - B_1'(0)x + B_2(0) - B\frac{x^2}{2} \qquad (5.11)$$

where $D_1 = \dfrac{E_1 h_1^3}{12(1-\mu_1^2)}$ is the flexural rigidity of the main strata.

Nether strata (over ribside): $\dfrac{\ell_1+w}{2} < x < \infty$

As in the case of the main strata, we can assume an expression for σ_x in terms of an unknown function of x G(x) like

$$\sigma_x = G(x)\left(y - \frac{h_2}{2}\right) \tag{5.12}$$

Then using the equilibrium equations (5.4) and proceeding along the same lines we find

$$\tau_{xy} = -\frac{1}{2} G'(x)\left(y^2 - h_2 y\right) \tag{5.13}$$

satisfying the conditions $(\tau_{xy})_{y=o} = (\tau_{xy})_{y=h_2} = o$.

We also get

$$\sigma_y = -(q_2 + X) + \frac{6}{h_2^3}(q_2 + X - k_2 v_1)\left(\frac{h_2 y^2}{2} - \frac{y^3}{3}\right) \tag{5.14}$$

with $$G''(x) = -\frac{12}{h_2^3}(q_2 + X - k_2 v_1) \tag{5.15}$$

where $k_2 = \dfrac{E_c}{H(1-\mu_c^2)}$ is the foundation modulus of the seam, E_c, μ_c being the elastic constants of the seam and H its thickness. v_1 are the bottom fibre deflections of the nether roof in the ribside region as explained before. Equ. (5.14) satisfies the conditions of normal stress on the upper and lower edges of the nether roof:

$$(\sigma_y)_{y=0} = -(q_2 + X), \quad (\sigma_y)_{y=h_2} = -k_2 v_1,$$

the second condition being in accordance with the theory of beams on elastic foundations.

Integrating $G''(x)$ of Equ. (5.15) once and twice and using relations (5.12) and (5.13), the stresses can be rewritten as

$$\left.\begin{aligned}
\sigma_x &= -\frac{12}{h_2^3}\left(q_2\frac{x^2}{2} + X_{II} - k_2 v_{1II}\right)\left(y-\frac{h_2}{2}\right) + C\left(y-\frac{h_2}{2}\right)\\
\sigma_y &= -\left(q_2 + X\right) + \frac{6}{h_2^3}\left(q_2 + X - k_2 v_1\right)\left(\frac{h_2 y^2}{2} - \frac{y^3}{3}\right)\\
\tau_{xy} &= \frac{6}{h_2^3}\left(q_2 x + X_I - k_2 v_{1I}\right)\left(y^2 - h_2 y\right)
\end{aligned}\right] \qquad (5.16)$$

The displacements along the contact plane between the two strata beams or the upper edge of the nether strata y = o can be determined in a similar manner as in the previous case of the main strata using (5.16) and the displacement relations (5.10). Mentioned here are only the vertical displacements v for relevance:

$$\begin{aligned}
v = {} & \frac{1-\mu_2^2}{E_2}\cdot\frac{12}{h_2^3}\left(q_2\frac{x^4}{24} + X_{IV} - k_2 v_{1IV}\right) - C\frac{x^2}{2}\\
& + \frac{\mu_2(1+\mu_2)}{E_2}\cdot\frac{6}{h_2^3}\left(q_2\frac{x^2}{2} + X_{II} - k_2 v_{1II}\right)\left(h_2 y - y^2\right)\\
& - \frac{1+\mu_2}{E_2}\cdot\frac{12}{h_2^3}\left(q_2\frac{x^2}{2} + X_{II} - k_2 v_{1II}\right)\left(h_2 y - y^2\right)\\
& - B_3'(y)\,x + B_4(y)
\end{aligned} \qquad (5.17)$$

From this, at the contact plane y = o,

$$(v)_{y=o} = \frac{1}{D_2}\left(q_2\frac{x^4}{24} + X_{IV} - k_2 v_{1\,IV}\right)$$

$$- B_3'(o)x + B_4(o) - C\frac{x^2}{2} \qquad (5.18)$$

where $D_2 = \frac{E_2 h_2^3}{12(1-\mu_2^2)}$ is the flexural rigidity of the nether roof.

Equ. (5.18) must be identical with Equ. (5.11) since both refer to the deflections at the same plane y = o. Equating the two right hand sides of these equations and differentiating four times with respect to x we get an expression for X, the unknown reactions at the contact plane:

$$X = \frac{q_1 D_2 - q_2 D_1 + D_1 k_2 v_1}{D_1 + D_2} \qquad (5.19)$$

The displacements at the lowest fibre of the nether roof or at the contact plane between the seam and the nether roof y = h_2 can be determined from Equ. (5.17):

$$v_1 = (v)_{y=h_2}$$

$$= \frac{1}{D_2}\left(q_2\frac{x^4}{24} + X_{IV} - k_2 v_{1\,IV}\right) - B_3'(h_2)x + B_4(h_2) - C\frac{x^2}{2}$$

Four times differentiation with respect to x gives us

$$D_2\frac{d^4 v_1}{dx^4} = q_2 + X - k_2 v_1$$

and substituting for X from (5.19) we get finally

$$(D_1 + D_2)\frac{d^4 v_1}{dx^4} = q_1 + q_2 - k_2 v_1 \qquad (5.20)$$

This is the differential equation for deflections v_1 of the lowest fibre of the nether strata over the ribside.

In order to evaluate the integration constants in the general solution of Equ. (5.20), expressions for bending moments and shear forces will be needed in terms of these deflections. Using stress equations (5.16) and the following definitions of bending moments and shear forces

$$M(x) = \int_0^{h_2} \sigma_x \, y \, dy$$

and $$Q(x) = \int_0^{h_2} \tau_{xy} \, dy$$

we find

$$M_1(x) = -\left(q_2 \frac{x^2}{2} + X_{II} - k_2 v_{1II} \right)$$

$$Q_1(x) = -\left(q_2 x + X_I - k_2 v_{1I} \right)$$

for the ribside region. Substituting for X from Equ. (5.19),

$$\left.\begin{aligned} M_1(x) &= -\frac{D_2}{D_1 + D_2} \left[(q_1 + q_2) \frac{x^2}{2} - k_2 v_{1II} \right] \\ Q_1(x) &= \frac{d}{dx} M_1(x) \end{aligned}\right] \qquad (5.21)$$

Now, the differential equation (5.20) has the general solution

$$v_1 = \frac{q_1 + q_2}{k_2} + e^{-\alpha x} \left(C_1 \cos \alpha x + C_2 \sin \alpha x \right) + e^{\alpha x} \left(C_3 \cos \alpha x + C_4 \sin \alpha x \right)$$

with $$\alpha = \left[\frac{k_2}{4(D_1 + D_2)} \right]^{1/4}$$

Considering that the coal seam is infinite in the region of v_1 we must satisfy the condition

$$(v_1)_{x=\infty} = \frac{q_1 + q_2}{k_2} \quad ,$$

so that the arbitrary constants $C_3 = C_4 = o$. Then

$$v_1 = \frac{q_1 + q_2}{k_2} + e^{-\alpha x}(C_1 \cos \alpha x + C_2 \sin \alpha x) \tag{5.22}$$

Substituting (5.22) in Equ. (5.21) we see that the bending moments and shear forces acquire the simpler forms

$$\left.\begin{aligned} M_1(x) &= -D_2 \frac{d^2 v_1}{dx^2} \\ Q_1(x) &= \frac{d}{dx} M_1(x) \end{aligned}\right] \tag{5.23}$$

It may be noticed that these are thin beam expressions for bending moments and shear forces because they are expressed in terms of the bottom fibre deflections.

Nether strata (over opening): $-\frac{l_1 + w}{2} < x < \frac{l_1 + w}{2}$

It only remains to work out the deflections in the hanging or unsupported part of the nether strata and satisfy the continuity conditions

on the ends so as to solve the situation in stage (1) completely.

The stress distribution in this part of the nether roof can be written down by the usual procedure:

$$\sigma_x = -\frac{6q_2}{h_2^3} x^2 \left(y - \frac{h_2}{2} \right) + B \left(y - \frac{h_2}{2} \right)$$

$$\sigma_y = -\frac{6q_2}{h_2^3} \left(\frac{y^3}{3} - \frac{h_2 y^2}{2} + \frac{h_2^3}{6} \right)$$

$$\tau_{xy} = \frac{6q_2}{h_2^3} x \left(y^2 - h_2 y \right)$$

From these expressions the final differential equation for deflections v_2 of the lowest fibre of the unsupported nether roof can be shown to be

$$D_2 \frac{d^4 v_2}{dx^4} = q_2 \qquad (5.24)$$

It has the solution

$$v_2 = \frac{q_2}{24 D_2} x^4 + C_3 x^2 + C_4 \qquad (5.25)$$

by symmetry about the ordinate. The bending moments and shear forces are given by

$$\left.\begin{aligned} M_2(x) &= -D_2 \frac{d^2 v_2}{dx^2} \\ Q_2(x) &= -D_2 \frac{d^3 v_2}{dx^3} \end{aligned}\right] \qquad (5.26)$$

We can now lay down the conditions of continuity for determining the integration constants C_1 to C_4 in Equ. (5.22) and (5.25). The continuity conditions in beams state that at the common line between two regions of the same beam, which are either differently supported or differently loaded, the deflections, slopes, bending moments and shear forces must be the same when obtained from either of the deflections in the two regions. Considering this definition and the expressions for bending moments and shear forces (5.23) and (5.26), the continuity conditions at the coal edge, which is the common line, become

$$\text{at } x = \frac{\ell_1 + w}{2} \; ; \quad \left\{ \begin{array}{l} v_1 = v_2 \;\; , \;\; v_1' = v_2' \;\; , \\ \\ v_1'' = v_2'' \;\; , \;\; v_1''' = v_2''' \end{array} \right. \qquad (5.27)$$

Putting v_1 and v_2 from Equ. (5.22) and (5.25) in these four conditions will give rise to four simultaneous linear algegraic equations whose solution will determine the integration constants $C_1 - C_4$, completely determining the deflections over the opening and the ribside in stage (1).

5.2.3.2 Stage (1): nether roof as several beams with broken cohesion between them

As mentioned earlier, stage (1) consists of creating an opening with a width $(\ell_1 + w)$. This working is more likely to induce breaks in the cohesion between different layers of the nether roof up to the cavity higher up. These breaks then represent just a loosening of contact reducing the overall flexural rigidity of the nether roof.

Let us initially assume that the nether roof has two beds of different thicknesses, the upper one resting on the lower one. Due to bending action this will generate normal reactions X_1, X_2 and X_3 as in Fig.5.5. The loadings, due to the dead weights of the two layers, will be q_2 and q_3, acting as shown on the upper edges of these layers. Only the bottom fibre deflections of the lower layer are of interest.

As in the previous case, the method of analysis consists of determining the unknown reactions X_1, X_2 and X_3 and eliminating them.

* Main strata (over coal): $\frac{l_1+w}{2} < x < \infty$

In the coordinate system shown in the figure, it can be proved that the deflections at the contact plane y = o between the main strata and the top nether roof are

$$(v)_{y=0} = \frac{1-\mu_1^2}{E_1} \cdot \frac{12}{h_1^3}\left(q_1 \frac{x^4}{24} - X_{1_{IV}}\right) - B_1'(o)x + B_2(o) \qquad (5.25)$$

Top nether roof (over coal): $\frac{l_1+w}{2} < x < \infty$

$$v = \frac{1-\mu_2^2}{E_2} \cdot \frac{12}{h_2^3}\left(q_2 \frac{x^4}{24} + X_{1_{IV}} - X_{2_{IV}}\right) -$$

$$+ \frac{\mu_2(1+\mu_2)}{E_2} \cdot \frac{6}{h_2^3}\left(q_2 \frac{x^2}{2} + X_{1_{II}} - X_{2_{II}}\right)\left(h_2 y - y^2\right)$$

$$- \frac{1+\mu_2}{E_2} \cdot \frac{12}{h_2^3}\left(q_2 \frac{x^2}{2} + X_{1_{II}} - X_{2_{II}}\right)\left(h_2 y - y^2\right) - B_3'(y)x + B_4(y)$$

---

* Constants B, C occurring earlier are excluded from further derivation since they do not affect deflections v.

FIG.5.5 - STAGE (1) - TWO-LAYER NETHER ROOF

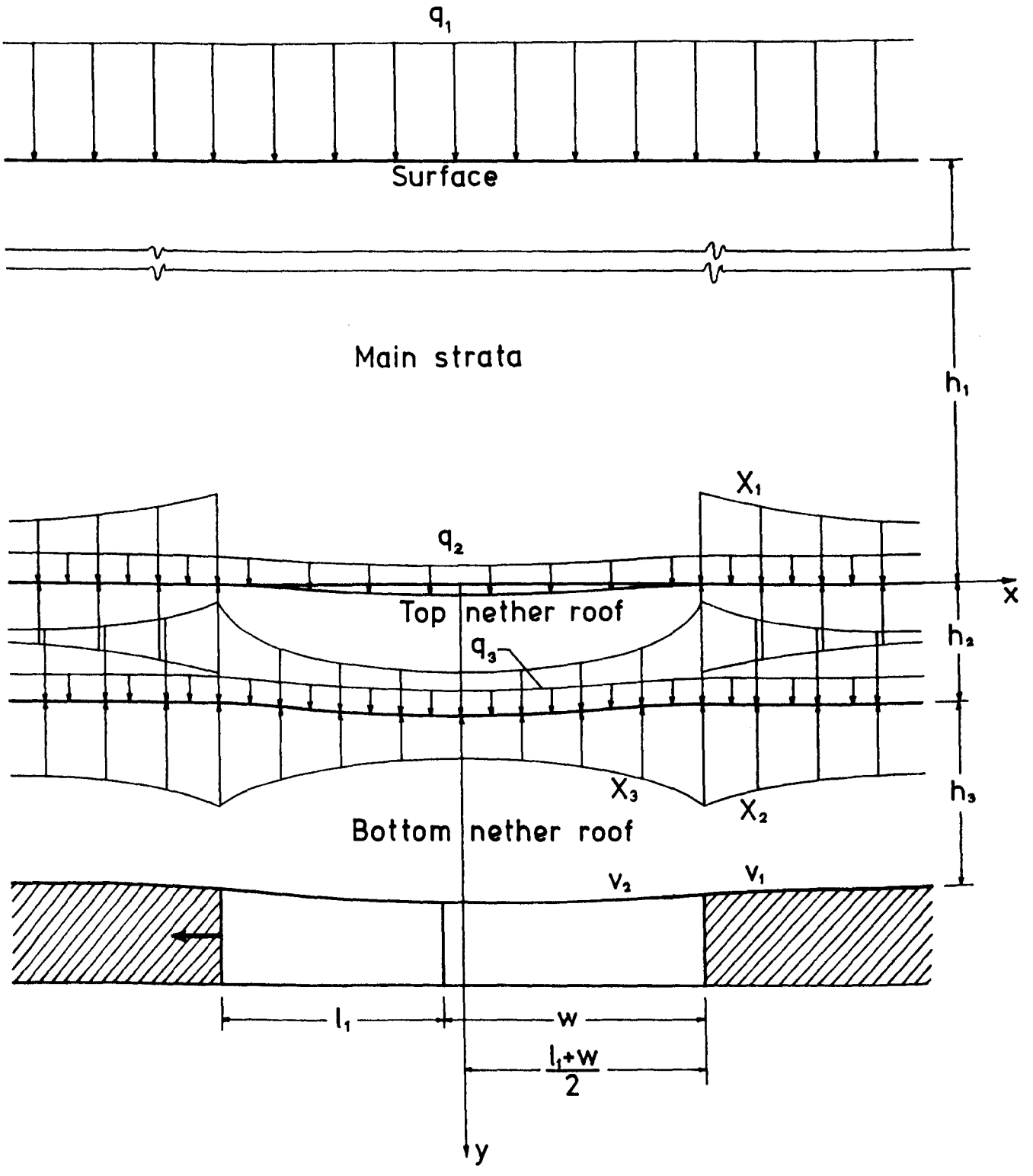

giving again the deflections at the contact plane y = o,

$$(v)_{y=0} = \frac{1-\mu_2^2}{E_2} \cdot \frac{12}{h_2^3} \left(q_2 \frac{x^4}{24} + X_{1_{IV}} - X_{2_{IV}} \right) - B_3'(o)x + B_4(o) \tag{5.29}$$

and the deflections at the contact plane y = h_2 between the two layers of the nether roof,

$$(v)_{y=h_2} = \frac{1-\mu_2^2}{E_2} \cdot \frac{12}{h_2^3} \left(q_2 \frac{x^4}{24} + X_{1_{IV}} - X_{2_{IV}} \right) - B_3'(h_2)x + B_4(h_2) \tag{5.30}$$

Equ. (5.28) and (5.29) must be identical, hence

$$X_1 = \frac{q_1 D_2 - q_2 D_1 + D_1 X_2}{D_1 + D_2} \tag{5.31}$$

where D_2 is the flexural rigidity of the upper nether roof.

Bottom nether roof (over coal): $\frac{l_1+w}{2} < x < \infty$

We similarly obtain at the contact plane y = h_2

$$(v)_{y=h_2} = \frac{1-\mu_3^2}{E_3} \cdot \frac{12}{h_3^3} \left(q_3 \frac{x^4}{24} + X_{2_{IV}} - k_2 v_{1_{IV}} \right) - B_5'(h_2)x + B_6(h_2) \tag{5.32}$$

At the bottom fibre of the lower nether roof we can write

$$\begin{aligned} v_1 &= (v)_{y=h_2+h_3} \\ &= \frac{1-\mu_3^2}{E_3} \cdot \frac{12}{h_3^3} \left(q_3 \frac{x^4}{24} + X_{2_{IV}} - k_2 v_{1_{IV}} \right) \\ &\quad - B_5'(h_2+h_3)x + B_6(h_2+h_3) \end{aligned} \tag{5.33}$$

Identifying (5.30) and (5.32)

$$X_2 = \frac{q_2 D_3 + X_1 D_3 - q_3 D_2 - D_2 k_2 v_1}{D_2 + D_3}$$

and with the help of Equ. (5.31)

$$X_2 = \frac{-(D_1 + D_2) q_3 + (q_1 + q_2) D_3 + (D_1 + D_2) k_2 v_1}{D_1 + D_2 + D_3}$$

where D_3 is the flexural rigidity of the bottom nether roof.
Differentiating Equ. (5.33) four times with respect to x and substituting this value of X_2, we finally obtain the differential equation in terms of deflections v_1 over the solid coal:

$$(D_1 + D_2 + D_3) \frac{d^4 v_1}{dx^4} = q_1 + q_2 + q_3 - k_2 v_1 \qquad (5.34)$$

We can similarly show that the deflection equation for the bottom nether roof over the opening is

$$(D_2 + D_3) \frac{d^4 v_2}{dx^4} = q_2 + q_3 \qquad (5.35)$$

A comparison of Equ. (5.34) and (5.35) with those for a single layer roof, Equ. (5.20) and (5.24), shows that they are very similar, with the flexural rigidity D_2 of the single layer roof being replaced by $D_2 + D_3$, the sum of the rigidities of the two layers.

It can similarly be proved by deduction that when there are several layers, say n, we have $\sum_1^n D_n$ instead of $D_2 + D_3$ and when all these layers have the same flexural rigidity D the differential equations are of the form

$$(D_1 + n D)\frac{d^4 v_1}{dx^4} = q_1 + q_2 - k_2 v_1 \qquad (5.36)$$

for the ribside and

$$n D \frac{d^4 v_2}{dx^4} = q_2 \qquad (5.37)$$

for the unsupported part over the opening. Here q_2 has now the same meaning as in Equ. (5.20) and (5.24) of the single layer case.

It is important to note that these two equations (5.36) and (5.37) assume that the flexural rigidity of the beam is nD over the opening which changes suddenly to $(D_1 + nD)$ over the ribside. Structurally this is not permissable in the same continuous beam. We must, therefore, assume that the equations have the form

$$D_2 \frac{d^4 v_1}{dx^4} = q_1 + q_2 - k_2 v_1$$

$$D_2 \frac{d^4 v_2}{dx^4} = q_2 \qquad (5.38)$$

instead of their earlier versions. Here nD has been replaced by D_2 for simplicity, with D_2 representing either the single-layered or multi-layered roof. Equ. (5.38) have the solutions

$$v_1 = \frac{q_1 + q_2}{k_2} + e^{-\alpha x}(C_1 \cos \alpha x + C_2 \sin \alpha x)$$

and $$v_2 = \frac{q_2}{24 D_2} x^4 + C_3 x^2 + C_4 \quad \Big] \qquad (5.39)$$

in which now $\alpha = \left(\frac{k_2}{4 D_2}\right)^{\frac{1}{4}}$. The arbitrary constants $C_1 - C_4$ can be determined from the continuity conditions (5.27) as explained before.

5.2.3.3 Stage (2)

Having made an opening of width $(\ell_1 + w)$ in stage (1) the first pack section is now erected and the short face advanced further by a distance ℓ. The length of the pack is also ℓ. When the opening is widened this way, it produces deflections additional to those existing already in the nether roof. These additional deflections occur over the pack, producing pack load. They also occur over the unsupported part of the opening and the ribside. Referring to Fig. 5.1 and 5.6 stage (2) shows that the new final deflections have been designated as follows:

v_3 - over the stagnant ribside, $(\ell_1 + \ell + w) < x < \infty$,

v_4 - over the trunk roadway, $(\ell_1 + \ell) < x < (\ell_1 + \ell + w)$,

v_5 - over the pack, $\ell_1 < x < (\ell_1 + \ell)$,

v_6 - over the working area at the face, $o < x < \ell_1$,

v_7 - over the faceside coal, $-\infty < x < o$.

The y-axis has been shifted to the face edge from its earlier position in stage (1) since this problem is no longer symmetrical in stage (2) $(\ell_1 \neq w)$.

FIG.5.6 - STAGE (2) OF FACE ADVANCE

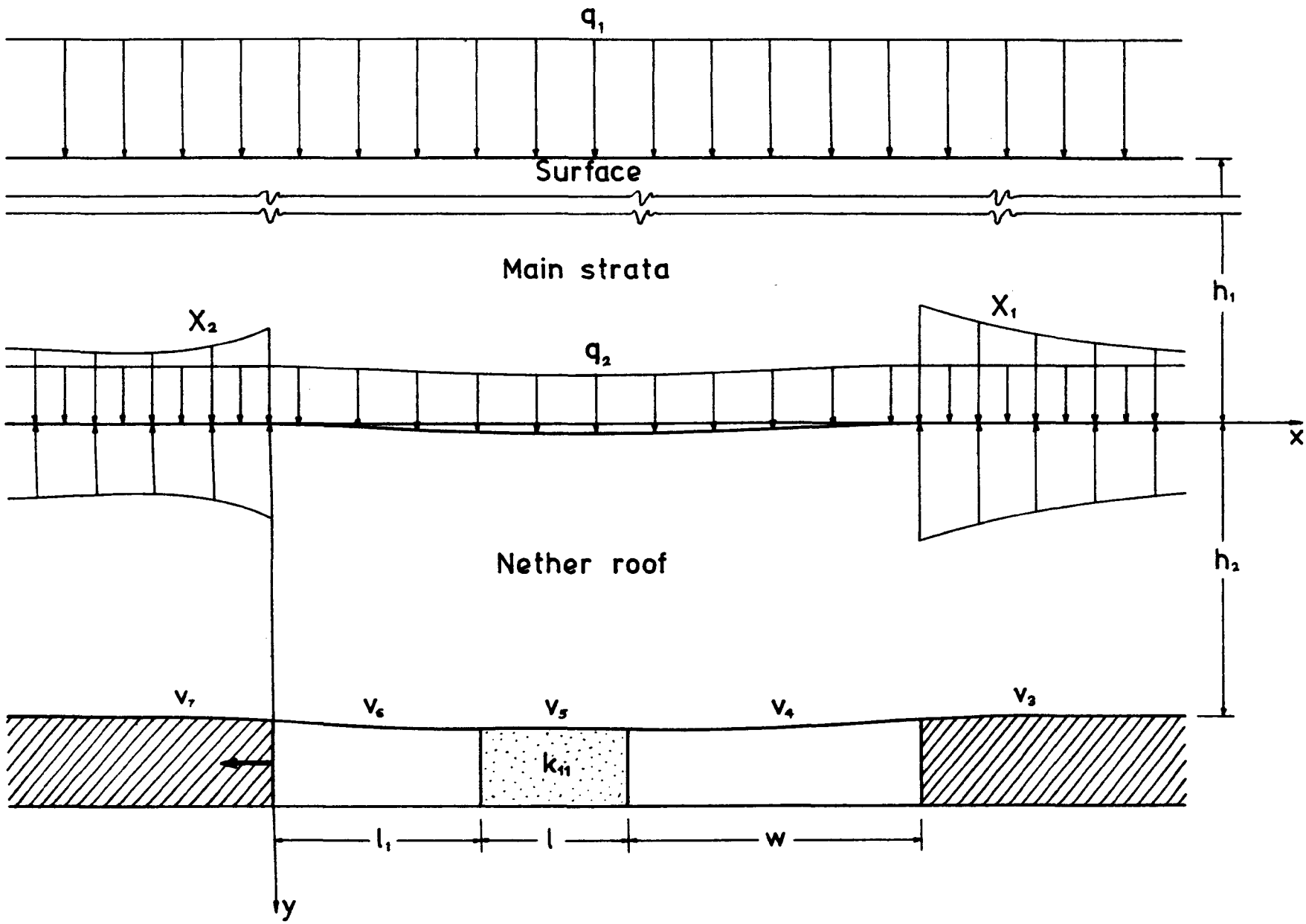

The pack was erected when the roof deflections were already v_2, as given by the second equation in (5.39). The new final deflections due to face advancement are v_5 so that the additional deflections responsible for pack compression are (v_5-v_2), and the pack load produced will be $k_{11}(v_5-v_2)$ where k_{11} is the pack foundation modulus at the instant the roof deflects in stage (2).

The unknown reactions X_1 and X_2 set up at the contact plane y = o between the main strata and the nether roof can be eliminated by the earlier procedure and it can be shown that (Fig. 5.6).

$$\left.\begin{aligned} v_3 &= \frac{q_1+q_2}{k_2} + e^{-\alpha x}(C_5 \cos \alpha x + C_6 \sin \alpha x) \\ v_7 &= \frac{q_1+q_2}{k_2} + e^{\alpha x}(C_{19} \cos \alpha x + C_{20} \sin \alpha x) \end{aligned}\right] \qquad (5.40)$$

the first equation satisfying the condition $(v_3)_{x=\infty} = \frac{q_1+q_2}{k_2}$ and the second one satisfying $(v_7)_{x=-\infty} = \frac{q_1+q_2}{k_2}$. These two separate equations are necessary for the two solid coal sides because the configuration is no more symmetrical, unlike stage (1). Similarly, for the unsupported parts of the nether roof

$$\left.\begin{aligned} v_4 &= \frac{q_2}{24 D_2} x^4 + C_7 x^3 + C_8 x^2 + C_9 x + C_{10} \\ v_6 &= \frac{q_2}{24 D_2} x^4 + C_{15} x^3 + C_{16} x^2 + C_{17} x + C_{18} \end{aligned}\right] \qquad (5.41)$$

again due to lack of symmetry.

Deflections over the pack, or pack compression, can now be considered under the following conditions on the two edges of the nether roof in the region of the pack:

$$\left.\begin{aligned} &(\tau_{xy})_{y=0} = (\tau_{xy})_{y=h_2} = 0 \\ &(\sigma_y)_{y=0} = -q_2 \quad , \quad (\sigma_y)_{y=h_2} = -k_{11}(v_5 - v_2) \end{aligned}\right] \qquad (5.42)$$

In order to determine v_5, the stresses in the nether roof in the pack region have to be determined. They can be written down as

$$\sigma_x = -\frac{12}{h_2^3}\left[q_2\frac{x^2}{2} - k_{11}(v_{5_{II}} - v_{2_{II}})\right]\left(y - \frac{h_2}{2}\right)$$

$$\sigma_y = -q_2 - \frac{6}{h_2^3}\left[q_2 - k_{11}(v_5 - v_2)\right]\left(\frac{y^3}{3} - \frac{h_2 y^2}{2}\right)$$

$$\tau_{xy} = \frac{6}{h_2^3}\left[q_2 x - k_{11}(v_{5_I} - v_{2_I})\right](y^2 - h_2 y)$$

which satisfy the edge conditions (5.42). From these equations we get the differential equation for deflections in the pack region in the usual manner:

$$D_2 \frac{d^4 v_5}{dx^4} = q_2 - k_{11}(v_5 - v_2) \tag{5.43}$$

The general solution of this equation can be obtained after substituting for v_2 from Equ. (5.39), modifying it to suit the new position of the y-axis at the coal face thus

$$v_2 = \frac{q_2}{24 D_2}\left(x - \ell - \frac{\ell_1 + w}{2}\right)^4 + C_3\left(x - \ell - \frac{\ell_1 + w}{2}\right)^2 + C_4$$

This expression when substituted in Equ. (5.43) gives its solution as

$$\begin{aligned} v_5 = {} & \frac{q_2}{24 D_2}\left(x - \ell - \frac{\ell_1 + w}{2}\right)^4 + C_3\left(x - \ell - \frac{\ell_1 + w}{2}\right)^2 + C_4 \\ & + e^{-\beta_1 x}\left(C_{11}\cos\beta_1 x + C_{12}\sin\beta_1 x\right) \\ & + e^{\beta_1 x}\left(C_{13}\cos\beta_1 x + C_{14}\sin\beta_1 x\right) \end{aligned} \tag{5.44}$$

in which

$$\beta_1 = \left(\frac{k_{11}}{4 D_2}\right)^{1/4}.$$

The five equations in (5.40), (5.41) and (5.44) are the complete deflection equations for the different regions in stage (2). They involve 16 integration constants C_5 - C_{20} which can be determined if the same number of algebraic equations can be framed. Continuity conditions like (5.27) can be applied to each pair of neighbouring regions. The pairs formed will be v_1-v_2, v_2-v_3, v_3-v_4, v_4-v_5, and since there will be four continuity conditions

for each of these pairs, we will get 16 simultaneous linear algebraic equations. As will be remembered, the four conditions are laid down in terms of deflection, slope, bending moment and shear force at the line of demarkation separating two neighbouring regions.

Stage (2) is then completely determined.

5.2.3.4 Stage (3)

A second section of the anhydrite pack is now placed adjacent to the first one of stage (2) and the short face is advanced further by a distance ℓ. The length of each of the two pack sections is also ℓ. This additional face movement causes further deflections to occur over both pack regions, compressing the first pack section further and the second section for the first time. At the instant the face moves, the foundation modulus of the first pack will have risen to another value k_{12}, $k_{12} > k_{11}$. The second section will have acquired the value k_{11}.

The deflections in the different regions are as designated in Fig. 5.1 and those over the coal sides and the unsupported regions of the opening can be shown to be similar to stage (2):

$$\left.\begin{aligned} v_8 &= \frac{q_1+q_2}{k_2} + e^{-\alpha x}(C_{21}\cos\alpha x + C_{22}\sin\alpha x) \\ v_{13} &= \frac{q_1+q_2}{k_2} + e^{\alpha x}(C_{39}\cos\alpha x + C_{40}\sin\alpha x) \\ v_9 &= \frac{q_2}{24 D_2}x^4 + C_{23}x^3 + C_{24}x^2 + C_{25}x + C_{26} \\ v_{12} &= \frac{q_2}{24 D_2}x^4 + C_{35}x^3 + C_{36}x^2 + C_{37}x + C_{38} \end{aligned}\right\} \quad (5.45)$$

Besides the usual conditions of zero shear stress on the upper and lower edges of the nether roof beam, the conditions for the vertical normal stress σ_y in the two pack regions are:

pack section (1): $(\sigma_y)_{y=0} = -q_2$,

$$(\sigma_y)_{y=h_2} = -k_{11}(v_5 - v_2) - k_{12}(v_{10} - v_5)$$

pack section (2): $(\sigma_y)_{y=0} = -q_2$,

$$(\sigma_y)_{y=h_2} = -k_{11}(v_{11} - v_6)$$

The second term in the second condition for pack section (1) corresponds to the additional loading thrown due to face movement in this stage. v_{10} and v_{11} are the final new deflections in stage (3) in the region of pack sections (1) and (2) respectively. We can then form the differential equation for deflections v_{10} over the first pack section:

$$D_2 \frac{d^4 v_{10}}{dx^4} = q_2 - k_{12}(v_{10} - v_5) - k_{11}(v_5 - v_2)$$

Changing v_2 of Equ. (5.39) and v_5 of Equ.(5.44) to suit the new position of the y-axis, we get the solution of this equation as a complementary function and a particular integral,

$$v_{10} = \frac{q_2}{24 D_2}\left(x - 2l - \frac{l_1 + w}{2}\right)^4 + C_3\left(x - 2l - \frac{l_1 + w}{2}\right)^2 + C_4$$
$$+ e^{-\beta_1(x-l)}\left[C_{11}\cos\beta_1(x-l) + C_{12}\sin\beta_1(x-l)\right]$$
$$+ e^{\beta_1(x-l)}\left[C_{13}\cos\beta_1(x-l) + C_{14}\sin\beta_1(x-l)\right]$$

$$+ e^{-\beta_2 x}\left(C_{27} \cos \beta_2 x + C_{28} \sin \beta_2 x \right)$$

$$+ e^{\beta_2 x}\left(C_{29} \cos \beta_2 x + C_{30} \sin \beta_2 x \right) \qquad (5.46)$$

with $\beta_2 = \left(\frac{k_{12}}{4 D_2} \right)^{1/4}$

Similarly, over pack section (2)

$$D_2 \frac{d^4 v_{11}}{dx^4} = q_2 - k_{11}\left(v_{11} - v_6 \right)$$

giving $v_{11} = \frac{q_2}{24 D_2}(x-\ell)^4 + C_{15}(x-\ell)^3 + C_{16}(x-\ell)^2 + C_{17}(x-\ell) + C_{18}$

$$+ e^{-\beta_1 x}\left(C_{31} \cos \beta_1 x + C_{32} \sin \beta_1 x \right)$$

$$+ e^{\beta_1 x}\left(C_{33} \cos \beta_1 x + C_{34} \sin \beta_1 x \right) \qquad (5.47)$$

changing v_6 of Equ. (5.41) to suit the new position of the y-axis and substituting in the differential equation.

Applying continuity conditions as usual we can determine the new set of 20 arbitrary constants $C_{21} - C_{40}$ involved in Equ. (5.45-47), completely solving the configuration of stage (3).

5.2.3.5 Further stages

Derivation can thus proceed up to whatever stage desired. In the instance of anhydrite packs it was carried out to stage (7), until when, it was felt, a sufficient part of the load acceptance curve of the pack would be obtained.

The load on any pack section considered can be seen to vary with face advance as given by the conditions for the normal stress σ_y on the lower edge of the nether strata. Taking each pack section stage by stage, at $y = h_2$,

Stage (2): pack (1) $\sigma_y = -k_{11}(v_5 - v_2)$

Stage (3): pack (1) $\sigma_y = -k_{11}(v_5 - v_2) - k_{12}(v_{10} - v_5)$

pack (2) $\sigma_y = -k_{11}(v_{11} - v_6)$

Stage (4) pack (1) $\sigma_y = -k_{11}(v_5 - v_2) - k_{12}(v_{10} - v_5) - k_{13}(v_{16} - v_{10})$

pack (2) $\sigma_y = -k_{11}(v_{11} - v_6) - k_{12}(v_{17} - v_{11})$

pack (3) $\sigma_y = -k_{11}(v_{18} - v_{12})$

Stage (5): pack (1) $\sigma_y = -k_{11}(v_5 - v_2) - k_{12}(v_{10} - v_5) - k_{13}(v_{16} - v_{10}) - k_{14}(v_{23} - v_{16})$

pack (2) $\sigma_y = -k_{11}(v_{11} - v_6) - k_{12}(v_{17} - v_{11}) - k_{13}(v_{24} - v_{17})$

pack (3) $\sigma_y = -k_{11}(v_{18} - v_{12}) - k_{12}(v_{25} - v_{18})$

pack (4) $\sigma_y = -k_{11}(v_{26} - v_{19})$

and so on up to stage (7).

Taking, for example, pack (1) the loading is seen to 'increase' step by step as for any other pack section. Deflection equations for stages (4) through (7) are given in Appendix I and may be referred to for interest. It will be seen that the integration constants from stages (4) to (7) are 24, 28, 32 and 36, the total constants from stage (1) to (7) being thus 160.

A suitable computer program was written for each stage in Fortran IV for the application of continuity conditions and solution of the resulting simultaneous equations. For the purpose of this numerical analysis, the conditions at Dawdon Colliery were taken. The computer program for stage (7), together with the output is given in Appendix II. A NAG Library Subroutine F04ATF was used for solution of the simultaneous equations (of which there are 36 in stage (7)).

5.2.4 Assumptions and data for numerical analysis on the computer

As already seen, there is a single rock (mudstone) in the nether roof above High Main seam at Dawdon up to a thickness of 10 m or more. It is more realistic to consider that the nether roof will be disturbed by breaking off of interstratum cohesion due to working up to the bed separation cavity. The assumptions made for the numerical analysis were therefore:

(a) When the short face is started, the roof develops a bed separation cavity at a height of 10 m (which appears to be a

a reasonable figure, considering the three heading widths of 12, 14 and 16 m, for which the situation has been analysed later) in stage (1). In spite of further face advance this cavity does not travel upward, since it would be limited by the width of the heading and not its length.

(b) The cohesion between layers is broken every 1 m in the nether roof mudstone, so that the flexural rigidity of the nether roof D_2 is 10D where D is the flexural rigidity of each such layer.

(c) The elastic properties used in the analysis were taken as an average of those for some Durham rocks and coals[64].

The following data for numerical analysis could then be

Depth of High Main seam from surface	365 m
Thickness of seam H	1.9 m
Modulus of elasticity of seam E_c	2.0×10^6 kN/m^2
Modulus of elasticity of nether roof (mudstone) E_2	1.35×10^7kN/m^2
Poisson's ratio (coal, rock, anhydrite) μ	0.25
Length of each pack section (or unit advance) ℓ	3.0 m
Width of trunk roadway w	6.0 m

Maximum unsupported span between the short face and the last pack section ℓ_1 5.0 m

Rock pressure per metre of depth ρ 22.8 kN/m^2

Three rates of advance, 9.0, 6.0 and 4.5 m/day, were used to obtain the pack load variation with face advance. The values of the foundation modulus, k_{11}, k_{12}, etc. will depend on the time interval between two successive face advances. The rate of advance will, therefore, affect pack load acceptance, even though this analysis is purely elastostatic and does not otherwise include time-dependent phenomena. All the results presented in this Chapter are elastostatic only.

5.2.5 Results of longitudinal considerations

The values of all the 160 integration constants could be determined from the computer programs, so that the deflection equations were completely known for all stages. Two points, A and B, were chosen on the top centre of pack sections (3) and (2) respectively, as shown in Fig. 5.1. No point was chosen on the first section as it was assumed to be close enough to the ribside to be influenced by it.

Deflections at A and B were obtained from before the placement of pack section below them to the last stage, i.e. from stage (3) and stage (2) to stage (7) respectively. From these deflections the load values at each stage of face advance were computed from the conditions given in Sec.5.2.3.5. These computations are given in the computer program of stage (7) in Appendix II. These load values form the load acceptance curve of the anhydrite pack

sections at points A and B, as presented in Fig. 5.7 and 5.8. The two figures indicate a somewhat different pack load behaviour, leading to the conclusion that point B is still a little influenced by the coalside across the trunk roadway, at least more so than point A. All subsequent work has, therefore, been carried out with reference to point A in the third pack section.

Elastically, the rate of advance is observed to have only a small effect on pack load acceptance, at least in these longitudinal considerations, in which the short face is infinitely long with a very large pack width, as pointed out earlier. It will be shown later that the rate of advance has a more significant influence when finite face lengths are taken. The loading curves will be discussed in greater detail for finite pack widths.

5.3 An elastic analysis by lateral considerations - an equivalent loading method

5.3.1 The first stage of pack loading

The short face advancing method, as analysed by the earlier longitudinal considerations, is shown is plan in Fig. 5.9, in which the section line marked BB represents the sectional elevation of Fig.5.1. It can be realised that the earlier derivation based on this configuration was purely hypothetical, since it assumes an infinite heading width and also because it assumes that the separated nether roof will be still 10 m in thickness. However, an analysis along the length of this infinitely wide heading was necessary as a first step to obtain the loading curves of a pack section for a later analysis of finite practical heading widths. The

FIG.5.7 - PACK LOAD VARIATION WITH FACE ADVANCE AT POINT A

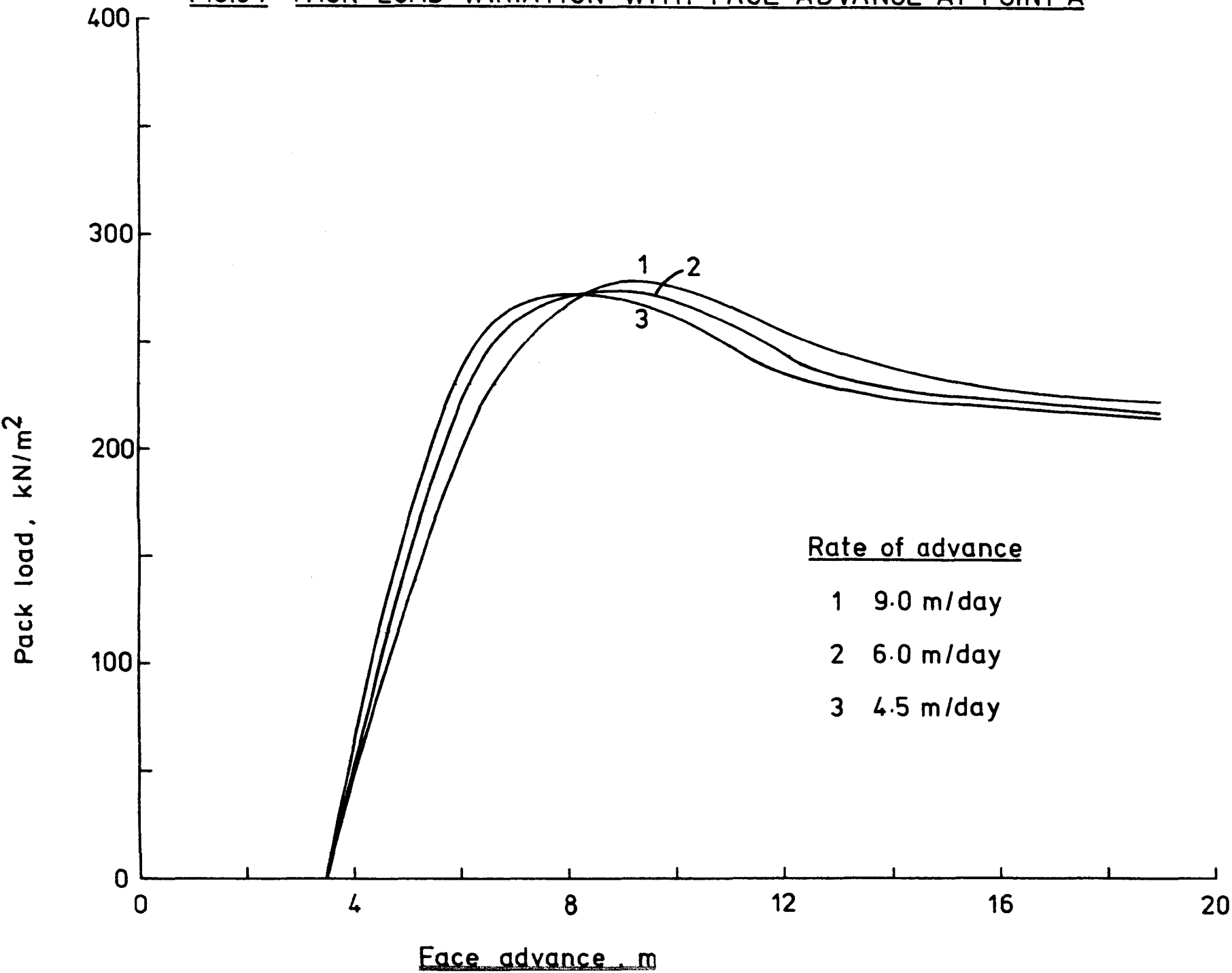

FIG.5.8-PACK LOAD VARIATION WITH FACE ADVANCE AT POINT B

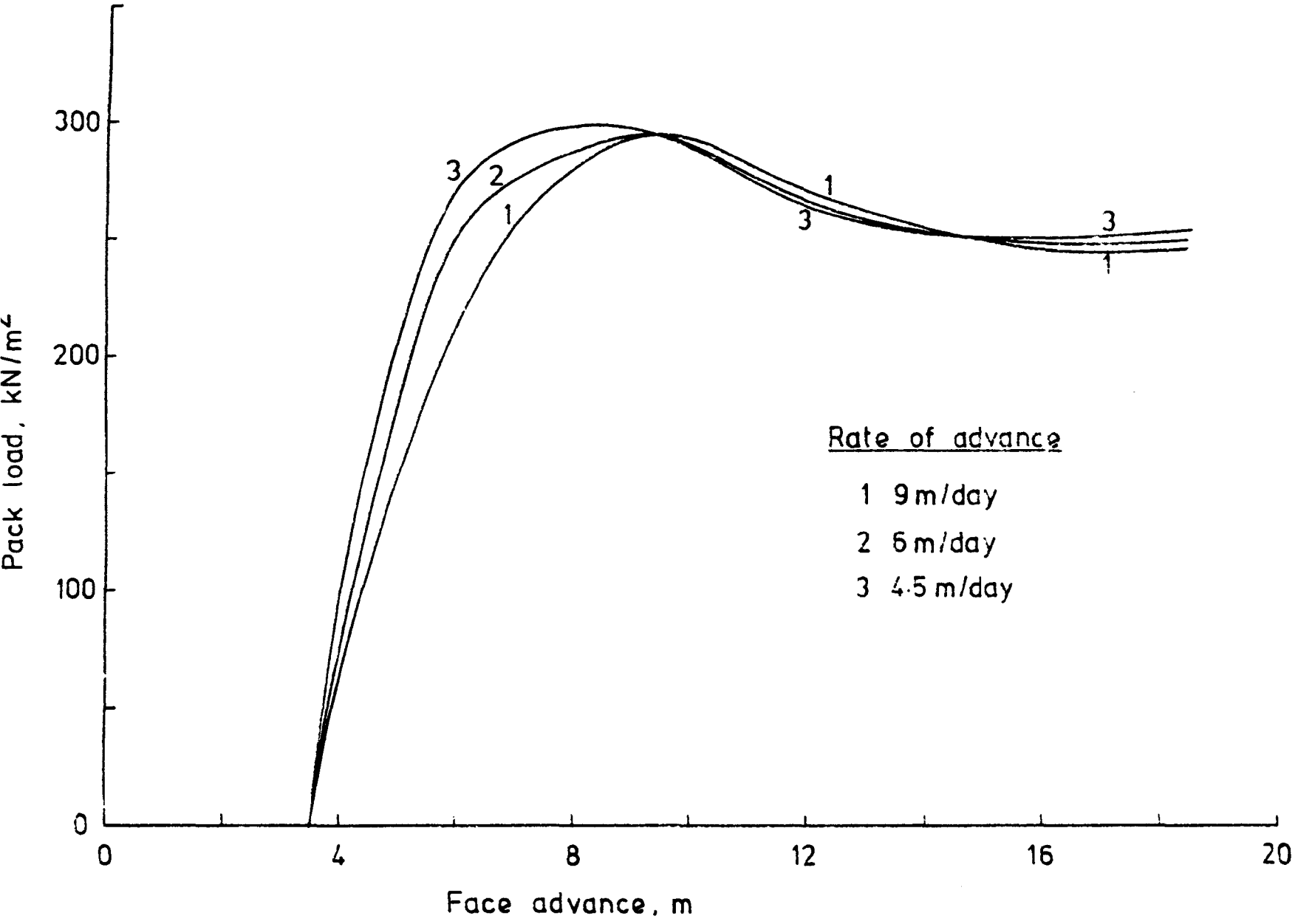

nether roof thickness of 10 m was hence chosen to correspond to these finite widths.

The point A has been marked in Fig. 5.9. Taking a lateral section CC across the heading through A, the situation looks as shown in the same figure. Point A received load due to roof deflection in stage (4) for the first time, as seen from Fig.5.1. If the load is designated as q_{21} and the deflection as δ_2 (their values are already known from the longitudinal analysis), the following equation is proposed for the deflection of the roof cross-section:

$$D_2 \frac{d^4 v_{31}}{dx^4} = q_{21} - k_{11}(v_{31} - \delta_1) \tag{5.48}$$

This equation accounts for the conditions that

(a) at an infinite distance from the roadways (i.e. at the centre of an infinite pack), the bending moment and hence the curvature, becomes zero, so that the loading on the upper and lower edges of the roof beam is q_{21}, the deflection being δ_2. Then

$$(\delta_2 - \delta_1) k_{11} = q_{21} \quad at \quad x = o$$

(b) k_{11} is the foundation modulus at the time δ_2 occurs,

(c) δ_1 is the initial deflection at x = o (i.e. at an infinite distance from the roadway).

All the three above conditions are satisfied by the previous longitudinal analysis so that Equ. (5.48) agrees with it. It can be rewritten as

FIG.5.9 - LATERAL CONSIDERATIONS

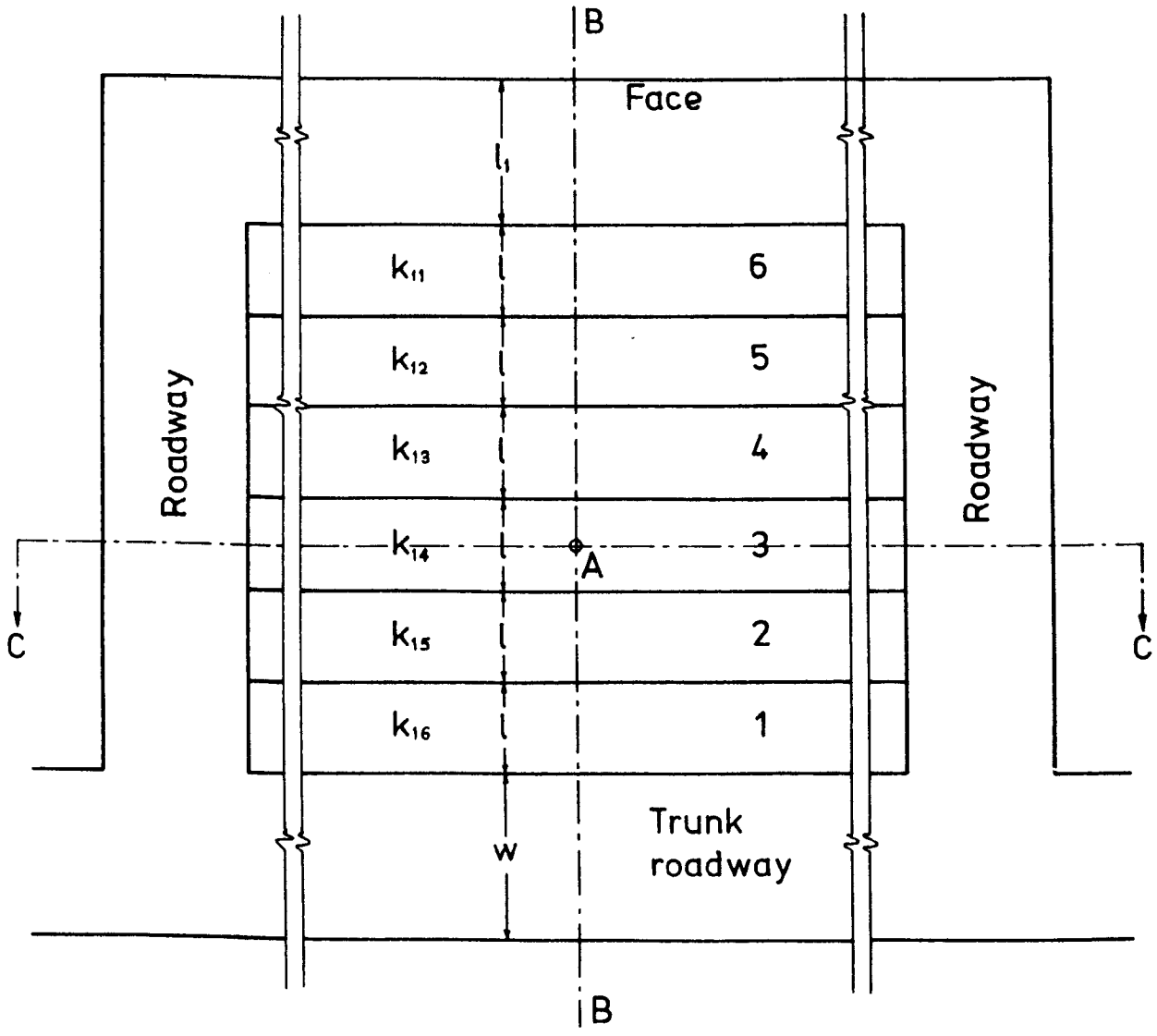

Plan

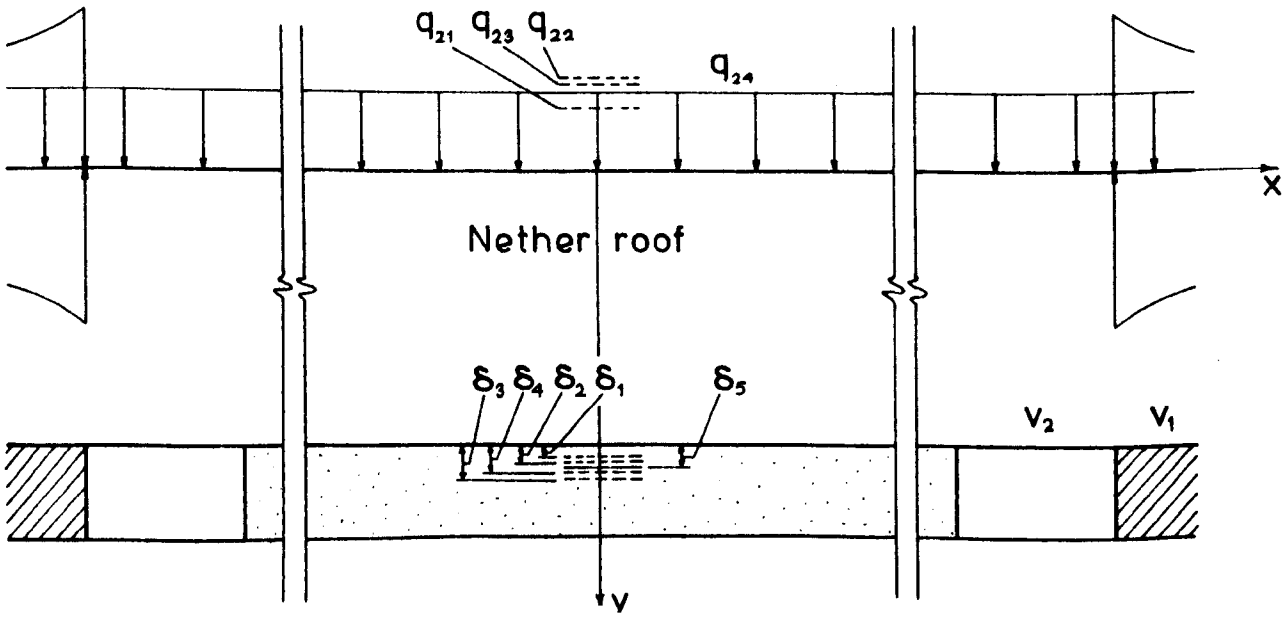

$$\frac{D_2}{k_{11}} \cdot \frac{d^4 v_{31}}{dx^4} = \delta_2 - v_{31}$$

according to condition (a). The deflections v_{31} describe the bending curve of the nether roof over the pack region between the two roadways. This equation has the solution

$$v_{31} = \delta_2 + A_1 \cosh \beta_1 x \cos \beta_1 x + A_2 \sinh \beta_1 x \sin \beta_1 x \tag{5.49}$$

When x is very large the terms containing hyperbolic and trigonometric functions vanish, leaving at x = o

$$v_{31} = \delta_2$$

for an infinite pack width. When the pack is finite

$$v_{31} = \delta_2 + A_1 \quad at \quad x = o$$

so that A acts as a correction to the deflection δ_2 when the pack, and also the short face, has a finite width. The last two terms containing functions in Equ. (5.49) thus describe correction values for different x in the pack region.

This, then, is an equivalent loading method by which a loading q_{21} obtained from the longitudinal considerations is placed on the beam instead of q_2, the loading due to its own weight, such that the condition at the centre of the beam (pack centre) is satisfied. The loading q_{21} thus takes into account the nearness of the short face, at least as far as the pack

centre is concerned. The limitations of such a method and the error involved will be discussed later in this Chapter.

5.3.2 Subsequent stages of pack loadings

In the next stage of face advance (stage (5)), point A deflects by an amount δ_3, the equivalent loading on the beam being q_{22}. These are again known from the longitudinal analysis and the differential equation for the pack region now becomes

$$D_2 \frac{d^4 v_{32}}{dx^4} = q_{22} - k_{11}(v_{31} - \delta_1) - k_{12}(v_{32} - v_{31}) \qquad (5.50)$$

where v_{32} are the new deflections over the pack due to face advance. Now, the longitudinal analysis gives

$$(\delta_2 - \delta_1) k_{11} + (\delta_3 - \delta_2) k_{12} = q_{22}$$

or $$\delta_3 = \frac{q_{22}}{k_{12}} + \delta_2 - \frac{k_{11}}{k_{12}}(\delta_2 - \delta_1)$$

so that Equ. (5.50) has the solution after substituting for v_{31} from (5.49)

$$\begin{aligned} v_{32} &= \delta_3 + A_1 \cosh\beta_1 x \cos\beta_1 x + A_2 \sinh\beta_1 x \sin\beta_1 x \\ &\quad + A_3 \cosh\beta_2 x \cos\beta_2 x + A_4 \sinh\beta_2 x \sin\beta_2 x \\ &= v_{31} + \delta_3 - \delta_2 \\ &\quad + A_3 \cosh\beta_2 x \cos\beta_2 x + A_4 \sinh\beta_2 x \sin\beta_2 x \end{aligned} \qquad (5.51)$$

Without writing the differential equations for further stages up

to (7), the expressions for defle ctions over the pack can be written down corresponding to equivalent loadings, q_{23}, q_{24}:

$$\left.\begin{aligned} v_{33} &= v_{32} + \delta_4 - \delta_3 \\ &\quad + A_5 \cosh \beta_3 x \cos \beta_3 x + A_6 \sinh \beta_3 x \sin \beta_3 x \\ v_{34} &= v_{33} + \delta_5 - \delta_4 \\ &\quad + A_7 \cosh \beta_4 x \cos \beta_4 x + A_8 \sinh \beta_4 x \sin \beta_4 x \end{aligned}\right] \qquad (5.52)$$

The constants β_1, β_2, etc. have the forms $(k_{11}/4D_2)^{\frac{1}{4}}$, $(k_{12}/4D_2)^{\frac{1}{4}}$, etc.

The deflection equations for the roadway region and the solid coal side can be written as usual:

$$\left.\begin{aligned} v_1 &= \frac{q_1 + q_2}{k_2} + e^{-\alpha x}(B_1 \cos \alpha x + B_2 \sin \alpha x) \\ v_2 &= \frac{q_2}{24 D_2} x^4 + B_3 x^3 + B_4 x^2 + B_5 x + B_6 \end{aligned}\right] \qquad (5.53)$$

where v_1 and v_2 are for the ribside and roadway respectively. The eight integration constants $A_1 - A_8$ in Equ. (5.49) and (5.51-52) can be evaluated in pairs by applying the usual continuity conditions between each of three equations and Equ. (5.53) turn by turn. This will also determine the values of $B_1 - B_6$.

5.3.3 Numerical Analysis

A suitable computer program in Fortran IV was written for the solution of the simultaneous equations resulting from applying the continuity conditions

to the above-mentioned equations of deflections. The program was designed to give

(a) Pack load acceptance with face advance.

(b) Bending moment distribution in the roadway roof, pack and ribside regions.

(c) Shear forces in the same regions.

(d) Ribside distribution of abutment pressure.

(e) Distribution of load on the pack.

Along with the earlier data for Dawdon Colliery, the heading width (or short face length) was chosen as 12, 14 and 16 m and the corresponding pack width as 2, 4 and 6 m, so that the roadways on either side of the pack had a constant width of 5 m. The rates of advance were taken as before at 9.0, 6.0 and 4.5 m per day.

As will be shown later, the solution is more accurate when the face has travelled a sufficient distance from the point under consideration (point A) so the bending moment, shear force and loading distributions were ascertained only for stage (7), calling them 'ultimate' values. Theoretically, the term ultimate is erroneous, since it can be used only for the situation when the face has moved an infinite distance. After stage (7), however, the changes in the picture are quite small and so this stage has been regarded as at infinity.

5.3.4 Results and discussion

5.3.4.1 Pack load variation with face advance

Figs. 5.10 - 12 display the load acceptance of the anhydrite centre pack with face advance for the three short face lengths (heading widths) of 12, 14 and 16 m. The general shape of the characteristic is similar in all the three cases of heading widths as well as rates of advance in that it indicates a rapid initial load build up to a peak value and a later, more gradual fall to a steady state value. All the curves have been plotted for loads at the pack centre. Peak load and ultimate or steady state load values are given in Table 5.1.

It is observed from Figs. 5.10 - 12 and Table 5.1 that the load increases if the heading width is increased from 12 to 16 m, except for the rate of advance of 4.5 m/day, when it remains virtually the same for heading widths of 14 and 16 m. The ultimate loads are really quite small. Obviously, the load values cannot be compared with those for a full-fledged longwall excavation, since the heading width is only 12 - 16 m. The reasons for such low loads are:

(a) Only the nether roof of 10-m thickness below the bed separation cavity throws load on the pack while deflecting downward, the ribside taking most of the strata weight (the dead weight of the nether roof is $230 kN/m^2$).

TABLE 5.1.

Peak and steady state loads on anhydrite packs during short face advancing

Heading width, m	Rate of advance, m/day	Peak load, kN/m^2	Steady State Load, kN/m^2
12	9.0	270	230
	6.0	336	295
	4.5	378	338
14	9.0	339	294
	6.0	373	327
	4.5	392	347
16	9.0	364	316
	6.0	382	334
	4.5	390	344

FIG.5·10 - PACK LOAD VARIATION WITH FACE ADVANCE

Heading width 12 m

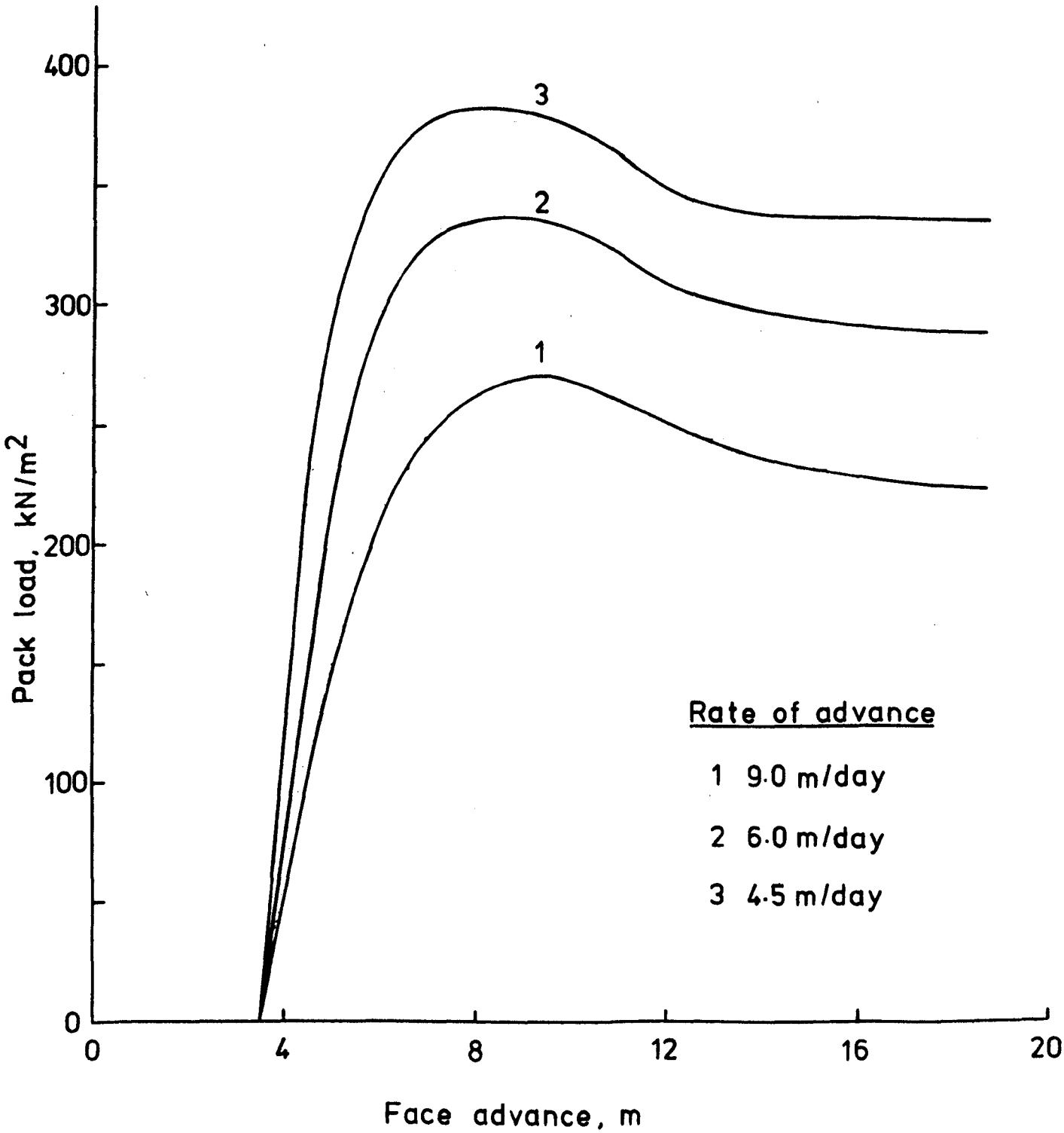

FIG.5.11 - PACK LOAD VARIATION WITH FACE ADVANCE

Heading width 14 m

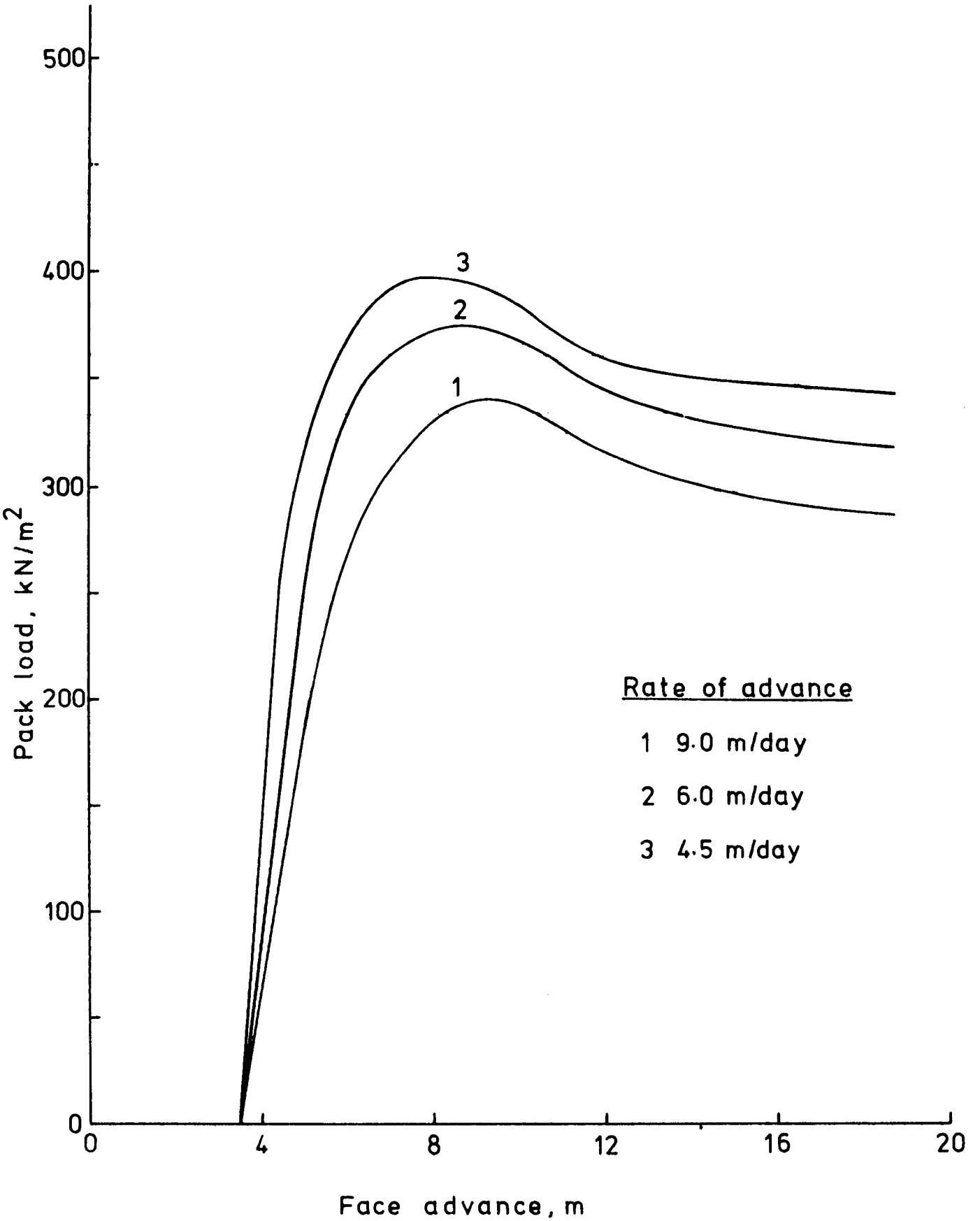

FIG.5.12 - PACK LOAD VARIATION WITH FACE ADVANCE

Heading width 16m

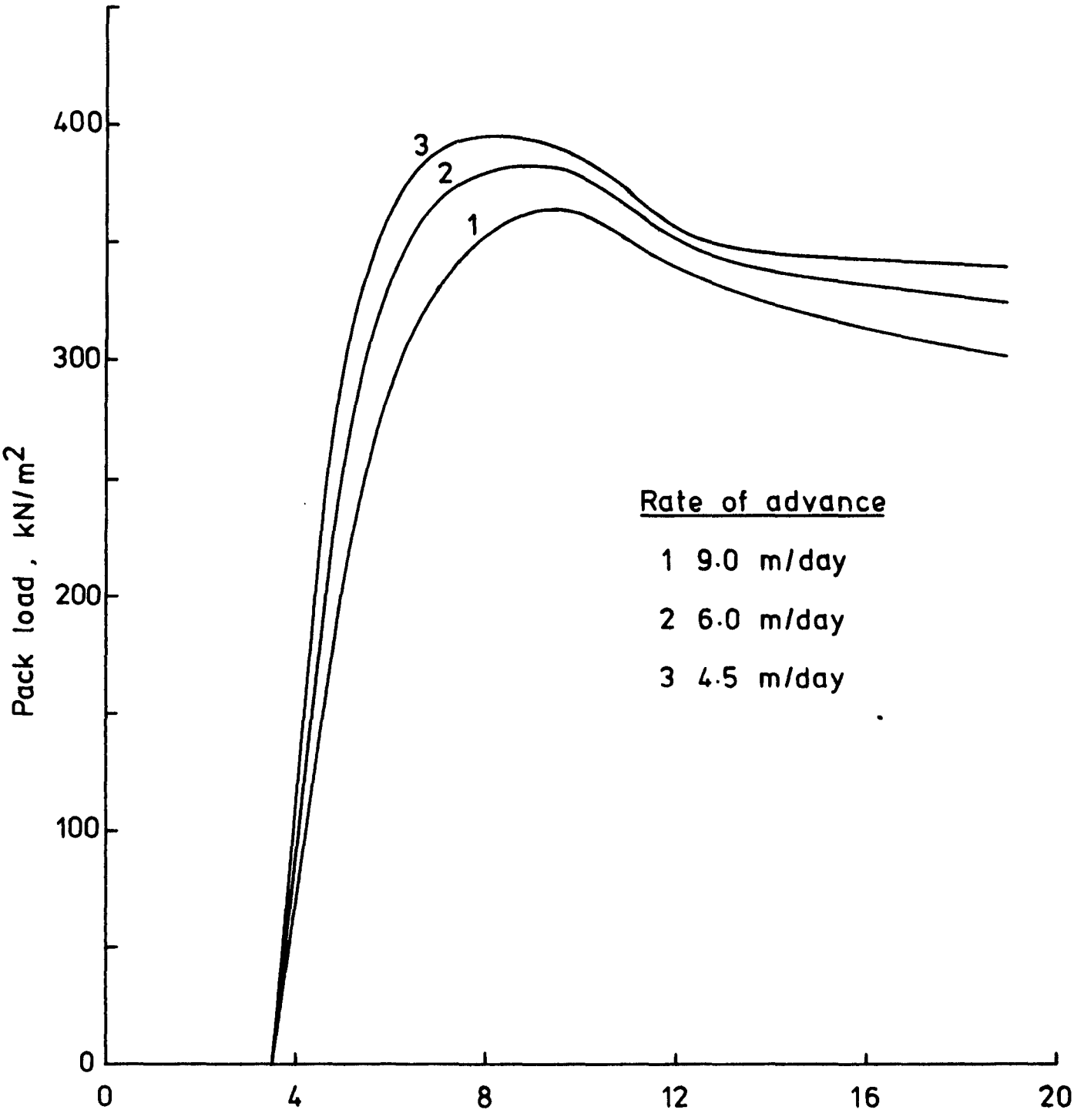

(b) a large part of the roof deflection occurs before the pack can be erected and so the pack cannot take care of the whole roof deflection.

Mathematically, the steady state load is reached at infinite face advance but practically at about 20 m to 25 m depending on the rate of advance. The rate of advance has a more pronounced effect for smaller loading widths, higher loads occurring at slower rates. The maximum change in the peak pack load which occurs for the 12-m case, is from 270 to 378 kN/m^2, corresponding to a change in the rate of advance from 9.0 to 4.5 m/day. The increase in load is thus 40%. The corresponding rise for a 16-m heading is only 7 %.

The wavy nature of load acceptance is attributable to the behaviour of an elastically supported beam as seen from the deflection equations for the various pack regions (see Appendix I). These equations were used to obtain the equivalent loadings q_{21}, q_{22}, etc. for the lateral analysis.

It is of interest to note that the shape of the loading characteristic is seen to agree with those observed underground by other workers (Fig. 2.6-7, Chapter 2), particularly the one for the anhydrite gateside pack at Easington Colliery (Fig. 2.7(b)). It may also be pointed out in this connection that there is apparently the difference that the load does not rise again in the steady state region, as it does in the underground curves mentioned. This is because the computations were not carried further than stage (7). A later rise in load would again be seen in the steady state region after stage (7), though it would

be small, because the deflection equations in the pack regions are of the form of quickly damped oscillations. This will be more clear from the abutment pressure curves and from Sec. 5.4.3.

5.3.4.2 Ultimate pack and ribside loading distribution

The steady state or ultimate load distribution across the section of the centre pack and on the ribside is shown in Figs. 5.13-15 for the three heading widths and three rates of advance mentioned earlier. Since the configuration is symmetrical about the heading centre, only the right half is shown plotted.

The load is seen to be maximum at the pack centre with a gradual fall toward the edge. This is because of the maximum central deflection of the roof over the pack. The edge load, as also the central load value, is seen to increase with heading width, the increase being greater from 12 m to 14 m than from 14 to 16 m heading widths, as in Table 5.2.

The ribside pressure forms a peak at the coal edge and falls curvilinearly with distance into the coal. It rises again to a very small extent and later falls to the depth pressure (8288 kN/m^2 for the depth at Dawdon in this instance). This later small rise is attributed to the wave-like nature of the deflection equation for solid coal and is commonly called the Weber wave[65].

The peak abutment pressure value is about 12 to 15% higher than the depth pressure, depending on the heading width and the rate of advance. It is seen to decrease very slightly with an increase in the heading width,

TABLE 5.2

Ultimate load values at the centre and edges of the anhydrite pack during short face advancing

Heading Width m	Rate of Advance m/day	Load at Centre kN/m^2	Edge Load kN/m^2
12	9.0	230	202
	6.0	295	259
	4.5	338	297
14	9.0	294	209
	6.0	327	228
	4.5	347	239
16	9.0	316	180
	6.0	334	183
	4.5	344	184

FIG.5.13 - ULTIMATE LOADING ON PACK & RIBSIDE

Heading width 12 m

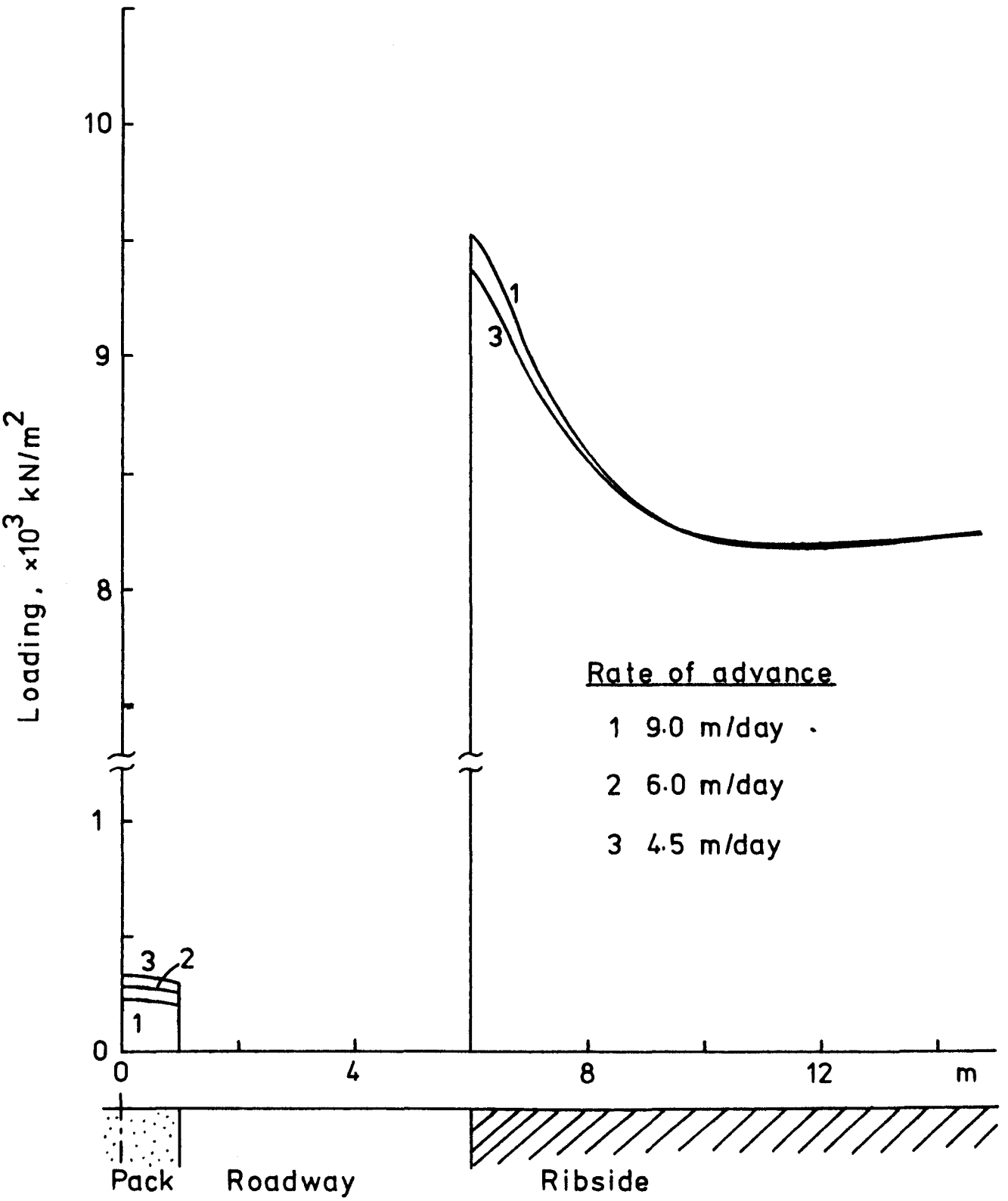

FIG.5.14 - ULTIMATE LOADING ON PACK & RIBSIDE

Heading width 14 m

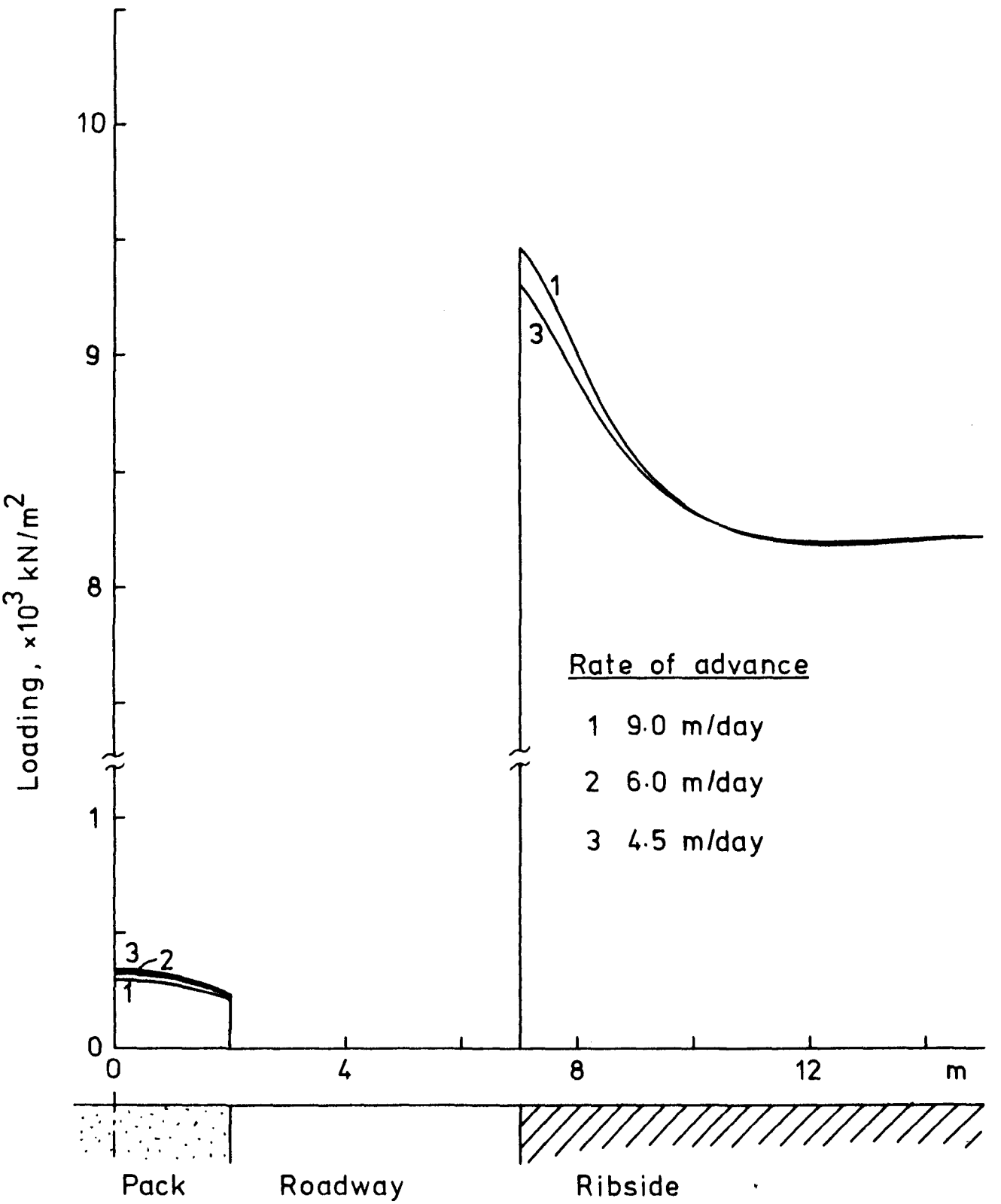

FIG.5.15 - ULTIMATE LOADING ON PACK & RIBSIDE

Heading width 16 m

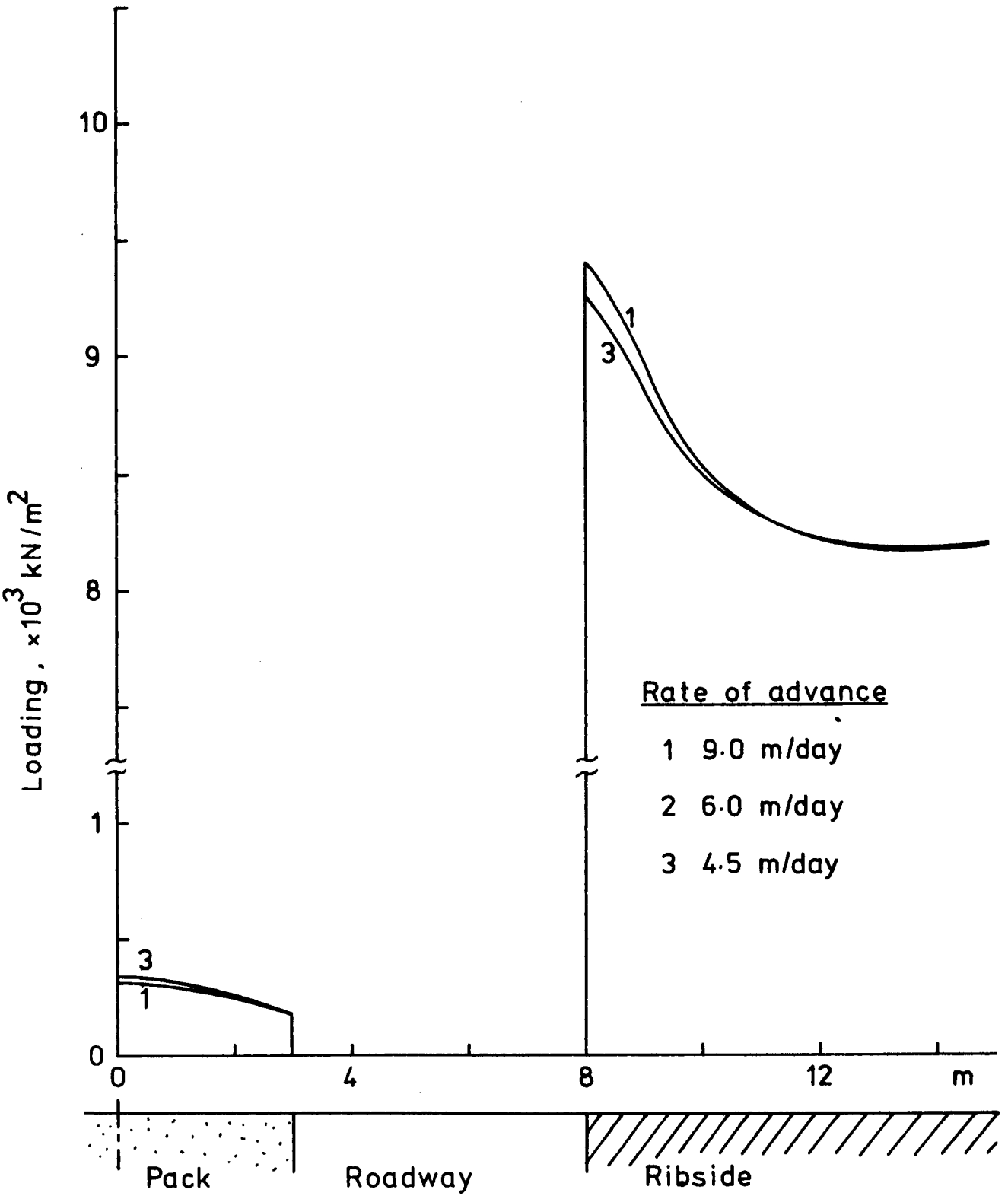

TABLE 5. 3.

Peak abutment pressure on the ribside during short face advancing using anhydrite packs (Depth pressure 8288 kN/m^2)

Heading Widths m	Rate of Advance m/day	Peak abutment pressure kN/m^2
12	9.0	9514
	6.0	9426
	4.5	9367
14	9.0	9456
	6.0	9358
	4.5	9298
16	9.0	9405
	6.0	9314
	4.5	9260

probably because the pack offers a better support resistance (see Table 5.3). The abutment pressure appears to be quite small as compared to a full longwall face (in which it may vary between 2 to 4 times the cover load) because the ribside has to support a much smaller rock mass, the heading width being quite small. This has been more elaborately explained in Chapter 7.

The abutment pressure forms a sharp peak at the coal edge which may (or may not) crush the ribside a little and shift the peak inward. The peak shown is thus the prefracture pressure. This aspect of a possible fracturing of the ribside will be covered in greater detail in Chapter 7.

5.3.4.3 Ultimate bending moments and shear forces in the nether roof

Shown in Figs. 5.16-18 are the bending moment and shear force distributions in the roof over the pack, roadway and ribside regions for the three heading widths and the two extreme rates of advance of 9.0 and 4.5 m/day, marked 1 and 3. Curves corresponding to the intermediate value of 6.0 m/day lie in between and are not shown.

All figures indicate the existence of a large negative bending moment about 1.2 to 1.4 m on the solid coal side, which falls quickly in a wavy form to the state of no bending after about 16 m in the ribside.*

---

*Negative moments mean bending convex upward and positive ones mean convex downward.

FIG.5.16 - ULTIMATE BENDING MOMENTS AND SHEAR FORCES IN THE ROOF

Heading width 12 m

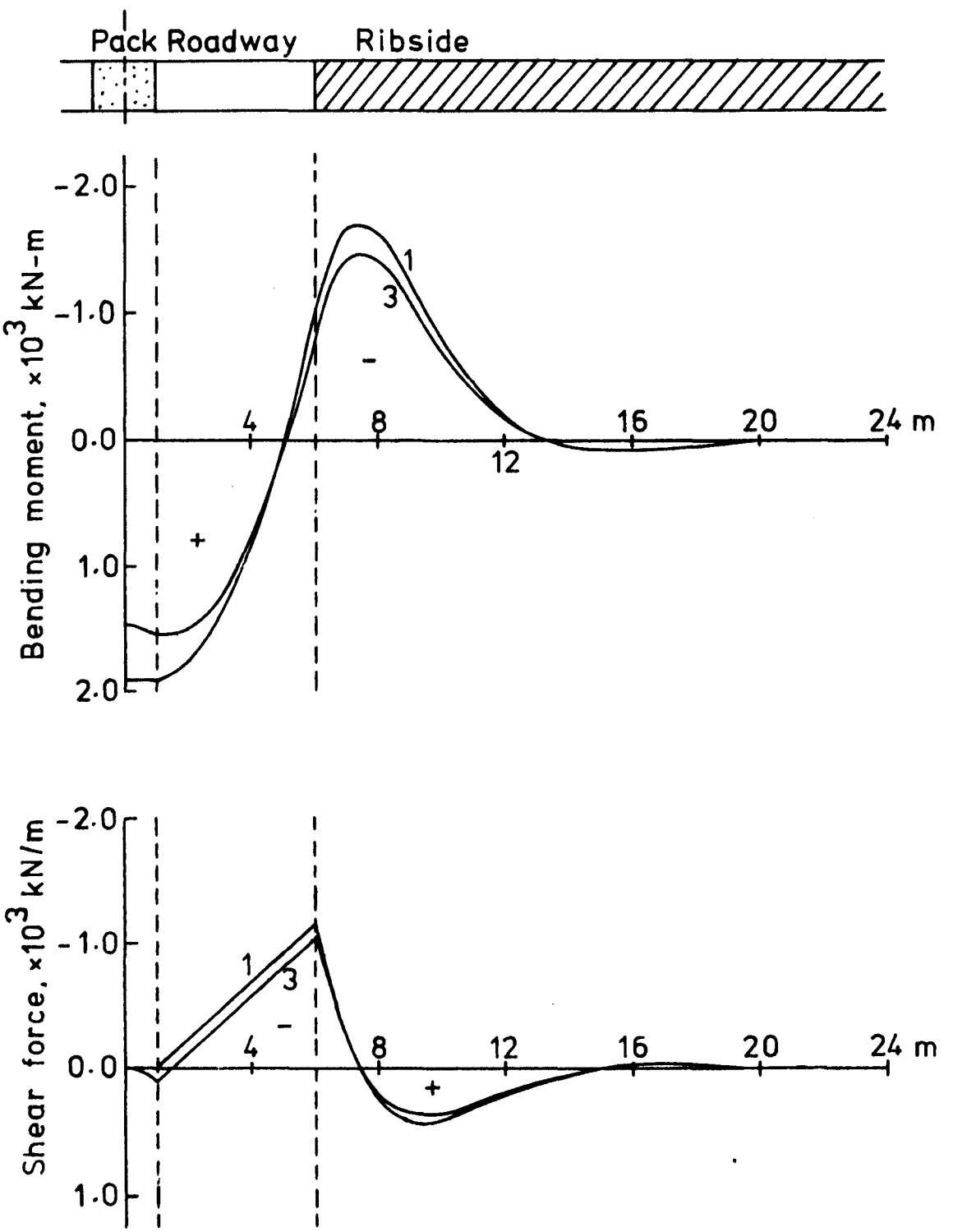

FIG.5.17 - ULTIMATE BENDING MOMENTS AND SHEAR FORCES IN THE ROOF

Heading width 14 m

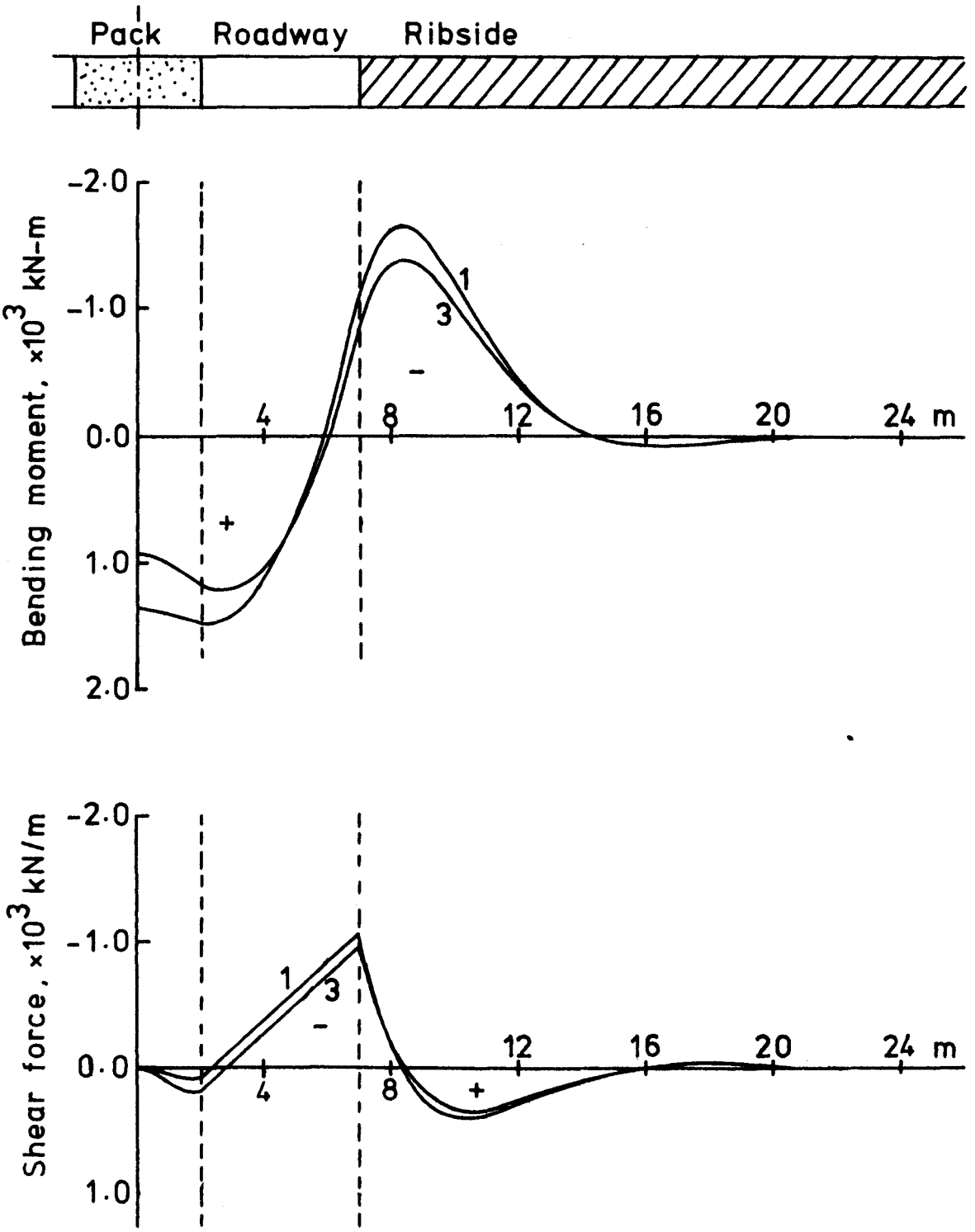

FIG.5.18 - ULTIMATE BENDING MOMENTS AND SHEAR FORCES IN THE ROOF

Heading width 16 m

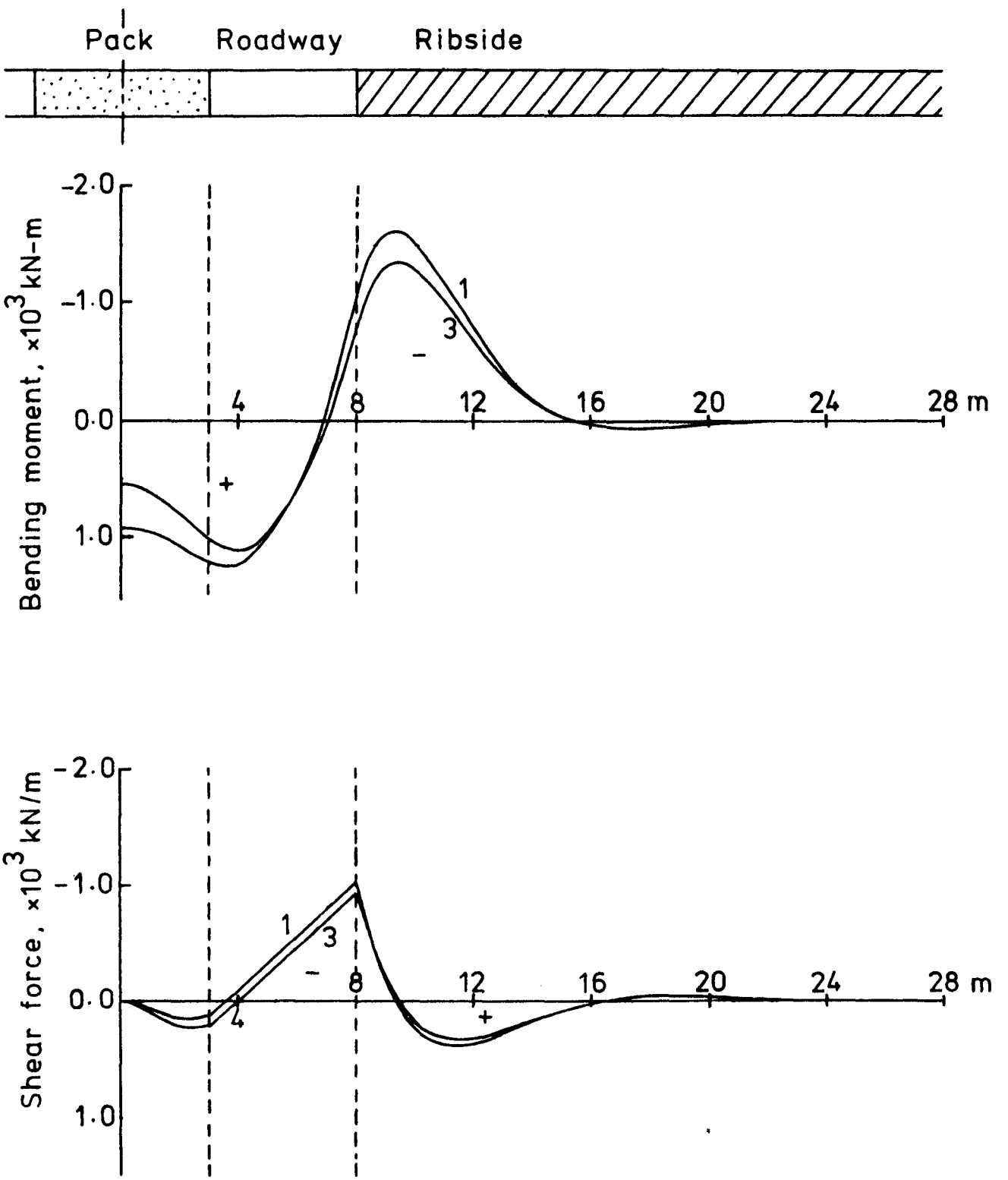

Bending moments of about the same magnitude are seen to occur in the roadway but are positive and generally fall in value into the pack. The maximum moment in the roadway is of importance for roof stability and is significantly affected by the rate of advance. The pack is thus seen to take care of a part of the bending process.

Because of increased pack load the maximum bending moment in the roadway as well as over the ribside falls with greater heading width, and also the rate of advance for the same reason. It occurs near the pack edge in the roadway when the heading width is 12 m and the rate of advance is 9.0 m/day, and farther into the roadway as the heading width increases and the speed of advance reduces.

The shear force variation shows the occurrence of a maximum shear force at the solid coal edge due to the cutting effect of the ribside, as might be expected. It is influenced by the speed of advance but not to the same extent as the bending moment.

Given in Table 5.4 are the values of the maximum tensile stress in the roof of the roadway. Since the tensile stress is proportional to the bending moment it varies the same way and reduces with increasing heading width. Considering the average tensile strength of some Durham rocks (about 6700 kN/m^2[64]), we see from Table 5.4 that the tensile strength is exceeded in most cases.

TABLE 5.4

Maximum roadway tensile stress during short face advancing using anhydrite packs

Heading Width m	Rate of Advance m/day	Maximum Tensile Stress kN/m^2
12	9.0	11,340
	6.0	10,020
	4.5	9,120
14	9.0	8,760
	6.0	7,740
	4.5	7,320
16	9.0	7,380
	6.0	6,960
	4.5	6,600

5.4 Validity and limitations of the equivalent loading method

As previously explained, the equivalent loading method consists of splitting the problem of a semi-infinite plate of finite width into two beam problems; the loading of the elastic foundation, obtained by considering the width of the plate as infinite and by solving the problem longitudinally, is placed on the plate and the problem is again solved laterally for finite widths of the plate. Obviously then the region of interest is the longitudinal central axis of the plate, or the centre line of pack in this instance.

The validity of this method, as well as the errors involved in it, can be shown by analytical solution of a parallel example, albeit a crude one. Very few plate problems are soluble analytically, so it was only possible to choose a comparatively much simpler situation than the short face advancing method.

Shown in Fig. 5.19 is a plate on elastic foundation with its edges simply supported. The plate is infinite along the positive direction of y and has a finite width a along x. There is a uniformly distributed load q on it. First a rigorous solution will be obtained for the downward deflection w perpendicular to the plane of the plate and later the same problem will be approached through the equivalent loading method.

5.4.1 Plate solution

The general differential equation for the deflections of an elastically supported plate is[61]

$$\frac{\partial^4 w}{\partial x^4} + 2\frac{\partial^4 w}{\partial x^2 \partial y^2} + \frac{\partial^4 w}{\partial y^4} = \frac{q}{D} - \frac{kw}{D} \tag{5.54}$$

where D is the fluxural rigidity of the plate and k is the modulus of the elastic foundation. Its solution can be expressed in the form

$$w = w_o + \sum_{m=1}^{\infty} Y_m \sin\frac{m\pi x}{a} \tag{5.55}$$

w_o being a particular solution of Equ. (5.54) representing a simply supported strip on elastic foundation. The infinite series is the general solution of the homogeneous equation

$$\frac{\partial^4 w}{\partial x^4} + 2\frac{\partial^4 w}{\partial x^2 \partial y^2} + \frac{\partial^4 w}{\partial y^4} + \frac{kw}{D} = 0 . \tag{5.56}$$

w_o can be obtained from the equation

$$D\frac{d^4 w_o}{dx^4} = q - kw_o \tag{5.57}$$

Choosing w_o to be of the series form

$$w_o = \sum_{m=1}^{\infty} A_m \sin\frac{m\pi x}{a}$$

and expressing the uniform load q as a Fourier series

$$q = \sum_{m=1}^{\infty} \frac{2q}{m\pi}(1 - \cos m\pi)\sin\frac{m\pi x}{a}$$

we get from Equ. (5.57) after substitution

FIG.5.19 - FOUNDATION LOADS BY EQUIVALENT LOADING & PLATE METHODS - Plate width 12 m

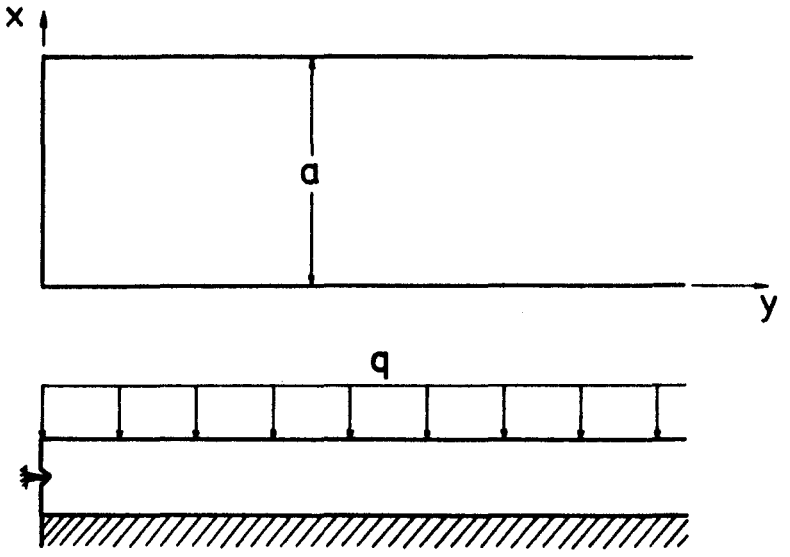

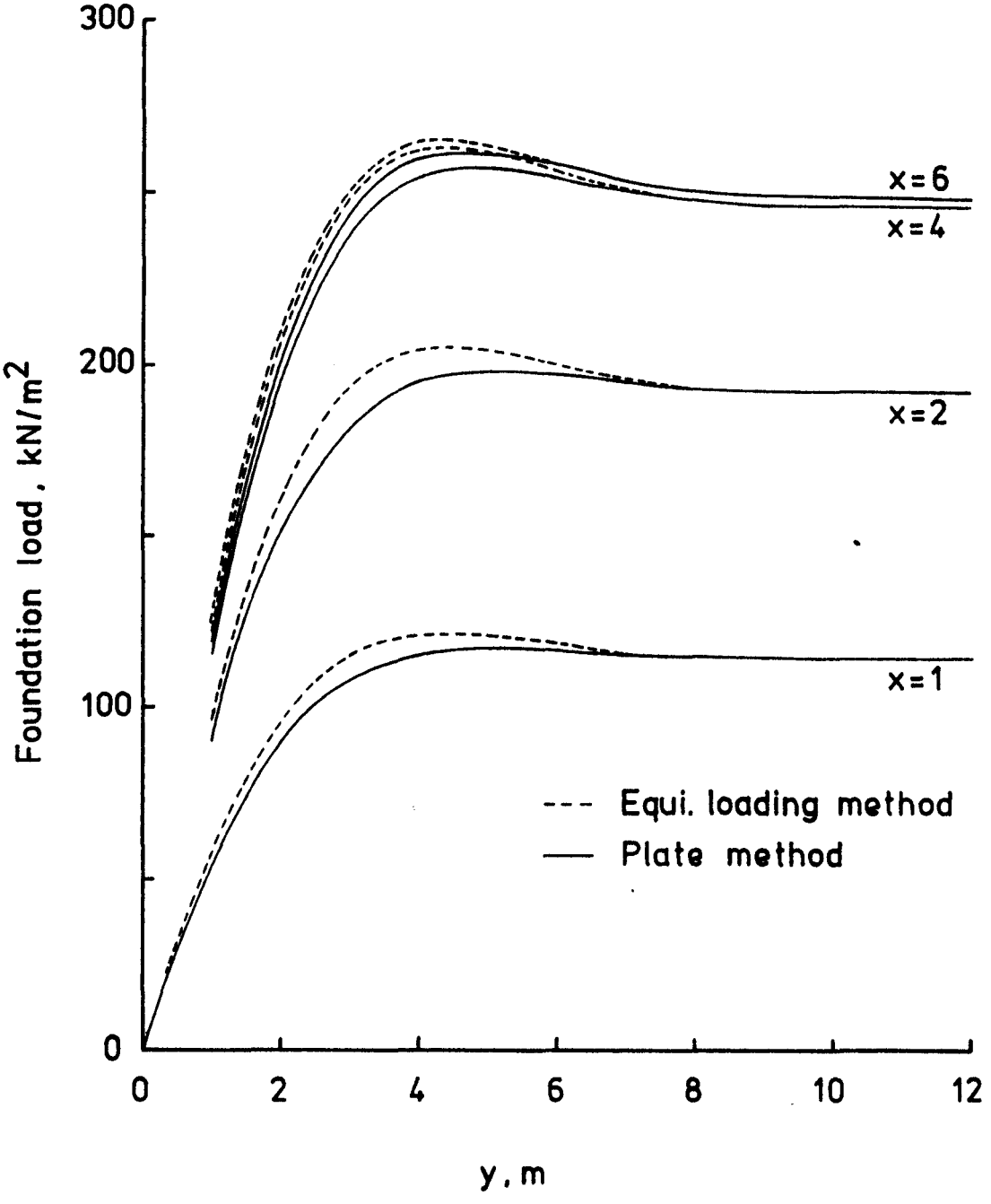

$$A_m = \frac{2q}{\pi D} \cdot \frac{1 - \cos m\pi}{m\left(\frac{m^4\pi^4}{a^4} + \frac{k}{D}\right)}$$

Only odd values of m can exist in the series because, when m is even, $A_m \equiv 0$. When m is odd

$$A_m = \frac{4q}{\pi D} \cdot \frac{1}{m\left(\frac{m^4\pi^4}{a^4} + \frac{k}{D}\right)}$$

so that

$$w_o = \frac{4q}{D\pi} \sum_{m=1,3,5\ldots}^{\infty} \frac{\sin \frac{m\pi x}{a}}{m\left(\frac{m^4\pi^4}{a^4} + \frac{k}{D}\right)} \qquad (5.58)$$

The second part of the solution can be obtained by substituting the series of Equ. (5.55) in Equ. (5.56) giving an ordinary differential equation in the functions Ym:

$$Y_m^{iv} - 2\frac{m^2\pi^2}{a^2} Y_m'' + \left(\frac{m^2\pi^2}{a^2} + \frac{k}{D}\right) Y_m = 0$$

This has a solution

$$Y_m = B_m e^{-\beta_m y} \cos \gamma_m y + C_m e^{-\beta_m y} \sin \gamma_m y \qquad (5.59)$$

in which

$$\beta_m = \frac{1}{\sqrt{2}} \left[\sqrt{\left(\frac{m^4\pi^4}{a^4} + \frac{k}{D}\right)} + \frac{m^2\pi^2}{a^2}\right]^{1/2}$$

$$\gamma_m = \frac{1}{\sqrt{2}} \left[\sqrt{\left(\frac{m^4\pi^4}{a^4} + \frac{k}{D}\right)} - \frac{m^2\pi^2}{a^2}\right]^{1/2}$$

The functions Ym vanish at $y = \infty$ and the deflections are given by $w = w_o$ so that the plate behaves like a uniformly loaded, simply supported strip on elastic foundation at $y = \infty$.

Substituting (5.58) and (5.59) in (5.55) it is seen that the deflections w satisfy the boundary conditions

$$(w)_{x=0,\, x=a} = 0 \quad , \quad \left(\frac{\partial^2 w}{\partial x^2}\right)_{x=0,\, x=a} = 0$$

To ascertain the values of the constants B_m and C_m the following boundary conditions can be applied to w at y = o

$$(w)_{y=0} = 0 \quad , \quad \left(\frac{\partial^2 w}{\partial y^2}\right)_{y=0} = 0$$

Then

$$B_m = - A_m \quad , \quad C_m = A_m \frac{m^2\pi^2}{a^2} \Big/ \sqrt{\frac{k}{D}}$$

Since B_m and C_m are proportional to A_m they too cannot exist for even values of m and thus we get finally the deflections w

$$w = \frac{4q}{D\pi} \sum_{m=1,3,5..}^{\infty} \frac{\sin \frac{m\pi x}{a}}{m\left(\frac{m^4\pi^4}{a^4} + \frac{k}{D}\right)} \left[1 - e^{-\beta_m y}\left(\cos \gamma_m y + \frac{\frac{m^2\pi^2}{a^2}}{\sqrt{\frac{k}{D}}} \sin \gamma_m y\right)\right] \qquad (5.60)$$

The load on the elastic foundation at any point (x,y) can be determined simply by multiplying this equation by the foundation modulus k.

5.4.2 Solution by the equivalent loading method

According to this method deflections along the centre line of the plate parallel to the y-axis are determined, assuming $a \to \infty$, two-dimensionally. These deflections are given by

$$w_c = \frac{q}{k} + e^{-\psi y}\left(C_1 \cos \psi y + C_2 \sin \psi y\right)$$

satisfying the condition $(w_c)_{y=\infty} = \frac{q}{k}$. Here $\psi = \left(\frac{k}{4D}\right)^{\frac{1}{4}}$. We have the simply supported conditions $(w_c)_{y=0} = (w_c'')_{y=0} = 0$ giving

$$C_1 = \frac{q}{k} \quad , \quad C_2 = 0$$

so that $w_c = \frac{q}{k}\left(1 - e^{-\psi y}\cos \psi y\right)$

This gives the loading on the foundation along the centre line as

$$k w_c = q\left(1 - e^{-\psi y}\cos \psi y\right) \qquad (5.61)$$

This loading can be placed on any lateral cross-section of the plate parallel to the x-axis, say y = L to give the deflection of that cross-section approximately. The equation for this deflection will be that of a beam on elastic foundation simply supported at its ends and uniformly loaded by $(kw_c)_{y=L}$. Now it will be remembered that when the load is q the deflections are given by the first series (w_o) in Equ. (5.60) for a beam.

Therefore, when the loading is $(kw_c)_{y = L}$ the deflections are

$$w_e = \frac{4 k w_c}{D\pi} \sum_{m=1,3,5..}^{\infty} \frac{\sin \frac{m\pi x}{a}}{m\left(\frac{m^4\pi^4}{a^4} + \frac{k}{D}\right)} \qquad (5.62)$$

This equation, when multiplied by k, will as usual give the foundation loads along any cross-section y = L.

The following numerical data were taken as an example:

Width of the plate, a	12, 14, 16 m
Uniform loading, q	230 kN/m^2
Flexural rigidity, D	1.2×10^7 kN-m
Foundation modulus, k	4.0×10^5 kN/m^3

The first three values are taken directly from the short face advancing situation considered before. k corresponds approximately to the ultimate foundation modulus of the anhydrite pack after setting for more than 6 weeks.

The loads on the foundation due to plate deflection were calculated from the edge x = o to the centre line of the plate x = $a/2$ at every metre by writing a simple computer program for both the methods. The results are plotted in Fig. 5.19-21. Foundation loads are shown to vary with y at different values of x.

5.4.3 A comparison of the two methods and limitations of the equivalent loading method

The foundation loading characteristics in Fig. 5.19-21 reveal the following salient features of the equivalent loading method as compared to the more rigorous plate method:

(a) The equivalent loading method is found to overestimate the foundation load slightly for all values of x, y ($x \neq o$, $y \neq o$) before reaching the steady state. Both the methods give virtually identical results when y is greater than nearly 7 m for all the three plate widths, i.e. when the edge y = o ('face') is more than 7 m distant. The over-estimation is a maximum of 6.6%, and occurs at y = 3 m along the longitudinal sections x = 1,2,3 m for all the plate widths. The error is least at the centre lines of the plate and is less than 1%.

(b) A peak load - hump - is found to occur in both the methods at a distance y = 5 m for the plate method and at y = 4 m for the equivalent loading method, which thus shows a somewhat early load peak. The wave-like load variation agrees with the load acceptance characteristics of the anhydrite centre pack. The distance y at which peak load occurs remains the same at the centre line and nearer the edges, i.e. for all values of $x > o$.

FIG.5.20 - FOUNDATION LOADS BY EQUIVALENT LOADING & PLATE METHODS - Plate width 14 m

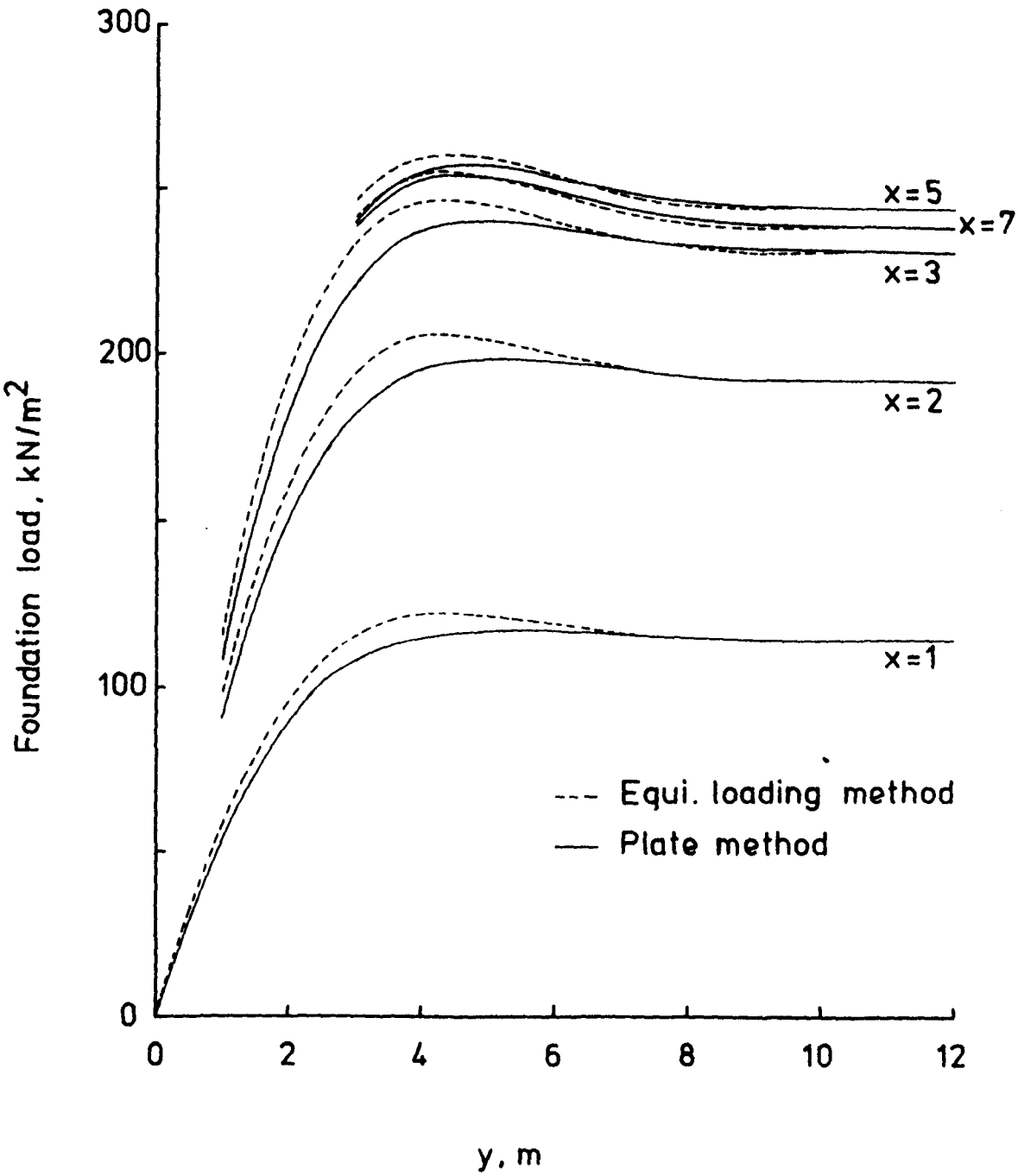

FIG.5.21 - FOUNDATION LOADS BY EQUIVALENT LOADING & PLATE METHODS - Plate width 16 m

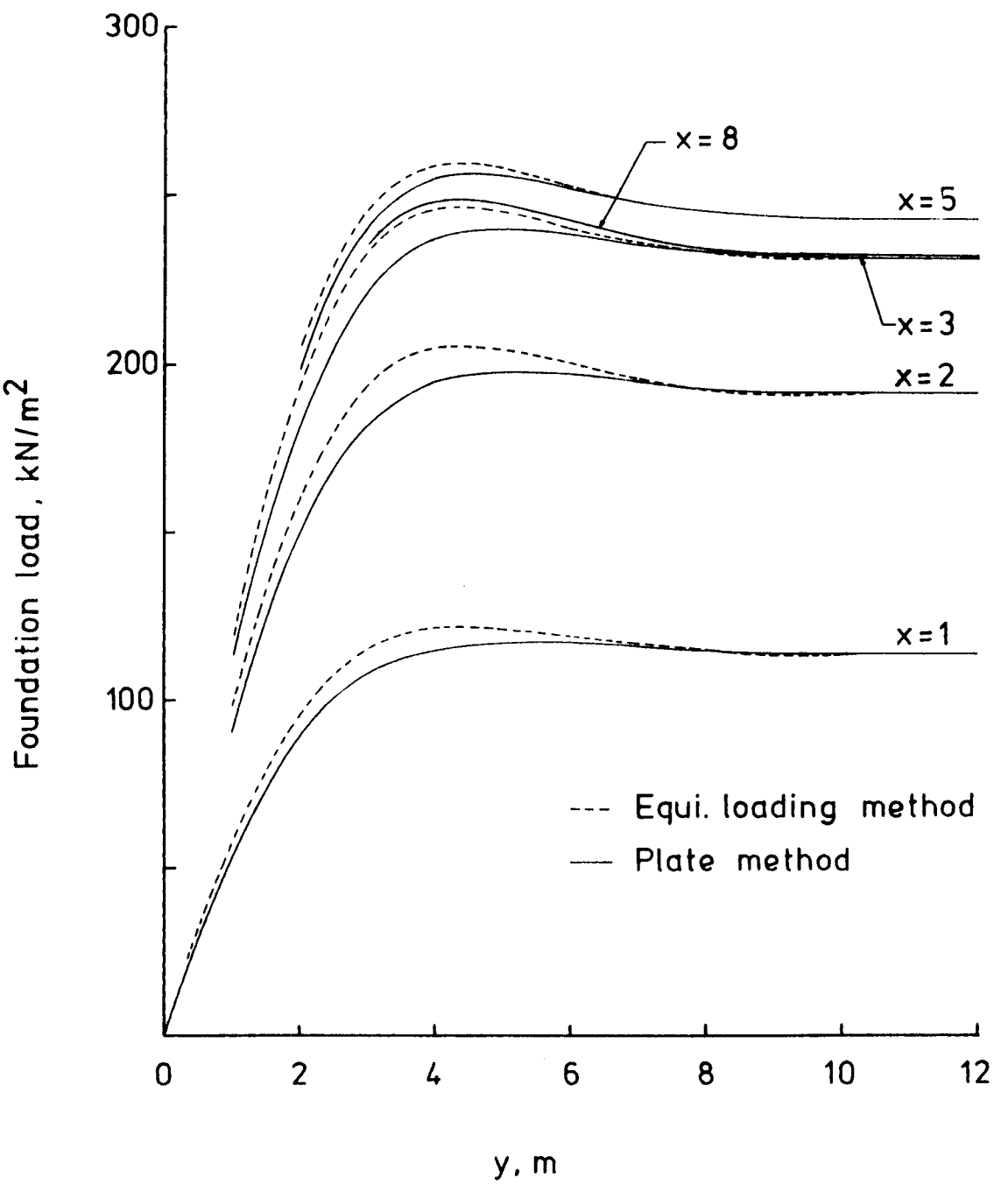

(c) Across any lateral section y = L, a hump is also seen to occur at x = 5 m from the longitudinal edges of the plate in the case of 14 and 16 m plate widths. This is the reason why the loading curves for x = 5 m lie uppermost, even above those for the centre lines x = 7 m and x = 8 m of the 14-m and 16-m plates. The equivalent loading method agrees with this behaviour, the distance being x = 4 m.

(d) In the steady state region the equivalent loading method gives slightly lower values (1 kN/m^2 or less) before giving the same values in the end as the plate method, as seen from some of the curves.

(e) Along the centre line x = 8 of the 16 m plate, both the methods give almost identical values, hence Fig.5.21 indicates only one curve for x = 8. Predictions by the equivalent loading method improve near the centre line, especially for wider plates.

(f) A slight rise again in the foundation load occurs at nearly 11 m in the steady state region, but the rise is too small to be noticeable (1 kN/m^2 or less) in most cases. (see Sec.5.3.4.1 in this connection).

It is thus seen that the equivalent loading method gives fairly reasonable estimates of foundation loads (and so plate deflections).

The example considered is that of a simply supported plate on elastic foundation which is much simpler that the situation of short face advancing with a centre pack. The main difference is that the foundation in the form of an anhydrite pack comes into existence only after a certain pack-free initial deflection occurs in the roof. This initial deflection, denoted by δ_1 in Equ. (5.48) of Sec.5.3.1, was obtained from longitudinal considerations at Point A (see Fig.5.9), so that δ_1, in fact, corresponds to an infinite heading width. When the loading has a finite width, however, δ_1 would be somewhat smaller. Also δ_1 would vary from one ribside to another and would be a maximum at the centre of the heading.

In Equ. (5.48) δ_1 has been taken as a constant which means that the occurrence of a uniform roof deflection has been assumed in the pack region in the lateral consideration. Since it is not necessary to take into account the initial deflections in the roadway region and ribside, the roof across the entire heading section was then assumed to deflect initially uniformly over the pack region and curvilinearly over the roadway and ribside. This form would entail introducing some errors, especially at the edges of the pack, in estimating pack load. The exact form of δ_1, on the other hand, is impossible to determine.

If in the longitudinal analysis it was seen that the ultimate deflection or deflection in the steady state, when the face was sufficiently distant, was greater than the pack-free deflection δ_1, errors due to assuming a uniform form would be minimised. This was essential to see, since over an anhydrite pack section deflections were found to

reduce (roof lifting) with face advance in the steady state region. For this, reference may be made to the output of the computer programme in Appendix II (deflections at A), in which it is seen that the deflection in the last stage is greater than the initial deflection. If this had not been the case, the roof would have lifted more than the initial pack-free position and the analysis by lateral considerations would have given negative pack loads.

δ_1 is seen to have three values for the three rates of face advance.

Thus it may be concluded that since the initial deflections δ_1 are assumed to be uniform in the pack region and of the same value for all the three heading widths of 12, 14 and 16 m, subsequent additional deflections over the pack after its erection will be somewhat underestimated, especially near pack edges. On the contrary, the equivalent loading method overestimates deflections and hence pack loads, so that it was likely that there would be some compensation. Central values of pack load would be more and more reliable as the heading width increased.

5.5 Conclusion

The equivalent loading method was found as an approximate approach to elastostatic analysis of the short face advancing situation for three probable heading widths. A comparison of this method with the rigorous plate method indicates that deflections of the plate on an elastic foundation are somewhat overestimated. The maximum error introduced was found

to be 6.6% in the case of a simpler parallel example of a rectangular semi-infinite plate on an elastic foundation, the edges being simply supported.

A compensating factor to this overestimation was that the initial deflection in the face area prior to pack setting (elastostatic face convergence) induced somewhat lower estimation of deflections in the pack region, as explained. With due consideration of the limitations of the equivalent loading method, the following conclusions can be drawn:

1. The anhydrite centre pack is found to build up load very quickly to a peak value which gradually falls to a steady state value. This initial build up of a hump and later fall is found to agree with observations underground by several workers. The load is found to increase with heading width and a reduced face advance. The values of load estimated are quite small (the maximum peak value is 392 kN/m^2) because of the small depth of the nether roof (10 m) below the bed separation cavity which is to be supported by the pack,and because a large part of the roof deflections take place before pack placement. The pack is found to be strong enough to take the load in all the three heading widths considered.

2. Loads at the edge of the pack are lower than at the centre because the roof deflections are higher at the centre. The pack load distribution is thus not uniform across the width of the pack.

3. The abutment pressure on the ribside is influenced by the pack load in that it shows a fall with higher loads accepted by the pack. The peak abutment pressure is found to be 12-15% higher than the depth pressure, which is quite small. This is because of the small size of the opening (12 to 16 m).

4. The maximum positive bending moment occurs in the roadway roof nearer the pack edge. Comparable negative moments occur 1.2 to 1.4 m inside the solid coal region.

In all the cases of heading widths and rates of advance, the maximum roadway tensile stress is found to exceed the average tensile strength of some Durham rocks. This would be expected, since the elastostatic analysis does not consider roadway supports and is merely an indication that steel supports in the roadway would be necessary.

Because of the lower loads accepted by the anhydrite pack in narrower headings, the roof has to be more self-supporting than in wider ones. This is the reason why lower maximum tensile stress values occur in the roadway

of a wider heading. This is a point in favour of wider headings. Excessively wide headings will, however, induce further bed separation in the roof, bringing greater loads on the roof layers and increasing the tensile stress. The qualitative assessment that lower tensile stresses in the roadway are encountered in wider headings is thus true only if no further bed separation takes place.

5. With better pack load acceptance there is some relief in the abutment pressure, reducing the maximum shear force at the coal edge. This might be of some advantage in decreasing floor heave. A detailed analysis for floor heave has been made in Chapter 7.

6. The rate of face advance influences the bending moment more significantly than it does the shear force. It also influences the pack load but its influence falls with increasing heading width. Lower rates of advance appear to be beneficial, if they can be adopted without detriment to productivity. The effect of rate of advance considered in this Chapter is purely elastostatic because the roof behaviour depends on the setting properties of anhydrite. This analysis does not include any viscoelastic or creep effects. In this connection it is important to note that the loading situation on packs reaches the steady state quite quickly, both in terms of time and distance and the

rate of advance is thus important, viscoelastically, for a short initial life of the heading only.

7. Judging by the load acceptance characteristic of pack obtained in this analysis and underground by other workers, the theory of beams on elastic foundations can be used as a possible explanation for the occurrence of peak pressure in the back abutment zone of a longwall face.

* * *

CHAPTER 6

Short face advancing with a centre pack of conventional non-setting materials

CHAPTER 6

Short face advancing with a centre pack of conventional non-setting materials - an elastostatic analysis

6.1 Introduction

In order to assess the advantages gained by using an anhydrite pack instead of a conventional non-setting pack and also to study the possibility of using a more compressible pack in the method of short face advancing with a central pack support, it was decided to analyse this situation elastostatically, introducing conventional packs. The influence of pack compressibility on the variation of the earlier factors of Chapter 5, pack load etc., was also studied to define the benefits of a stiffer pack. As in the case of anhydrite centre packs, the analysis was done longitudinally and laterally.

The basic difference between a material like anhydrite and a non-setting one like dirt packs, wood chocks, etc., is the setting property of the former, by virtue of which it hardens and becomes less compressible with time, as given by Equ.(5.1). The usual non-setting materials are much more compressible, as seen in Chapter 2, and also their modulus of elasticity does not change with time in the sense of setting. As observed in the previous Chapter, the foundation modulus of each anhydrite pack section acquires different values, k_{11}, k_{12}, etc. with face advance, while a conventional pack would have the same value k_1 at all stages of advance (assuming the load-yield characteristic of a conventional pack to be linear).

6.2 Roof deflection equations for various stages of face advance

6.2.1 Longitudinal analysis

Equations for the deflection of the nether roof were again developed along the longitudinal section of the heading, taking initially an infinite pack width. The mechanical model for the nether roof with regard to bed separation was the same as in the previous case of anhydrite packs. Stage (1) represents the maximum pack-free advance of the short face and, therefore, coincides with the earlier analysis for anhydrite packs (see Fig.5.4). The deflection equations are thus identical to Equ. (5.39) which are reproduced here for convenience:

Stage (1)

$$\left.\begin{aligned} v_1 &= \frac{q_1+q_2}{k_2} + e^{-\alpha x}\left(C_1 \cos \alpha x + C_2 \sin \alpha x\right) \\ v_2 &= \frac{q_2}{24 D_2} x^4 + C_3 x^2 + C_4 \end{aligned}\right\} \qquad (6.1)$$

where the different symbols have the same meanings as given in Chapter 5.

In stage (2) a pack section is erected and the face is advanced further. From this stage onward the pack modulus remains unchanged with face advance and we thus get a series of pack sections, all of the same modulus. The roof deflection before placement of each pack section is, however, different from those for the neighbouring sections until the face is sufficiently far away. Hence it was necessary to develop a differential equation for deflections

over each pack section separately, just as in the case of anhydrite packs.

As seen from Appendix I the deflection over a pack section is given by expressions of the form of damped oscillations or damped waves, the parameters β_1 , β_2, etc. occurring in the exponential functions being termed damping coefficients. In the case of an anhydrite pack section, the deflection comprises a number of such waves, the number being higher the farther the face is. These damping coefficients determine the distance necessary to damp a wave to reach the steady state. From the nature of the deflection equations for anhydrite packs it is impossible, theoretically, to predict such a distance, but for a conventional pack, for which the damping coefficient remains constant at a value β whatever the face advance, this distance is given by $5/\beta$[33]. Like β_1, β_2, etc. β is defined by

$$\beta = \left(\frac{k_1}{4 D_2}\right)^{1/4}$$

Considering the range of foundation moduli k_1 taken for a numerical analysis of this problem (given later in this Chapter), it was decided that the longitudinal analysis would have to be carried out up to stage (9) of face advance, the unit advance, width of the trunk roadway and working area at the face remaining the same.

Stages (1) to (5) are shown in Fig. 6.1. Then for the position of the y-axis indicated, the deflections v_3, v_4, etc. in stage (2) can be written down as

FIG.6.1 - ROOF DEFLECTIONS ETC. ALONG THE HEADING SECTION WITH CONVL. CENTRE PACKS

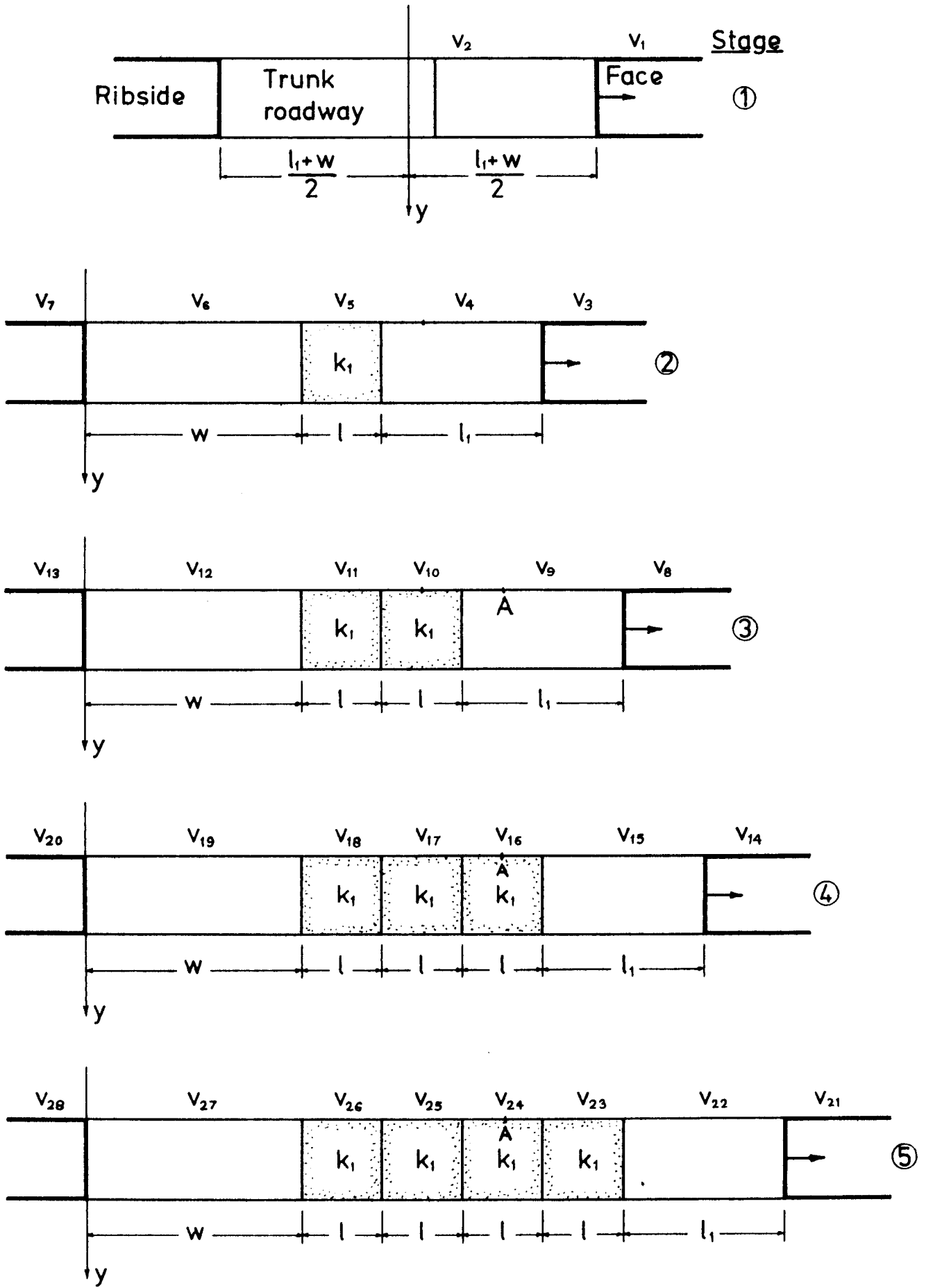

Stage (2):

$$
\begin{aligned}
v_3 &= \frac{q_1+q_2}{k_2} + e^{-\alpha x}\left(C_5 \cos \alpha x + C_6 \sin \alpha x\right) \\
v_4 &= \frac{q_2}{24 D_2} x^4 + C_7 x^3 + C_8 x^2 + C_9 x + C_{10} \\
v_5 &= \frac{q_2}{24 D_2}\left(x - \frac{\ell_1+w}{2}\right)^4 + C_3\left(x - \frac{\ell_1+w}{2}\right)^2 + C_4 \\
&\quad + e^{-\beta x}\left(C_{11} \cos \beta x + C_{12} \sin \beta x\right) \\
&\quad + e^{\beta x}\left(C_{13} \cos \beta x + C_{14} \sin \beta x\right) \\
v_6 &= \frac{q_2}{24 D_2} x^4 + C_{15} x^3 + C_{16} x^2 + C_{17} x + C_{18} \\
v_7 &= \frac{q_1+q_2}{k_2} + e^{\alpha x}\left(C_{19} \cos \alpha x + C_{20} \sin \alpha x\right)
\end{aligned}
\qquad (6.2)
$$

In stage (3), a second pack section is placed and the face is advanced further, causing compression of the first section once more and of the second section for the first time. The differential equations for these two sections are then

Section (1):

$$D_2 \frac{d^4 v_{11}}{dx^4} = q_2 - k_1 (v_{11} - v_5) - k_1 (v_5 - v_2)$$

$$= q_2 - k_1 (v_{11} - v_2)$$

Section (2):

$$D_2 \frac{d^4 v_{10}}{dx^4} = q_2 - k_1 (v_{10} - v_4)$$

Their solutions are written with the rest of the deflection equations for stage (3):

Stage (3)

$$\left.\begin{aligned}
v_8 &= \frac{q_1 + q_2}{k_2} + e^{-\alpha x} (C_{21} \cos \alpha x + C_{22} \sin \alpha x) \\
v_9 &= \frac{q_2}{24 D_2} x^4 + C_{23} x^3 + C_{24} x^2 + C_{25} x + C_{26} \\
v_{10} &= v_4 + e^{-\beta x} (C_{27} \cos \beta x + C_{28} \sin \beta x) \\
&\quad + e^{\beta x} (C_{29} \cos \beta x + C_{30} \sin \beta x)
\end{aligned}\right\} \qquad (6.3)$$

$$
\left.
\begin{aligned}
v_{11} &= \frac{q_2}{24 D_2}\left(x - \frac{l_1 + w}{2}\right)^4 + C_3\left(x - \frac{l_1 + w}{2}\right)^2 + C_4 \\
&\quad + e^{-\beta x}\left(C_{31}\cos\beta x + C_{32}\sin\beta x\right) \\
&\quad + e^{\beta x}\left(C_{33}\cos\beta x + C_{34}\sin\beta x\right) \\
v_{12} &= \frac{q_2}{24 D_2}x^4 + C_{35}x^3 + C_{36}x^2 + C_{37}x + C_{38} \\
v_{13} &= \frac{q_1 + q_2}{k_2} + e^{\alpha x}\left(C_{39}\cos\alpha x + C_{40}\sin\alpha x\right)
\end{aligned}
\right\} \qquad (6.3)
$$

Further deflection equations could similarly be written down up to stage (9). The integration constants, C_1, C_2, etc. would be 244 for all the stages together which could be determined, as before, by applying continuity conditions (5.27) in terms of deflections, slopes, bending moments and shear forces to any two neighbouring deflection regions in each stage.

The assumptions and data for a numerical analysis of this situation were taken again to correspond to the conditions at Dawdon Colliery (see Sec. 5.2.4). A suitable computer program was written as in Appendix III

for applying continuity conditions to Equ. (6.1-3) and all equations up to stage (9) to give the 244 integration constants and obtain finally the deflections and pack loads at Point A (Fig.6.1) as before.

Since this pack foundation modulus does not change with time, and hence face advance, the elastostatic influence of rate of advance could not be included. The pack elastic modulus was varied from 3.5×10^4 to 1.75×10^5 kN/m^2, taking five values at equal intervals of 3.5×10^4 kN/m^2. The least value of 3.5×10^4 kN/m^2 was approximately estimated for a stone pack tested by Barraclough et al.[10] (see Chapter 2, Fig 2.2(b). The rest of the values are just multiples of this value and do not necessarily belong to any particular pack type. This was done to study the influence of varying pack compressibility.

6.2.2 Lateral considerations

A lateral analysis of this situation is comparatively simple when compared with the case of anhydrite packs. After an initial pre-setting deflection δ, compressions of the pack take place with its foundation modulus remaining constant at a value k_1. At infinite advance of the face the roof settles down over the pack section under consideration (Point A), causing deflections v_3 in the pack region in addition to the deflection δ. The roof deflections in the roadways and the ribside are v_2 and v_1 respectively. δ is the elastostatic convergence at the face and has five values corresponding to the five pack foundation moduli. These are the first values in the output of the computer program of Appendix III.

The differential equation for the deflections v_3 at Point A for

infinite face advance will be

$$D_2 \frac{d^4 v_3}{dx^4} = q_2 - k_1 (v_3 - \delta)$$

It has the solution

$$v_3 = \frac{q_2}{k_1} + \delta + A_1 \cosh \beta x \cos \beta x + A_2 \sinh \beta x \sin \beta x \qquad (6.4)$$

by symmetry of the heading about the pack centre, the y-axis being positive downward through the pack centre. For an infinite pack width, the last two functional terms in the solution vanish for x = o so that

$$v_3 = \frac{q_2}{k_1} + \delta$$

and for a finite pack width we have for x = o

$$v_3 = \frac{q_2}{k_1} + \delta + A_1$$

Thus A_1 acts as a correction term for the deflections at the pack centre when the pack width is finite and the two functional terms for the deflections elsewhere in the pack.

The deflection equations for the roadway and ribside are written down as usual:

$$\left.\begin{aligned} \text{Ribside:} \quad & v_1 = \frac{q_1 + q_2}{k_2} + e^{-\alpha x} (B_1 \cos \alpha x + B_2 \sin \alpha x) \\ \text{Roadway:} \quad & v_2 = \frac{q_2}{24 D_2} x^4 + B_3 x^3 + B_4 x^2 + B_5 x + B_6 \end{aligned}\right\} \qquad (6.5)$$

It can thus be seen that the lateral analysis in the case of conventional centre packs is much simpler than for the earlier case of anhydrite packs. It was not necessary to resort to the equivalent loading method to obtain the ultimate roof deflections because the pack foundation modulus k_1 remains constant.

The integration constants A_1, A_2, B_1-B_6 in the deflection equations (6.4-5) could be determined by applying the usual continuity conditions to give sets of 8 simultaneous equations. A similar computer program was written to obtain the variation of pack load, ribside load, bending moments, etc. for the five pack moduli mentioned and for the three heading widths 12, 14 and 16 m.

6.3 Results and Discussion

6.3.1 Pack load variation with face advance

The acceptance of load by a conventional pack is seen to be of the form shown in Fig. 6.2. These load characteristics were obtained by longitudinal analysis. Lateral considerations would yield similar curves, as was the case with anhydrite. Only the steady state or ultimate loads were hence calculated for the three heading widths by lateral analysis.

The load build up is observed to be slower for conventional non-setting packs than for anhydrite packs. The figure shows that the load builds up to a flat peak slowly and later falls gradually (cf. Fig.5.10-12). For low values of pack moduli the peak is hardly noticeable and occurs at a greater distance from the short face than for higher moduli.

FIG.6·2 - PACK LOAD VARIATION WITH FACE ADVANCE

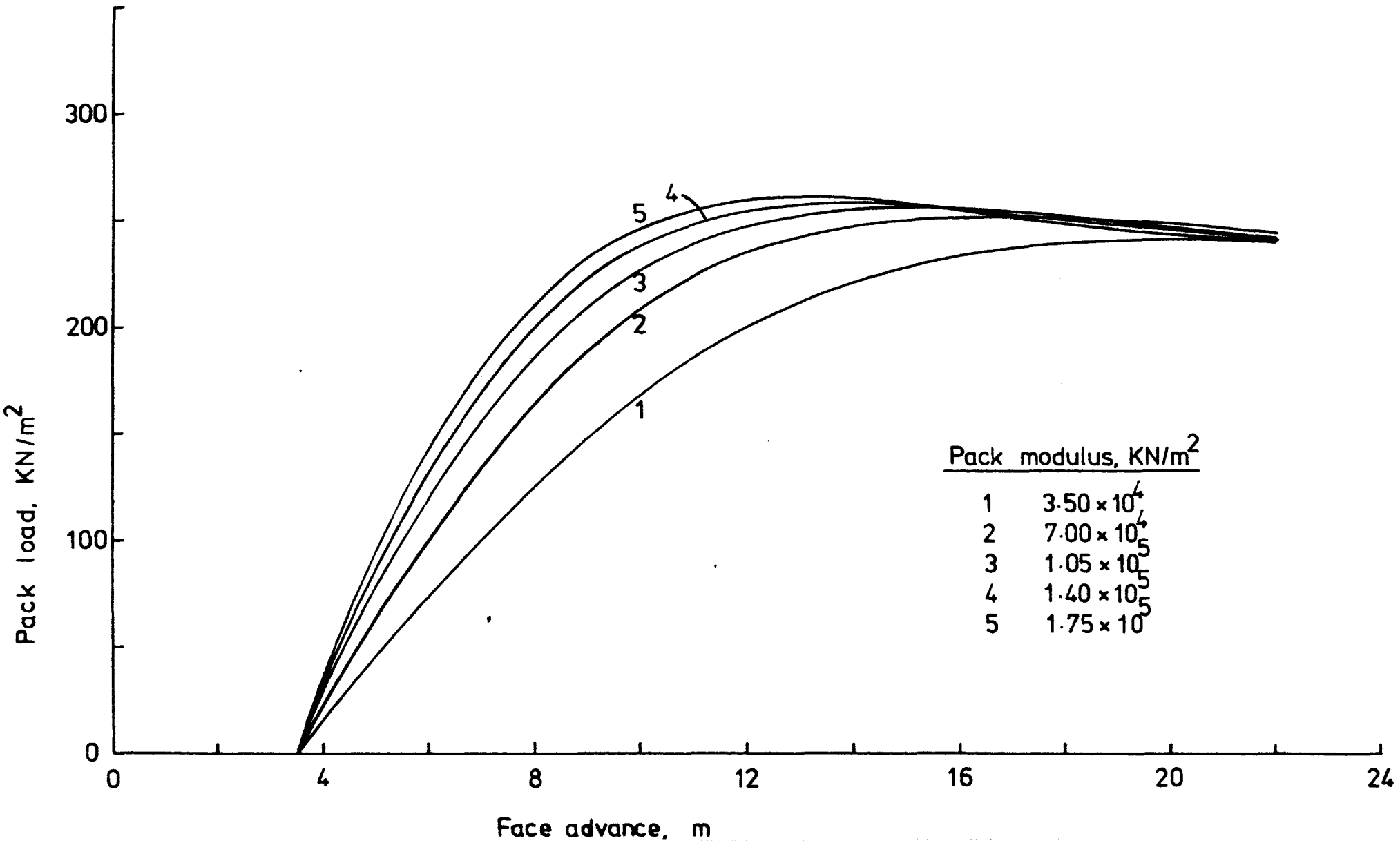

As mentioned earlier in Sec. 6.2.1, it is possible to predict the distance at which the steady state would be reached. This distance, $5/\beta$, varies between 20 and 30 m for the five values of pack moduli considered as given in Table 6.1.

The ultimate loads obtained by lateral analysis for the three heading widths and five moduli are given in Table 6.2. Lower pack moduli and narrower heading widths give very low values of ultimate pack load as in the Table, indicating that the strata have to be virtually self-supporting. Conventional packs of low moduli like stone packs or wood chocks serve hardly any purpose by way of support in the short face advancing method.

6.3.2 Ultimate load distribution on pack and ribside

Fig 6.3-5 indicate the ultimate or steady state load distribution in the pack and ribside for the three heading widths of 12, 14 and 16 m respectively. The ribside loading looks similar to the anhydrite case (cf. Fig. 5.13-15), but the loading on the pack is more flatly distributed. Pack load increases with the heading width and pack modulus. Overall, the pack load is found to increase and the ribside abutment pressure to fall with rising pack modulus. The abutment peak is greater for all values of moduli than for anhydrite (because anhydrite accepts load better), the highest value being about 25% greater than the depth pressure which occurs in case of the 16-m heading with the pack modulus of 3.5×10^4 kN/m^2. The corresponding highest value was found to be about 15% greater than the cover load for anhydrite packs. This is a point in favour of anhydrite as a packing medium in that it reduces the unevenness of loading across the roadway.

TABLE 6.1

Face Advance for reaching steady state load on conventional packs during short face advancing

Pack Modulus kN/m^2	Face advance for steady state m
3.50×10^4	30.5
7.00×10^4	26.0
1.05×10^5	23.0
1.40×10^5	21.5
1.75×10^5	20.5

TABLE 6.2

Steady state loads for different heading widths
(Conventional packs)

Heading width m	Pack Modulus kN/m^2	Steady State load kN/m^2
12	3.50×10^4	15
	7.00×10^4	40
	1.05×10^5	68
	1.40×10^5	95
	1.75×10^5	120
14	3.50×10^4	39
	7.00×10^4	80
	1.05×10^5	116
	1.40×10^5	146
	1.75×10^5	172
16	3.50×10^4	70
	7.00×10^4	122
	1.05×10^5	160
	1.40×10^5	189
	1.75×10^5	212

FIG.6.3 - ULTIMATE LOADING ON CONVL. PACK & RIBSIDE

Heading width 12 m

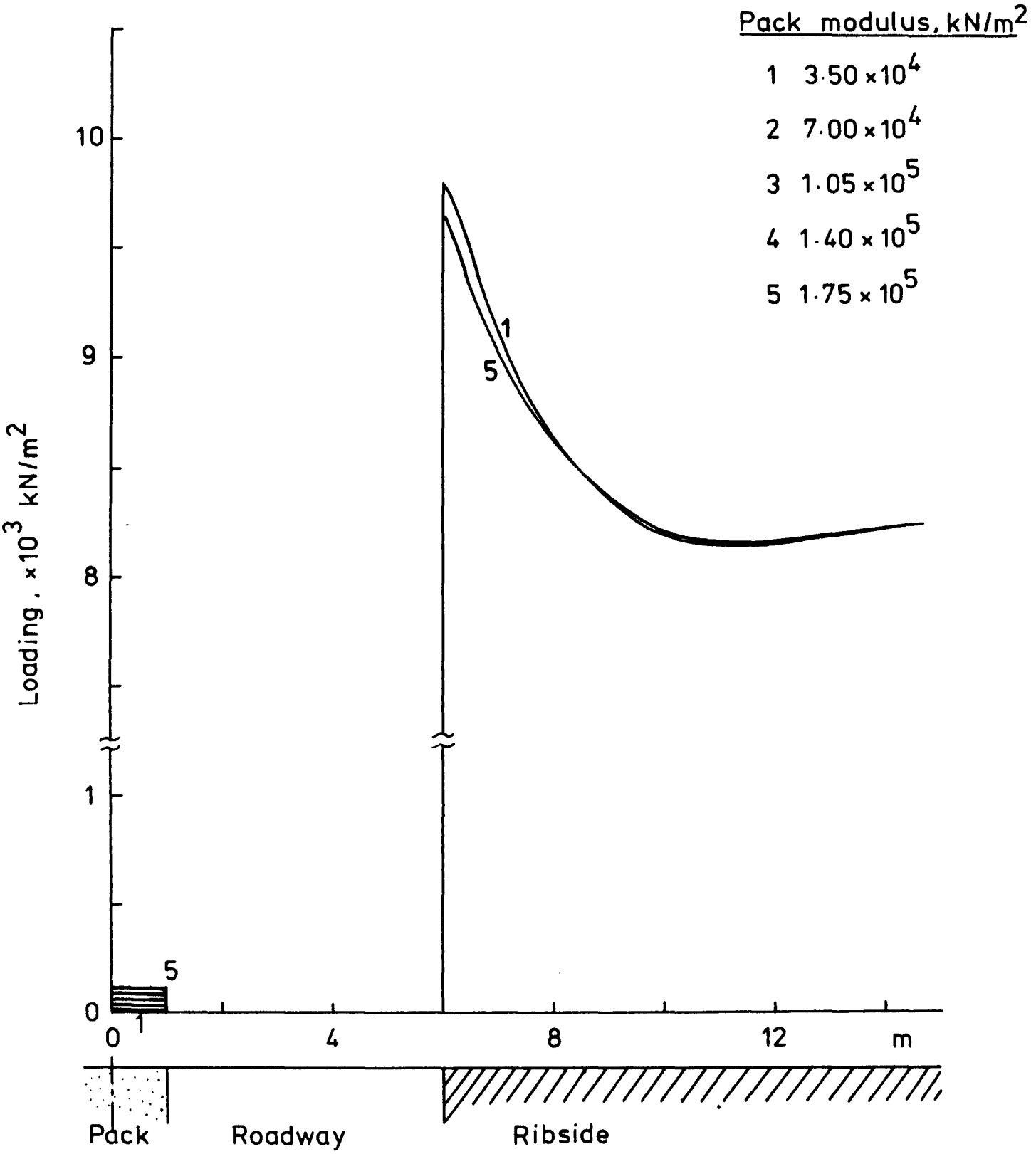

FIG.6·4 - ULTIMATE LOADING ON CONVL. PACK & RIBSIDE

Heading width 14 m

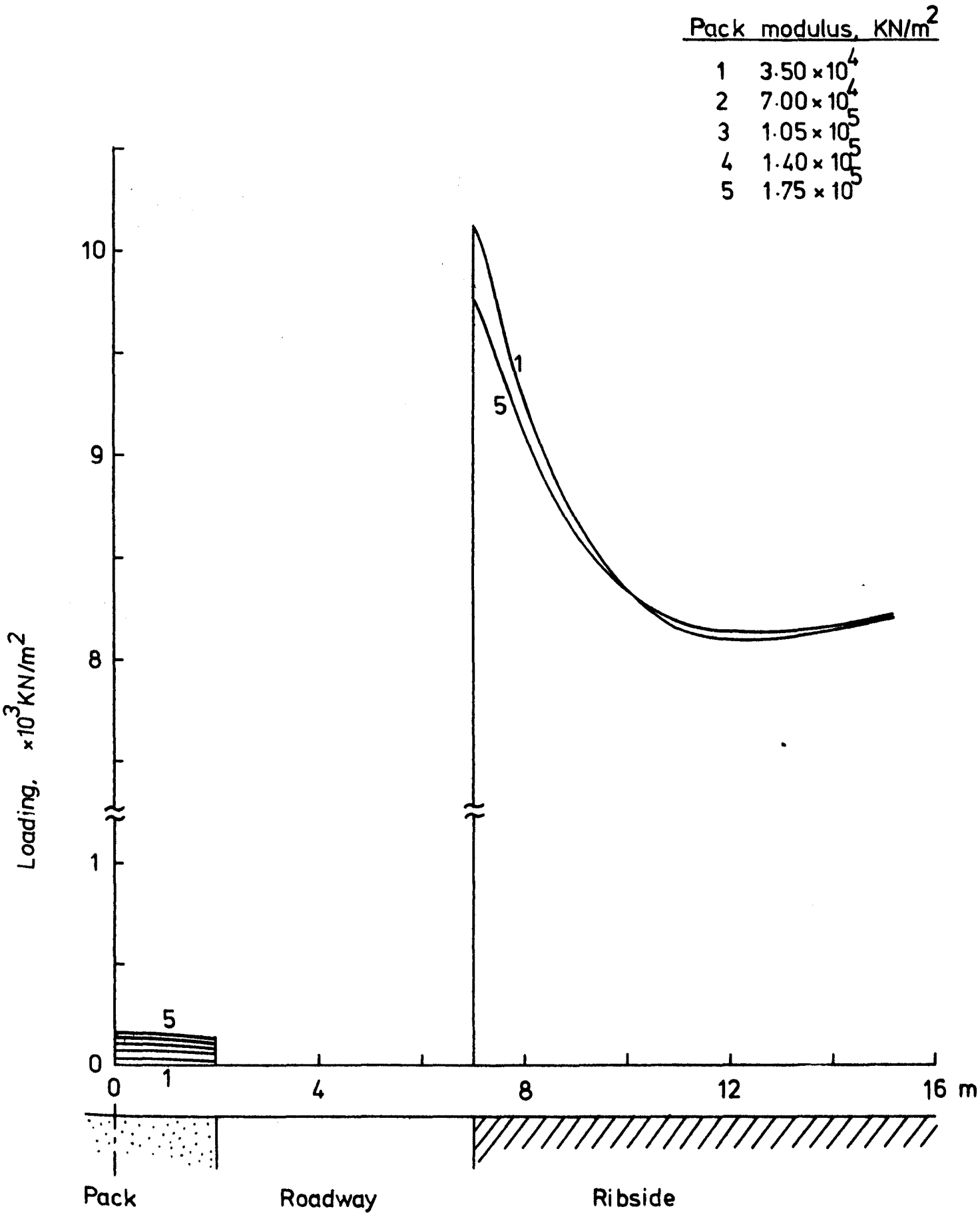

FIG.6.5 - ULTIMATE LOADING ON CONVL. PACK & RIBSIDE

Heading width 16m

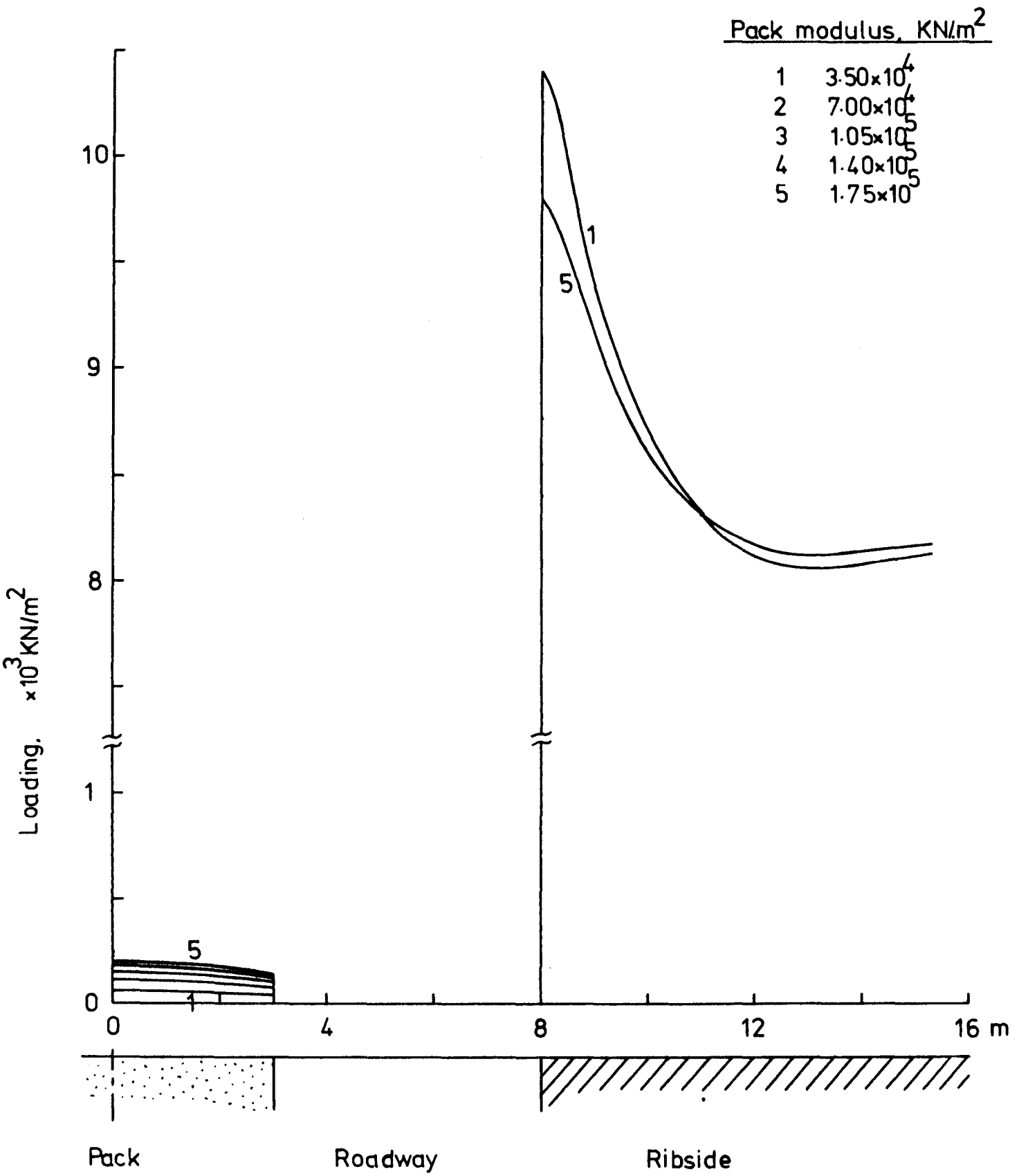

6.3.3 Variations of pack load and ribside abutment pressure with pack modulus

The ultimate loads on the pack centre and the ribside abutment peak pressure are plotted against pack modulus in Figs. 6.6 and 6.7 respectively. Pack load is seen to increase considerably with pack modulus and heading width, with very low values of load occurring at the lowest modulus of 3.5×10^4 kN/m^2. For a 12-m heading a fourfold increase in pack modulus increases the pack load 8.0 times, which in 14-m and 16-m headings rises 4.4 and 3.0 times. Thus a centre pack will be more effective in narrower headings if it is stiffer.

The ribside abutment pressure of Fig.6.7 and Table 6.3 shows a fall with increasing pack modulus, obviously because of an improvement in pack load acceptance. The fall is slower for smaller heading widths. In fact, for the 12-m case the fall is almost negligible. This again indicates that the behaviour of the nether roof is less dependent on the stiffness of the pack in narrower headings.

6.3.4 Ultimate bending moments and shear forces

The pack modulus is found to influence the roof bending picture as is seen from Figs. 6.8-10, in which curve 1 corresponds to the pack modulus of 3.5×10^4 kN/m^2 and curve 5 is for 1.75×10^5 kN/m^2. The curves for the rest of the values lie between these two and are not shown plotted. Bending moments increase with the heading width and vary inversely as the pack modulus. The influence of pack modulus is very pronounced for higher heading widths.

FIG.6·6 - VARIATION OF ULTIMATE PACK LOAD WITH MODULUS OF ELASTICITY

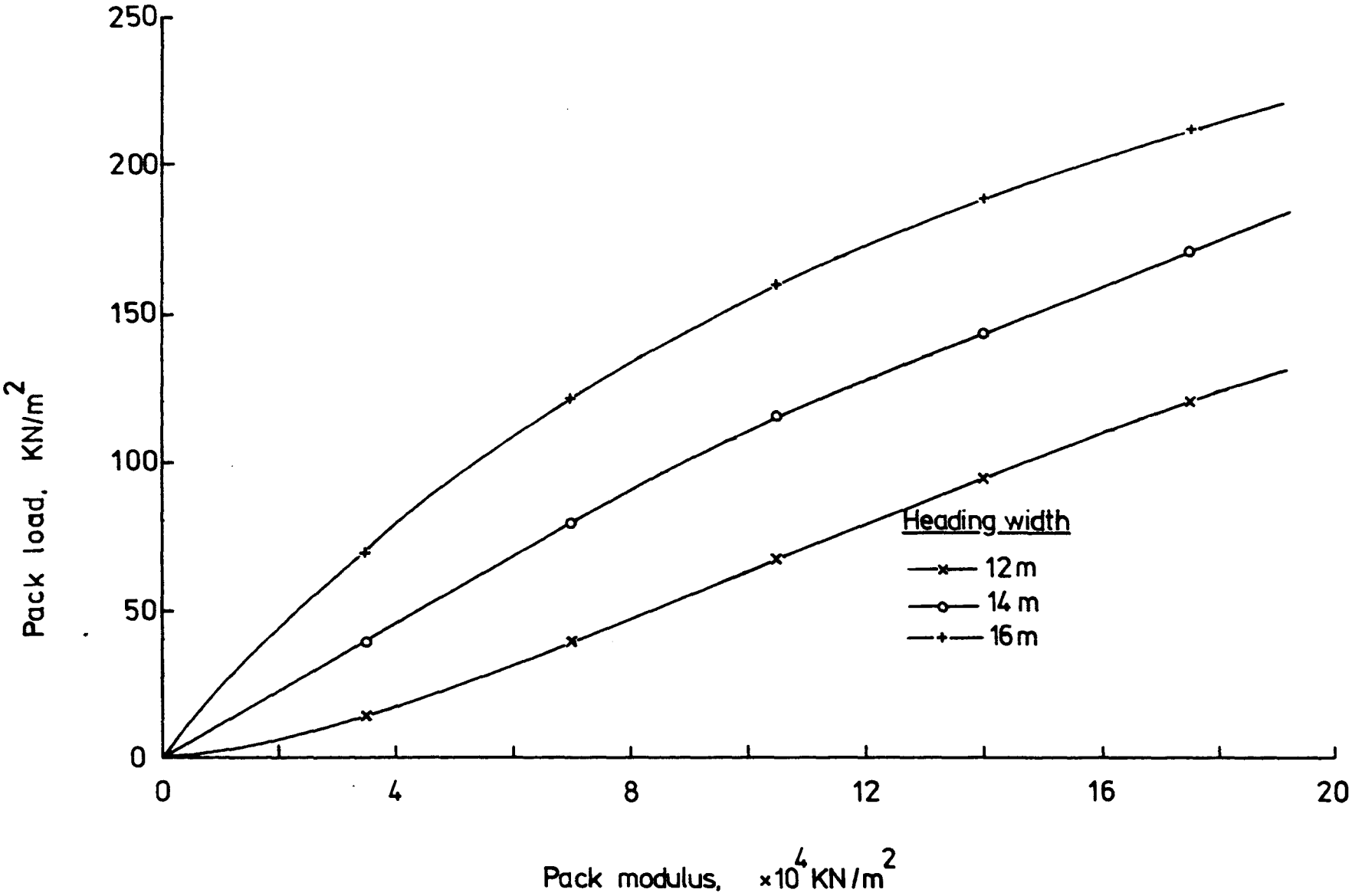

FIG.6·7 - VARIATION OF RIBSIDE ABUTMENT PRESSURE WITH PACK MODULUS OF ELASTICITY

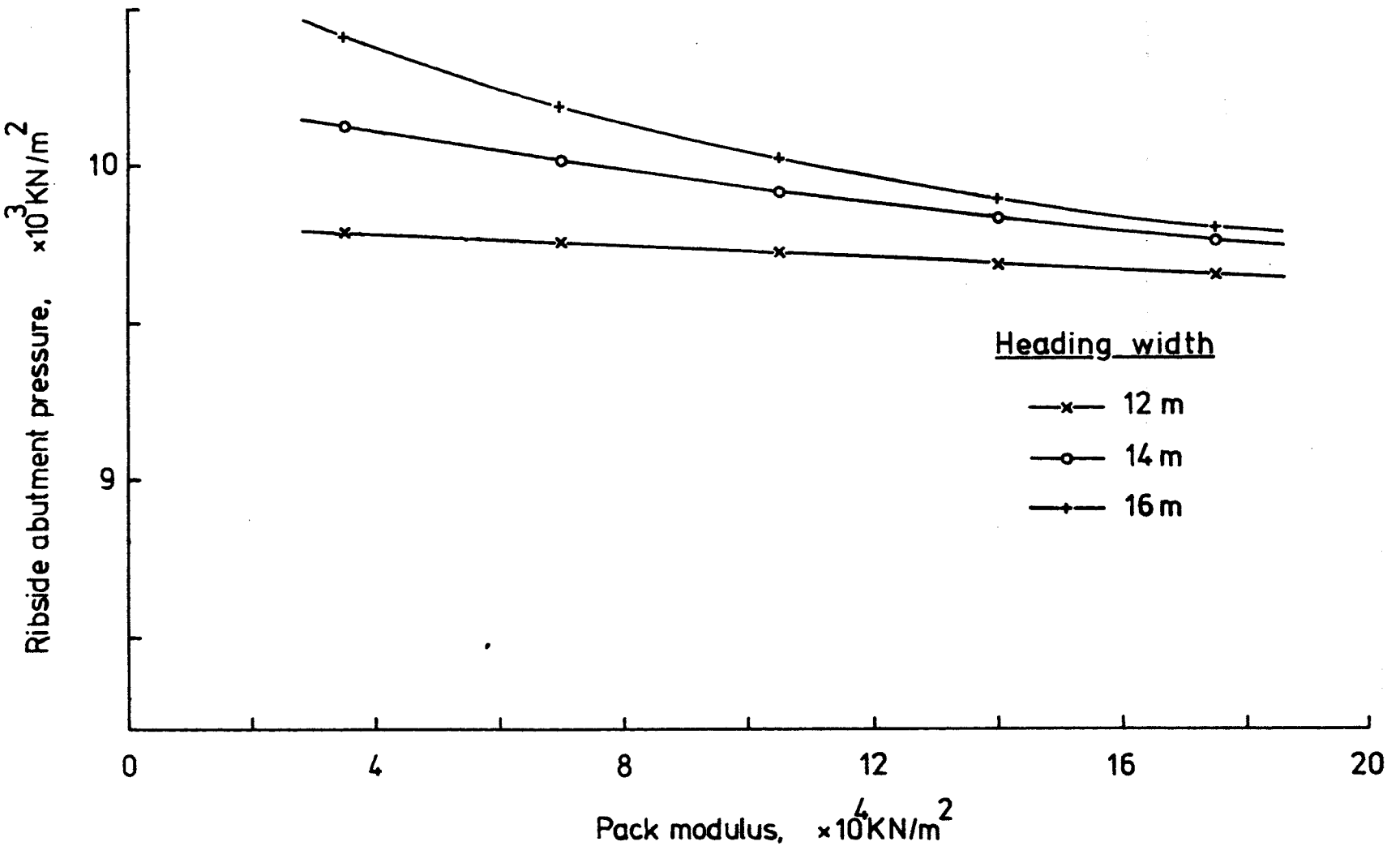

TABLE 6.3

Peak abutment pressure on the ribside during short face advancing using conventional packs

(Depth pressure - 8288 kN/m^2)

Heading width m	Pack modulus kN/m^2	Abutment pressure kN/m^2
12	3.50×10^4	9,786
	7.00×10^4	9 753
	1.05×10^5	9,718
	1.40×10^5	9,683
	1.75×10^5	9,650
14	3.50×10^4	10,125
	7.00×10^4	10,014
	1.05×10^4	9,916
	1.40×10^4	9,833
	1.75×10^4	9,764
16	3.50×10^4	10,403
	7.00×10^4	10,181
	1.05×10^5	10,019
	1.40×10^5	9,897
	1.75×10^5	9,801

FIG.6.8 - ULTIMATE BENDING MOMENTS & SHEAR FORCES IN THE ROOF (CONVL. PACKS)

Heading width 12 m

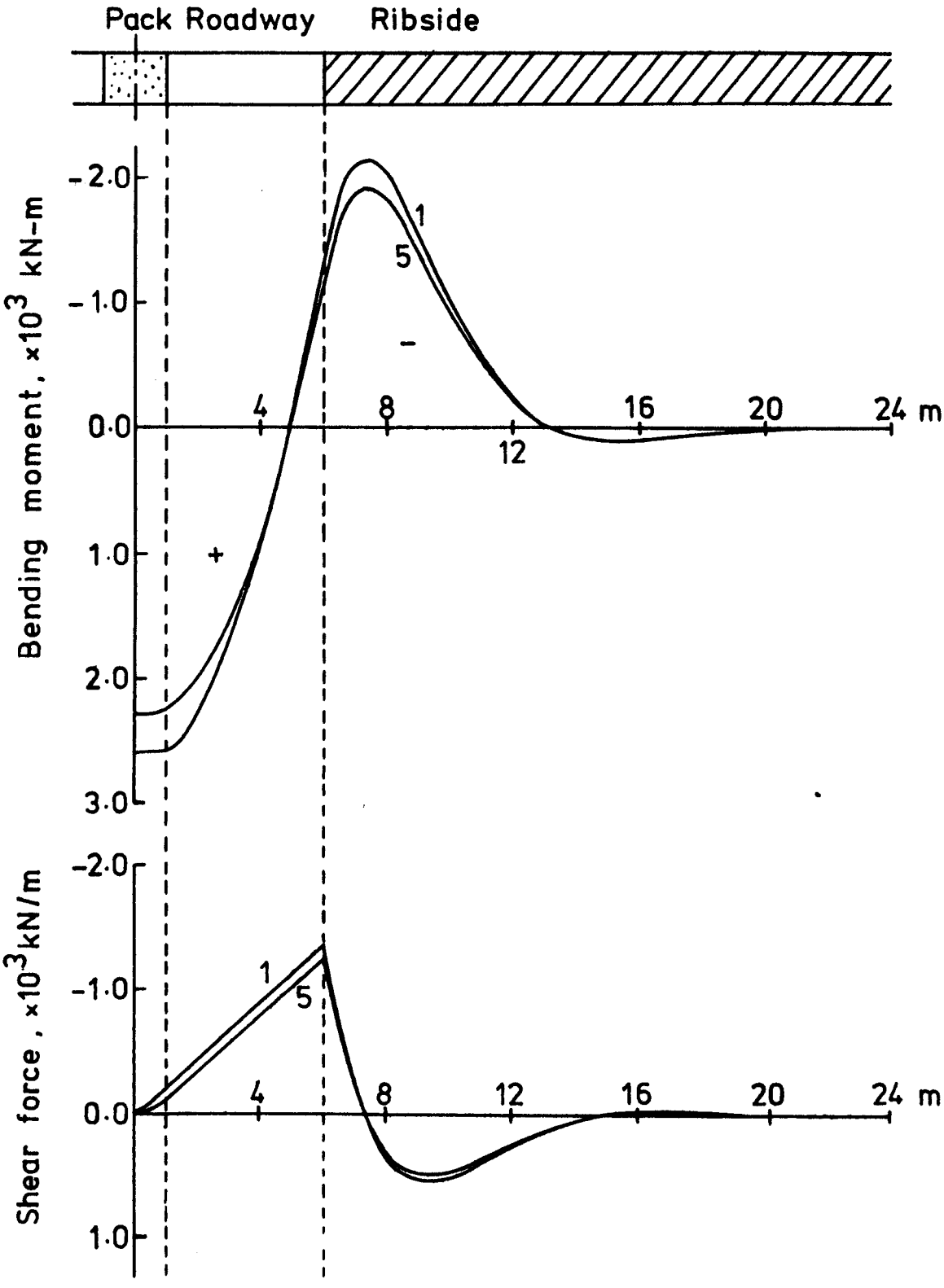

FIG.6.9 - ULTIMATE BENDING MOMENTS & SHEAR FORCES IN THE ROOF (CONVL. PACKS)

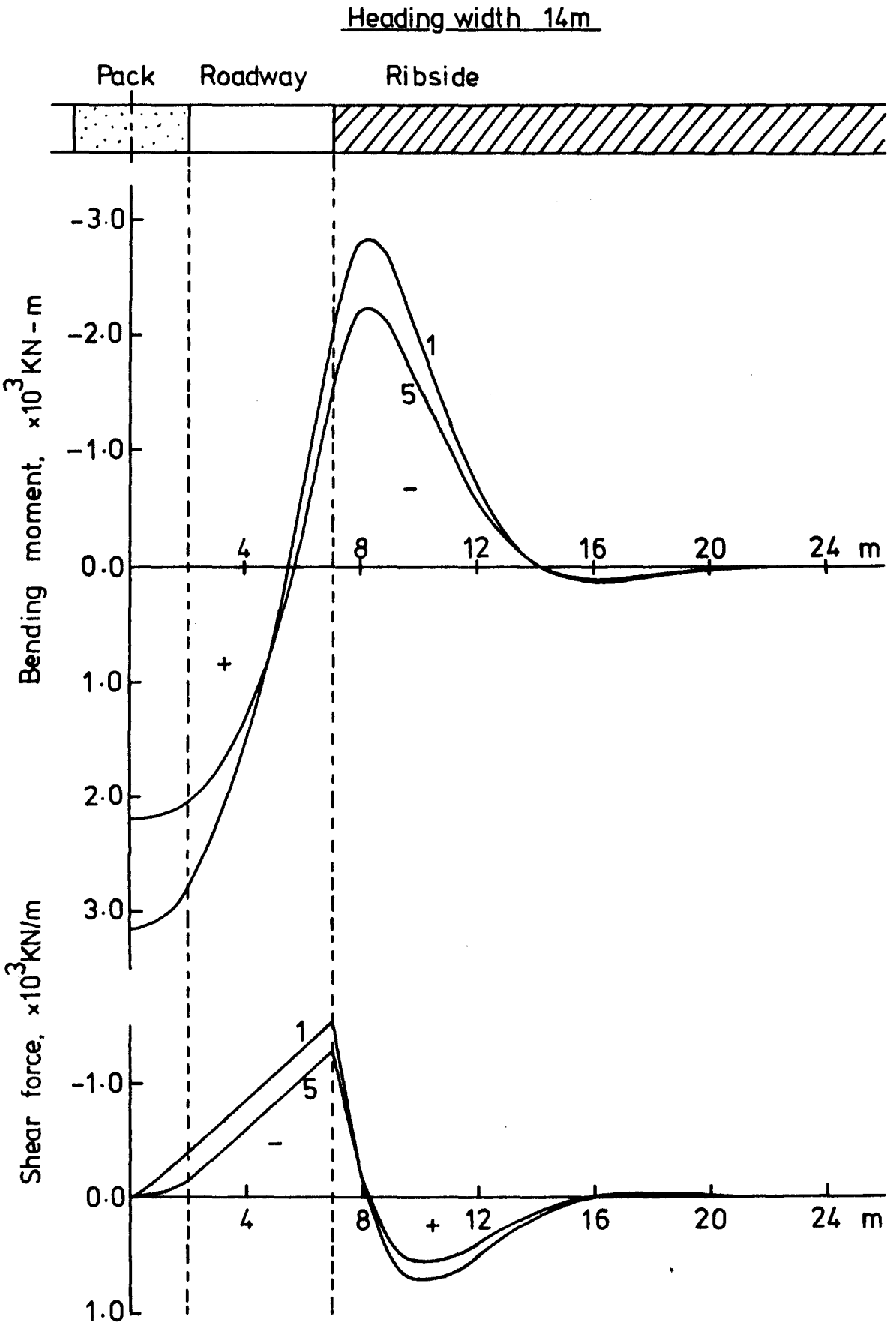

FIG.6.10 - ULTIMATE BENDING MOMENTS & SHEAR FORCES IN THE ROOF (CONVL PACKS)

Heading width 16m

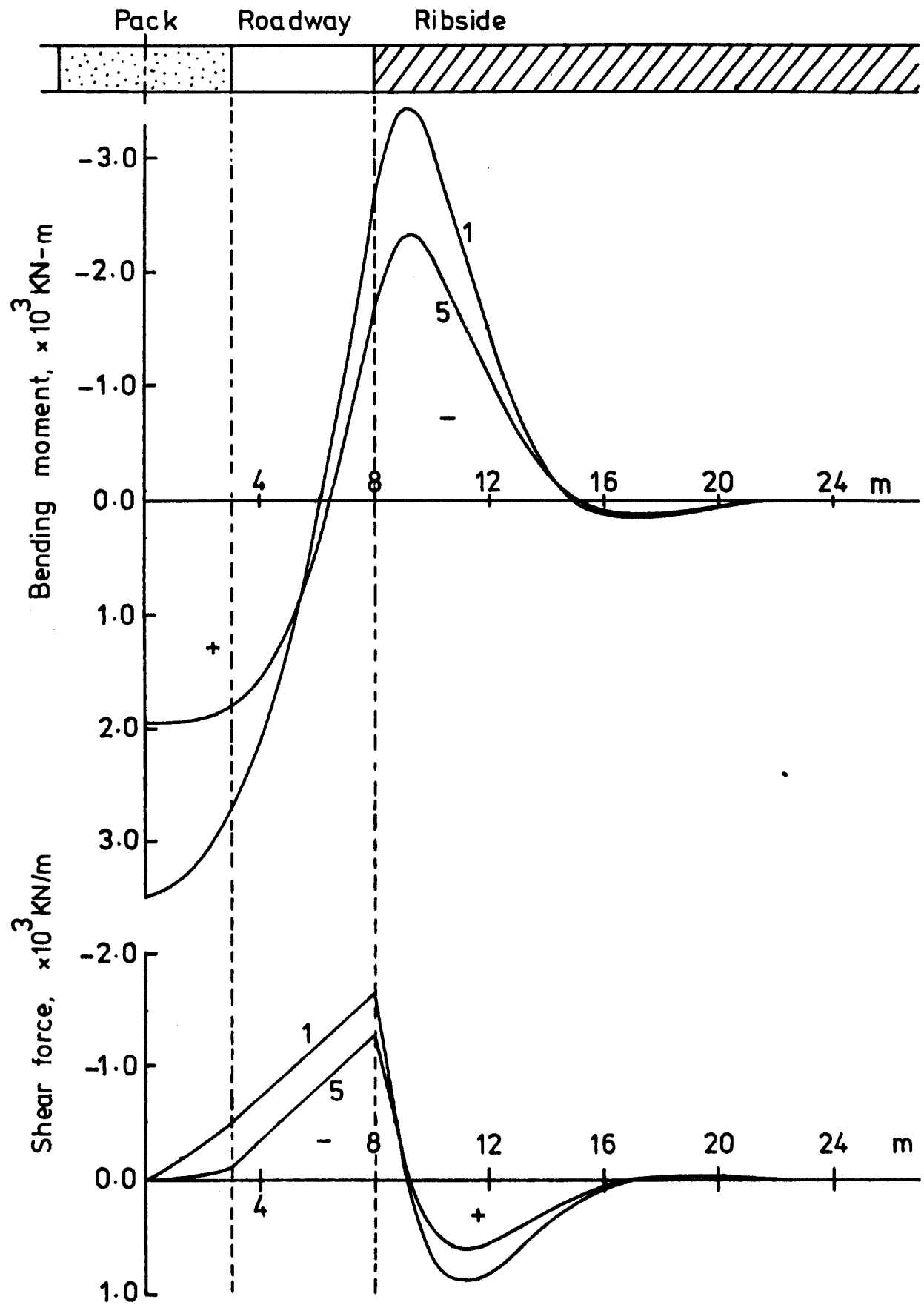

The maximum positive moment is found to occur over the pack instead of in the roadway or pack edge, as opposed to the anhydrite case (cf. Figs. 5.16-18). Bending moments are significantly higher for conventional packs than anhydrite packs.

The shear force is distributed across the heading in much the same manner, the maximum value, which lies at the coal edge, being greater than when using anhydrite packs. This may induce higher floor heave.

6.3.5 Maximum tensile stress in the roadway roof

The pack modulus influences the maximum roadway tensile stress in the same manner it does the bending moment. It has been plotted in Fig. 6.11 against the pack modulus and in general indicates a fall with a rising pack modulus (see Table 6.4).

For the 12 m heading the stress fall is virtually linear within the range of the modulus taken, i.e. the benefit of introducing a stiffer pack increases linearly, while in 14-m and 16-m headings, the stress decreases more slowly for higher moduli.

The maximum improvement in the stress picture takes place in a 16-m heading with a rising pack stiffness and a minimum in the 12-m case.

At very low values of the pack modulus the 12-m heading develops the least tensile stress but at higher values it has the greatest tensile stress of all three widths, again indicating that the utilisation of a centre pack as a support element is less effective in narrower headings and the roof has to be more self-supporting.

FIG.6.11 - MAXIMUM ROADWAY TENSILE STRESS VS. PACK MODULUS

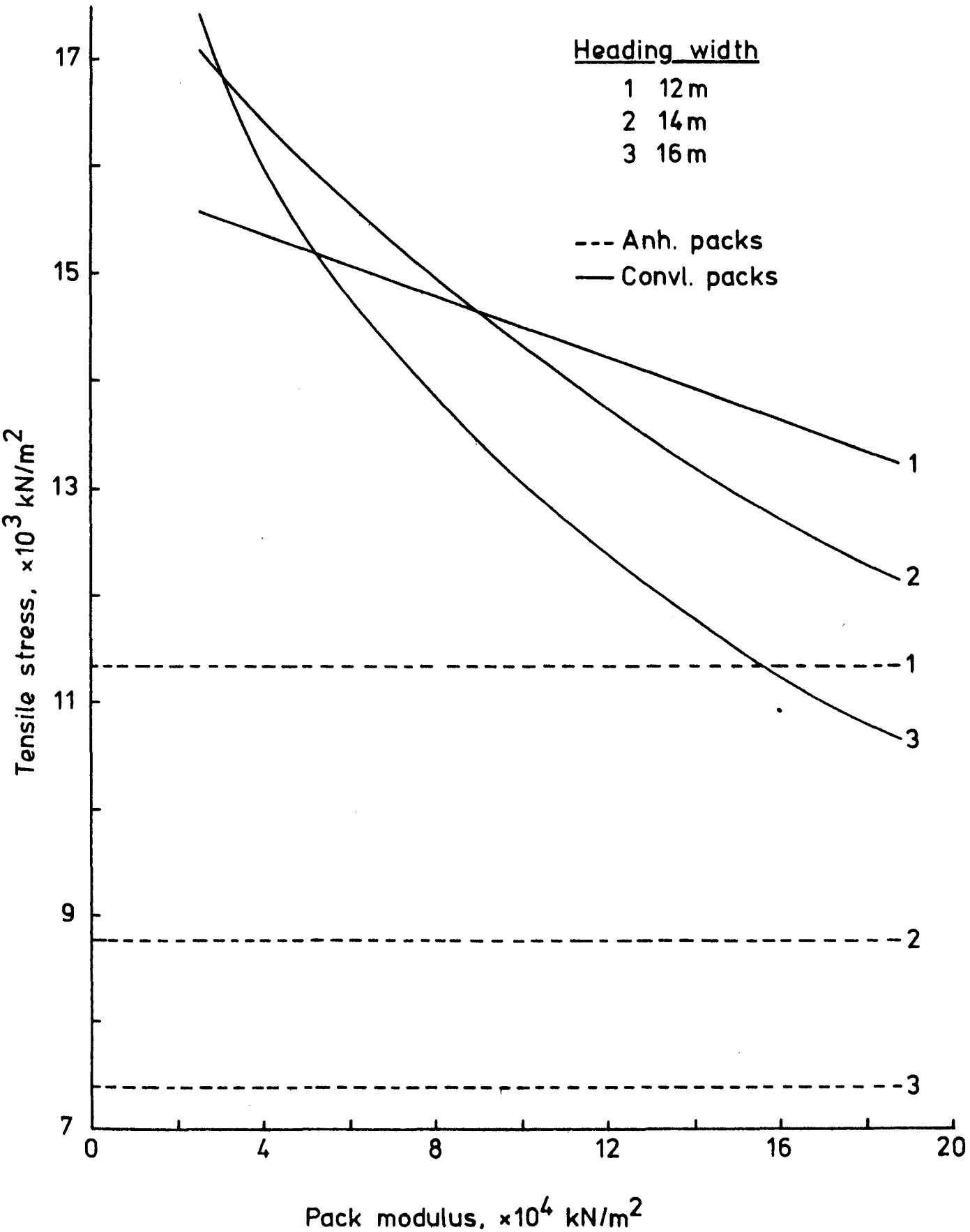

TABLE 6.4

Maximum Roadway tensile stress during short face advancing using conventional packs

(Ultimate roof strength = 6700 kN/m^2)

Heading width m	Pack Modulus kN/m^2	Maximum tensile stress kN/m^2
12	3.50×10^4	15,420
	7.00×10^4	14,940
	1.05×10^5	14,400
	1.40×10^5	13,920
	1.75×10^5	13,380
14	3.50×10^4	16,620
	7.00×10^4	15,360
	1.05×10^5	14,160
	1.40×10^5	13,200
	1.75×10^5	12,360
16	3.50×10^4	16,380
	7.00×10^4	14,340
	1.05×10^5	12,840
	1.40×10^5	11,760
	1.75×10^5	10,860

6.4 Conclusion

1. Loads on conventional non-setting centre packs during short face advancing are lower than anhydrite packs. The general nature of the load acceptance characteristic follows a similar pattern, i.e. the load rises to a peak value and later falls and steadies off gradually. The load reaches, comparatively slowly, a flat peak, the conventional pack material being more compressible than anhydrite. The load acceptance characteristic again supports the back abutment pressure hypothesis.

2. For narrower headings like 12 m, conventional packs of low moduli (e.g. stone packs) exhibit very poor acceptance of load, showing nearly zero loads. This shows that the roof has to be virtually self-supporting when the pack is highly compressible. Load acceptance improves considerably with the pack modulus.

3. The ribside abutment pressure is higher than for anhydrite packs. It is influenced by the pack load so that it shows a fall if the pack accepts load better or if the pack modulus is higher.

4. The maximum bending moment in the roadway is higher than when anhydrite packs are used. Bending moments are found to reduce with increasing heading width when using non-setting packs of higher moduli as with anhydrite packs. With the modulus on the lower side, the opposite is the case.

5. Conventional packs give rise to a greater shear force at the coal edge than anhydrite.

6. The pack modulus influences the maximum tensile stress in the roadway. In general, there is a fall in the stress level with an increasing pack modulus, the fall being slower for narrower headings such as 12-m. At very low values of the modulus the 12-m heading develops the least tensile stress but at higher values the tensile stress is more than in a 16-m heading. This indicates that the utilisation of a centre pack as a support to the roof is less in narrower headings and the roof has to be more self-supporting. For all the values of pack moduli considered the maximum roadway tensile stress exceeds the ultimate strength of the roof rock, which is indicative of the need for roadway supports. The stress level is higher than with anhydrite packs.

7. In general, stiffer packs such as anhydrite show better load acceptance, less bending moment in the roadway (hence tensile stress), less shear force at the coal edge and a smaller abutment pressure than conventional non-setting packs. Hence introducing a stiffer pack instead of a highly compressible one does appear to lead to better overall structural stability.

* * *

CHAPTER 7

Estimation of floor heave during short face advancing and subsequent retreating

CHAPTER 7

Estimation of floor heave during short face advancing and subsequent retreating

7.1 Introduction

Floor lift seriously affects longwall operations by virtue of closure in gateroads, especially in deeper mines and can sometimes be the most important consideration in adopting a particular method of longwall mining. Having considered the behaviour of the roof in the method of short face advancing with centre packs of anhydrite and also of conventional non-setting materials, it now remains to estimate the extent of heave likely to occur in conditions like those at Dawdon, while using this method.

Floor heave occurs due to the removal of the virgin pressure in forming a gate roadway and since this pressure is proportional to the depth of the workings, more severe floor heaving is seen to occur at greater depths. Floor heave is also governed by the vertical restraint applied to the floor by the ribside abutment pressure (its magnitude and proximity) and by the roadside pack. If the resulting stresses in the roadway floor are high and the floor is weak, fracture may commence, increasing the lift due to a volume increase in the broken rock and causing relative pack penetration. In addition to this elastostatic behaviour before and after failure, floor lift goes on increasing with time, viscoelastically, due to creep effects. We thus get a rising heave characteristic with face movement, which is the

combined effect of

(a) increase in the floor stress level from the start line of the face,

(b) build-up of fractures in the floor, affecting increasingly deeper levels and causing an apparent 'swelling',

(c) further 'softening' of the floor due to breaking,

(d) creeping of the floor material, and

(e) swelling, due to wet clay minerals, if present.

In this Chapter it is proposed to analyse the situation of centre-pack short face advancing and subsequent retreating for estimating the floor lift due to the first four factors. Since the floor stress distribution depends on pack load, ribside abutment pressure distribution and also the load on the floor in the goaf of a longwall face, it was first necessary to obtain a complete picture of floor loading. In the previous two Chapters, pack load and ribside abutment pressure distribution have already been obtained for short face advancing and we thus know the floor loads during advancing. Presented below is a method to estimate the ultimate or steady-state floor loading in a longwall panel for use in subsequent retreating.

7.2 Loading on the floor of a longwall panel including a method to determine the zone of ribside crushing

Experience has shown that there exists a high peak stress some distance

into the ribside which falls with distance to the depth pressure. The shape generally accepted for this abutment pressure distribution on the ribside of a longwall panel is shown in Fig. 2.1, Chapter 2, showing a zero stress at the coal edge. The supporting capacity of the coal increases with depth into the ribside, because of lateral confinement while at the edge is at its lowest. The build-up of a peak pressure at the edge due to bending of rock strata in the goaf causes rib edge crushing and shifts the peak inward until equilibrium is re-established.

7.2.1 Wilson's method

A method proposed by Wilson[66] to estimate the zone of crushing in ribside coal pillars and the magnitude of abutment pressure is described here in some detail.

The forces on an element of coal in the ribside pillar is shown in Fig.7.1(a). The thickness of the element is δy and it lies at a distance y from the pillar edge. If σ_v is the vertical stress on the element and σ_H , $\sigma_H + \delta\sigma_H$ are the lateral confining stresses on two sides of the element, the equilibrium equation for the element becomes

$$(\sigma_H + \delta\sigma_H)\, m l - \sigma_H\, m l = \delta\sigma_H\, m l$$

$$= 2\sigma_v \tan\phi \cdot l\, \delta y \qquad (7.1)$$

where m is the seam thickness, l is the element length and tan ϕ is the roof-seam-floor interface friction (which Wilson erroneously terms internal friction).

FIG.7.1(a) - FORCES ON A RIBSIDE ELEMENT

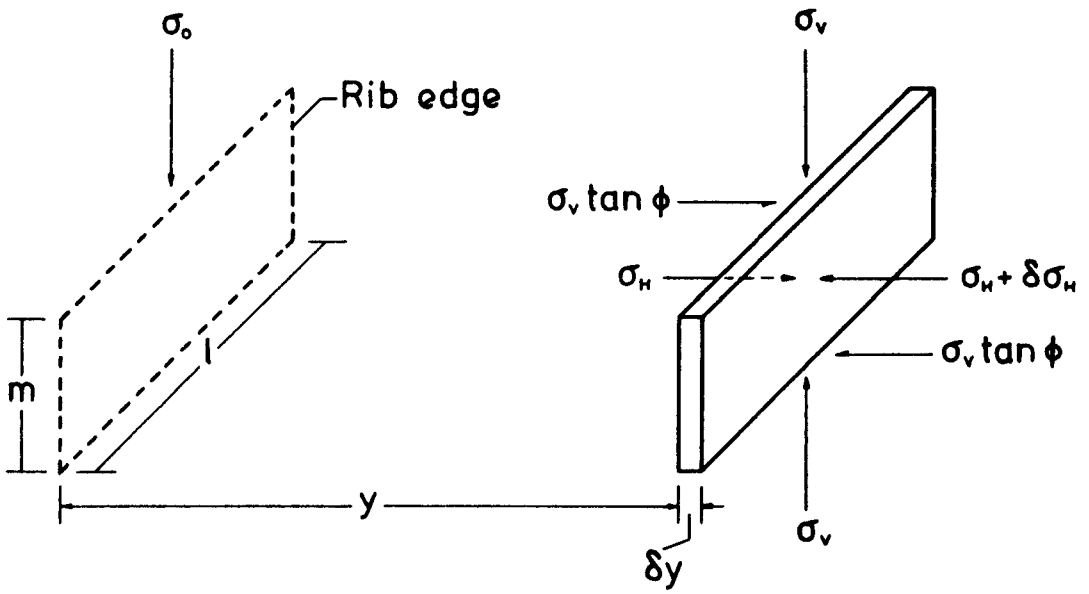

FIG.7.1(b) - ABUTMENT PRESSURE SCHEMATIC

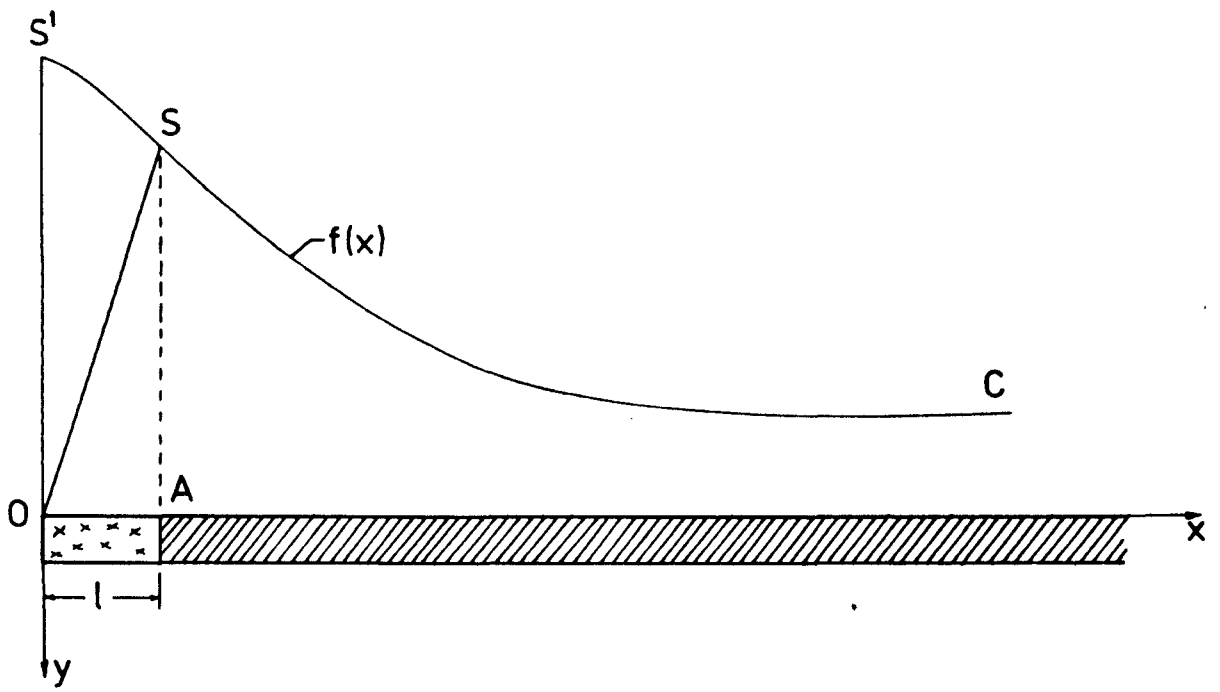

Hobbs[67] tested several British coals under triaxial compression and has proposed the general relation between triaxial fracture strength σ_1, and confining pressure σ_3

$$\sigma_1 = \sigma_o + \sigma_3 + a\,\sigma_3^{\,b} \tag{7.2}$$

where a and b are empirical constants and σ_o is the uniaxial strength. Wilson simplifies this relation to the linear form

$$\sigma_1 = \sigma_o + \sigma_3 \tan\beta$$

and further to the form

$$\sigma_1 = \sigma_3 \tan\beta$$

assuming σ_o to be negligible. $\tan\beta$ is the slope of the linear relation of Wilson. This gives

$$\delta\sigma_H = \frac{1}{\tan\beta}\,\delta\sigma_v$$

Equ. (7.1) then becomes

$$\delta\sigma_v \frac{1}{\tan\beta}\, m = 2\sigma_v \tan\phi \cdot \delta y$$

or $$\frac{dy}{d\sigma_v} = \frac{m}{2\tan\beta\tan\phi} \cdot \frac{1}{\sigma_v}$$

now $\tan\beta$ and $\tan\phi$ are related according to

$$\tan \phi = \frac{\tan \beta - 1}{2\sqrt{\tan \beta}} \tag{7.3}$$

so that

$$\frac{dy}{d\sigma_v} = \frac{m}{\sqrt{\tan \beta}\,(\tan \beta - 1)} \cdot \frac{1}{\sigma_v}$$

integrating with respect to σ_v,

$$y = \frac{m}{\sqrt{\tan \beta}\,(\tan \beta - 1)} \cdot \log \frac{\sigma_v}{\sigma_o} \tag{7.4}$$

which satisfies the condition $(\sigma_v)_{y=o} = \sigma_o$. The following values have been proposed for using this equation:

$$\tan \beta = 4 \;,\quad \sigma_v = 4\rho h \;,\quad \sigma_o = 1 \text{ p.s.i.}$$

The value of $\tan \beta = 4$ is in keeping with the linear relation of Wilson for the triaxial strength of coal based on Hobbs' results. The value of $\sigma_v = 4\rho h$ assumes that the abutment pressure is always 4 times the depth pressure ρh and the value $\sigma_o = 1$ p.s.i. has been arbitrarily fixed by Wilson assuming that σ_o is very small at the coal edge because of crushing.

The following criticisms can be expressed against this method:

(a) Hobbs' triaxial strength relation (7.2) has been simplified to a linear form. This may mean over-simplification, since Equ. (7.2) predicts very rapid

initial increments in the fracture strength with small increases in confining pressure.

(b) tan ϕ is assumed to be the coefficient of internal friction, which it is not, hence Equ. (7.3) may not be valid.

(c) The magnitude of the abutment peak pressure and the extent of ribside crushing are independent of the face length. This does not appear probable, since the weight of the hanging rock between a pair of longwall ribs that has to be supported by them depends on face length.

(d) σ_o is admittedly small as compared to the abutment pressure but the value σ_o = 1 p.s.i. is arbitrary. As per the normally accepted practice of equating negligible quantities to zero, if σ_o = o in Equ. (7.4), we get $y = \infty$. However, even if we accept that $\sigma_o \neq o$ and assign another small value say σ_o = 2 or 3 p.s.i., Equ. (7.4) still gives greatly different values of y.

Due to these discrepancies in Wilson's hypothesis, it was decided to develop a method of calculating the abutment pressure and define the zone of crushed coal in the ribside of a longwall panel.

7.2.2 Alternative method

Due to strata crushing in the goaf a pressure distribution, say OS^1C, builds up over the ribside as shown in Fig. 7.1(b). The sharp peak stress OS^1 causes crushing to commence in the coal, reducing the supporting capacity of the rib and shifting the peak deeper into the coal to a new position S. Once again equilibrium is established and the post-failure pressure distribution is OSC. OA is the crushed coal zone, its limit being right below the new abutment peak S.

The stress condition at the coal edge is biaxial before failure commences, the vertical stress σ_y being the pre-fracture abutment peak OS^1. From Hobbs' experiments on coal under biaxial compression[68] it is seen that when the lateral stress is $\frac{1}{4}$ of the vertical stress the rise in strength from uniaxial to biaxial is about 10%. Under biaxial confinement the edge undergoes a vertical stress σ_y and a lateral stress $\mu\sigma_y$, the third lateral stress being zero. If $\mu = 0.25$, we get a rise in coal strength by about 10% at the edge. This same rise in strength is obtained in triaxial compression when the confining pressure is, say, c times the vertical stress, where c is a fraction. The equivalent triaxial state of stress giving the same strength at the edge is then

$$[\ \sigma_y = f(o)\ ,\ \sigma_x = c\sigma_y\ ] \qquad (7.5)$$

when $f(x)$ is the pressure distribution OS^1C.

Now deep inside the seam, the depth pressure acts, with the horizontal confinement σ_x being $\frac{\mu}{1-\mu}$ times the depth pressure. Hence the stress levels are

$$\left[\sigma_y = \rho h \ , \ \sigma_x = \frac{\mu}{1-\mu} \rho h \right] \tag{7.6}$$

Results of Hobbs' triaxial tests on 9 coals are shown in Fig.7.2. An average best fit by numerical iteration for 7 out of these 9 coals was obtained. Pentremawr and Barnsley Hards were not included as being of rather high strength, in keeping with the medium strength of Durham coals[64]. The best fit is given by

$$\sigma_1 = 2200 + \sigma_3 + 250 \left(\sigma_3 \right)^{0.45} \qquad \text{lb/in}^2$$

$$\sigma_1 = 15190 + \sigma_3 + 724 \left(\sigma_3 \right)^{0.45} \qquad \text{kN/m}^2 \tag{7.7}$$

When the line

$$\sigma_x = \frac{\mu}{1-\mu} \sigma_y$$

is plotted in Fig 7.2 it is seen that it does not intersect the curve given by Equ.(7.7) indicating that the state of stress deep inside the coal defined by (7.6) is stable. The limit of the zone of crushed coal and the process of crushing occur at stress levels between the two extremes (7.5) and (7.6). These two stress levels can be marked as two points on Fig.7.2. Then a straight line joining these two points will consist of two parts: one above the failure envelope (7.7) indicating crushing and the other below it showing stability. Such a straight line will have the equation

FIG.7.2 - TRIAXIAL FRACTURE STRENGTH OF COAL
(After Hobbs)

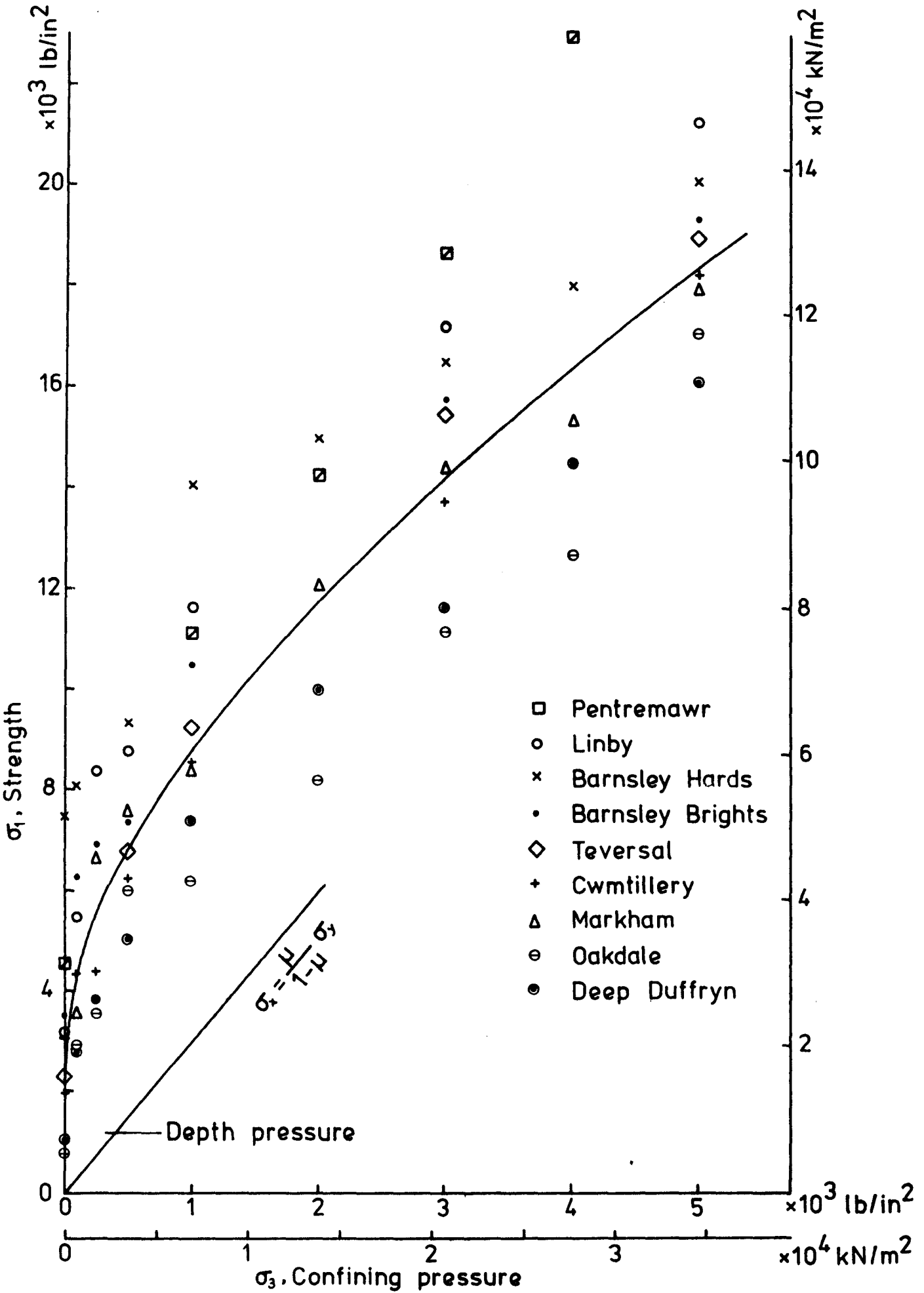

$$\sigma_y = a\,\sigma_x + b \qquad (7\,8)$$

where

$$a = -\frac{f(o) - \rho h}{\frac{\mu}{1-\mu}\rho h - c f(o)}$$

$$b = f(o)\rho h\,\frac{\frac{\mu}{1-\mu} - c}{\frac{\mu}{1-\mu}\rho h - c f(o)}$$

$f(o)$ = pre-fracture abutment peak pressure $f(x)_{x=o}$

ρh = depth pressure

The point of intersection of the two curves (7.7) and (7.8) then defines the state of stress at which failure just ceases and, therefore, corresponds to the limit of the crushed zone or the position of the new abutment peak. To determine this point, the pre-fracture pressure distribution on the ribside $f(x)$ must be known.

Consider the situation of Fig. 7.3 showing the lateral section of a longwall working. Equivalent material mine modelling has given an indication[62] that the roof in the goaf breaks down and collapses to a certain height, depending on the excavation width (face length), and the height of collapse in the goaf for competent brittle coal measures could be taken to vary between 1.3L and 1.7L, where L is the excavation width. In widening the excavation, the roof rock initially breaks down into small pieces, which quickly become very large slabs with further widening, so

that most of the broken rock above the nether roof consists of large slabs rather systematically arranged, as shown in Fig. 7.3. It is also seen that the intact rock hardly touches the broken rock, indicating that the goaf rock is not disintegrated enough and also settles down due to its own dead weight so that the goaf volume is not completely occupied by it. The floor in the goaf then gets only the dead weight of the broken rock, the intact rock pressure being carried by the ribsides and to some extent by the roadside packs. The same type of behaviour is assumed here to apply to British rocks. The average value of 1.5L for the height of collapse in the goaf is taken for further calculation. Though these observations are contrary to popular belief, they do corroborate the observations taken underground as quoted by Wilson[66] that the load taken by the centre of the goaf can be 1.66 $L\rho$ while in our case the value is 1.5$L\rho$.

The mechanism of loading of a roadside pack is still unknown, mainly because of the unstable nature of the roof, and analytically it is not possible to arrive at a suitable load value. In this analysis, it was, therefore, decided to assign different values to the pack load, assuming that the pack receives load partly due to the dead weight of some rock fractured above it and partly due to the bending action of the main rock mass higher up. This is equivalent to replacing the pack as a structural element by an upward reaction to the roof rock which is equal to the pack load.

In the model of Fig. 7.3 for a longwall panel there will be a shear force Q acting to the left of the pack, the bending moment being taken zero.

FIG.7.3-MECHANICAL MODEL FOR RIBSIDE LOADING

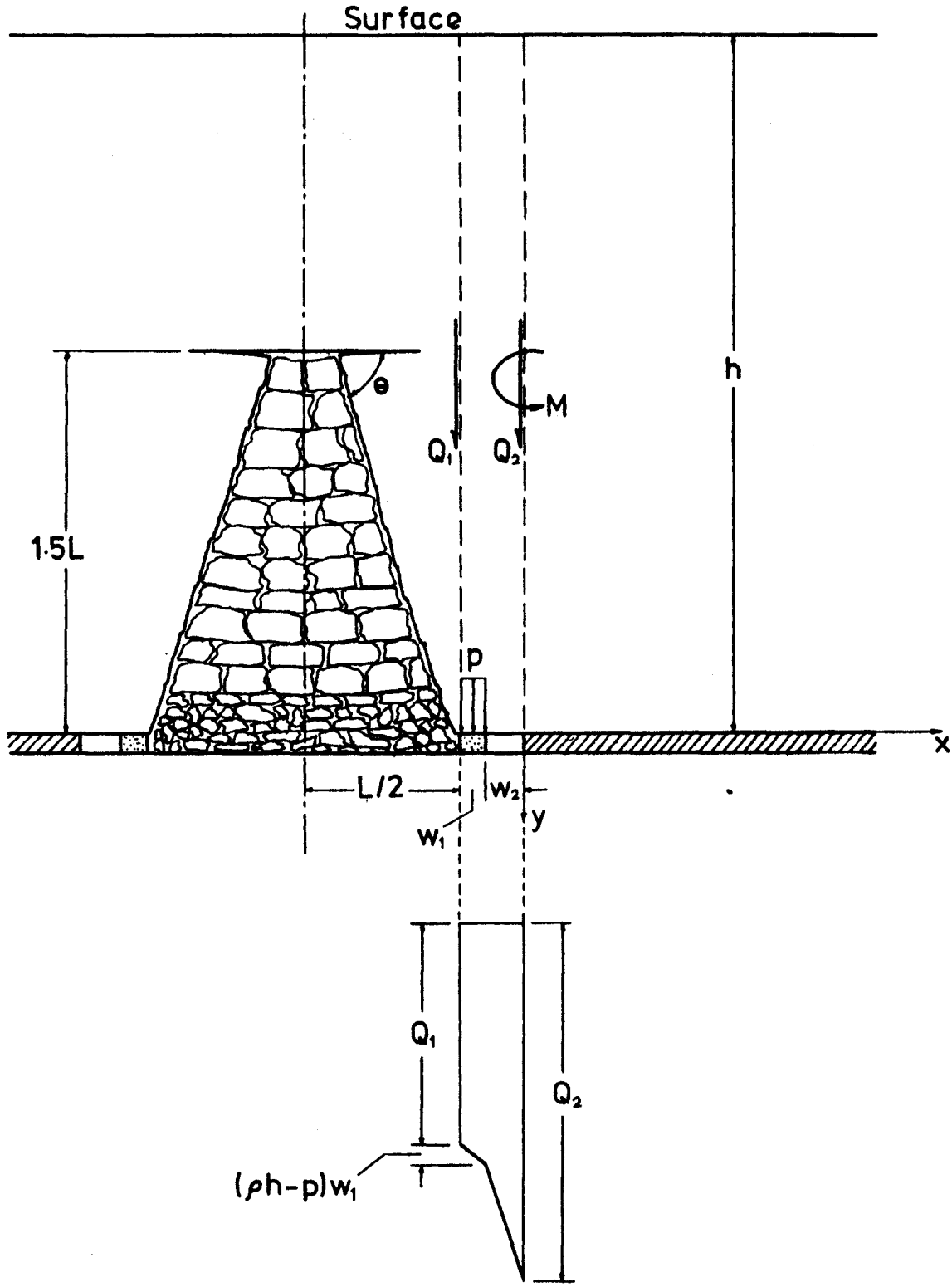

S.F. Diagram

Also at the rib edge there will be a shear force Q_2 and a bending moment M. The shear force diagram is shown in the same figure for the pack and roadway region. Q_1 is obtained as the weight of the intact rock to the left of the pack up to the centre line of the goaf:

$$Q_1 = \rho\left[(h - 1{\cdot}5L)\frac{L}{2} + \frac{1}{2}(1{\cdot}5L)^2 \cot\theta\right]$$

where θ is the angle of fracture shown in Fig. 7.3. Then the shear force Q_2 at the rib edge is obtained as

$$Q_2 = Q_1 + (\rho h - p)w_1 + w_2 \rho h$$

and the bending moment M can be written down very approximately as

$$M = -Q_1(w_1 + w_2) - \rho h \frac{(w_1 + w_2)^2}{2} + p w_1\left(\frac{w_1}{2} + w_2\right)$$

where p = pack load,

w_1 = pack width,

w_2 = roadway width.

Now the equation for deflections v of the lowest fibre of the strata above the ribside is

$$D\frac{d^4v}{dx^4} = \rho h - k_2 v$$

which gives $v = \frac{\rho h}{k_2} + e^{-\alpha x}(A_1 \cos\alpha x + A_2 \sin\alpha x)$ (7.9)

satisfying the condition $(v)_{x=\infty} = \frac{\rho h}{k_2}$. Here $\alpha = \left(\frac{k_2}{4D}\right)^{1/4}$

Applying the following conditions to the deflections v:

$$\left(\frac{d^3v}{dx^3}\right)_{x=0} = \frac{Q_2}{D} \quad , \quad \left(\frac{d^2v}{dx^2}\right)_{x=0} = \frac{M}{D}$$

the arbitrary constants A_1 and A_2 are obtained as

$$A_1 = \frac{2Q_2\alpha}{k_2} + \frac{2M\alpha^2}{k_2} \quad , \quad A_2 = -\frac{2M\alpha^2}{k_2}$$

The pre-fracture pressure distribution on the ribside f(x) is then simply written down from (7.9) as

$$\begin{aligned} \sigma_y = f(x) &= k_2 v \\ &= \rho h + 2\alpha e^{-\alpha x}\left[(Q_2 + M\alpha)\cos\alpha x - M\alpha \sin\alpha x\right] \end{aligned} \tag{7.10}$$

We can then determine the vertical pressure at the point of intersection of curves (7.7) and (7.8) by simultaneous solution of the equations to these curves. Thus

$$\sigma_{y(l)} = 15190 + \frac{\sigma_{y(l)} - b}{a} + 724\left[\frac{\sigma_{y(l)} - b}{a}\right]^{0.45} \tag{7.11}$$

and the length l to which fracturing will occur in the ribside is given from Equ. (7.10) by

$$\begin{aligned} \sigma_{y(l)} &= f(l) \\ &= \rho h + 2\alpha e^{-\alpha l}\left[(Q_2 + M\alpha)\cos\alpha l - M\alpha \sin\alpha l\right] \end{aligned} \tag{7.12}$$

Equ. (7.11) and (7.12) are two simultaneous trancendental equations in $\sigma_{y(l)}$ and l and can only be solved graphically or numerically.

7.2.2.1 Lateral confinement deep inside the coal seam

The assumption used in this method that deep inside the seam the lateral confining stress σ_x takes a value $\sigma_x = \frac{\mu}{1-\mu}\sigma_y$ may be open to scepticism, since at greater depths conditions of near-hydrostatic or hydrostatic stress may exist; it is proposed here, however, as a hypothesis, that Poisson's ratio μ itself will change with depth.

It is seen from compression tests to register stress-volumetric strain curves of a rock specimen that μ increases roughly after half the uniaxial fracture load until it reaches values of 0.5 or greater at failure[69]. This happens due to microcracking along the load axis of the specimen at approximately half the failure stress (fracture initiation), producing larger and larger lateral strains as the applied stress approaches the failure value. This may explain why higher lateral confinements are generally observed in deeper mines. At great depths, the high vertical stress level tends to fail the rock if it is exposed and Poisson's ratio values of about 0.5 will occur, giving us $\sigma_x = \frac{\mu}{1-\mu}\sigma_y \approx \sigma_y$ which is hydrostatic stress.

Poisson's ratio μ changes with the axial stress σ_1 according to the theoretical equation[69].

$$\mu = \left(1 - \frac{E_i}{K}\right)\frac{\sigma_1 - \sigma_1^i}{2\sigma_1} + \mu_i\frac{\sigma_1^i}{\sigma_1} + \frac{E_i N}{2\sigma_1}\left[\frac{\sigma_1 - \sigma_1^i}{\sigma_1^i}\right]^m \qquad (7.13)$$

where E_i = tangent elastic modulus at microcrack initiation,

K = linear bulk modulus,

σ_1 = axial stress,

σ_1^i = axial stress at microcracking,

μ_i = Poisson's ratio at microcracking,

N,m = volumetric microcrack strain-hardening parameters.

In our case at Dawdon Colliery, the depth pressure is 8288 kN/m^2 and the average coal strength is 15190 kN/m^2 as per Equ. (7.7), i.e. the strength is approximately twice the depth pressure. Since the stress level at microcracking $\sigma_1{}^i$ is roughly half the failure stress, we can take $\sigma_1{}^i \approx$ 8288 kN/m^2. At this stress level in the coal seam $\sigma_1 = \sigma_1^i$ and we get from Equ. (7.13) $\mu = \mu_i$. Thus the usual normal value of Poisson's ratio, 0.25, can be taken for this analysis, since up to microcrack initiation μ does not change significantly.

7.2.2.2 Numerical analysis

Taking the data for Dawdon Colliery given earlier in Chapter 5, Equ. (7.11) and (7.12) were solved numerically on the computer with the help of a simple program in Fortran IV, incorporating the following variations:

Pack width = 1.5 to 6 m at every 0.5 m.

Face Length = 120, 140, 160, 183 m.

Pack load = 3000 to 7000 kN/m^2 at every 1000 kN/m^2.

The angle of fracture θ was taken as 75° and the constant α was calculated to be 3.69×10^{-2} m^{-1} assuming that bed cohesion was broken over every 20 m up to a height of 280 m, which is the height corresponding to about 1.5 x the maximum face length. This is rather arbitrary, but it is necessary to know beforehand the spacing of weakness planes in the rock mass along which cohesion would be expected to break horizontally, and in this case this was not possible.

7.2.3 Results

7.2.3.1 Abutment pressure distribution

Fig. 7.4 shows the abutment pressure distribution over the ribside of a longwall face for the two extreme face lengths of 120 and 183 m considered. Just at the rib edge the pressure is zero but it rises steeply to its peak value just over the limit of the crushed zone. The fall after the peak is somewhat slower and the depth pressure is reached at nearly 50 m from the coal edge. A greater extent of crushing and a higher pressure is observed for the longer face length.

7.2.3.2 Influence of pack load and width and face length on abutment pressure

There is a fall in the abutment peak pressure with both increasing pack width and pack load, both factors influencing it more significantly before ribside crushing than after (see Fig.7.5). When the pack is narrow, the shear force over the coal edge Q_2 is not significantly reduced, in spite of sufficiently high pack loads and, therefore, the reduction in abutment pressure consequent upon increasing pack load is small for narrow packs. In

FIG.7.4 - ABUTMENT PRESSURE DISTRIBUTION ON THE RIBSIDE

Pack load 3000 kN/m^2 Pack width 1·5 m

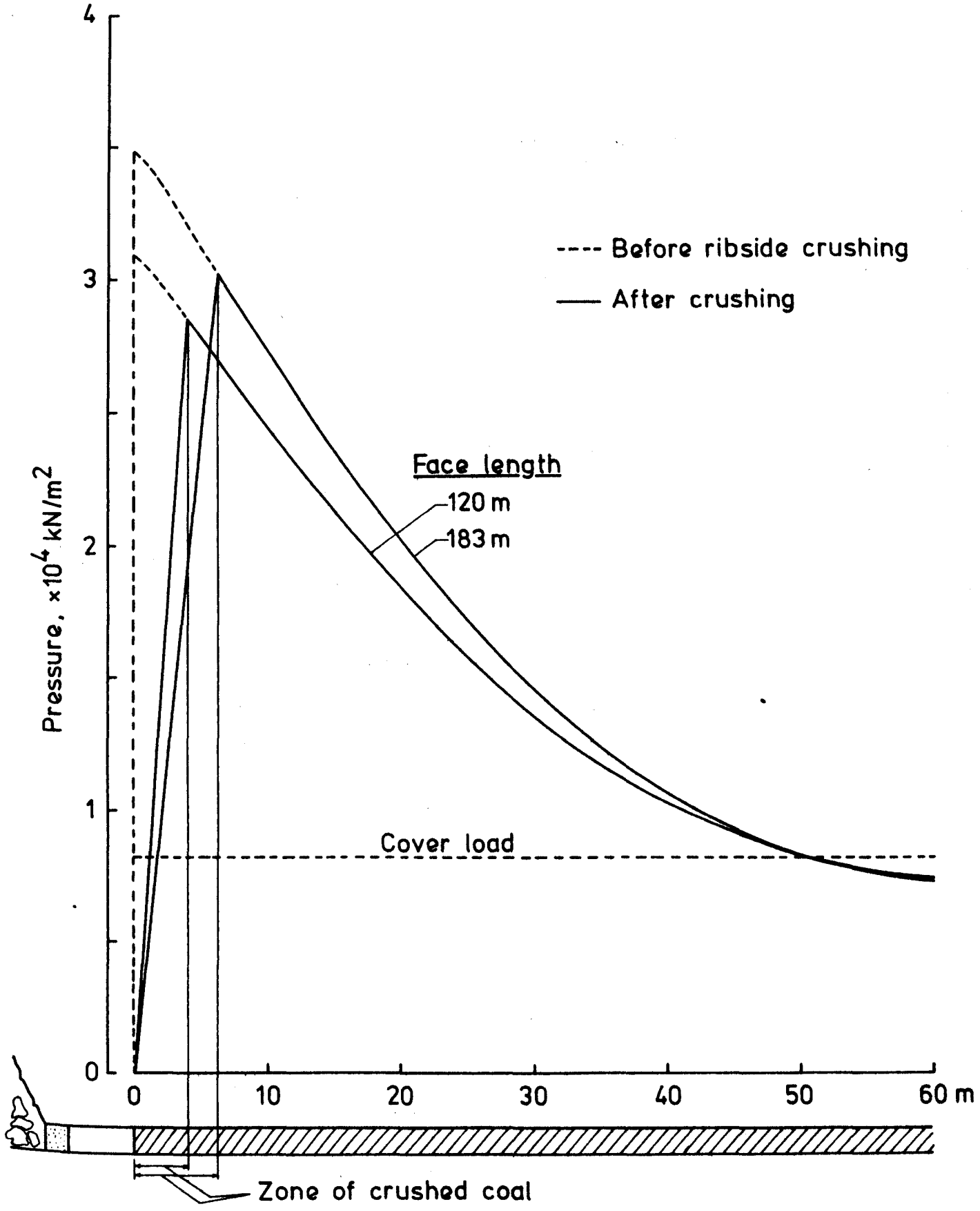

FIG.7.5-ABUTMENT PRESSURE VS. PACK LOAD AND WIDTH

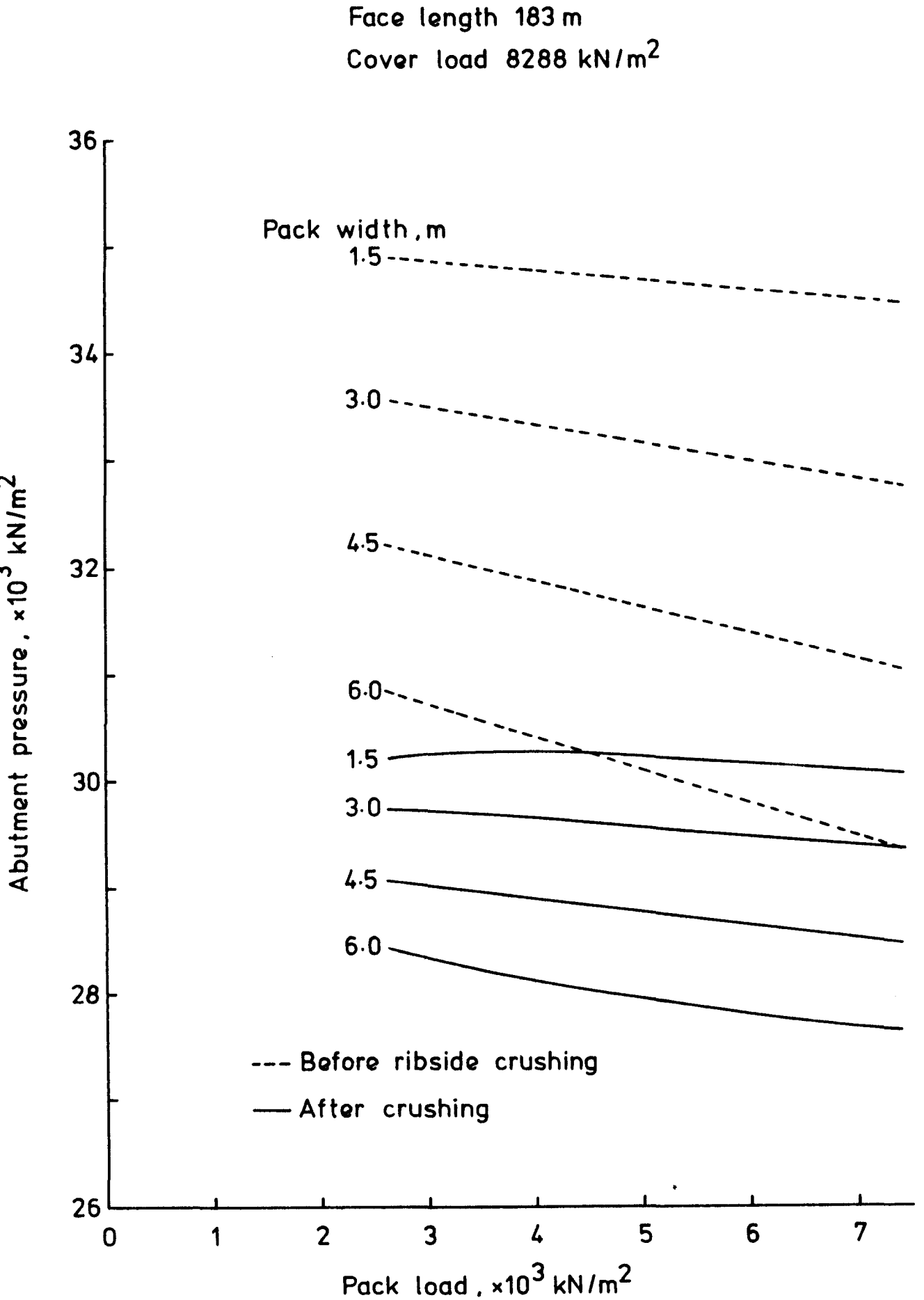

FIG.7.6 - VARIATION OF RIBSIDE ABUTMENT PRESSURE WITH FACE LENGTH

Pack load 3000 kN/m^2 Pack width 1.5 m

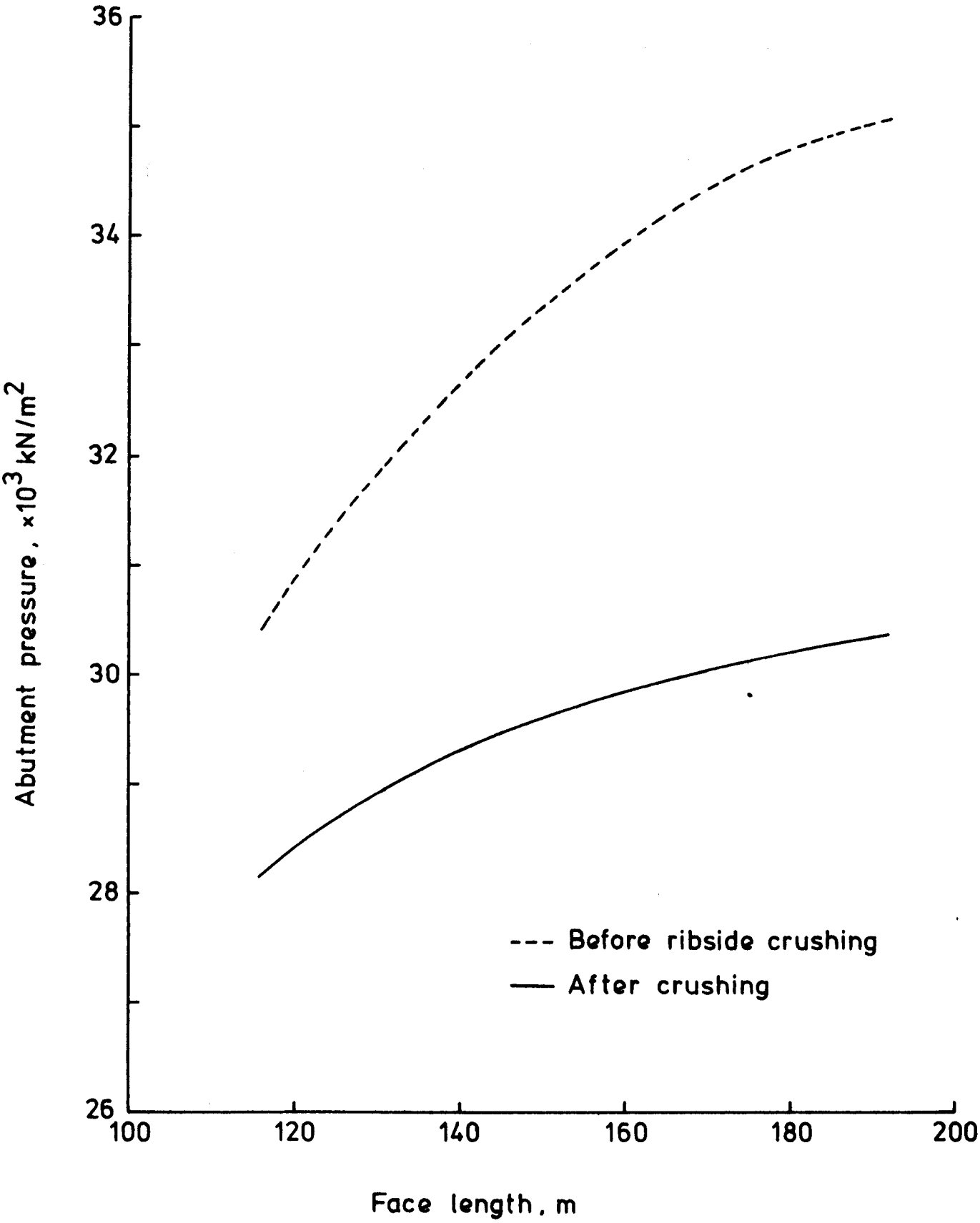

fact, for a pack width of 1.5 m the post-failure abutment peak stress shows almost no change. As the pack width increases, load changes are seen to affect the abutment stress more prominently. Table 7.1 gives values of the abutment peak stress as multiples of the depth pressure. The fall from a 1.50-m to a 6-m pack is observed to be significant.

A longer face means a higher shear force Q_2 at the coal edge and so a higher pressure. The influence of face length on abutment pressure increases at a reducing rate. At a certain face length which can be calculated as about 240 m (for a depth of 365 m at Dawdon), the fracture lines in the goaf will reach the surface and any further increase in the face length will cease to raise the abutment pressure. The curves of Fig. 7.6 tend to become flatter with face length such that their slope will become zero at a value of 240 m.

7.2.3.3 Extent of ribside crushing due to abutment stress

The length of the crushed zone inside the rib is affected by pack load, width and face length in much the same manner as the abutment pressure, as seen from Figs. 7.7 and 7.8. Increasing pack load and width reduce the extent of crushing, as is logical, since the pre-fracture abutment falls. The reduction in the crushing is almost exactly linear for any pack width.

7.2.4 Ultimate floor loading

From the triaxial strength relation of Hobbs, Equ.(7.7), and the magnitude of the pre-fracture abutment pressure during short face advancing with centre packs, it could be concluded that there would be little crushing

FIG.7.7-EFFECT OF PACK LOAD & WIDTH ON THE EXTENT OF RIBSIDE CRUSHING

Face length 183m

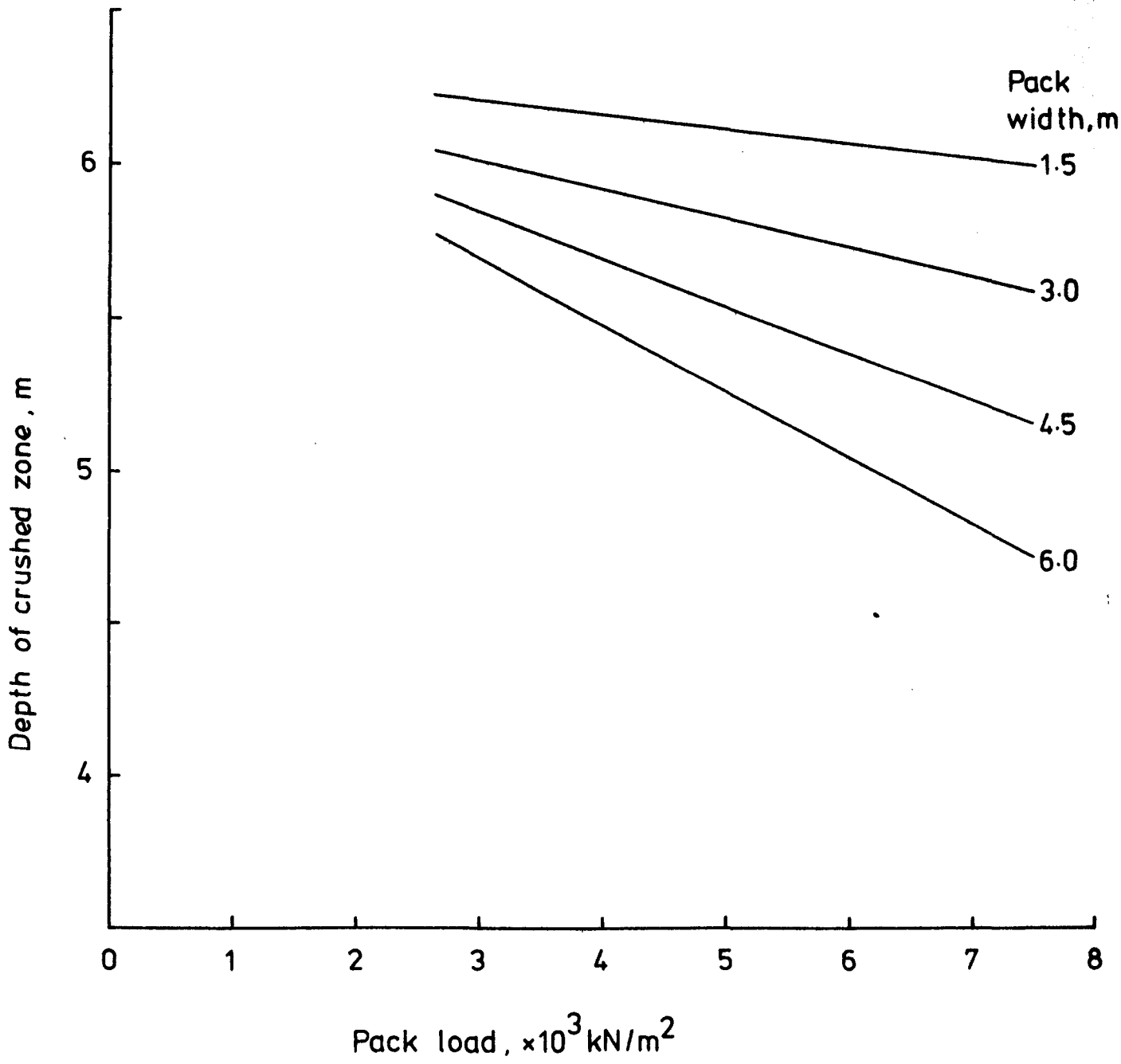

FIG.7.8 - EFFECT OF FACE LENGTH ON THE EXTENT OF RIBSIDE CRUSHING

Pack load 3000 kN/m^2 Pack width 1.5 m

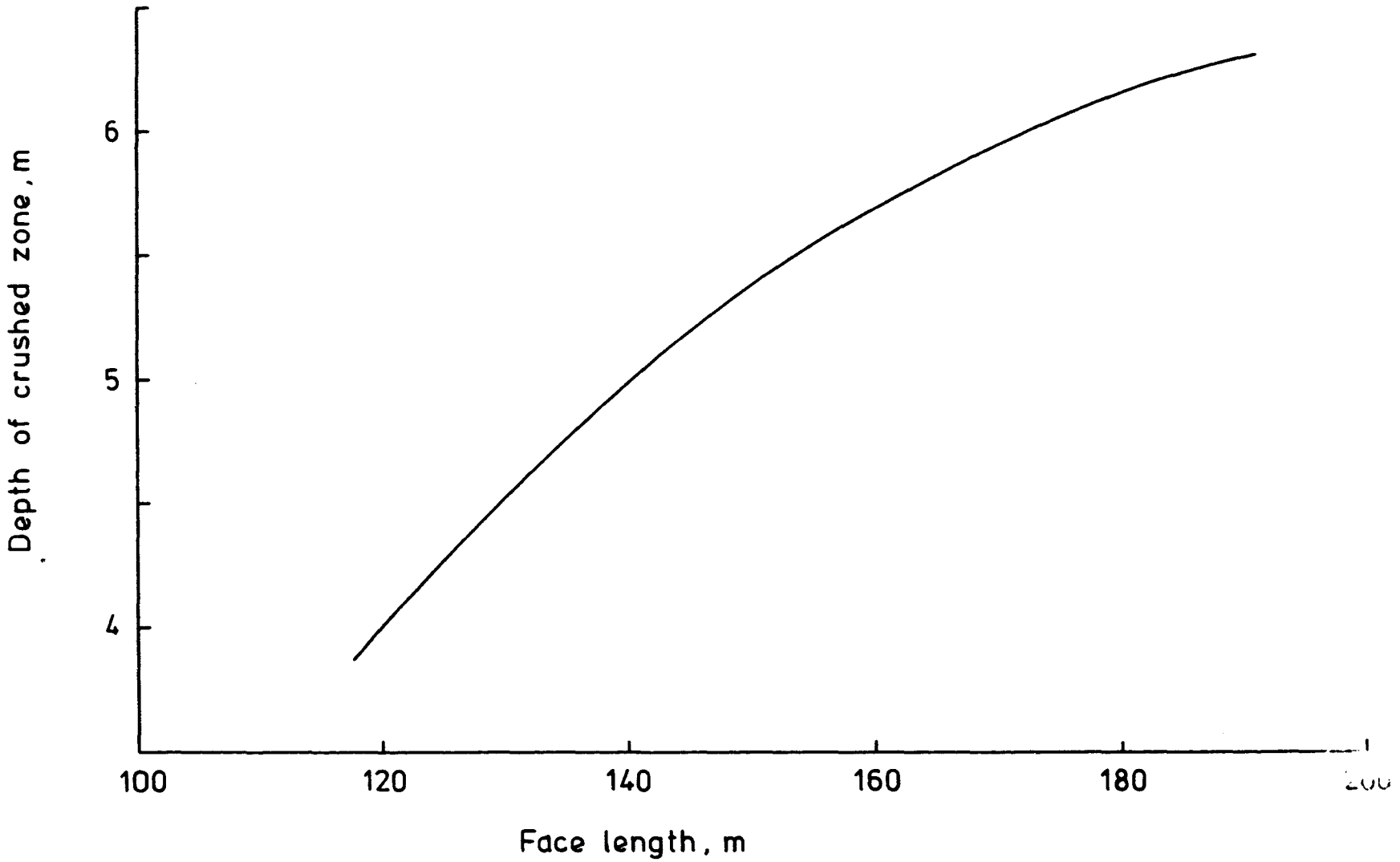

TABLE 7.1

Abutment peak stress after ribside crushing

(a) Face length 183 m

Pack width, m	Pack Load, kN/m^2	Abutment pressure, x depth pressure
1.5	3000	3.65
	4000	3.65
	5000	3.64
	6000	3.64
	7000	3.63
3.0	3000	3.58
	4000	3.57
	5000	3.56
	6000	3.55
	7000	3.54
4.5	3000	3.50
	4000	3.49
	5000	3.47
	6000	3.46
	7000	3.44
6.0	3000	3.41
	4000	3.39
	5000	3.38
	6000	3.36
	7000	3.34

(b) Influence of face length - pack load 3000 kN/m^2, pack width 1.5 m

Face length, m	Abutment pressure, X depth-pressure
120	3.42
140	3.53
160	3.60
183	3.65

of coal in this stage of the working. The floor loading is thus given by the elastostatic ribside loading and the pack load already obtained in Chapters 5 and 6.

During subsequent retreating, floor heaving of a point marked x in Fig 2.8 on the floor will be considered. To the right of this point there is a virgin ribside and after the retreating face in panel 1 passes this point, the situation becomes as in Fig.7.3. Thus, during retreating, the floor loading for the ribside obtained in the previous sections will take place. The load on the pack has been already assumed to vary between 3000 and 7000 kN/m^2. In order to complete the picture of floor loading during retreating, the load in the goaf must now be mentioned. As per the model of Fig. 7.3, it is already known that the goaf will receive the dead weight of the broken rock which is piled up to a trapezium shape. The loading in the goaf is then simply the weight of a rock pile of this shape, which throws no load near the pack and a maximum at the goaf centre.

7.3 An elastostatic analysis for floor stresses and heaving

After obtaining the complete load distribution on the floor, it was necessary to study the stresses in the floor as a result of this loading and also the lift produced elastostatically upon fracture, if any, and viscoelastically with face movement.

For this purpose the floor was treated as a semi-infinite medium with one straight boundary receiving the aforementioned loading distribution.

The floor section shown in Fig.5.3 indicates that there is a seatearth at Dawdon Colliery below the High Main seam with an average thickness of 0.23 m. In this analysis it was assumed that the entire semi-infinite medium was made up of this seatearth.

7.3.1 Face element method for elastostatic lift

It was decided to use the face element method for the initial elastostatic analysis of this situation during short face advancing and subsequent retreating. The face element method is of recent origin and comprises a numerical procedure for elastostatic stress analysis by means of a surface distribution of potential functions[60]. The process involves division of the surface into discrete elements over which boundary conditions, e.g. the loading distribution in the present instance, are known. The advantages over the better known finite-element method are that only the surface, not the volume, is discretised and an artificial boundary need not be formed in semi-infinite or infinite media, as the conditions at infinity are automatically taken care of.

Figs. 7.9 and 7.10 show the formation of the elements on the surface line of the floor for the cases of short face advancing and later retreating respectively. The scheme of loading in Fig. 7.9 on the floor, correspond to Fig. 5.13 of Chapter 5 for a pack width of 2 m. Fig. 7.10 shows the loading obtained by calculation in this Chapter. The modulus of elasticity for the floor material was taken as 5.02×10^6 kN/m^2[64], and Poisson's ratio as 0.25. The pack width was varied from 1.5 to 6 m and the face length and pack load in the case of retreating were varied from 120 to 183 m

FIG.7·9-FACE ELEMENT SCHEME FOR FLOOR- SHORT FACE ADVANCING

Heading width 12 m

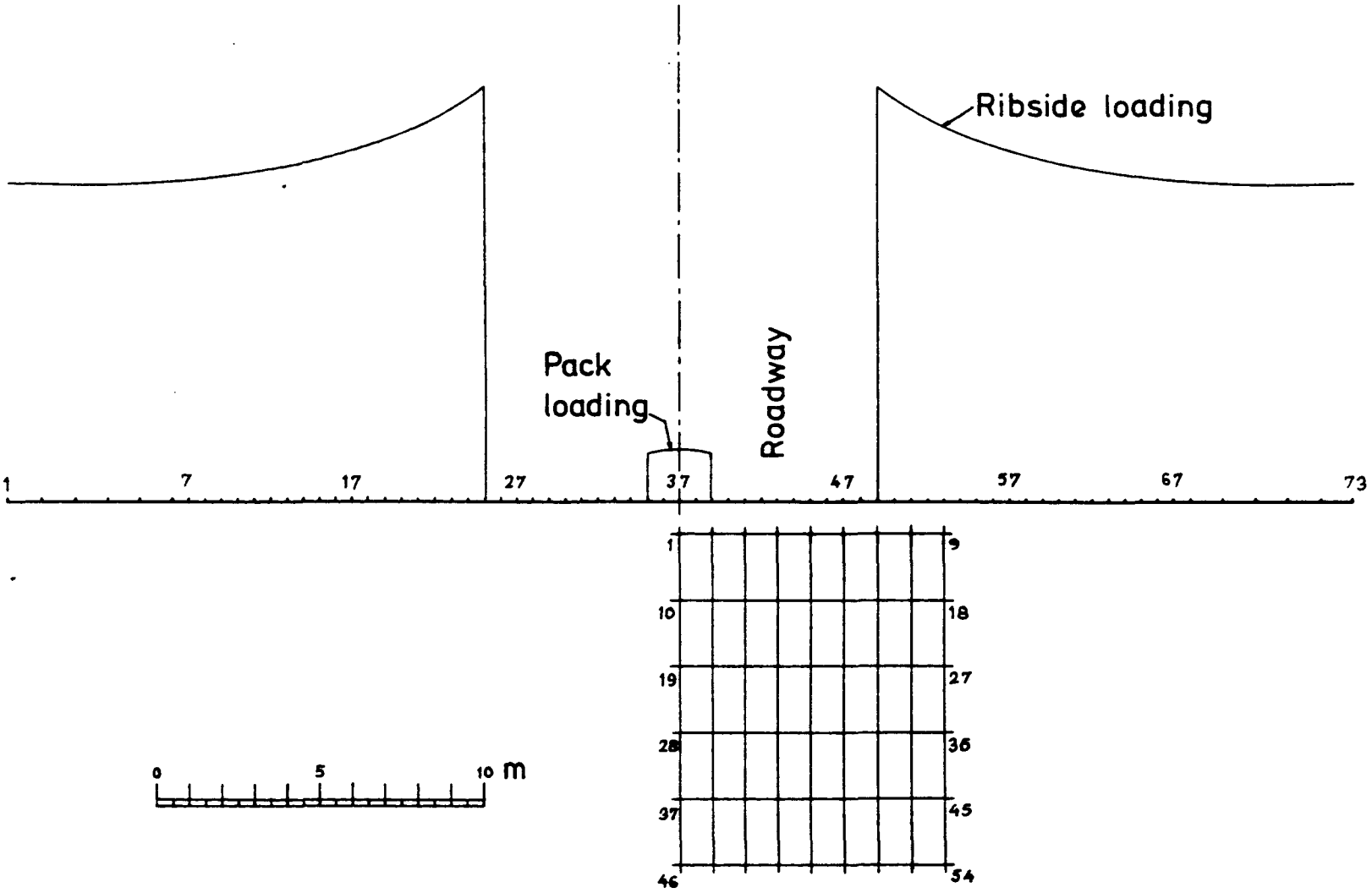

FIG.7.10-FACE ELEMENT SCHEME FOR FLOOR- RETREATING

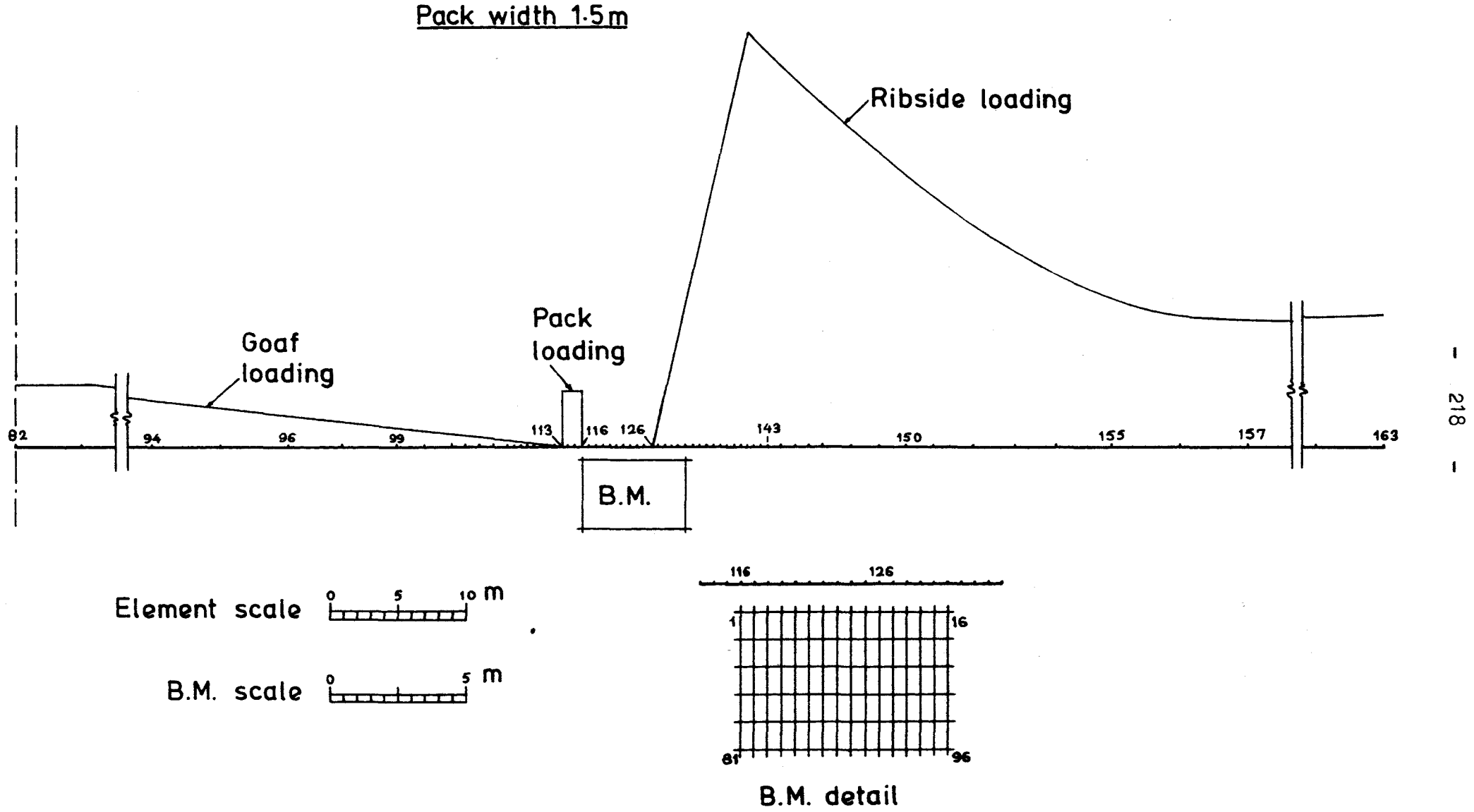

and 3000 to 7000 kN/m^2 respectively. In the short face advancing situation only two face lengths (heading widths) of 12 and 16 m were taken.

7.3.2 A criterion of failure in the face element method

Since it would be necessary to see whether the floor would undergo fracturing, if any, due to the stress distribution obtained in the face element analysis, it was decided to adopt a suitable failure criterion for the floor. Kidybinski and Babcock[70] have used three variations of the Mohr-Coulomb failure criterion for studying the failure pattern of a longwall roof. The method described here is a different form of the same criterion of Mohr-Coulomb.

Consider the tensile and compressive failure Mohr's circles in Fig. 7.11. Then the failure envelope which is tangential to both these circles will have the equation

$$\tau = \tau_c + \sigma \tan \phi \tag{7.14}$$

in a rectangular coordinate system σ, τ. The coefficient of internal friction tan ϕ and the cohesive strength τ_c can be written down as

$$\tan \phi = \frac{\sigma_c - \sigma_t}{2\sqrt{\sigma_c \sigma_t}}$$

$$\tau_c = \frac{1}{2}\sqrt{\sigma_c \sigma_t} = \frac{\sigma_c}{2} \tan\left(45 - \frac{\phi}{2}\right) \tag{7.15}$$

in which σ_c and σ_t are the compressive and tensile failure stresses for a rock.

FIG.7.11 - FAILURE CRITERION

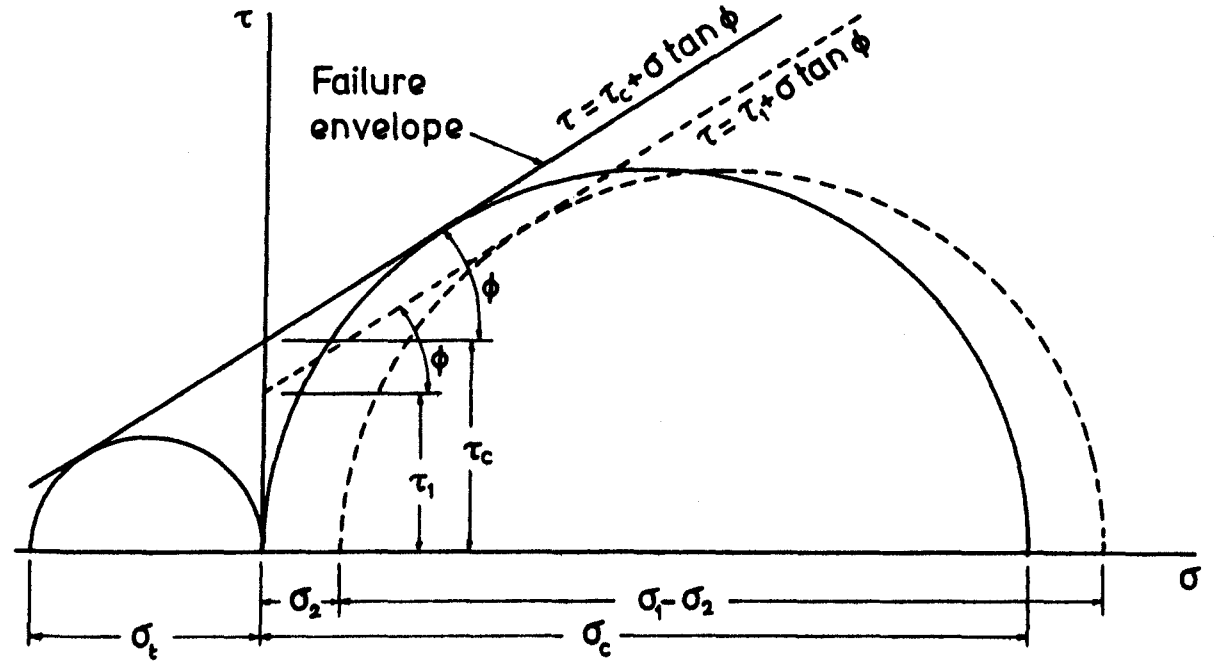

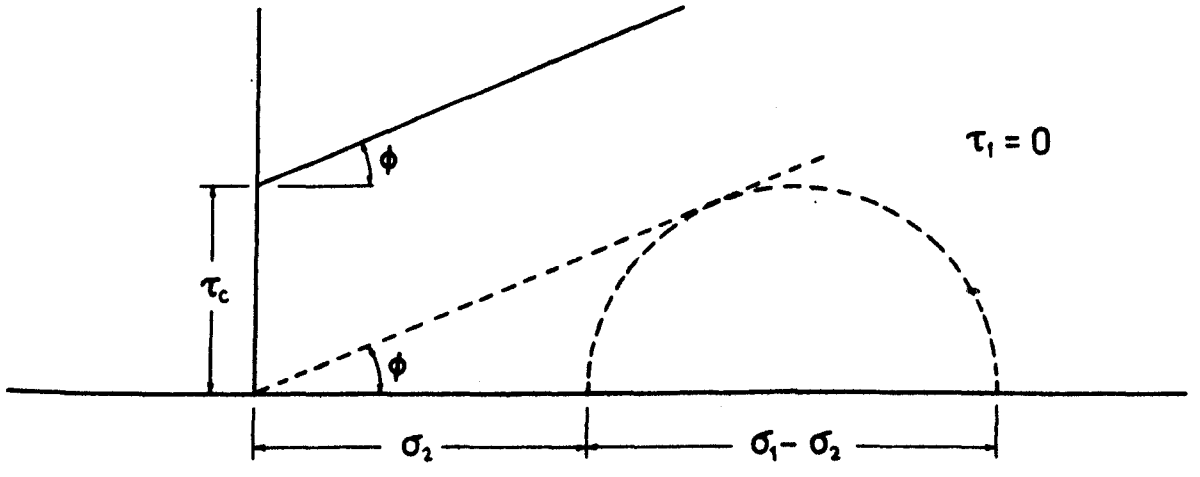

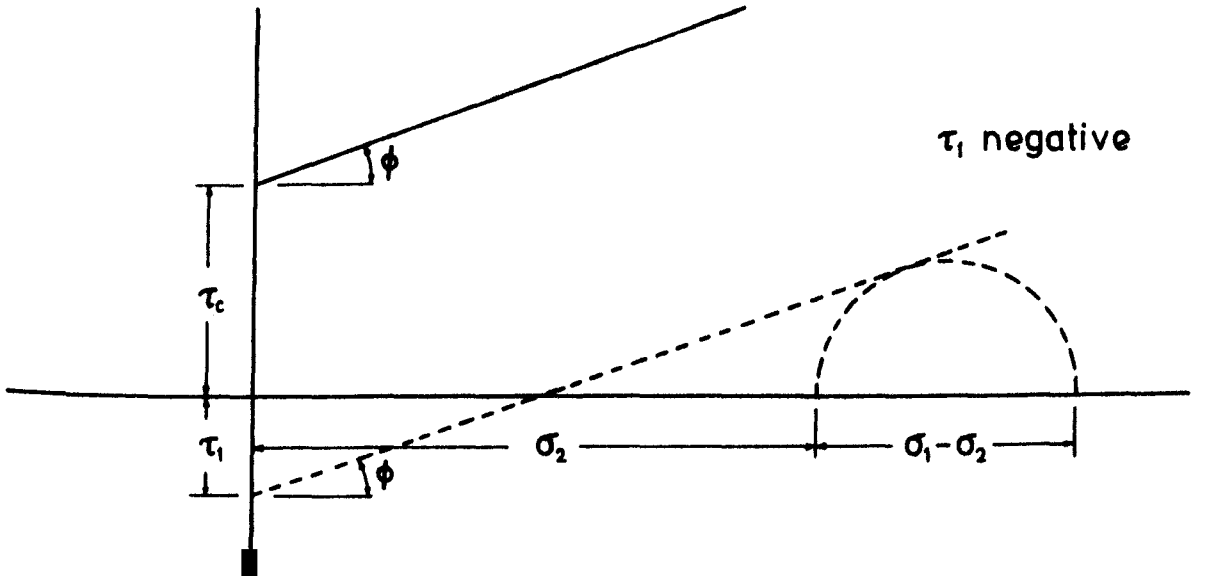

Now if we have a point in a stressed rock mass with the general stress condition (σ_1, σ_2) in terms of two principal stresses, the Mohr circle corresponding to this state of stress will be as shown by the broken circle. The Mohr-Coulomb criterion then states that failure will commence at that point if this circle touches or intersects the failure envelope (7.14). The variation of this theory suggested here is that a tangent parallel to the failure envelope drawn to this circle will have an intercept on the τ-axis greater than or equal to the cohesive strength for failure to commence. The parallel envelope will have the equation

$$\tau = \tau_1 + \sigma \tan \phi$$

where the cohesive intercept τ_1 will be given by

$$\tau_1 = \frac{\sigma_1 - \sigma_2}{2} \tan (45 - \frac{\phi}{2}) - \sigma_2 \tan \phi \ , \qquad (7.16)$$

when both the principal stresses are compressive (taken positive here). When both are negative (tensile),

$$\tau_1 = \frac{-\sigma_1 + \sigma_2}{2} \tan (45 - \phi/2) + \sigma_2 \tan \phi \qquad (7.17)$$

and when σ_1 is positive but σ_2 is negative,

$$\tau_1 = \frac{\sigma_1 + \sigma_2}{2} \tan (45 - \phi/2) + \sigma_2 \tan \phi \qquad (7.18)$$

τ_1 can occur in three forms, positive, zero or negative, as in Fig 7.11. When positive, failure is indicated if $\tau_1 \geq \tau_c$. If τ_1 is less than τ_c or if it is zero or negative it indicates stability. This then

affords us a simple criterion of failure for the floor rock.

The original face element program on the computer does not include a failure criterion. To obtain the state of stress deep into the floor, 54 bench marks were chosen below the floor level as in Fig. 7.9 for the short face advancing case. Their number was 96 in the case of retreating (Fig.7.10). The face element source program was modified to include this failure criterion represented by Equ. (7.14-18). Appendix IV shows the editing commands, together with the modification statements for incorporating in the face element source program.

As per the face element program manual[60], initial pre-excavation virgin stresses corresponding to the depth at Dawdon (365 m) were specified in the data so as to produce an upward lift in the floor when they were removed and the floor loading was applied. The modified version of the source program was run for each pack width, pack load and face length chosen for retreating and for the loadings corresponding to the two heading widths with only one rate of advance of 9.0 m/day for anhydrite packs and the five pack moduli for conventional packs in the case of short face advancing. The total runs were 27.

7.3.3 Discussion of results for elastostatic lift

7.3.3.1 Elastostatic floor heave during short face advancing

Figs. 7.12 and 7.13 show the elastostatic upward deflection of the floor in 12 and 16-m wide short face headings using centre packs when the face has advanced sufficiently. Very little difference in the lift occurred when the

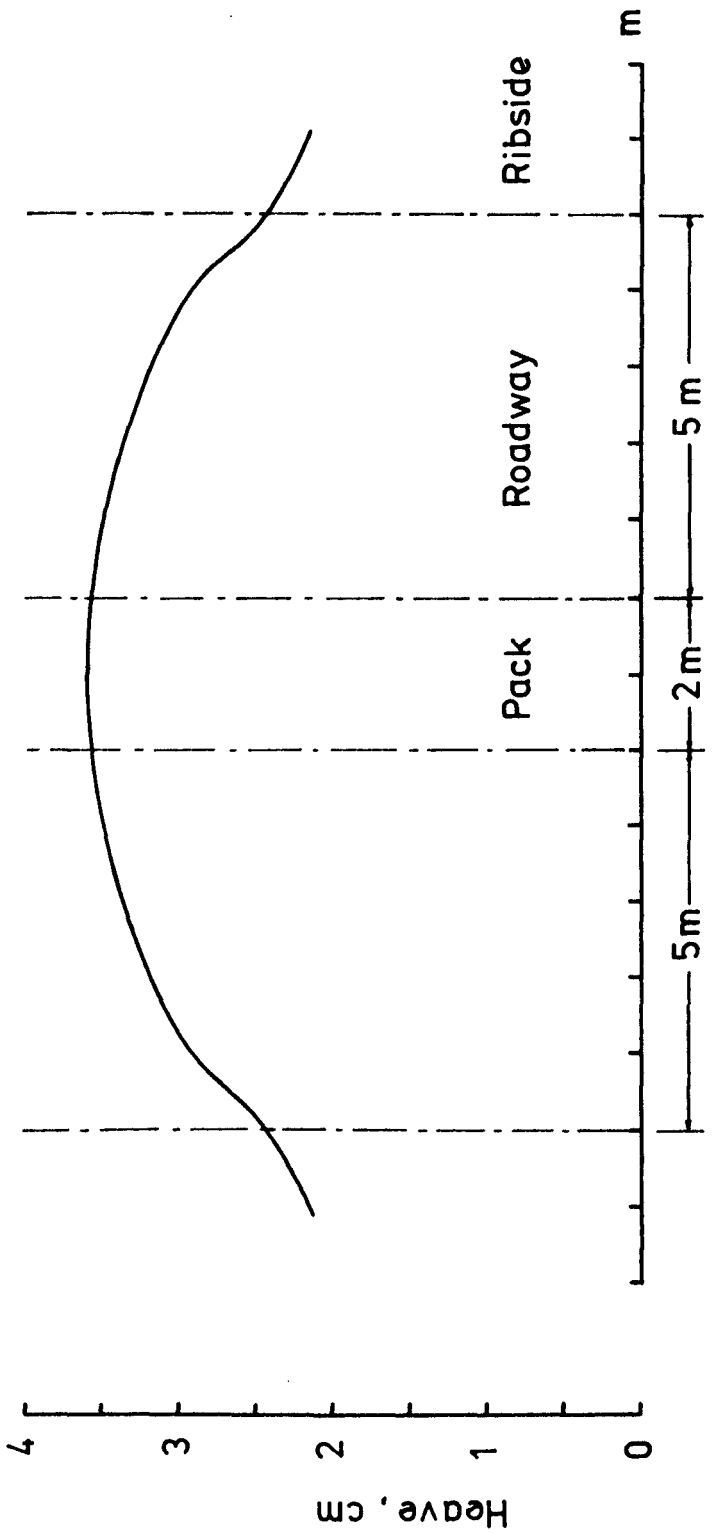

FIG.7.12-ELASTOSTATIC FLOOR LIFT IN A 12-m HEADING

FIG.7·13 - ELASTOSTATIC FLOOR LIFT IN A 16-m HEADING

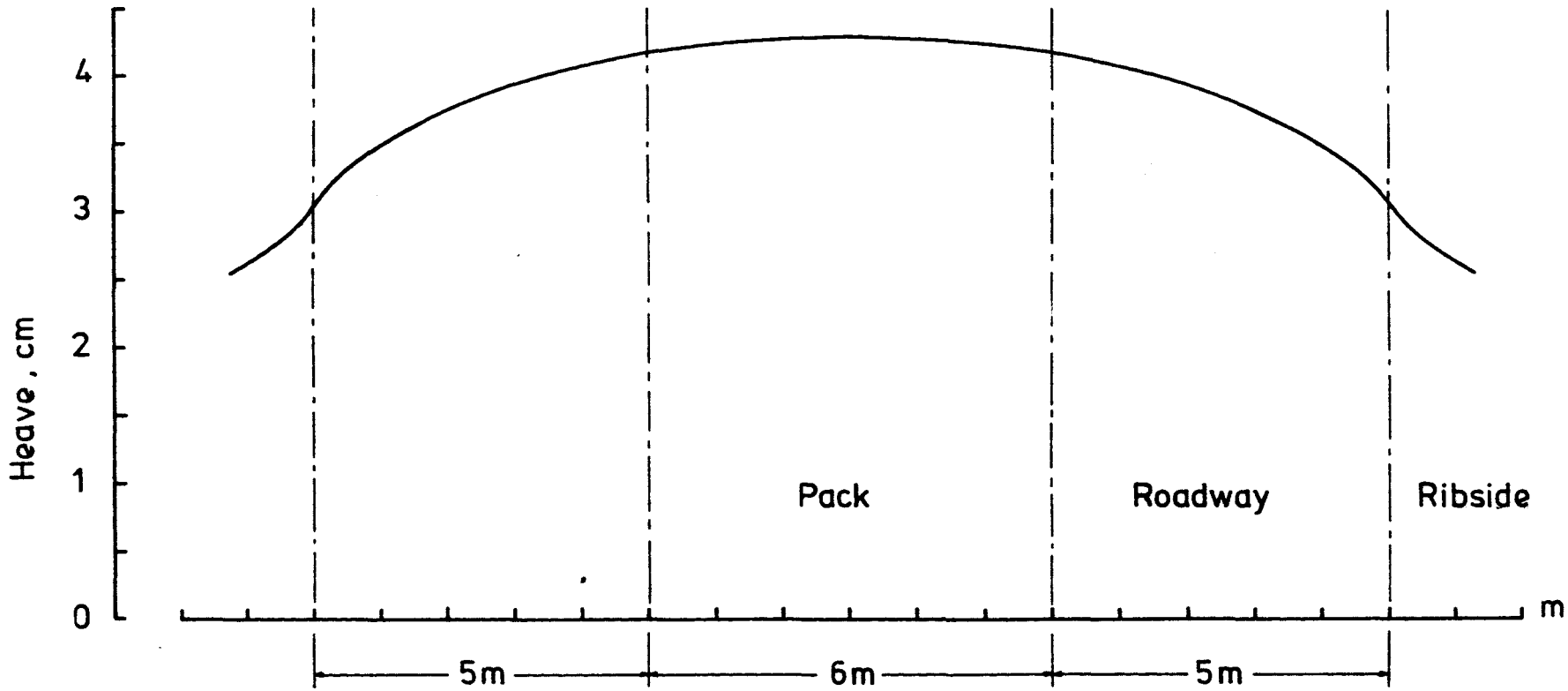

pack material was changed from anhydrite to a soft pack material with a pack modulus of 3.5×10^4 kN/m^2 (which is the smallest value considered in Chapter 6). These figures, therefore, represent all pack materials considered till now. This indicates that the pack is not very effective in influencing the floor lift during short face advancing.

The maximum lift occurs in the heading centre below the pack and the main factor governing it appears to be the heading width. In a 16-m heading the maximum central lift is nearly 4.3 cm as opposed to 3.6 cm of the 12-m heading, which is 19.4% greater.

The 54 bench marks in the floor were chosen in a rectangular grid to the right of the centre line of the heading as in Fig. 7.9. The lowest row of bench marks, nos. 46 to 54, represents a depth of 11 m below the floor level. The upward displacement of all the bench marks is plotted in Fig.7.14, showing that considerable depths are affected by the movement. The movement is greatest at the top row, nos. 1 to 9, and it falls gradually to the lowest row, nos. 46 to 54. The top row, which is 1 m below the floor level, shows displacements which are very little different from those at the floor level, being less than 2 mm smaller.

7.3.3.2 Floor stress during advancing

Distribution of the three stresses σ_x, σ_y and τ_{xy} has been plotted in Fig. 7.15 across each of the 9 columns of bench marks, the first column representing the centre line of the heading and the ninth one being below

FIG.7.14-DISPLACEMENTS AT FLOOR BENCH MARKS

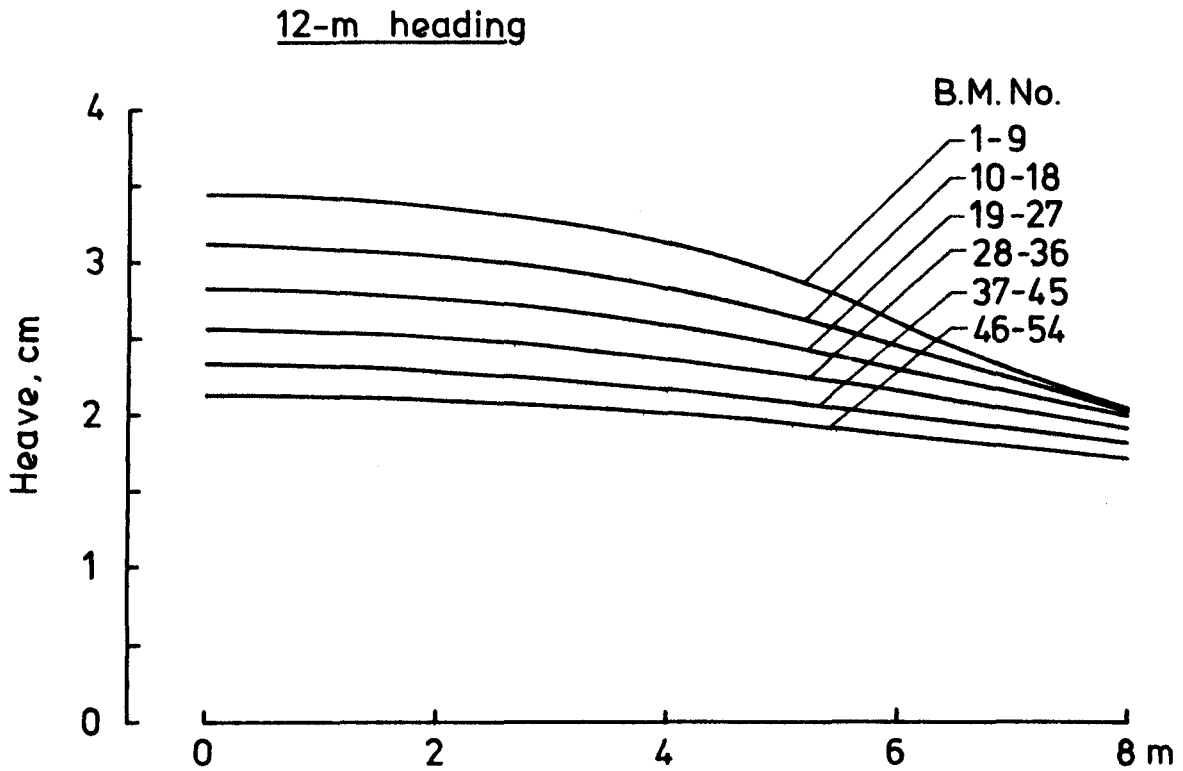

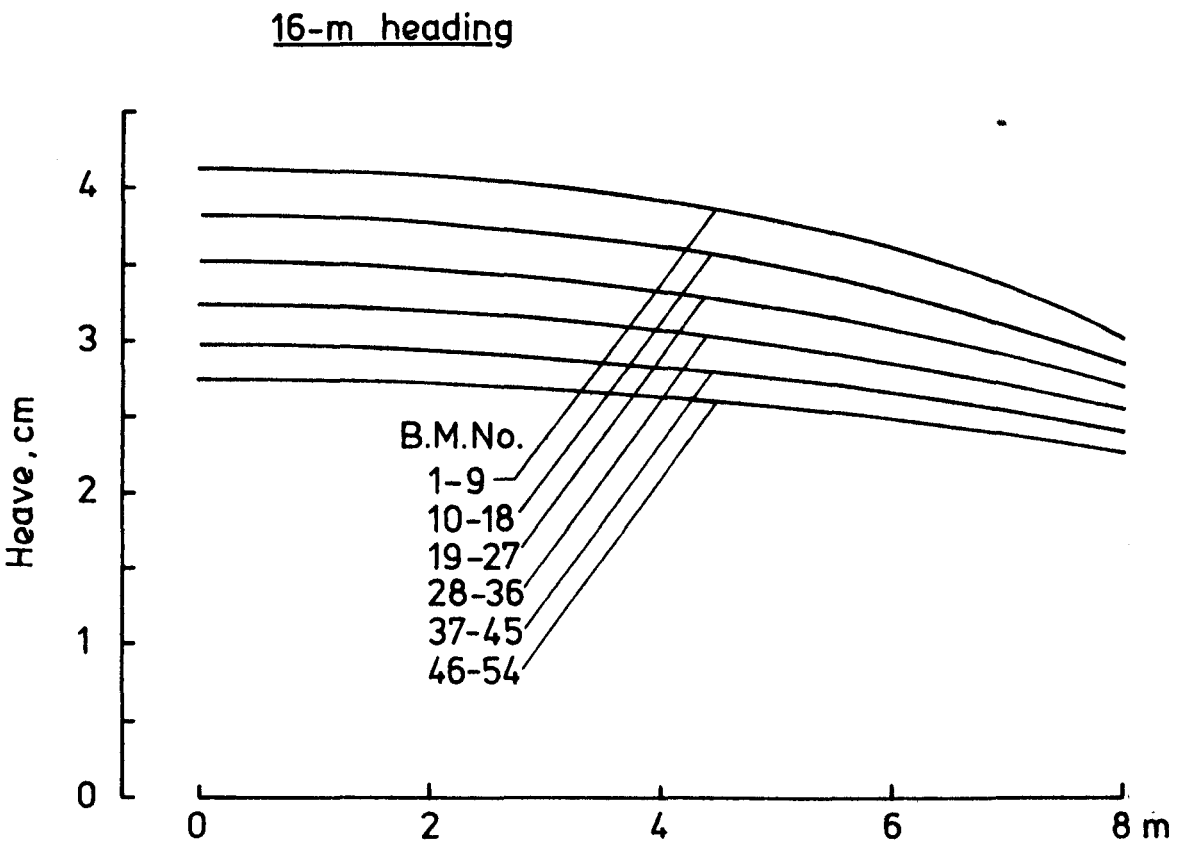

FIG. 7.15 - STRESSES AT FLOOR BENCH MARKS - 12-m HEADING

Vertical scale : 1 cm = 2 m Horizontal stress scale : 1 cm = 1000 kN/m^2

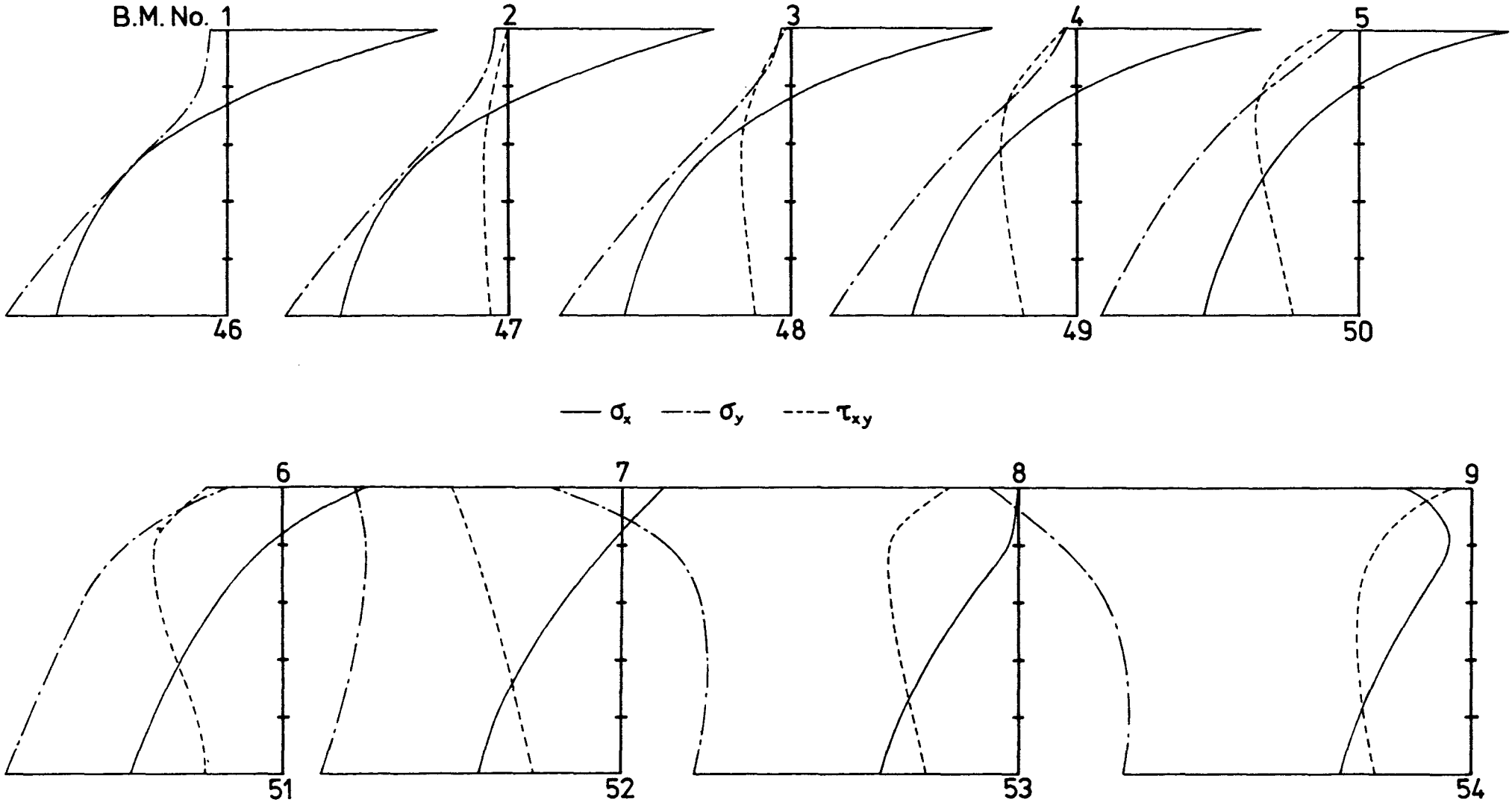

the ribside. All the three stresses do not exhibit a significant change up to the fifth column which is 2 m away from the ribside. From the sixth to the ninth column the effect of the ribside is quite noticeable, the vertical stress σ_y showing a great rise due to the abutment pressure. The shear stress is zero along the first column due to symmetry of the configuration and rises gradually toward the ribside. In this figure, negative values of σ_x , σ_y indicate compression.

The face element program also gives the values of principal stresses at bench marks. Its modified version includes the failure criterion explained earlier. Fig. 7.16 and 7.17 show the safety factor (s.f.) contours for anhydrite packs and conventional non-setting packs of modulus 3.5×10^6 kN/m^2 respectively. The safety factor at a point is defined here as the ratio τ_c / τ_1 according to the failure criterion. Curves joining points of equal safety factors are called safety factor contours. When τ_1 is zero or negative the safety factor is taken as infinity. Contours were plotted up to a maximum value of s.f. = 3.0, reasons for which will be given later.

Both Fig. 7.16 and 7.17 show virtually the same s.f. contours, again indicating that the floor stresses, and hence lift, are not significantly affected by the pack quality during short face advancing. The s.f. contours travel deeper below the ribside than below the pack, the probability of failure being to a greater depth below the ribside. However, since the rock is stratified there is a possibility that the fractures would occur along bedding planes rather than follow exactly the shape of the contour.

FIG.7.16-SAFETY FACTOR CONTOURS IN THE FLOOR
-ANHYDRITE CENTRE PACK

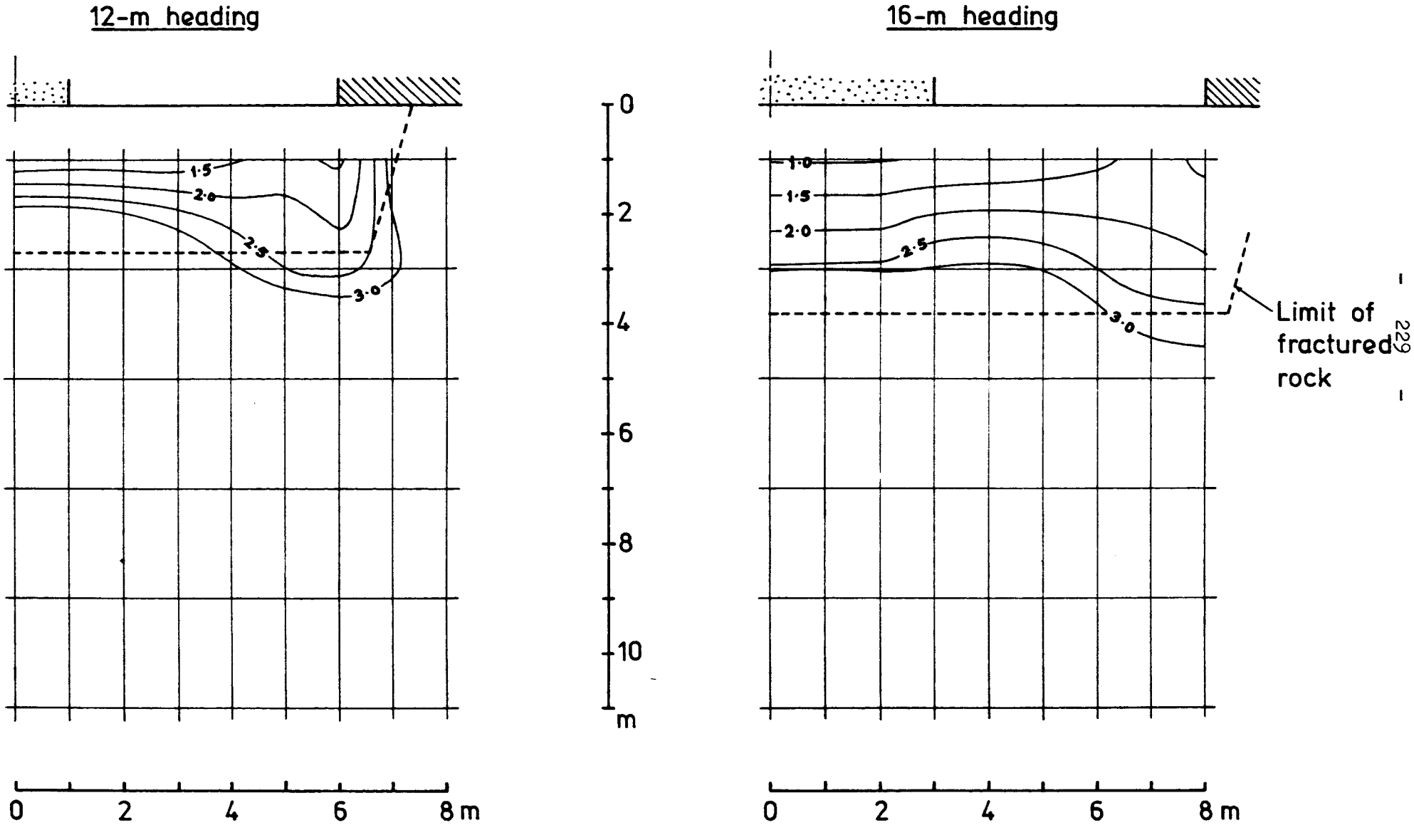

FIG. 7·17 - SAFETY FACTOR CONTOURS IN THE FLOOR - CONVL. CENTRE PACKS

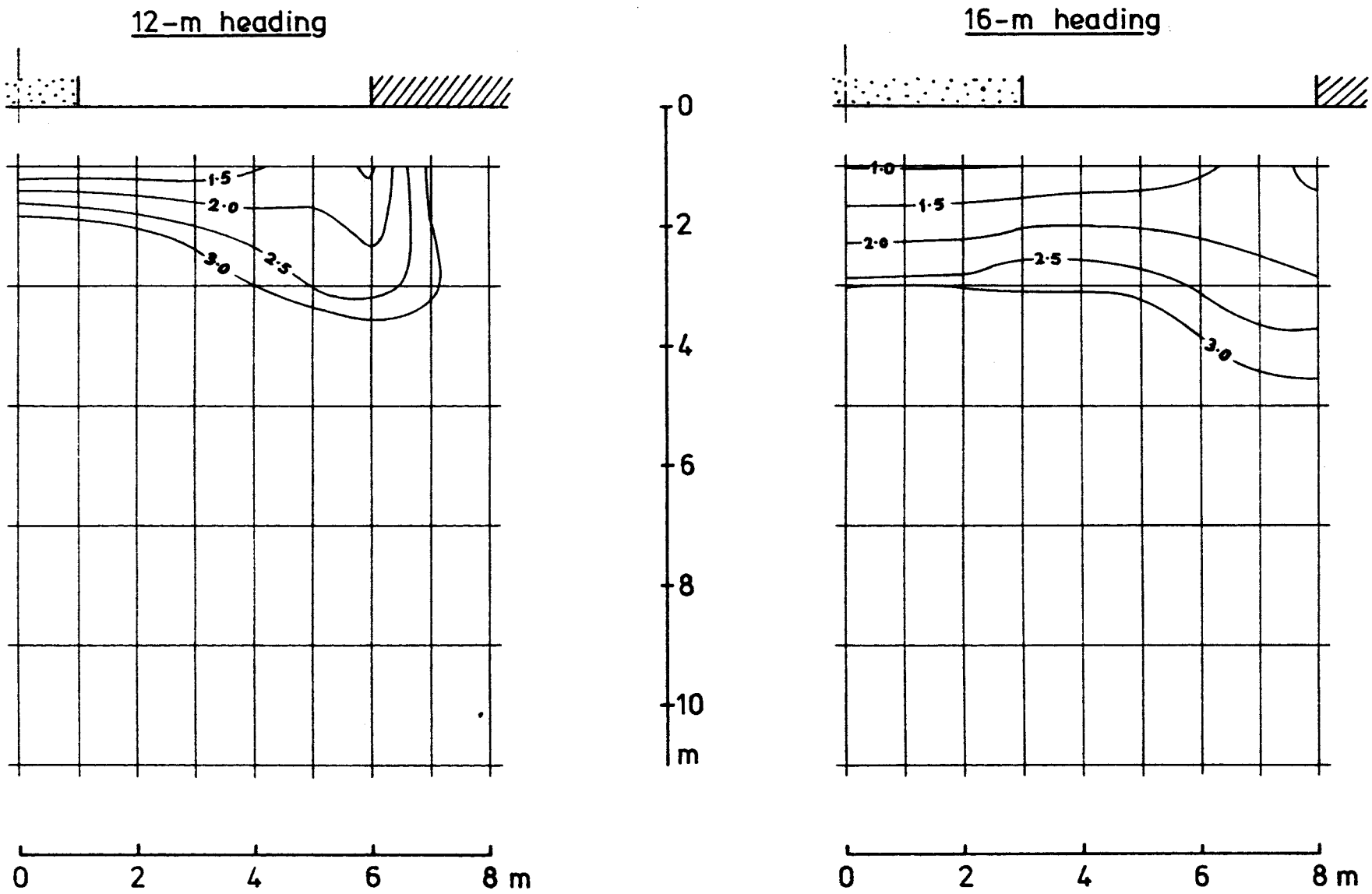

More will be said about s.f. contours in the section on post-failure analysis of floor heave.

7.3.3.3 Heave during retreating

During the retreating stage after short face advancing, the face element analysis covered the influence on lift of pack load, pack width and face length. In Fig.7.18 and 7.19 is shown the heaving of the floor surface at five pack load values of 3000 to 7000 kN/m^2 the pack width being 1.5 m and 6.0 m respectively. The face length in both the figures is 183 m. The heaving curve shows a downward curvature in the pack region and upward in the roadway region. The downward curvature is seen to be more noticeable at higher pack loads. As the pack load rises, the whole heaving curve shifts downward in all regions. At lower values of pack load the downward curvature below the pack is almost negligible. A 6-m pack shows a greater change in the lift with pack load than a 1.5-m pack, as might be expected. A twofold increase in the pack load from 3000 to 6000 kN/m^2 reduces the maximum roadway lift by about 8.6% in the case of a 1.5-m pack and by about 23.2% when a 6-m pack is used.

If the pack load remains the same an increase in the width of the pack produces increased floor heaving as in Fig.7.20. This is somewhat surprising, but is probably because of the fall in abutment pressure being produced upon a pack width increase. Though this is so, it will be seen later that the curvature drops for higher pack widths, giving more advantageous floor stress patterns.

FIG.7·18-ELASTOSTATIC LIFT DURING RETREATING-EFFECT OF PACK LOAD

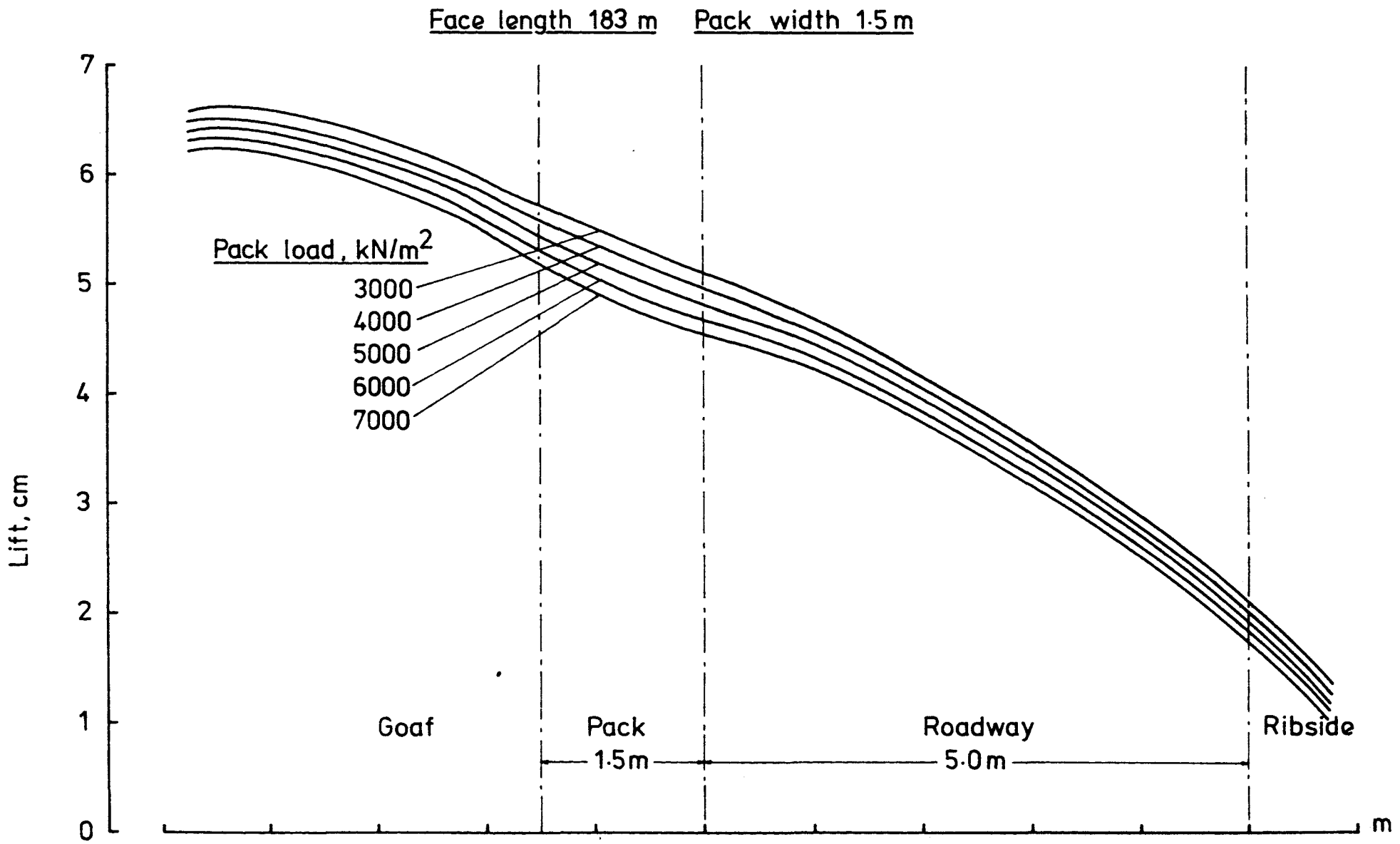

FIG.7.19 - ELASTOSTATIC LIFT DURING RETREATING - EFFECT OF PACK LOAD

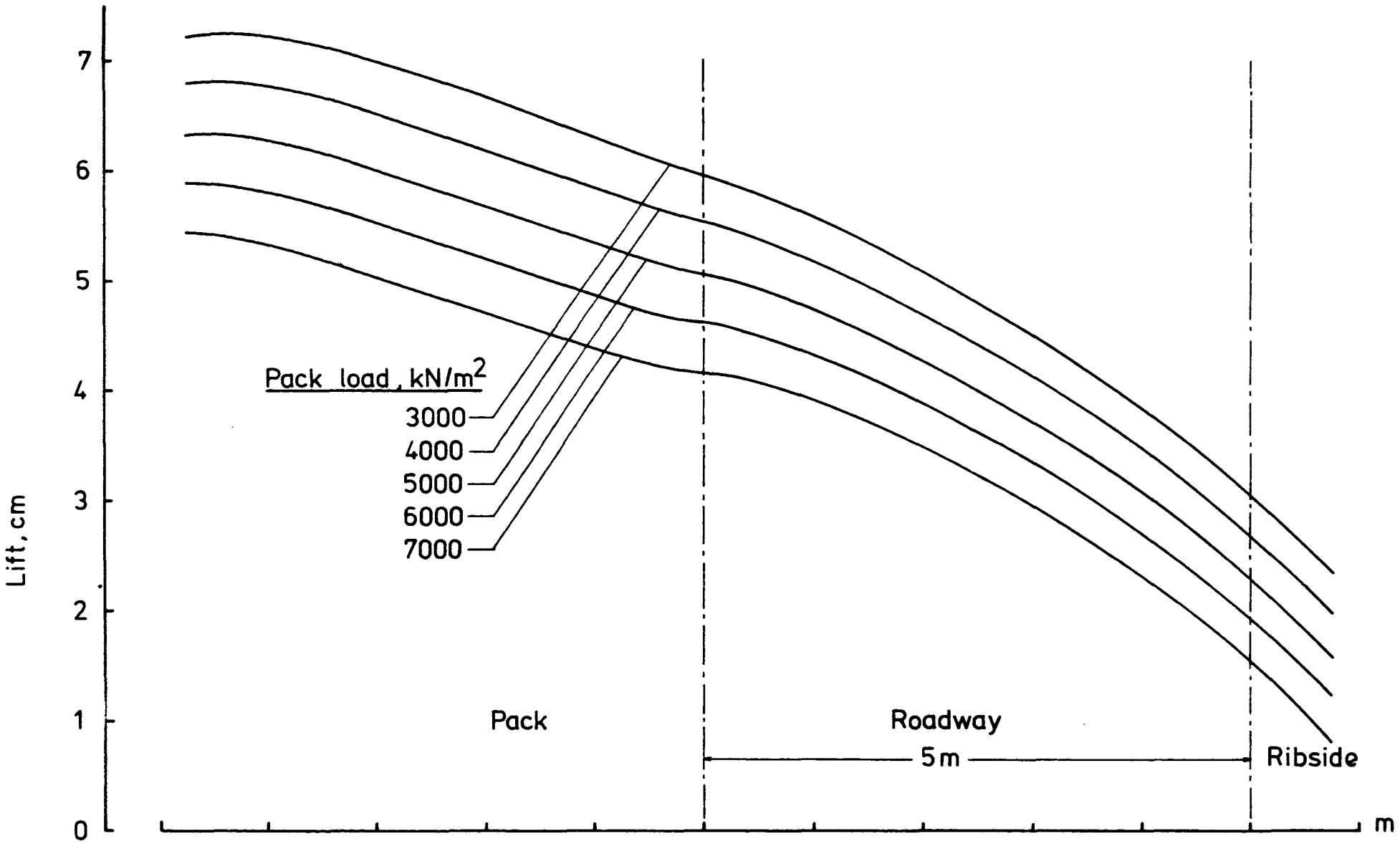

FIG.7·20 - ELASTOSTATIC LIFT DURING RETREATING - EFFECT OF PACK WIDTH

Face length 183 m Pack load 3000 kN/m^2

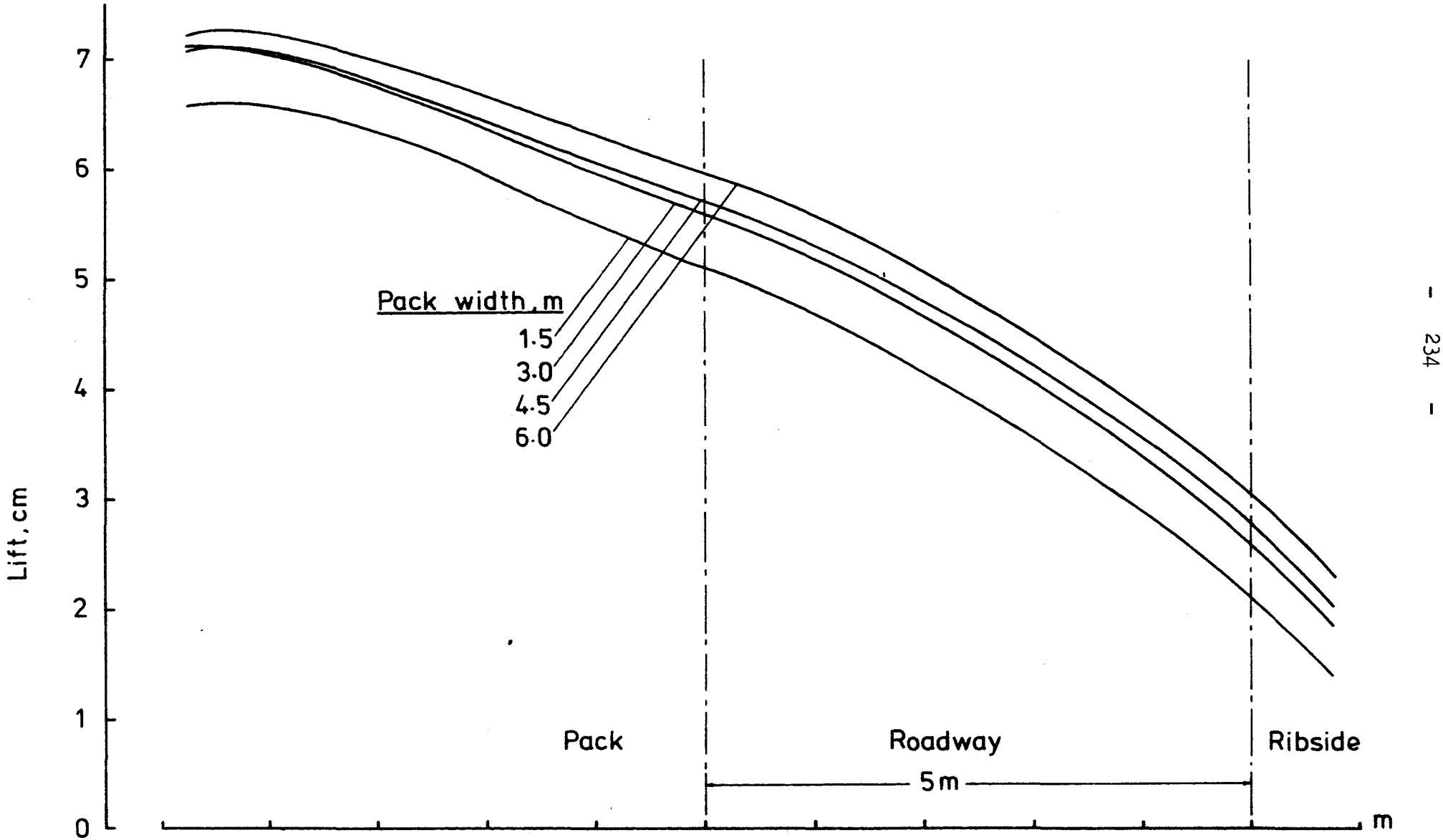

FIG. 7·21 - ELASTOSTATIC LIFT DURING RETREATING - EFFECT OF FACE LENGTH

Pack width 1·5 m Pack load 3000 kN/m^2

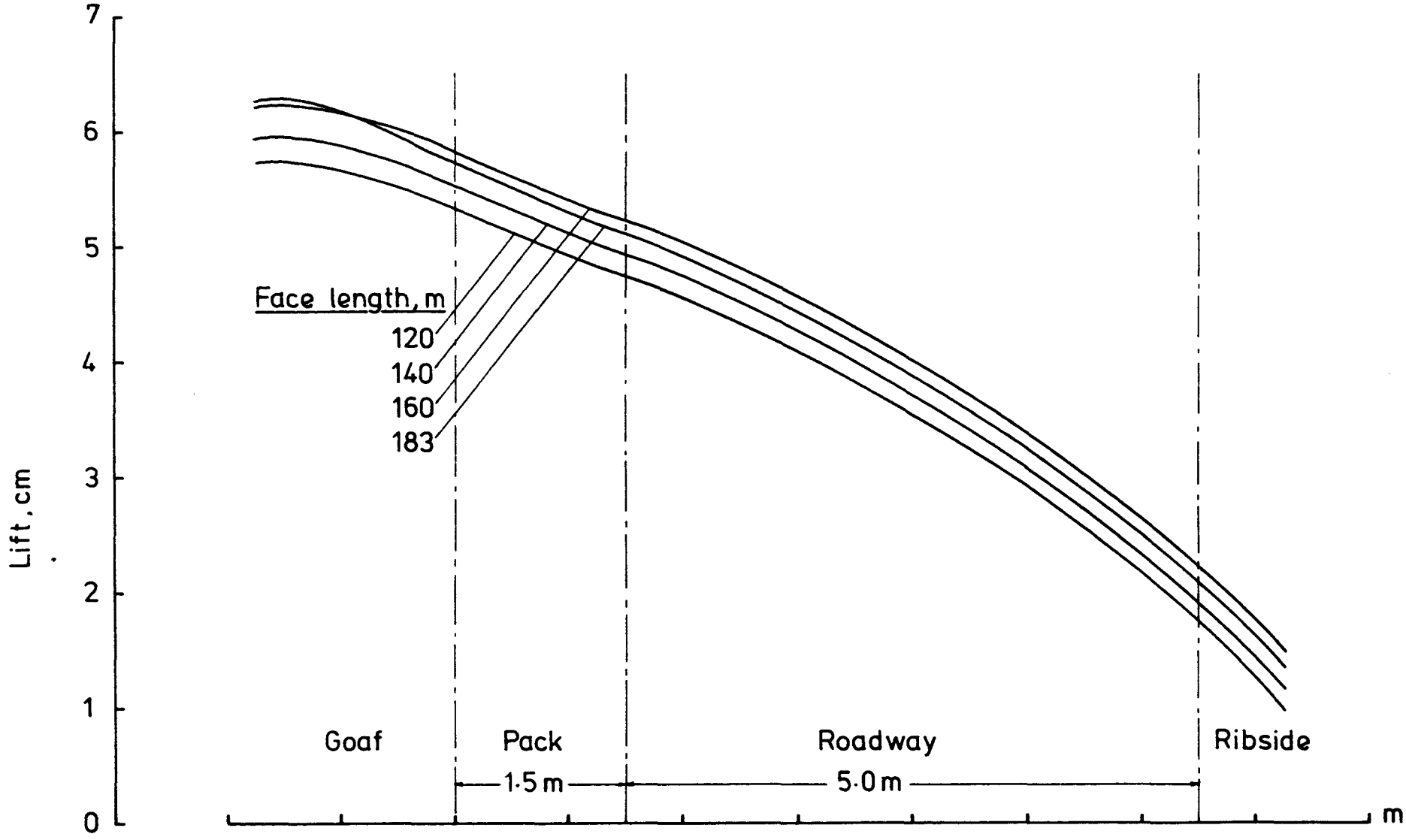

The length of the longwall face for the same pack load of 3000 kN/m^2 and pack width of 1.5 m influences the floor heave curve as indicated in Fig. 7.21. Amongst the four face lengths considered, the greatest roadway lift occurs for a length of 160 m instead of for the highest value of 183 m.

7.3.3.4 Safety factor contours during retreating

The change in the safety factor contour pattern with pack load can be noticed from Fig. 7.22 and 7.23 for a 1.5-m pack and from Fig. 7.24 and 7.25 for a 6-m pack. Increasing the pack load reduces the depth of contours for both pack sizes. In the 1.5-m case the contours change in the roadway region more than near the pack. Especially noteworthy are the contours in the case of a 6-m pack with a load of 7000 kN/m^2 (Fig.7.25). Very short contour lines exist just at the corner area between bench marks Nos. 1 and 3. The probability of a deep fracture is thus greatly reduced.

Similar is the effect of widening the pack from 1.5 to 6 m at a constant pack load, as observed from Figs. 7.22, 7.24, 7.25 and 7.27. The contour depth goes on reducing.

From all the figures of s.f. contours during retreating the following conclusions can be drawn:

(a) No probability of failure is indicated near the ribside up to about 1 m from it.

(b) The contour lines have the greatest depth near the pack edge and about 3.0 m from the pack edge in the roadway.

FIG.7·22 - S.F. CONTOURS DURING RETREATING

Pack width 1·5 m Pack load 3000 kN/m^2

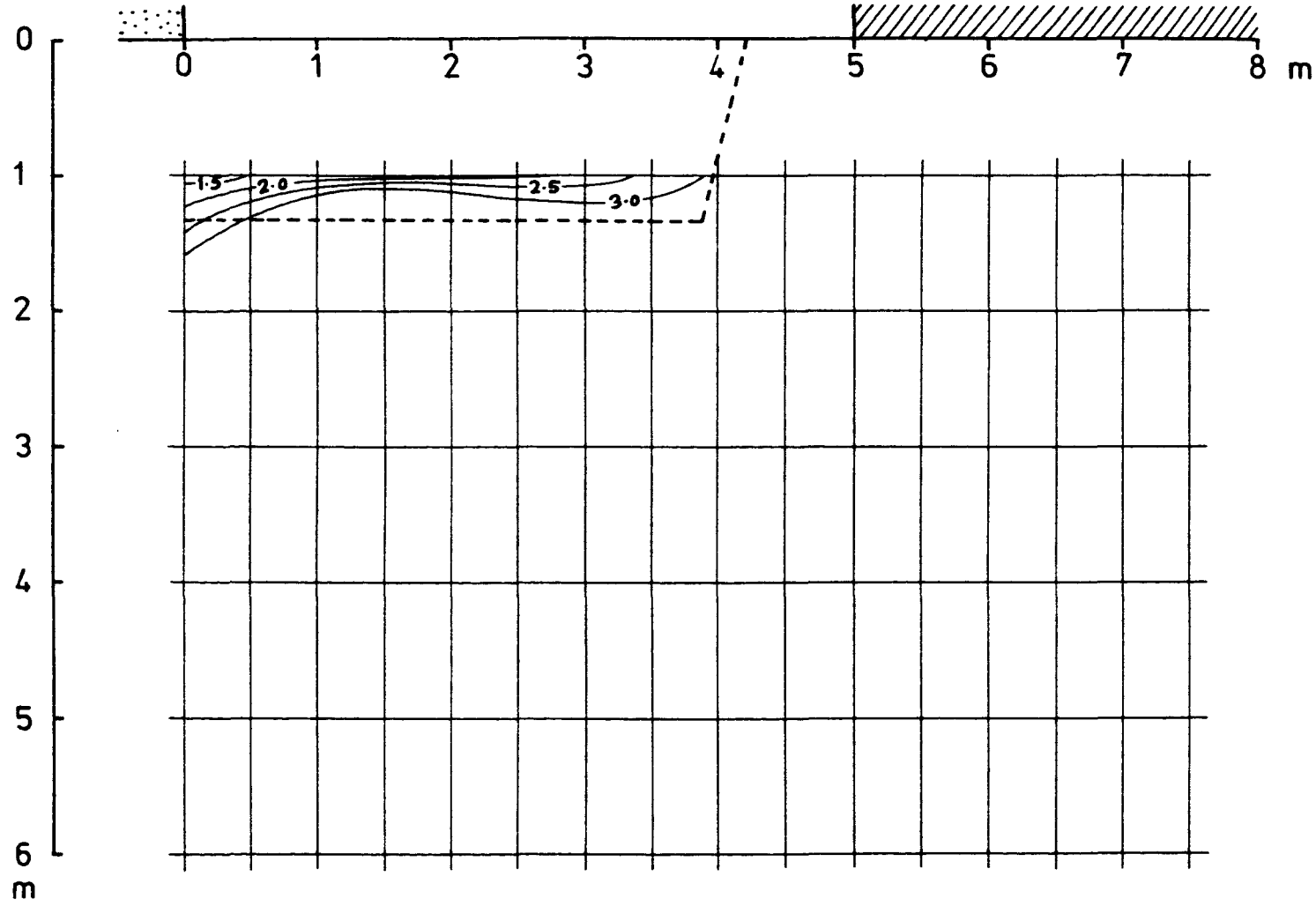

FIG.7·23 - S. F. CONTOURS DURING RETREATING

Pack width 1·5 m Pack load 7000 kN/m^2

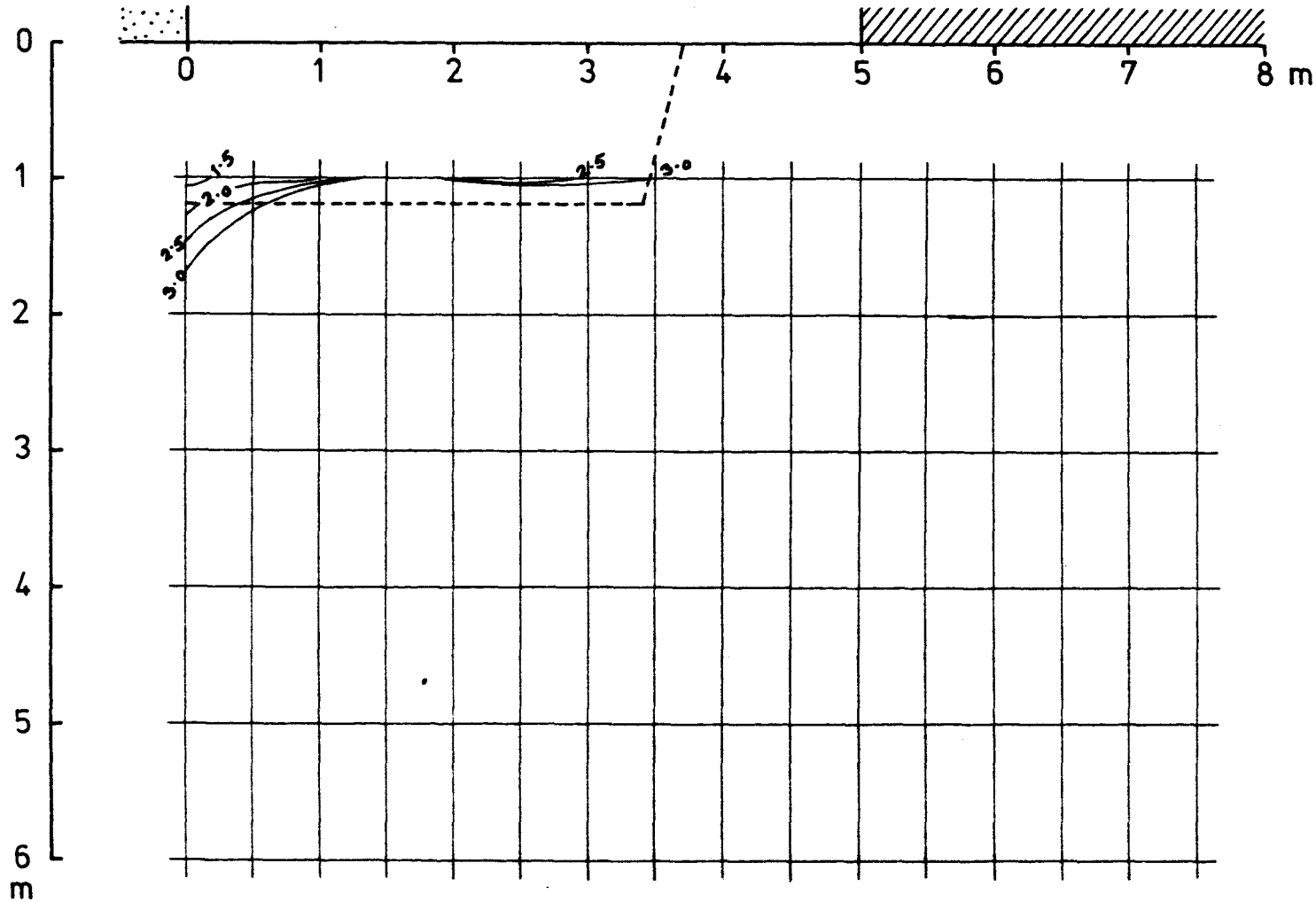

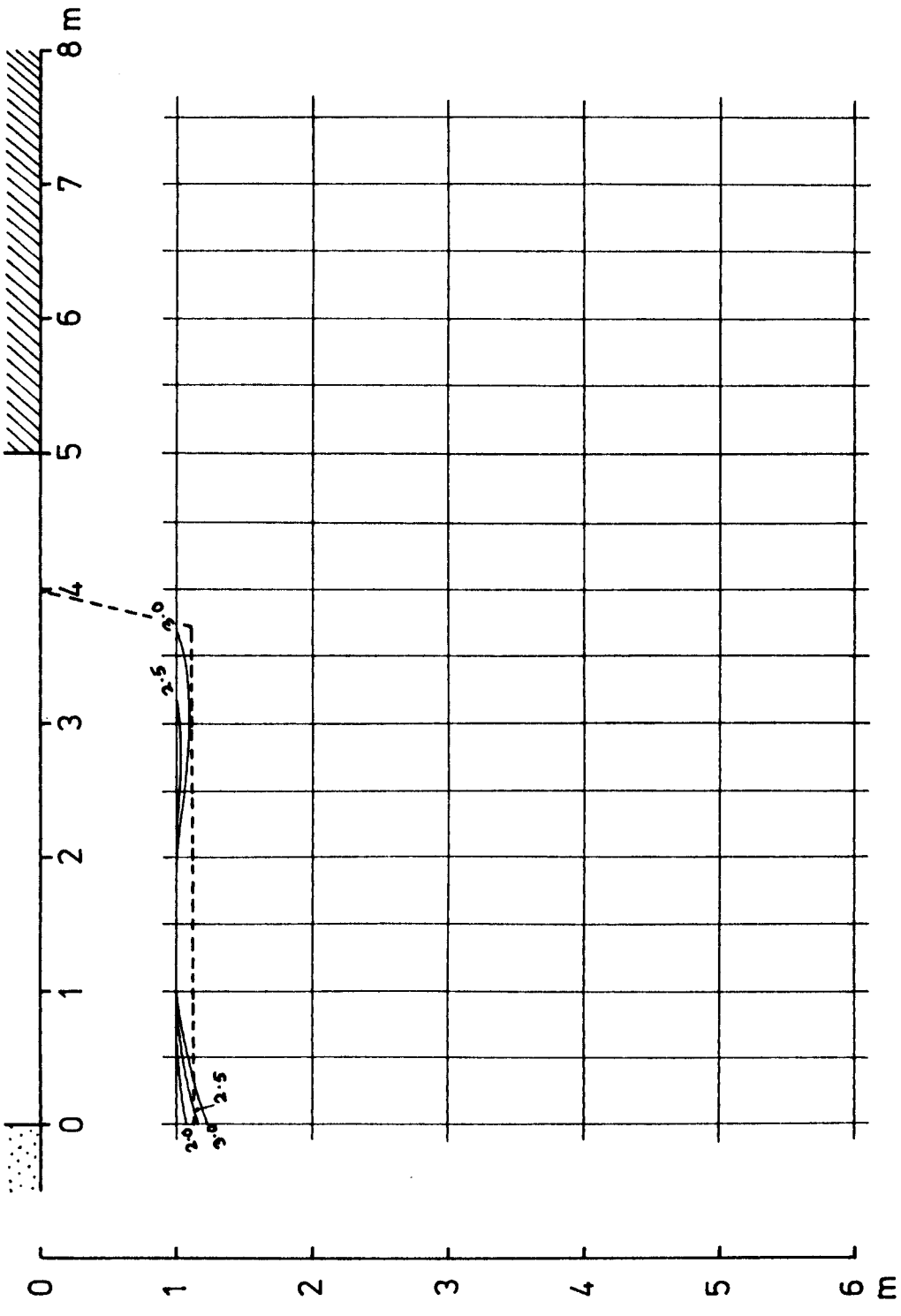

FIG.7.24 - S.F. CONTOURS DURING RETREATING.

FIG.7·25 - S. F. CONTOURS DURING RETREATING

Pack width 6·0 m Pack load 7000 kN/m^2

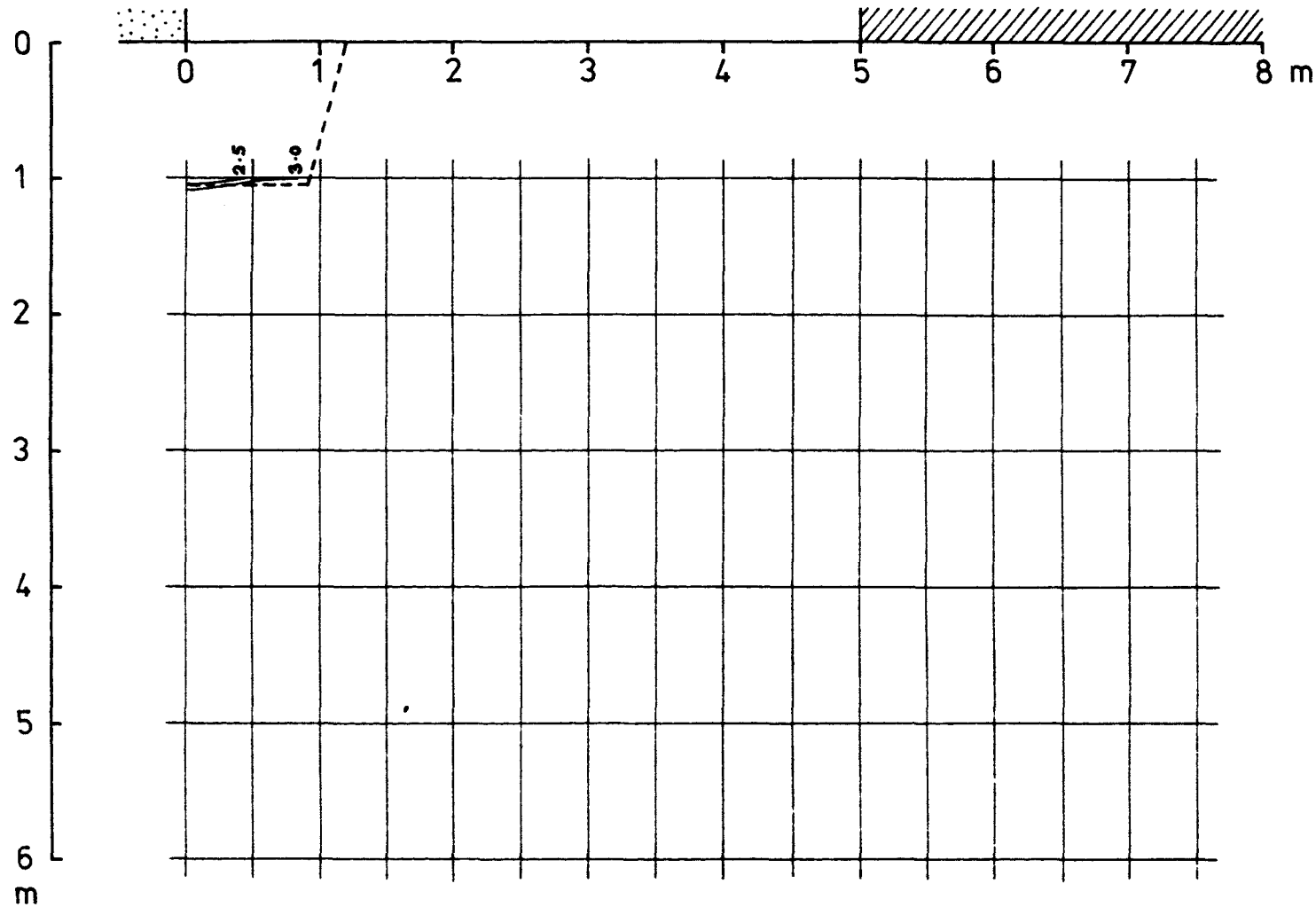

FIG.7·26 - S. F. CONTOURS DURING RETREATING

Pack width 3·0 m Pack load 3000 kN/m^2

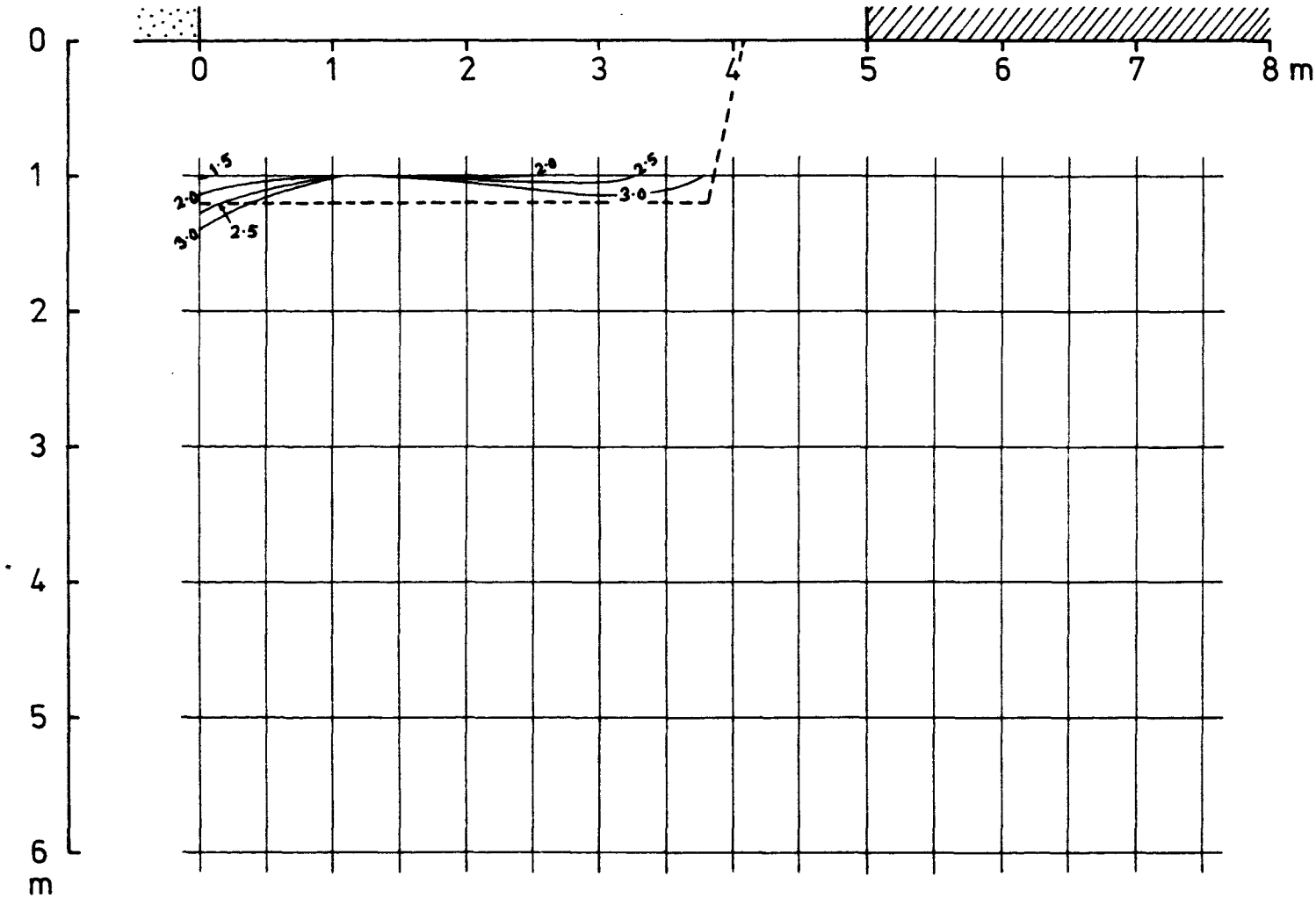

FIG.7·27- S. F. CONTOURS DURING RETREATING

Pack width 4·5 m Pack load 3000 kN/m^2

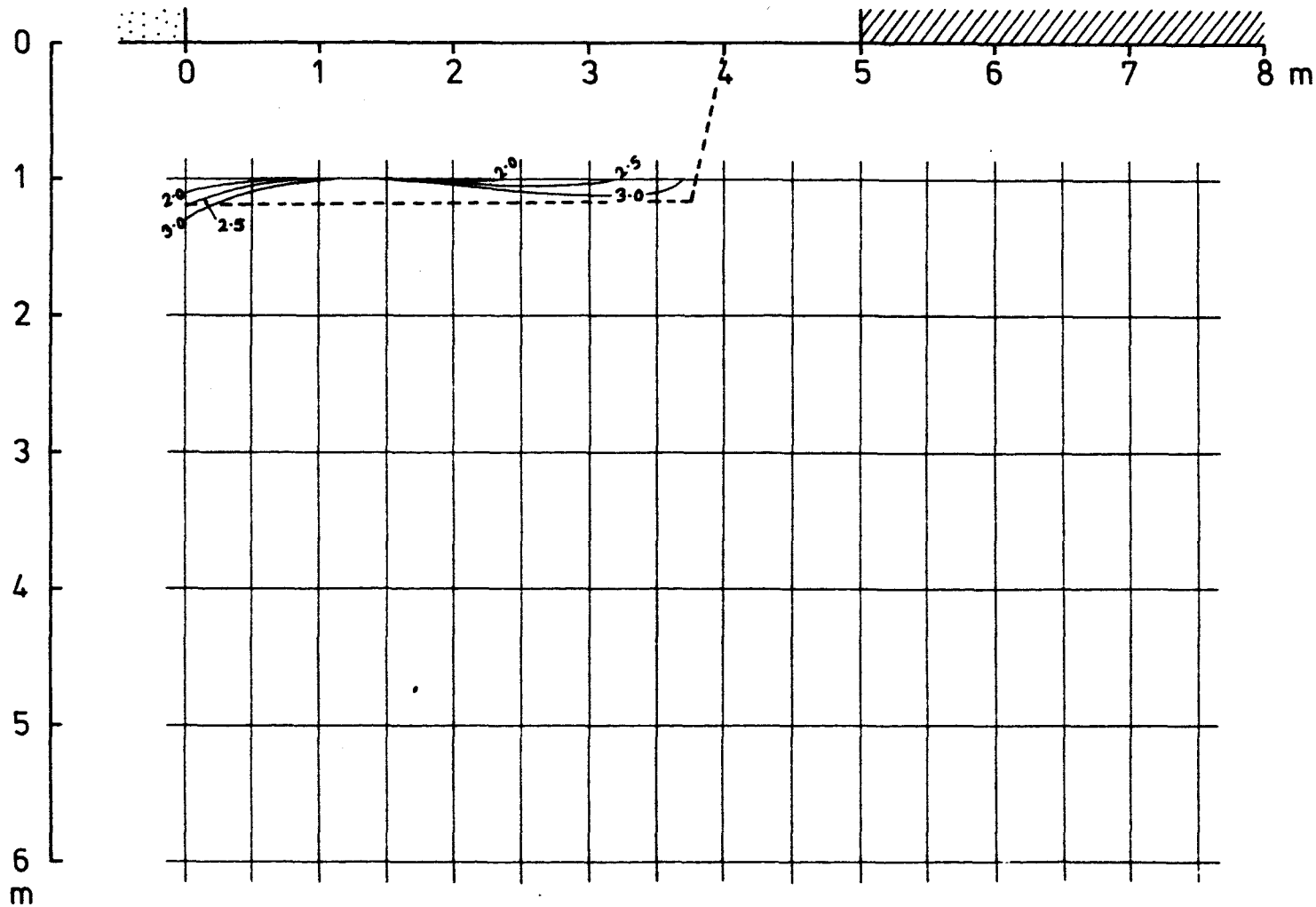

(c) Probability of failure is greatest near the pack edge as opposed to the case of short face advancing in which it is at the ribside.

(d) The effect of widening the pack is less than increasing the pack load.

(e) A probability of deeper fractures exists while advancing than while retreating.

The last conclusion makes it obvious that deeper fractures than the subsequent retreating is likely to give rise to may already exist in the floor because of short face advancing. This conclusion is important since if the longwall face were advancing instead of retreating after short face advancing, the s.f. contours would be as in Figs. 7.22-27 and we would obtain much shallower fracture areas in the floor than are obtained in Fig. 7.16. This is a point in favour of simple advancing than retreating after short face advancing. A detailed post-failure viscoelastic analysis is, however, necessary to estimate whether the creep will be excessive by this method.

7.3.3.5 Safety factor variation

The change in the least safety factor in the bench mark region of the floor is represented by Fig. 7.28. The least s.f. rises with pack load almost linearly, more quickly for a 6-m pack than for a 1.5-m one. The increase with pack width is curvilinear, widening the pack beyond 5 or 6 m not being of much consequence.

The safety factor reduces steeply if the face length is increased beyond 160 m. Faces shorter than 160 m do not appear to be of any great benefit because the safety factor changes little. The least safety factors are given in Table.7.2.

FIG.7.28 - LEAST SAFETY FACTOR IN THE B.M. REGION DURING RETREATING

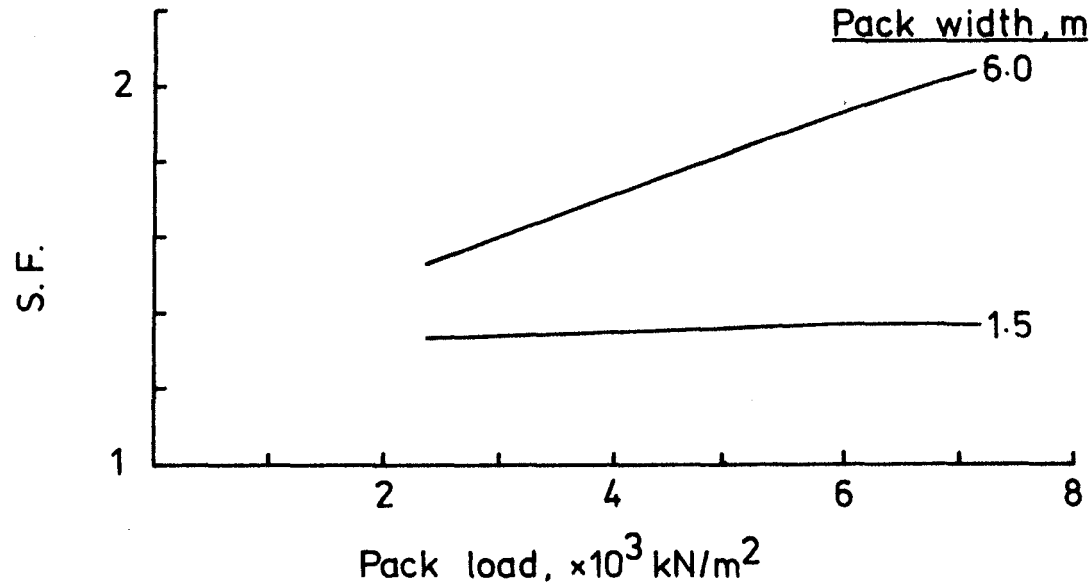

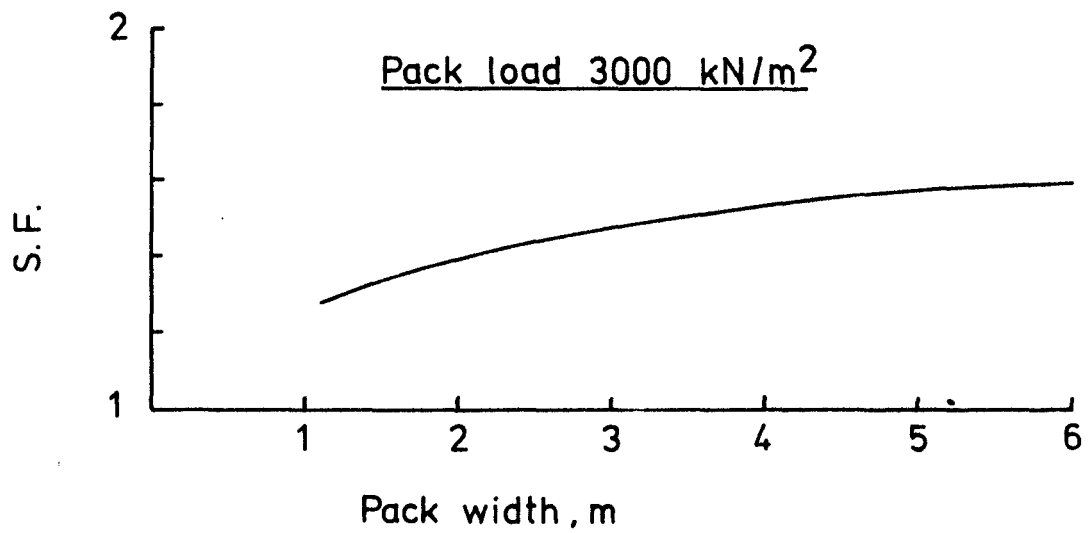

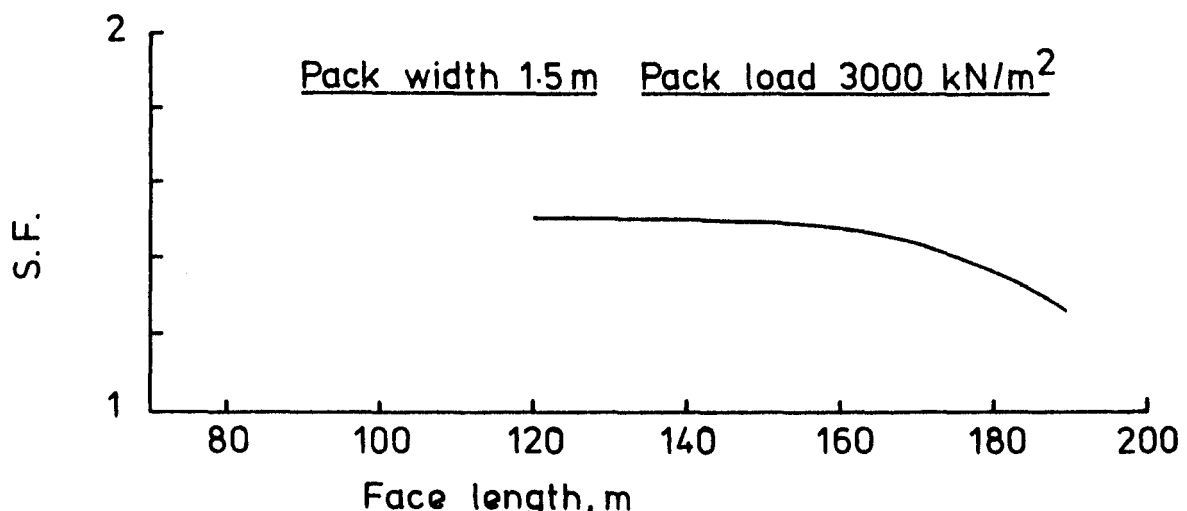

TABLE 7.2

Least safety factors in the bench mark region of the floor during retreating

(a) Safety factor vs. pack load - face length 183 m

Pack width m	Pack load kN/m^2	s.f.
1.5	3000	1.34
	4000	1.35
	5000	1.36
	6000	1.37
	7000	1.37
6.0	3000	1.60
	4000	1.71
	5000	1.82
	6000	1.93
	7000	2.03

(b) Safety factor vs. pack width -pack load 3000 kN/m^2, face length 183 m

Pack width,m	s.f.
1.5	1.34
3.0	1.48
4.5	1.56
6.0	1.60

(c) Safety factor vs. face length -pack load 3000kN/m^2, pack width 1.5m

Face length, m	s.f.
120	1.51
140	1.50
160	1.48
183	1.34

7.4 Post-failure floor heave analysis

From Fig. 7.16 for short face advancing and Figs. 7.22 - 27 for subsequent retreating, it is felt that there will be fractures in the floor. Assuming a safety factor of 3.0 as the limiting value for fracture, the contour lines for this value are then the limits of failure or fracture surfaces. This value of 3.0 was taken based on the ratio of laboratory and in-situ values of the elastic modulus of rock proposed by Kidybinski and Babcock[70]. It was assumed that the ratio would be the same for strengths for the purpose of this analysis, so it was decided to draw the s.f. contours only up to the value of 3.0.

Now, it was already mentioned that the fracture surface would not exactly follow the s.f. contour lines because of the stratifications. The breaks would occur along bedding planes horizontally, and at $\theta = 75^{\circ}$ to the stratification as per the angle of fracture. Mean horizontal lines have been drawn in the region of the s.f. contour of 3.0 and another line at 75° to this line, near the ribside in Fig. 7.16 and Figs.7.22 - 27. It is at once seen that the depth affected by fractures during short face advancing, which is 2.7 m for a 12-m heading and 3.8 m for a 16-m heading, is greater than in any case of subsequent retreating. So during retreating floor heave will occur due to the deformation of an already broken floor. In advancing,the breaks will develop gradually and reach their final picture of Fig. 7.16 when the short face is sufficiently far away.

In soil mechanics it is well known that during a plate bearing test,

some heave at the soil surface occurs when the bearing plate undergoes pressure. The behaviour of a pack on broken rock is akin to a plate bearing test. In the absence of any definite conclusive evidence regarding the amount of heave vis-à-vis plate load and soil property, it was decided to estimate the post-failure heave by elastic analysis of the broken rock zone. A finite element elastic analysis of the longwall roof after failure can be seen in reference (70). The method followed here is basically the same except that it is analytical and not numerical.

It is known from experiments that the progressive failure of rock in compression, expressed in terms of a decreasing bearing capacity of a specimen, is connected with a gradual drop in the modulus of elasticity related to the entire acting section of the material[71]. Fig. 7.29 shows the curve of post-failure elastic behaviour of a sandstone sample, where E_o is the initial maximum value of the modulus of elasticity, E_n is the actual E value due to the process of failure, σ_c is the critical maximum stress and σ_n is the residual resistance stress during the process of failure. Kidybinski and Babcock[70] have proposed that

$$\frac{\sigma_c}{\sigma_n} = \frac{1}{S}$$

where S is the safety factor ($S < 1$). In our case failure is indicated up to $S = 3.0$, so that

$$\frac{\sigma_c}{\sigma_n} = \frac{3}{S} \qquad (7.19)$$

This relation gives the value of the ratio σ_c / σ_n which can in turn give the post-failure modulus values E_n from Fig. 7.29.

FIG.7.29 - POST-FAILURE ELASTICITY OF SANDSTONE
(After Bieniawski)

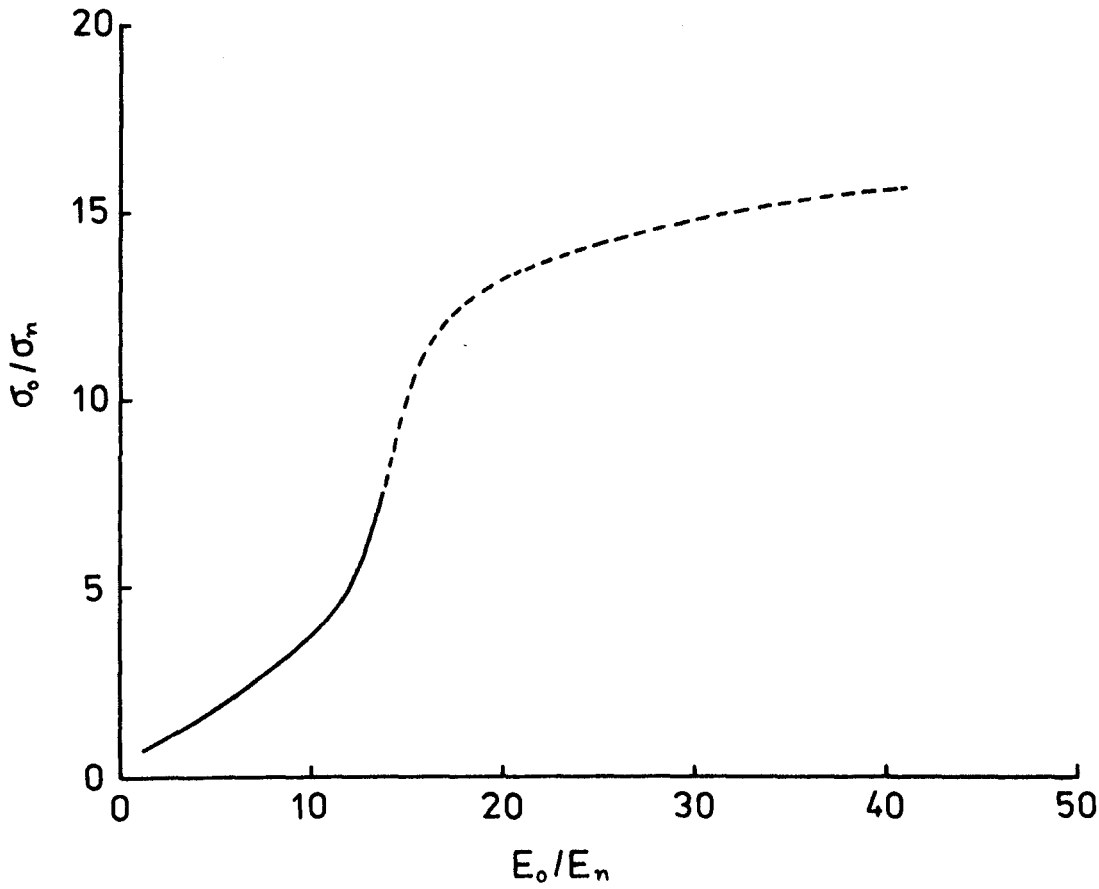

FIG.7.30 - MODEL FOR POST-FAILURE FLOOR LIFT

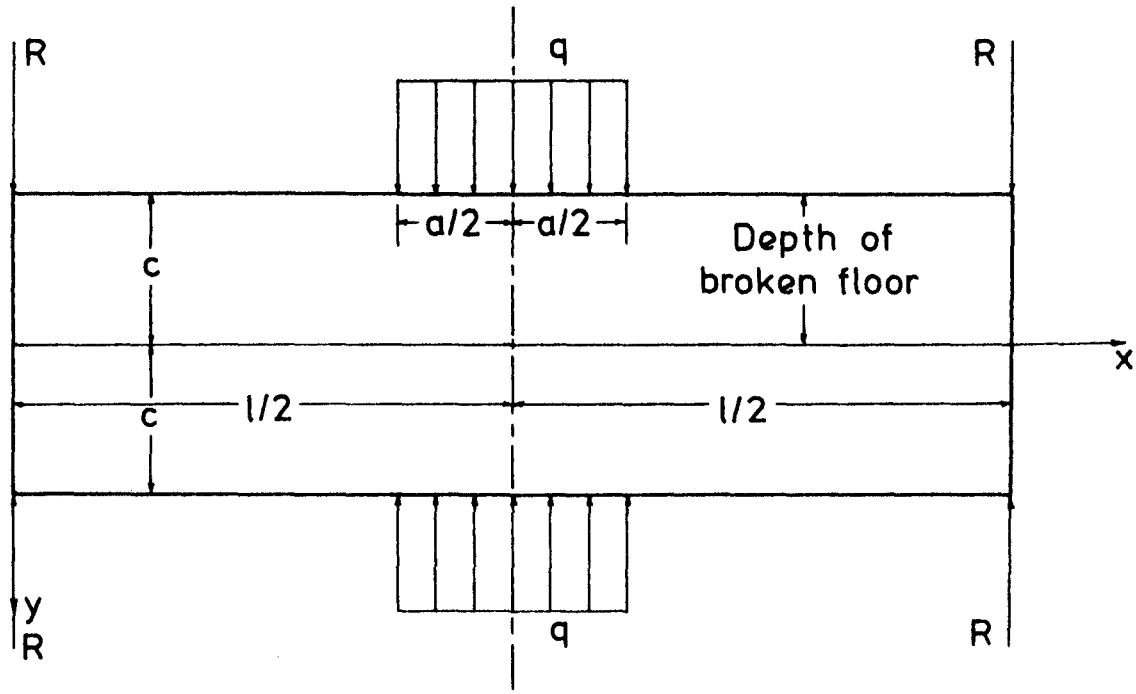

7.4.1 Elastostatic solution for the broken zone

The broken rock zone of Fig. 7.16 has been analysed for two loading conditions corresponding to short face advancing and retreating. Since the configuration of the broken zone remains the same during both phases of working, all that was necessary was to vary the loading condition on the pack and ribside. The following simplifying assumptions were made:

(a) Instead of the fracture surface at the end of the broken zone being inclined at 75°, it was assumed to be vertical.

(b) The broken rock was assumed to rest on solid rock with initial deflection values being zero. Deflections at the surface of the floor so obtained were superimposed on those obtained by the face element analysis.

(c) The extent of the broken zone in the goaf was the same as in the roadway.

(d) The ribside, being solid and infinite, did not actually cause penetration into the broken rock, but merely acted as a restraint to the broken rock, keeping its deflection zero below the ribside.

(e) The same restraining force was applied on the goaf-side.

Due to these assumptions the model of broken rock appeared as in Fig. 7.30. Because of the symmetrical loading on the top and bottom of the

beam, the model satisfies the assumption (b) giving zero displacements v at the middle plane $y = 0$. The depth of the broken rock during short face advancing and also during retreating is represented by c in the figure, so that the bottom half of the beam of thickness 2c gives deflections which are mirror images of those of the top half. Such a model of double the broken rock thickness was necessary to create zero deflections at y = o. The pack load is q and the restraining forces R of unknown magnitude have been applied on the beam ends to satisfy assumptions (d) and (e). Since the condition related to R (zero end displacement) is given, the absolute magnitude of R need not be known.

For a rigorous analysis of the situation, the loading on the top and bottom edges of the beam is represented by the Fourier series

$$f(x) = \sum_{m=1}^{\infty} A_m \sin \frac{m\pi x}{l}$$

for the coordinate system (x,y) of Fig.7.30, the length of the broken zone being l. The constants A_m can be obtained by Fourier analysis as

$$A_m = \frac{1}{l} \int_{\frac{l-a}{2}}^{\frac{l+a}{2}} q \sin \frac{m\pi x}{l} \, dx$$

$$= \frac{2q}{m\pi} \sin \frac{m\pi}{2} \sin \frac{m\pi a}{l}$$

Putting $\alpha = \frac{m\pi}{l}$, the stresses are given by[72]

$$\sigma_x = 2A_m \left[\frac{\alpha c \cosh \alpha c - \sinh \alpha c}{\sinh 2\alpha c + 2\alpha c} \cosh \alpha y - \frac{\sinh \alpha c}{\sinh 2\alpha c + 2\alpha c} \alpha y \sinh \alpha y \right] \sin \alpha x$$

$$\sigma_y = -2A_m \left[\frac{\alpha c \cosh \alpha c + \sinh \alpha c}{\sinh 2\alpha c + 2\alpha c} \cosh \alpha y - \frac{\sinh \alpha c \cdot \alpha y \sinh \alpha y}{\sinh 2\alpha c + 2\alpha c} \right] \sin \alpha x$$

$$\tau_{xy} = -2A_m \left[\frac{\alpha c \cosh \alpha c \cdot \sinh \alpha y}{\sinh 2\alpha c + 2\alpha c} - \frac{\sinh \alpha c}{\sinh 2\alpha c + 2\alpha c} \alpha y \cosh \alpha y \right] \cos \alpha x$$

Hence the displacement relation

$$\frac{\partial v}{\partial y} = \frac{1}{E_n} \left[(1-\mu^2) \sigma_y - \mu (1+\mu) \sigma_x \right]$$

gives $$v = -\frac{2A_m}{E_n} \sin \frac{m\pi x}{l} \left[(1-\mu^2) g_{2_I}(y) + \mu(1+\mu) g_{1_I}(y) \right] + C_1(x) \quad (7.20)$$

in which $g_1(y)$ and $g_2(y)$ are the functions of y in the expressions for σ_x and σ_y respectively. Now the vertical displacements v must satisfy the condition $(v)_{y=0} = 0$, so that from Equ. (7.20)

$$C_1(x) = \frac{2A_m}{E_n} \left[(1-\mu^2) g_{2_I}(0) + \mu(1+\mu) g_{1_I}(0) \right] \sin \frac{m\pi x}{l}$$

It can be shown by direct substitution for g_2 and g_1 that the quantity in brackets is identically zero so that

$$C_1(x) = 0$$

Thus from Equ. (7.20) we get

$$v_c = (v)_{y=-c} = \frac{4(1-\mu^2)}{E_n} \sum_{m=1}^{\infty} A_m \frac{l}{m\pi} \cdot \frac{\sinh^2 \frac{m\pi c}{l}}{\sinh \frac{2m\pi c}{l} + \frac{2m\pi c}{l}} \sin \frac{m\pi x}{l} \quad (7.21)$$

which are the vertical displacements at the floor level. A superimposition of these displacements over the earlier floor level face element displacements

will give us the total post-failure elastostatic floor lift.

7.4.2 Results

The situation was numerically analysed writing a computer program for Equ.(7.21) for short face advancing and retreating. The important data were

Pack width a = 2, 6 m

Broken zone l = 14, 18 m corresponding to 2, 6 m pack

Corresponding broken rock depth c = 2.7, 3.8 m

Corresponding pack loads during advancing q = 215, 275 kN/m^2

Pack loads during retreating q = 3000 - 7000 kN/m^2

E_n = 1.25×10^6 kN/m^2, μ = 0.2

The value of the post-failure elastic modulus E_n was obtained from Equ. (7.19) and Fig.7.29 after estimating the average value for the safety factor S in the broken zone. For this the highest modulus E_o before failure was taken as 5.02×10^6 kN/m^2 as before. Poisson's ratio μ was 0.2, representing a totally disintegrated rock[73]. Deflections obtained by this analysis, the face element pre-fracture lift and the final lift (elastostatic post-failure) are given in Tables 7.3 and 7.4 for advancing and retreating.

It is noticed from these Tables that the difference in lift due to breaking is not very significant. It must, however, be remembered that a

TABLE 7.3

Elastostatic pre-fracture and post-failure floor heave in advancing by short faces

Heading width m	Distance from pack edge m	Pre-fracture lift cm	Post-failure lift cm
12	0	3.577	3.566
	1	3.525	3.522
	2	3.428	3.427
	3	3.279	3.279
	4	3.060	3.060
	5	2.672	2.672
16	0	4.173	4.153
	1	4.074	4.068
	2	3.933	3.930
	3	3.743	3.743
	4	3.484	3.484
	5	3.061	3.061

TABLE 7.4

Elastostatic pre-fracture and post-failure lift during retreating

Pack width m	Pack load kN/m^2	Distance from pack edge m	Pre-fracture lift cm	Post-failure lift cm
2.0	3000	0	5.112	4.958
		1	4.685	4.651
		2	4.167	4.162
		3	3.577	3.577
		4	2.901	2.903
		5	2.102	2.105
	4000	0	4.969	4.764
		1	4.563	4.517
		2	4.054	4.047
		3	3.468	3.467
		4	2.796	2.798
		5	1.998	2.002
	5000	0	4.842	4.586
		1	4.458	4.401
		2	3 956	3.447
		3	3.377	3.376
		4	2.708	2.711
		5	1.913	2.916
	6000	0	4.705	4.398
		1	4.340	4.271
		2	3.847	3.836
		3	3.273	3.272
		4	2.609	2.612
		5	1.816	1.821

TABLE 7.4 (contd)

Pack width m	Pack Load kN/m^2	Distance from pack edge m	Pre-fracture lift cm	Post-failure lift cm
2.0	7000	0	4.573	4.215
		1	4.229	4.149
		2	3.745	3.733
		3	3.176	3.175
		4	2.516	2.520
		5	1.725	1.732
6.0	3000	0	5.968	5.742
		1	5 571	5.501
		2	5.076	5.047
		3	4.503	4.500
		4	3.840	3.840
		5	3.050	3.053
	4000	0	5.523	5.224
		1	5.162	5.068
		2	4.685	4.646
		3	4.124	4.120
		4	3.470	3.470
		5	2.685	2.689
	5000	0	5.055	4.681
		1	4.727	4.610
		2	4.267	4.218
		3	3.717	3.712
		4	3.070	3.070
		5	2.288	2.243

TABLE 7.4 (contd)

Pack width	Pack Load kN/m^2	Distance from pack edge m	Pre-fracture lift cm	Post-failure lift cm
6.0	6000	0	4.617	4.168
		1	4.322	4.181
		2	3.880	3.821
		3	3.342	3.337
		4	2.704	2.704
		5	1.925	1.931
	7000	0	4.164	3.640
		1	3.902	3.738
		2	3.476	3.408
		3	2.950	2.946
		4	2.320	2.321
		5	1.543	1.550

considerable difference in the lift will be made due to 'swelling' or an apparent increase in the rock volume upon breaking. This has been accounted for in the last phase of this analysis, viz. viscoelastic post-failure heave including swelling.

7.5 A linear viscoelastic approach to floor heave and swelling effects

Having estimated the elastostatic post-failure lift, it now remains to ascertain the behaviour of the floor with time due to viscoelastic or creep effects. For this a linear viscoelastic approach has been adopted.

7.5.1 The correspondence principle

One approach to solving viscoelastic or creep problems consists of using the correspondence principle, whereby viscoelastic solutions can be deduced from the corresponding elastic solutions for the same configuration by applying the Laplace transformation technique[74]. This technique has been used by several workers[75-77]. The Laplace transformation can be employed if at all material points the conditions demanded by the system do not change during load application, and if the body shape does not change. If these conditions are satisfied and if the material is 'initially dead', the Laplace transformation is defined by

$$f(s) = L\left[f(t)\right] = \int_0^\infty f(t)e^{-st}dt$$

where f(s) is the Laplace transform of f(t), s is the transform parameter and L is the Laplace transform operator.

Bland[74] expresses the correspondence principle as: "If the dependent variables and the boundary conditions in the elastic solution are replaced by their Laplace transforms and the elastic moduli by the corresponding parameter (s) varying moduli, then the viscoelastic solution for these variables is obtained by inversion of the expressions so obtained for the transforms of the dependent variables."

For an isotropic elastic body the stress-strain relation is

$$\sigma = E.\varepsilon$$

and for a linear viscoelastic material

$$F.\sigma(t) = G.\varepsilon(t)$$

where σ and ε are now functions of time and F and G are linear differential operators with constant coefficients:

$$F\left(\frac{\partial}{\partial t}\right) = \sum_{i=0}^{m} f_i \left(\frac{\partial^i}{\partial t^i}\right) \quad , \quad G\left(\frac{\partial}{\partial t}\right) = \sum_{i=0}^{n} g_i \left(\frac{\partial^i}{\partial t^i}\right)$$

where f_i and g_i are material constants defining viscoelastic behaviour. The four basic rheological models representing time-dependent behaviour of mine rocks are the Maxwell, Kelvin, three-element and Burgers model. The last one is considered the most realistic of the four and, as shown in Fig. 7.31, consists of a spring and dash-pot in series with another spring and dash-pot in parallel. Its stress-strain relation is

$$c_2 \sigma''(t) + c_1 \sigma'(t) + c_0 \sigma(t) = \varepsilon''(t) + d_1 \varepsilon'(t) \qquad (7.23)$$

FIG.7.31 - BURGERS RHEOLOGICAL MODEL & ITS CREEP CURVE

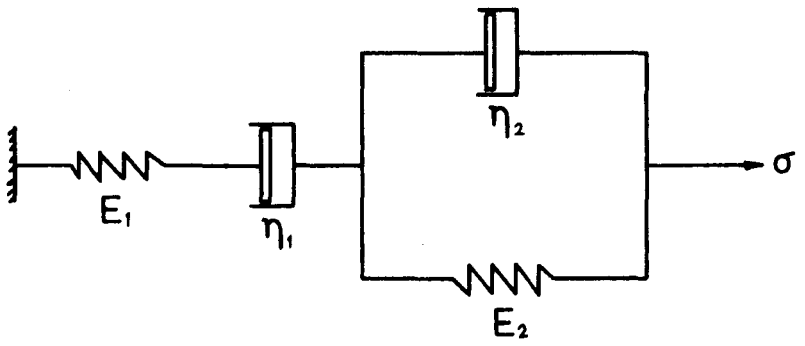

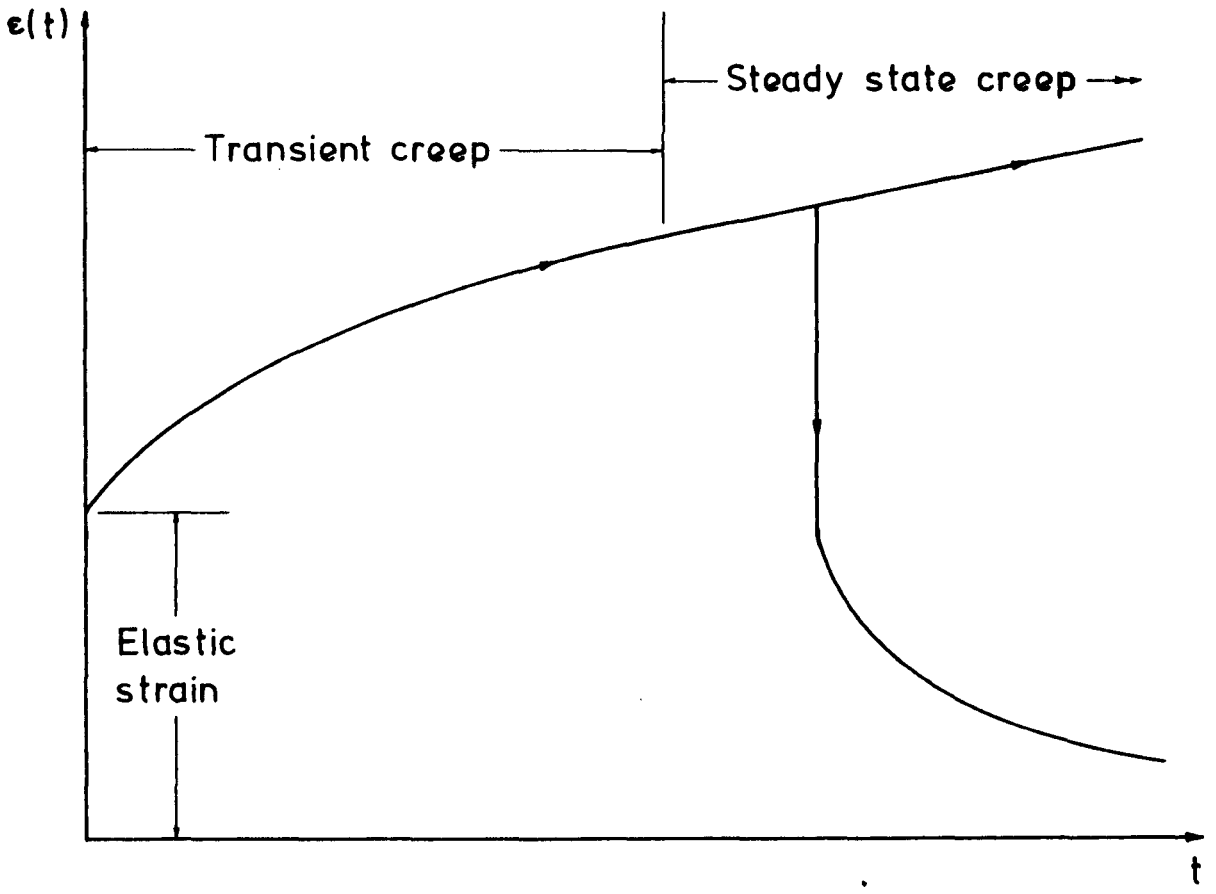

where $c_o = \frac{E_2}{\eta_1 \eta_2}$, $c_1 = \frac{E_2}{E_1 \eta_2} + \frac{1}{\eta_1} + \frac{1}{\eta_2}$

$c_2 = \frac{1}{E_1}$, $d_1 = \frac{E_2}{\eta_2}$

Upon integration we find

$$\varepsilon(t) = \left[\frac{1}{E_1} + \frac{t}{\eta_1} + \frac{1}{E_2} \left(1 - e^{-E_2 t/\eta_2} \right) \right] \sigma(t) \qquad (7.24)$$

The behaviour of this model is shown by the creep curve of Fig.7.31. It includes the instantaneous elastic deformation, the transient creep and the steady-state creep which is non-recoverable upon removal of stress. Equ. (7.23) is of the linear differential form (7.22) and the Laplace transform of the corresponding Young's modulus is[76]

$$\bar{E}(s) = \left(s^2 + d_1 s \right) / \left(c_2 s^2 + c_1 s + c_o \right) \qquad (7.25)$$

7.5.2 General solution in plane strain

Suppose a plane strain elastic problem gives the solution for stresses as

$$\sigma_x = f_1(x, y) \ , \ \sigma_y = f_2(x, y) \ , \ \tau_{xy} = f_3(x, y)$$

then the relation for vertical displacements

$$\frac{\partial v}{\partial y} = \frac{1}{E} \left[(1 - \mu^2) \sigma_y - \mu (1 + \mu) \sigma_x \right]$$

gives

$$v = \frac{1-\mu^2}{E} \int \sigma_y \, dy - \frac{\mu(1+\mu)}{E} \int \sigma_x \, dy + A_1(x)$$

Since $A_1(x)$ is an arbitrary function of x this can be written in the form

$$v = \frac{1}{E} \left[g_1(x,y) + g_2(x,y) + A_1(x) \right]$$

without loss of generality. As Poisson's ratio is assumed time-independent it has been merged with the unknown functions. At any given point (x_1, y_1), say at the floor level,

$$v\,(x_1,y_1) = \frac{\delta}{E}$$

Now the deflections $v(x_1,y_1)$ at any point on or within the floor has already been obtained by the face element analysis so that δ can be determined from

$$\delta = v(x_1,y_1) \times E \qquad (7.26)$$

i.e. by multiplying each elastostatic displacement already obtained by E. In terms of Laplace transforms this can be written as

$$\bar{v}(s) = \frac{\bar{H}(s)}{\bar{E}(s)} \qquad (7.27)$$

where $\bar{H}(s)$ is the transform of the loading history H(t). Since the constant δ has the units of (stress x length), H(t) will tell the manner in which the ultimate loading condition in a given viscoelastic body has been reached, or its loading history.

It must be noted here that the loading history is actually the change of stress taking place in the floor at any point (x_1,y_1). Since the stresses

are two in the equation for vertical strain $\frac{\partial v}{\partial y}$, the combined effect produced due to a change in both these stresses is the real loading history. Now at the floor level we have a free surface so that only σ_x changes with face advance, σ_y being zero in the roadway. Then the loading history in the roadway is really a change in σ_x only. Below the pack and ribside, however, the problem of loading history is much more complicated because both σ_x and σ_y will change with face advance.

7.5.3 Loading history in short face advancing and retreating

As seen from the pack load acceptance curves of Chapter 5, the steady state of stress for the section of the heading reaches within about 20 to 25 metres, or in terms of time, in 2 to 3 days, when the rate of advance is 9.0 m per day. Assuming that the short faces are driven to a distance of 900 m at this rate of advance, the time required for driving the heading will be 100 days. If we consider a section of the heading which is 450 m from the start line, the loading history for this section will, for the most part, consist of the steady state, only the first 2 to 3 days being transient. It was, therefore, decided to choose the loading history during short face advancing as of a constant load as in Fig. 7.32.

During retreating, however, general experience has shown that a point reaches steady state after about 100 m or so of face travel. It is thus transient over a long period. Also, some floor heave already occurs during advancing under the earlier loading history. Added to this is the transient loading due to retreating. If the constant δ has the value δ_1

FIG.7.32 - LOADING HISTORY OF POINT X

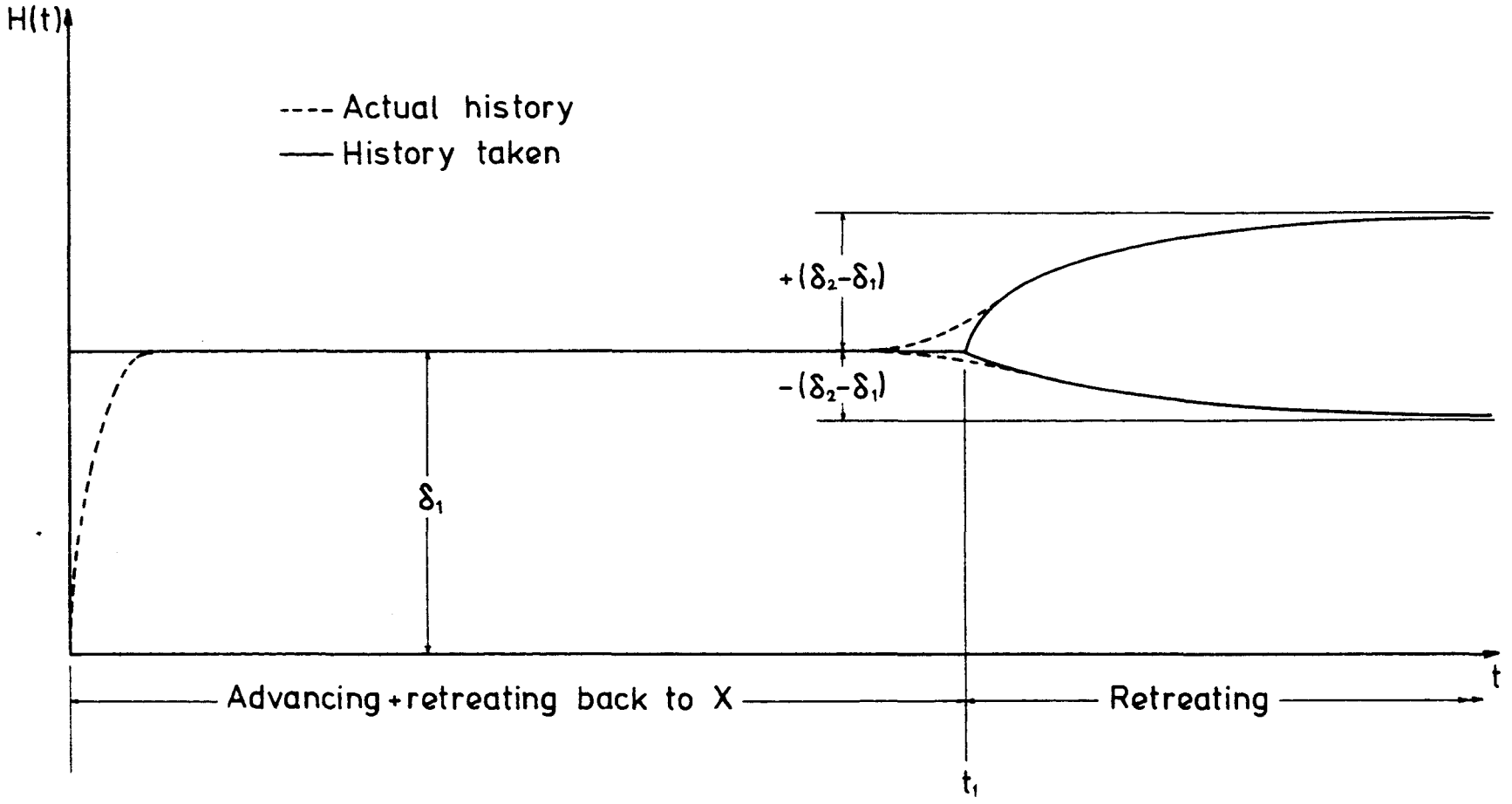

during advancing and an ultimate value δ_2 during retreating the loading histories are:

(a) Short face advancing:

$$H(t) = \delta_1 \tag{7.28}$$

(b) Subsequent retreating:

$$H(t) = \delta_1 + (\delta_2 - \delta_1)(1-e^{-\alpha t}) \tag{7.29}$$

where $\alpha = 0.06$, which roughly corresponds to a steady state in retreating reaching after about 100 m of face travel at the rate of 1.5 m/day.

The history (7.29) during retreating can be of two kinds: (a) $\delta_2 > \delta_1$ (b) $\delta_2 < \delta_1$. These two conditions are shown in Fig. 7.32.

7.5.4 Total post-failure viscoelastic floor heave

During advancing by short faces, the loading history (7.28) gives according to Equ (7.27) and Equ. (7.25)

$$\bar{v}(s) = \delta_1 \frac{1}{s} \Big/ \frac{s^2 + d_1 s}{c_2 s^2 + c_1 s + c_0}$$

where $\frac{\delta_1}{s}$ is the Laplace transform of $H(t) = \delta_1$. An inverse transformation of this expression gives

$$v(t) = \delta_1 \left[\frac{1}{E_1} + \frac{t}{\eta_1} + \frac{1}{E_2} \left(1 - e^{-E_2 t / \eta_2} \right) \right] \tag{7.30}$$

During subsequent retreating the loading history (7.29) has to be applied, which involves a constant term δ_1 for advancing and an additional transient term signifying the change in the history due to retreating. The floor lift due to the constant term δ_1 is already known from Equ. (7.30). So it is necessary to determine the lift only due to the transient term, which gives

$$\bar{v}(s) = (\delta_2 - \delta_1)\left(\frac{1}{s} - \frac{1}{s+\alpha}\right) \Big/ \frac{s^2 + d_1 s}{c_2 s^2 + c_1 s + c_0}$$

and by inverse transformation

(a) $\delta_2 > \delta_1$:

$$v(t) = (\delta_2 - \delta_1)\Big[\frac{1}{E_1} + \frac{t}{\eta_1} + \frac{1}{E_2}\left(1 - e^{-E_2 t/\eta_2}\right) - \frac{1}{\eta_1 \alpha} + \frac{1}{E_2 - \eta_2 \alpha} e^{-E_2 t/\eta_2} + \left(\frac{\frac{\alpha}{E_1} - \frac{E_2}{\eta_2 E_1} - \frac{1}{\eta_1} - \frac{1}{\eta_2}}{\frac{E_2}{\eta_2} - \alpha} + \frac{\frac{E_2}{\eta_1 \eta_2}}{\alpha\left(\frac{E_2}{\eta_2} - \alpha\right)}\right) e^{-\alpha t}\Big] \qquad (7.31)$$

(b) $\delta_2 < \delta_1$:

When $(\delta_2 - \delta_1)$ is negative, there is a process of gradual transient unloading during retreating from the value δ_1 of advancing. The steady state creep is, however, non-recoverable, so that in this case the floor lift will be obtained by putting $1/\eta_1 = 0$ in Equ. (7.31), thus:

$$v(t) = (\delta_2 - \delta_1)\Big[\frac{1}{E_1} + \frac{1}{E_2}\left(1 - e^{-E_2 t/\eta_2}\right) + \frac{1}{E_2 - \eta_2 \alpha} e^{-E_2 t/\eta_2} + \left(\frac{\frac{\alpha}{E_1} - \frac{E_2}{\eta_2 E_1} - \frac{1}{\eta_2}}{\frac{E_2}{\eta_2} - \alpha}\right) e^{-\alpha t}\Big] \qquad (7.32)$$

Thus the floor lift in retreating is obtained by superimposing (7.31) or (7.32) on the lift obtained in advancing by Equ. (7.30) for $t \geqslant t_1$ where t_1 is the time required for the short face to move to the end from the point under consideration plus the time required for the retreating face to come back to the same point.

Added to this floor lift must be the lift due to swelling of the rock upon breaking. If the coefficient of apparent volume increase due to breaking is 1.4, then the coefficient of linear increase will be $(1.4)^{\frac{1}{3}} = 1.12$. So there will be a 12% increase in the thickness of the broken zone, lifting the rock upward. Since rock breaking is completed in advancing itself, the additional heave due to swelling is just added to that given by Equ.(7.31) or (7.32). The total lift in retreating is thus

$$\text{Total } v(t) = v(t) \text{ (advancing)} + v(t) + 0.12\ c \qquad (7.33)$$

where c is the depth of the broken rock zone.

7.5.5 Numerical analysis and results

For estimating the total floor heave, a point X 450 m from the start line of the short face, or midway between its total travel of 900 m, was chosen at 2 m from the edge of the pack into the roadway. The constants in the Burgers model were determined from the creep curve for Dawdon seat-earth[64], Fig.7.33, as

$$E_1 = E_n \text{ (post-failure)} = 1.25 \times 10^6 \text{ kN/m}^2$$

$$E_2 = 2.6 \times 10^7 \text{ kN/m}^2$$

$$\eta_1 = 1.62 \times 10^8 \text{ kN/m}^2 \text{ - day}$$

$$\eta_2 = 1.88 \times 10^7 \text{ kN/m}^2 \text{ - day}$$

FIG.7.33 - CREEP CURVE FOR DRY SEATEARTH FROM DAWDON COLLIERY (AFTER CLOOK)

Constant applied stress = 24111 kN/m^2 = 75.4 % U. C. S.

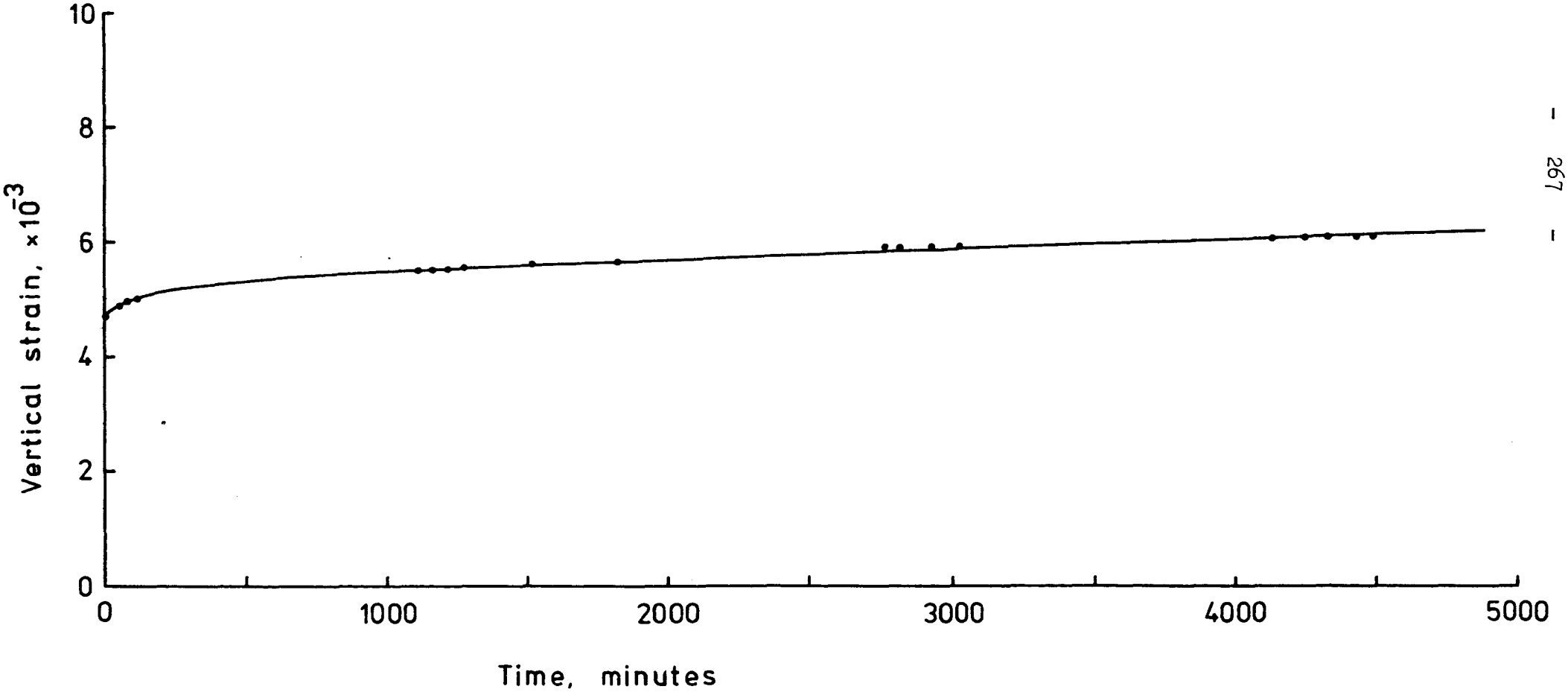

The post-failure elastostatic deflections at point X are given in Table 7.5, from which δ_1 and δ_2 could be calculated from the relation (7.26) by simply multiplying by E_1. The value of t_1, the time required for the short face to travel from X to the end at 9.0 m/day and retreat back to X at 1.5 m/day, was 350 days.

The total floor heave was obtained by writing a Fortran program for Equ. (7.30 - 33). The results are shown in Figs. 7.34 and 7.35 corresponding to retreating after advancing by a short face of 12 m and 16 m respectively. The results have the following main features:

(a) A large part of the floor heave takes place during short face advancing itself, mainly from floor breaking. The heave due to breaking is constant in retreating and has values of 32.4 and 45.6 cm corresponding to the two heading widths of 12 m and 16 m, so that breaking alone is responsible for a closure of 17% and 24% of the working height.

(b) Pack load does not change the lift as significantly corresponding to a 12-m heading as in the case of a 16-m heading. A higher pack load will obviously increase floor penetration so that although the lift falls, the overall closure due to downward pack movement may not necessarily fall. It is not possible to estimate this effect and the overall closure. Changing the pack load because of the quality of the pack thus does not significantly alter floor heave.

TABLE 7.5

Post-failure elastostatic lift at point X

(a) Short face advancing

Heading width m	lift cm
12	3.427
16	3.930

(b) Subsequent retreating

Peak load kN/m^2	Lift, cm	
	Pack width 2 m	Pack width 6 m
3000	4.162	5.047
4000	4.047	4.646
5000	3.947	4.218
6000	3.836	3.821
7000	3.733	3.408

FIG.7.34-FLOOR HEAVE DURING RETREATING

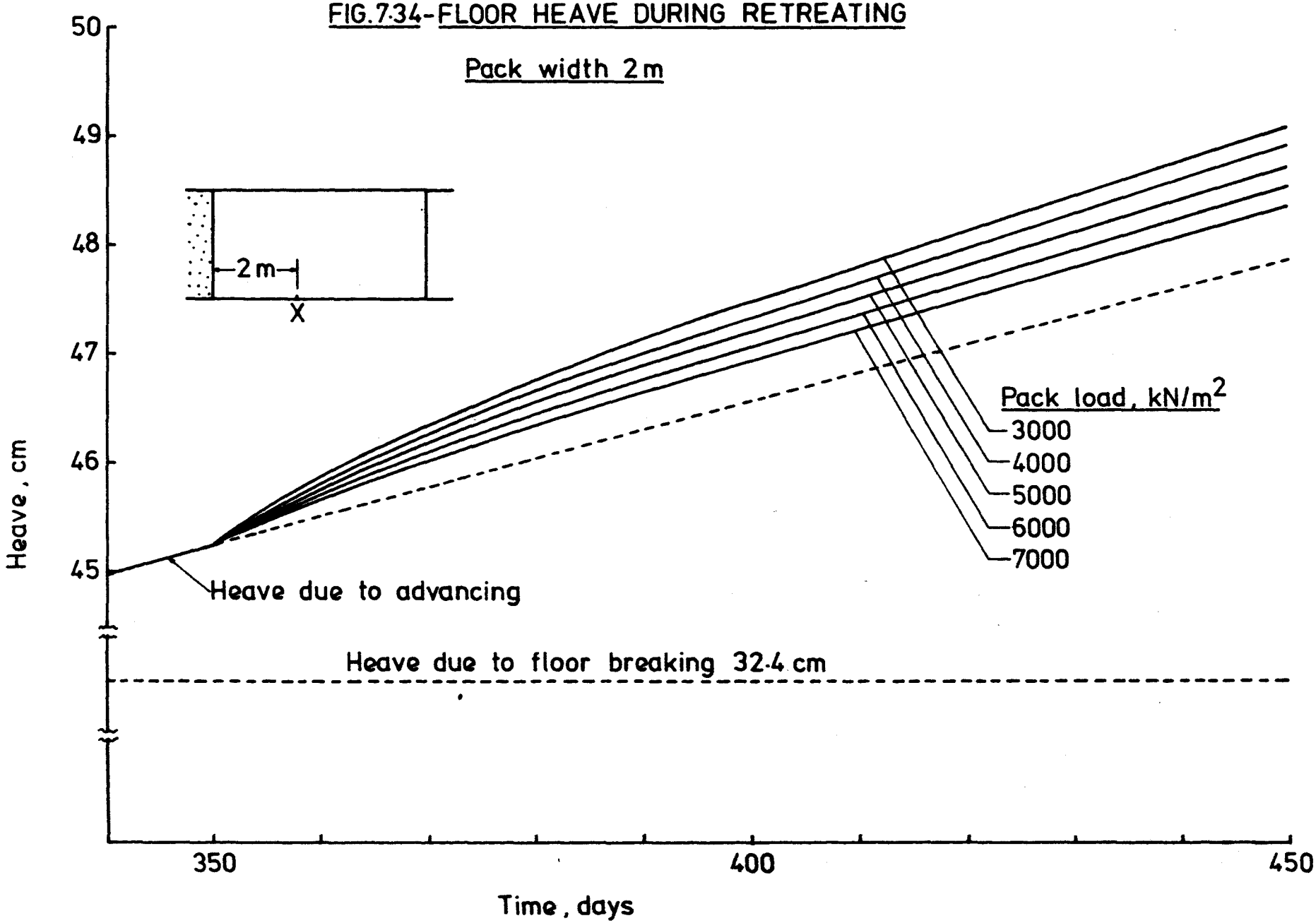

FIG. 7·35 - FLOOR HEAVE DURING RETREATING

Pack width 6 m

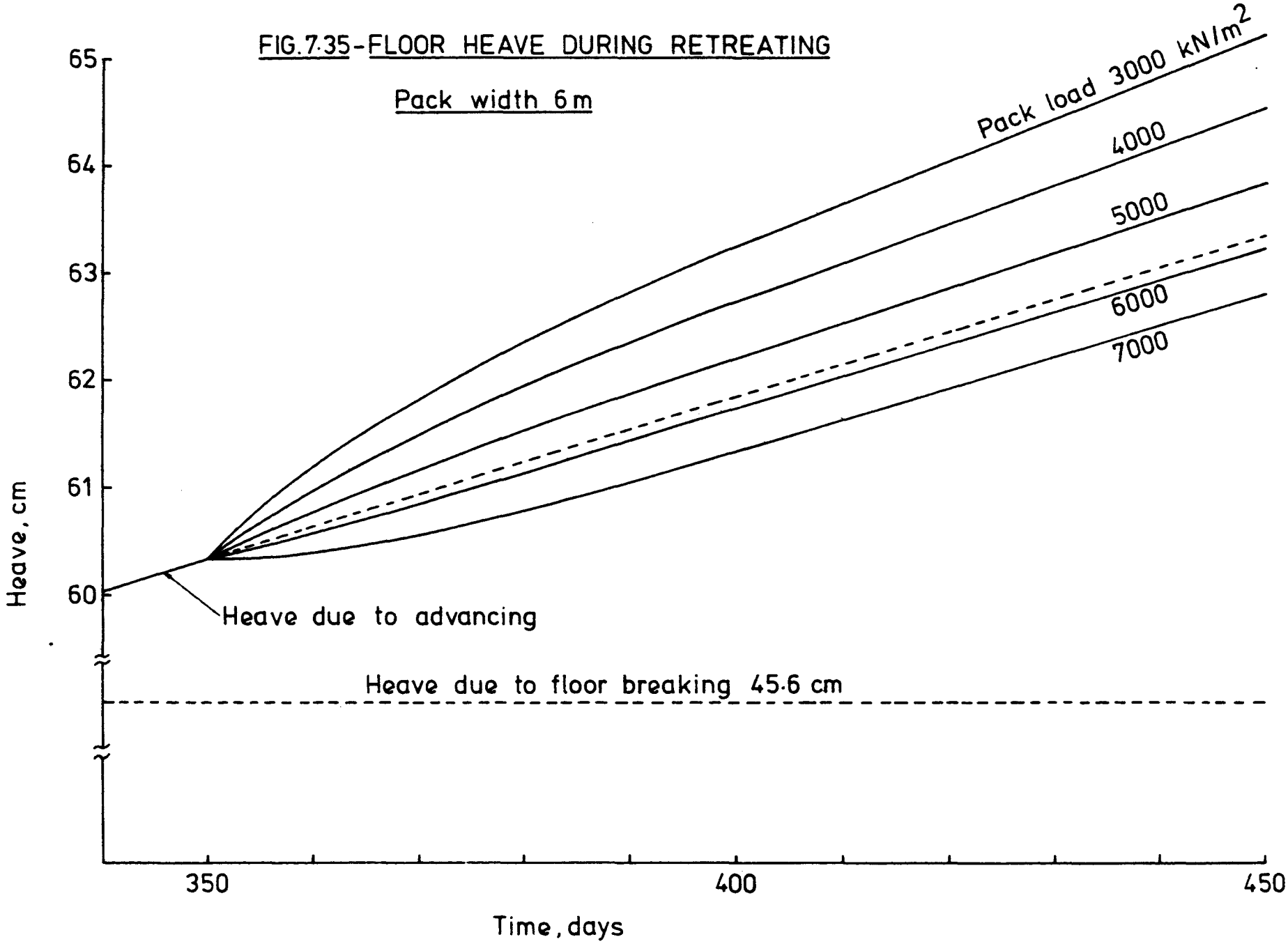

(c) Only two cases of pack load of 6000 and 7000 kN/m^2, Fig.7.35, correspond to the condition of a falling load history. The heave, even for these cases, appears to rise because the steady state creep is not recoverable, and the Burgers model behaves like a three-element model under loading.

(d) Judging by the heave curves, the total floor lift at point X is likely to be, at the finish of the retreating operation, as much as 29% or 37% depending on the heading width initially adopted for advancing, and the pack load subsequently developed.

7.5.6 Application of the theoretical method to the example of Easington Colliery

From Easington Colliery, where anhydrite packing is being used, underground measurements of floor heave are available. It was considered worthwhile estimating the floor heave there theoretically by the method so far developed and comparing these results with underground measurements.

For this, it was necessary first to obtain the zone of crushed coal and the loading on the ribside abutment. The pack load in the steady state was measured underground as 4500 kN/m^2[28]. The panel under consideration here has the following particulars:

Depth from surface 548 m

Section of the roadway as shown in Fig. 7.36 (except that the roadway width is taken here as 5.0 m instead of 4.7 m).

Face length 180 m

Pack width 1.5 m.

The workings are being carried out by longwall advancing with advanced headings in the Low Main seam.

The same procedure of analysis was followed. The length of the crushed coal zone in the ribside due to abutment pressure was obtained as nearly 11.5 m, the Poisson ratio for this purpose being estimated at 0.4 instead of the usual 0.25, considering Equ.(7.13), because Easington is deeper than Dawdon. The maximum abutment pressure at this distance was obtained as 46000 kN/m^2, about 3.7 times the depth pressure. The goaf loading on the floor was estimated as usual from the weight of the fallen rock.

A face element run for this case gave the s.f. contours as in Fig.7.36. This gave the depth of the broken zone as c = 2.5 m with the value of the post-failure modulus as $E_n = 7.7 \times 10^5$ kN/m^2. The usual post-failure analysis yielded the value of the floor lift as 17.85 cm at a point 3 m from the pack edge.

This problem has been worked out assuming that no advanced headings were present ahead of the face for simplicity. The loading history for a floor point would then be

FIG.7·36 - S. F. CONTOURS IN THE FLOOR AT EASINGTON

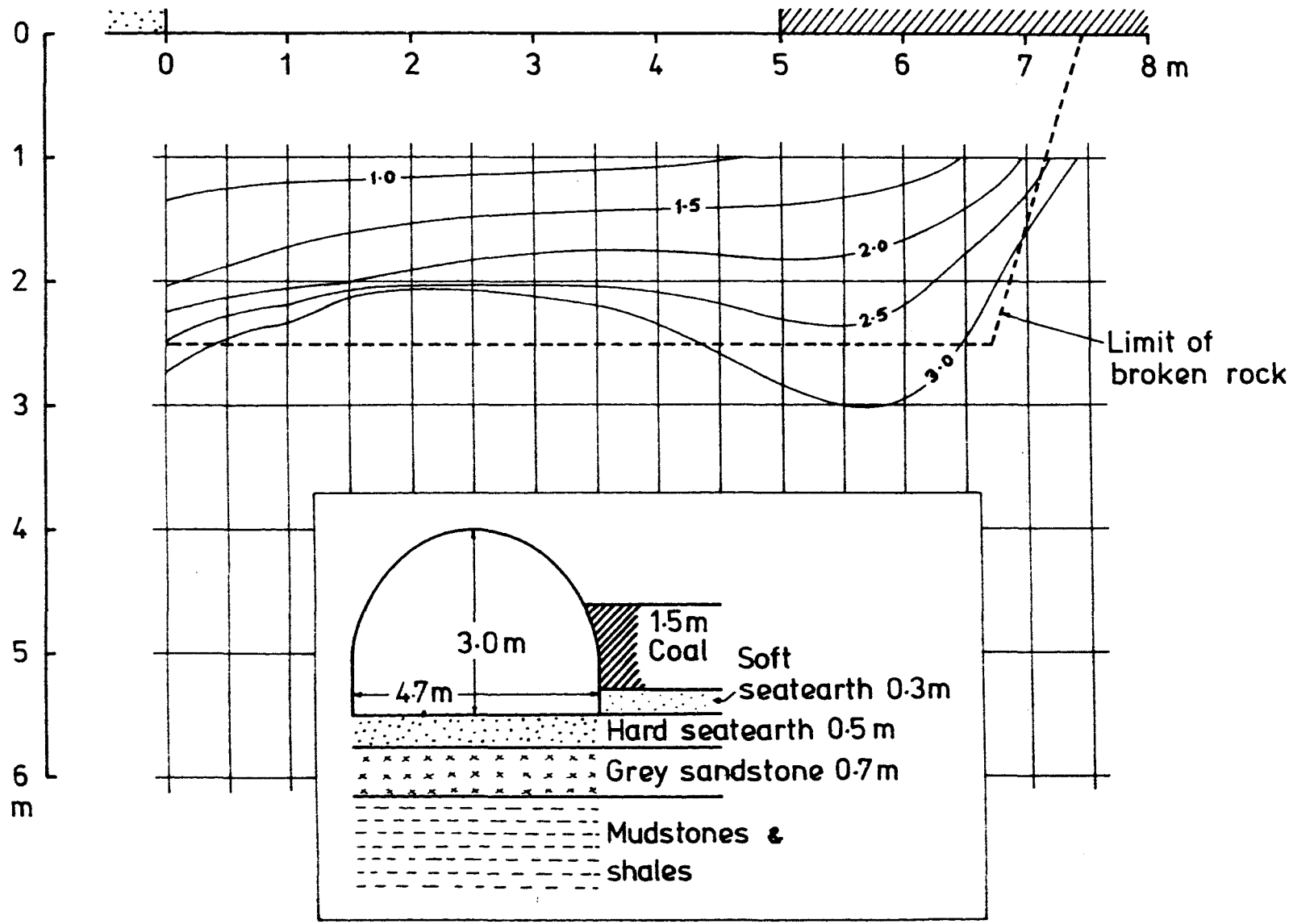

$$H(t) = \delta\ (1 - e^{-\alpha t})$$

where $\delta = 0.1785 \times 7.7 \times 10^5$ kN/m^2 and $\alpha = 0.06$. Then using Equ.(7.31) substituting δ instead of $(\delta_2 - \delta_1)$, the floor lift could be estimated. To this floor lift had to be added the swelling of the broken rock. A reasonable assumption was that the process of breaking commenced from the start of the face ($t = o$) and reached its ultimate value in the steady state of the loading history, so that the lift due to swelling could be expressed by

$$v(t) \text{ swelling} = 0.12c\ (1 - e^{0.06t})$$

$$= 0.12 \times 2.5\ (1 - e^{-0.06t})$$

This was superimposed on the viscoelastic lift already determined and the results are plotted in Fig. 7.37 along with the observed underground results[28] which are shown assuming zero displacements when the face is at the measuring station (as if the advanced heading is removed).

There appears to be a reasonably good agreement between the two results.

7.6 Conclusion

(a) The method proposed for estimation of the zone of crushing in the ribside and the abutment pressure curve appears to give satisfactory results. The solution given by Equ. (7.11) and (7.12) is sensitive to changes in the constants a and b which define the straight line joining the two states of stress at the rib edge and deep inside.

FIG.7.37 - THEORETICAL AND MEASURED FLOOR HEAVE AT EASINGTON COLLIERY

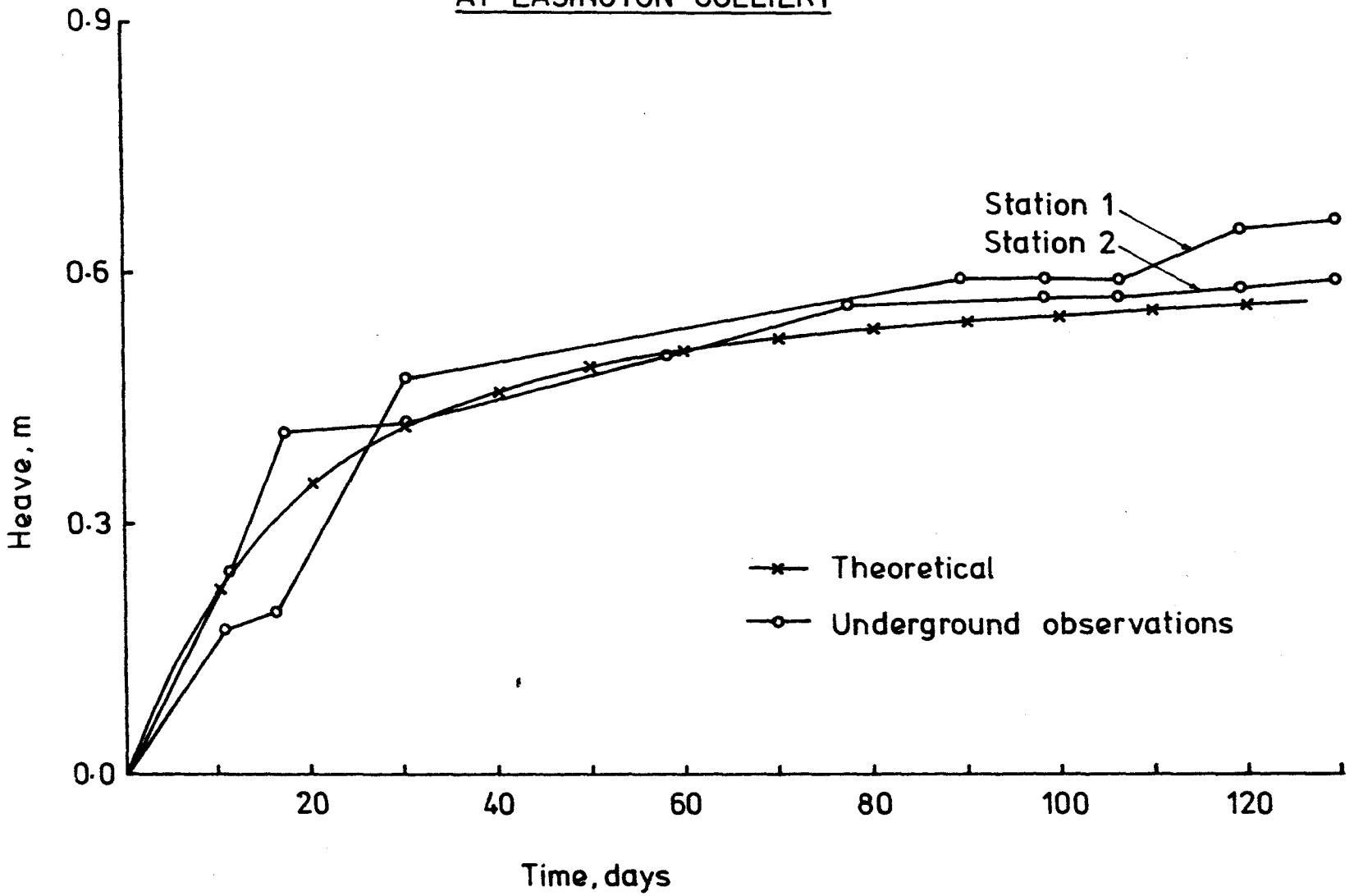

The equivalent triaxial state at the edge takes the confinement as 1% of the vertical stress, which is only approximate. This value needs to be determined precisely since the resulting values of the crushed length and abutment peak are sensitive to this initial confinement before crushing. The lateral restraining stress deep inside the seam is taken as $\frac{\mu}{1-\mu}$ times the cover load, with a changing value of μ as per Equ (7.13). This requires good estimates of the crushing strength of the seam for obtaining a proper value of μ.

The results of abutment pressure and zone of crushing are also sensitive to the value of the flexural rigidity of the roof strata. A fall in the flexural rigidity has the effect of increasing the abutment pressure before crushing and reducing the distance at which the cover load is reached by the pressure wave. An accurate knowledge of the horizontal weakness planes and reasonable estimates of E of roof strata are required for good accuracy of results.

(b) The elastostatic face element analysis shows that this method of short face advancing with retreating may produce deeper fractures in the floor than simple advancing and there is a probability that floor heave will be greater by the former method. This may place a limitation on the depth to which this method of initial development may be adopted. By the time retreating finishes in the first panel after short face

advancing, the roadway on the outer side of the pack will have undergone floor heave which could be roughly up to one third the roadway height, making it difficult to use as a tailgate for the second panel. The floor heave in this roadway depends on the width of the heading adopted in short face advancing, wider headings being disadvantageous.

(c) Floor heave also appears to be influenced by pack load and width, wide packs loaded well put a restraining effect on the floor and reduce floor heave to some extent. Narrow packs like 1.5 or 2 m do not show much benefit when the pack load is increased. It does not, therefore, appear greatly beneficial to have a highly resistant pack like anhydrite if it is to be narrow from the stand point of floor heave. Overall, a control of floor heave by changing the pack width or pack load can be achieved only to a small extent. The probable reason is that a roadside pack is really a relatively small element of the complete longwall structure.

(d) To alleviate bad roadway conditions due to floor heave, pack load, pack width and face length may be changed (i.e. put a stiffer, wider pack and a shorter face) though a change in just one of these factors may not bring about appreciable improvement. The main factors influencing floor heave appear to be the depth of working and the floor strength, since they govern the depth to which a fracture zone may develop in the floor. A large part of the floor heave is accounted for by the increase in the apparent volume of

the rock upon breaking. It is always advantageous to reduce floor breaking. In the method of short face advancing it is seen that the quality of pack does not affect floor stress significantly. It will, however, be wiser to adopt a stiffer pack like anhydrite and use as narrow a heading as permitted by the economics of advancing.

(e) The method of floor heave estimation gives reasonable estimates of heave at Easington when compared with underground measurements taken there. Even then, it will be necessary to carry out extensive field experiments to corroborate the findings of this Chapter.

* * *

CHAPTER 8

Conclusions and recommendations for future work

CHAPTER 8

Conclusions and recommendations for future work

The method of short face advancing with a centre pack for in-seam development was investigated for feasibility. The elastostatic analysis for roof behaviour leads to the following conclusions:

1. Stiff packs of setting materials like anhydrite accept load more quickly than conventional non-setting packs. Both kinds of pack show an initial load build-up to a peak value, a subsequent fall and steadying off with advance of the short face. The initial build-up to a hump is pronounced in the case of anhydrite packs, while it is flat in conventional packs. Load acceptance increases with the pack modulus.

The values of pack load obtained during short face advancing are quite small. Wide headings give rise to higher loads.

The pack loading curve agrees with those observed underground by other workers and supports the back abutment pressure concept.

2. The maximum tensile stress, which occurs in the roadway on either side of the centre pack, shows a slight fall with higher pack loads, i.e. with increasing pack stiffness and heading width. It exceeds the ultimate tensile strength

(taken as an average for some Durham rocks) in most cases of packs, indicating the need for roadway supports.

The centre pack is seen to take care of only a part of the bending moments in the roof, a large amount of roof deflection taking place before pack erection.

3. The ribside abutment pressure is seen to fall with increasing pack load. A higher pack load thus appears desirable in reducing the unevenness of load distribution across a roadway.

4. The beam theory, as applied to the short face advancing situation, shows that a short face behaves in a manner similar to a full-fledged longwall face in that it gives a pack load characteristic with an initial peak (back abutment), a ribside abutment pressure, smaller values of load at the pack edge than at the centre and a flat, delayed load acceptance by soft non-setting packs.

A laboratory investigation of anhydrite properties indicates that

1. Anhydrite becomes stiffer with time, the elastic modulus reaching a plateau value greater than or comparable with many coals after 6 to 7 weeks (Equ. 4.1).

2. The strength falls significantly with an increase in the test specimen size, the fall from a laboratory small speciman to a regular pack being 50% or more. Accounting for this property and the width-height ratio of a pack, a strength formula

(Equ.4.5) has been proposed.

The method developed for obtaining the post-failure ribside abutment pressure and the extent of crushing of the ribside during retreating leads to the conclusions below:

1. The method is found to give reasonable values of the abutment pressure and extent of crushing. The solution by this method is sensitive to the initial pre-fracture biaxial confinement at the rib edge, the strength of the seam and the flexural rigidity of the rock mass in the roof. Their accurate determination is, therefore, necessary for the success of the method.

2. Both abutment pressure and ribside crushing are reduced with an increase in pack load and width.

3. A reduction in the face length has the same effect.

The situation of floor heaving in short face advancing and subsequent retreating can be summarised from the post-failure viscoelastic analysis thus:

1. The method used for floor heave estimation gives satisfactory results in the test case of Easington Colliery.

2. The method of short face advancing with subsequent retreating may produce deeper fractures in the floor than simple advancing, so that there is a probability that floor heave will be greater by this method. This

may place a limitation on the depth to which this method of working can be adopted. By the time retreating finishes in the first panel after short face advancing, the roadway on the outer side of the pack will have undergone floor heave which could be up to $\frac{1}{3}$ the roadway height, making it difficult to be used for the second panel.

3. The floor heave during subsequent retreating is greater if the short face heading during development is wider. No additional fracturing appears to occur in the floor while retreating, so that the floor condition is mainly governed by the width of the development heading adopted. It is thus difficult to recommend short face headings wider than 10 to 12 m.

4. It does not appear greatly beneficial to have a highly resistant pack like anhydrite from the stand point of floor heave. Overall, a control of floor heave by changing only the pack load and width can be achieved only to a small extent.

5. A large part of the floor lift occurs due to an increase in the apparent rock volume upon fracturing. During short face advancing, the quality of the pack does not affect floor breaking significantly. It is,

however, better to use a stiffer pack like anhydrite to improve roof behaviour.

6. Floor heave in roadways, in general, may be reduced by putting a wider pack and a shorter longwall face, though a change in just one of these factors may not bring about appreciable improvement. The main factors influencing floor heave appear to be the depth of the working and floor strength.

Recommendations for future work

There has recently been a proposal to adopt the method of short face advancing with a central pumped pack in one of the Areas of the National Coal Board. This could be a good opportunity for underground investigations for corroborating the findings of this Thesis, for an experimental confirmation of these theoretical results is much needed. It will be of practical interest to investigate the findings with reference to pack load acceptance and floor heave, while using the short face method, and also compare the results with a conventional advancing face in the same area.

A method, at least an empirical thumb rule, is needed to establish the relationship between pack quality and the resulting pack load.

* * *

REFERENCES

1. Binns, P.D. - "New techniques in roadway support", Symp.Mining Methods, Harrogate (1974)

2. Keirs, J.B. - "Retreat mining in the Barnsley area", Min.Engr. 197-206 (Jan. 1976)

3. Whittaker, B.N. and Titley, C.H. - "Improvement of gate roadway stability with special reference to roadside support", Coll. Guard. 470-76 (Oct. 1971)

4. Jenkins, J.D., Davies, D.O. and Prasad, A.S. - "Roadside conditions in longwall gateways", Symp. Strata Control in Roadways, Nottingham (1970)

5. Hobbs, D.W. - "Scale model studies of strata movement around mine roadways", Inter.J. Rock Mech.Min.Sci. 3, 101-27 (1966); 5, 219-35 (1968); 5, 237-44 (1968); 5, 245-51 (1968); 6, 365-404 (1969); 6, 405-14 (1969)

6. Breer, W. - "Gateroad support problems in the West German coal mining industry", 5th Inter.Strata Control Conf. London (1972)

7. Spruth, F. - "The necessity of securing the sides of gateroads", Gluckauf, 105, 981-86 (1969)

8. Farmer, I.W. and Robertson, J.T. - "The effect of pack construction on roadway stability behind working faces", Min.Engr. (Dec. 1976)

9. Genthe, M. - "Gateroad side packs made of hydraulically setting materials", Gluckauf, 106, 67-74 (1970)

10. Barraclough, L.J., Dixon, S.M. and Hogan, M.A. - "Tests on packs", Coll. Guard. 484-87 (March, 1934)

11. Sanders, G.W. - "Improving the efficiency of face ends", Min.Engr. 193-210 (Jan 1968)

12. Lewis, S. - "Systems of roadway support", Symp. Strata Control in Roadways, Nottingham (1970)

13. Heinrich, F. - "Technical experience gained with gateroad side packs made from anhydrite or from Blitzdammer quicksetting cement", Gluckauf, 107, 51-63 (1971)

14. Arioglu, E. , and Dunham, R.K. - "Physical properties of anhydrite/ accelerator mixtures for use as a gateside packing medium", Coll. Guard. 224, 31-33 (1976)

15. Lenge, G., Rauss, B. and Garte, R. - "Experience with side packs built as stoppings with rapidly setting materials", Gluckauf, 107, 482-88 (1971)

16. Robinson, G. and Coates, H. - "Surface and underground handling of dirt", Colloquium on Transport (1973)

17. Blades, M.J. and Whittaker, B.N. - "Longwall layouts and roadway design for effective strata control in advance and retreat mining", Min.Engr. 277-88 (April 1974)

18. Blades, M.J. and Whittaker, B.N. - "Aspects of improved roadway stability (Abstract)", Min.Engr. 331-40 (May 1974)

19. Phillips, D.W. and Walker, L. - "Control of longwall roadways by means of packs", Trans. Instn. Min. Eng., 96, 124-41 (1938)

20. Evans, W.H., Hogan, M.A. and Vallis, E.H. - "An investigation of the loads on packs at moderate depths", Trans.Instn. Min. Eng. 100, 340-54 (1941)

21. Phillips, D.W. - "Research problems on falls of ground", Trans. Instn. Min. Eng. 102, 122-40 (1943)

22. Phillips, D.W. and Jones, T. J. - "Strata movements ahead of and behind longwall faces", Trans. Instn. Min. Eng. 101, 346-57 (1942)

23. Winstanley, A. - "Strata control in mechanical working of coal seams", Inter. Conf. Rock Pressure and Supports in Underground Workings, Liège (1951)

24. Price, N.J. and May, N. - "The use of pack dynamometers", Coll. Engg. 37, 379-82 (1960)

25. Jacobi, O. - "The pressure on seam and goaf", Inter. Strata Control Cong., Essen (1956)

26. Creuels, F.H. and Hermes, J.M. - "Measurement of the change in rock pressure in the vicinity of a working face", Inter. Strata Control Cong., Essen (1956)

27. Thomas, L.J. - "Pack pressure measurements", Coll. Guard. 218, 503-09 (1970)

28. Arioglu, E and Dudley W.R. - "Progress in the investigations into the use of crushed anhydrite as a packing medium", Confidential Rep. N.C.B., University of Newcastle (Nov. 1974)

29. Timoshenko, S. and Woinowsky-Krieger, S. - "Theory of Plates and Shells", pp.4-5, McGraw Hill, New York (1959)

30. Hetenyi, M. - "Beams on Elastic Foundations", University of Michigan Press, Ann Arbour (1946)

31. Tincelin, E. and Sinou, P. - "Collapse of areas worked by the small pillar method", 3rd Inter. Conf. Strata Control, Paris, 571-89 (1960)

32. Adler, L. - "Rib control of bedded roof stresses", 4th Symp. Rock Mech., Penn. State University, 205-09 (1961)

33. Timoshenko, S. - "Strength of Materials, Part II", pp. 1-20 Van Nostrand, New York (1956)

34. Kerr, A.D. - "Elastic and viscoelastic foundation models", J.Appl. Mech., 31, 491-98 (1964)

35. Höfer, K.H. and Menzel, W. - "Vergleichende Betrachtungen uber die mathematisch und aus Messungen unter Tage ermittelten Pfeiler Belastungen im Kalibergbau", Bergakamie 15, 326-34 (1963)

36. Stephansson, O. - "Stability of single openings in horizontally bedded rock", Engg. Geol. 5, 5-71 (1971)

37. Sheorey, P.R. and Singh, B. - "A two-dimensional analysis of stresses on mine pillars at the goaf edge during depillaring with caving", Symp. Rock Mech., Dhanbad, 122-30 (1972)

38. Timoshenko, S. and Woinowsky-Krieger, S. - "Theory of Plates and Shells", pp. 259-80, McGraw Hill, New York (1959)

39. Timoshenko, S. and Goodier, J.N. - "Theory of Elasticity", p.48, McGraw Hill Kogakusha, Tokyo (1970)

40. Albritton, G.E. - "Review of literature pertaining to the analysis of deep beams", U.S. Army Engrs.Waterways Expt.Stn., Vicksburg, Tech.Rep.no. 1-701 (1965)

41. Sheorey, P.R. - "Discussion of O. Stephansson's paper": "Stability of single openings in horizontally bedded rock," Engg.Geol.6, 313-4 (1972)

42. Mandel, J. - "Les Calculs en matiere de pressions des terrains", Rev. de l'Indus.Minerale, 41, 78-92 (1959)

43. Sheorey, P.R. and Singh, B. - "Estimation of pillar loads in single and contiguous seam workings", Inter. J. Rock Mech.Min.Sci., 11, 97-102 (1974)

44. Timoshenko, S. and Woinowsky-Krieger S. - "Theory of Plates and Shells", pp. 166-70, McGraw Hill, New York (1959)

45. Timoshenko, S. and Goodier, J.N. - "Theory of Elasticity", pp.57-8, McGraw Hill, Kogakusha, Tokyo (1970)

46. Sheorey, P.R. - "An approach to thick beam analysis for roof strata", Inter. J. Rock Mech. Min.Sci., Geomech.Abstr. 12, 373-77 (1975)

47. Salustowicz, A. - "The influence of excavation on the extent of deformation and value of stresses in a coal seam. Archiwum Gornictwa, 5, 91-8 (1960)

48. Borecki, M and Salustowicz, A. - "Experimental work in the field of rock mechanics", 3rd Inter. Conf. Strata Control, Paris, 487-98 (1960)

49. Sheorey, P.R., Barat, D. and Singh, B. - "Assessment of barrier stability in a pyrite mine", Inter.J.Rock Mech. Min. Sci. Geomech.Abstr., 13, 31-4 (1976)

50. Epstein, B. - "Statistical aspects of fracture problems", J. Appl. Phys. 19, 140-47 (1948)

51. Grobbelaar, C. - "A Theory for the Strength of Pillars", pp. 7-19, Voortrekkers, Johannesburg (1970)

52. Bieniawski, Z.T. - "The effect of specimen size on compressive strength of coal", Inter. J. Rock Mech. Min.Sci. 5, 325-35 (1968)

53. Greenwald, H.P., Howarth, H.C. and Hartman, I. - "Experiments on strength of small pillars of coal in the Pittsburgh Bed", U.S. Bur. Mines Rep. Inv. 3575 (1941)

54. Steart, F.A. - "Strength and stability of pillars in coal mines", J.Chem. Metall.Min.Soc.S.Africa, 54, 309-25 (1954)

55. Holland, C.T. and Gaddy, F.L. - "Some aspects of permanent support of overburden on coal beds", Proc. W. Virginia Coal Min. Inst., 54-55 (1956)

56. Salamon, M.D.G. - "A method of designing bord and pillar workings", J.S.Afr. Inst.Min.Metall. 58, 68-78 (1967)

57. Dudley, W.R. - Personal communication, University of Newcastle upon Tyne (1975)

58. Sheorey, P.R. and Singh, B. - "Strength of rectangular pillars in partial extraction", Inter.J.Rock Mech.Min.Sci. 11, 41-4 (1974)

59. Desai, C.S. and Abel, J. - "Introduction to the Finite Element Method", Van Nostrand Reinhold, New York (1970)

60. Thompson, M. - "The Face Element Method: Numerical Solution of Elastostatic Problems by the Use of Harmonic Functions", Ph.D. Thesis, University of Newcastle upon Tyne (1975)

61. Timoshenko, S. and Woinowsky-Krieger, S. - "Theory of Plates and Shells", pp. 269-71, McGraw Hill, New York (1959)

62. Singh, T.N. - Personal Communication, Central Mining Research Station, Dhanbad (1974)

63. Norbury, B. - "A Field Investigation into Strata Displacements around Roadways Associated with Advancing and Retreating Longwall Faces", Ph.D. Thesis, University of Newcastle upon Tyne (1975)

64. Clook, P. - "Theoretical and field investigations into the behaviour of some mine roadway floors associated with longwall extraction", Ph.D. Thesis, University of Newcastle upon Tyne (1973)

65. Spackeler, G. - "The so-called pressure wave", Gluckauf. 64, 873-80 (1928)

66. Wilson, A. H. - "Research into the determination of pillar size", Min.Engr. 131, 409-16 (1972)

67. Hobbs, D.W. - "Strength and stress-strain characteristics of coal in triaxial compression., J.Geol.72, 214-31 (1964)

68. Hobbs, D.W. - "The strength of coal under biaxial compression", Colly.Eng. 39, 285-90 (1962)

69. Bordia, S.K. - "Complete stress-volumetric strain equation for brittle rock up to strength failure", Int. J.Rock Mech. Min. Sci. 9, 17-24 (1972)

70. Kidybinski A. and Babcock, C.O. - "Stress distribution and rock fracture zones in the roof of longwall face in a coal mine", Rock Mech. 5, 1-19 (1973)

71. Bieniawski, Z.T. - "Deformation behaviour of fractured rock under multiaxial compression", C.S.I.R. Rep. MEG 708, Pretoria (S.A.) (1968)

72. Timoshenko, S. and Goodier, J.N. - "Theory of Elasticity", pp.53-5, McGraw Hill Kogakusha Tokyo (1970)

73. Gerrard, C.M. and Morgan, J.R. - "Application of layered elastic theory to practical problems", 7th Inter.Conf.Soil Mech. Foundation Engg., Vol.1, Mexico, 143-57 (1969)

74. Bland, D. R. - "The theory of linear viscoelasticity", Pergamon Press, New York (1960)

75. Lee, E.H. - "Stress analysis in viscoelastic bodies", Quarterly Appl.Math. 13, 183-90 (1955)

76. Lu, P.H. and Wright, F.D. - "Stess-strain analysis of a viscoelastic mine roof", 10th Symp.Rock Mech., Texas University, 811-53 (1968)

77. Gnirk, P.E. and Johnson, R.E. - "The deformational behaviour of a circular shaft situated in a viscoelastic medium under hydrostatic stress", 6th Symp. Rock Mech., University of Missouri, 231-59 (1964)

* * *

APPENDIX I

APPENDIX I

Deflection equations for stages 4 to 7 for short face advancing with anhydrite centre packs

As the face moves in each stage, the y-axis is also shifted. If the deflection over a pack section is given by v_m in a stage of advance and if it changes to v_n in the next stage, the expression for v_n will include v_m such that (x-1) is written instead of x in v_m, due to the shift in the y-axis by 1, the unit advance. For brevity v_n can then be written down as

$$v_n = (v_m)_{x \rightarrow (x-1)} + f(x)$$

This convention has been adopted for writing down the delfection equations for stages 4 to 7. Also, the following notations have been used:

$$\frac{q_1+q_2}{k_2} = a_1 \quad , \quad \frac{q_2}{24\,D_2} = a_2 \, ,$$

$$e^{-\alpha x}\cos\alpha x = e_1(\alpha) \, , \quad e^{-\alpha x}\sin\alpha x = e_2(\alpha) \, ,$$

$$e^{\alpha x}\cos\alpha x = e_3(\alpha) \, , \quad e^{\alpha x}\sin\alpha x = e_4(\alpha) \, ,$$

$$e^{-\beta_i x}\cos\beta_i x = e_1(\beta_i) \, , \quad e^{-\beta_i x}\sin\beta_i x = e_2(\beta_i) \, ,$$

$$e^{\beta_i x}\cos\beta_i x = e_3(\beta_i) \, , \quad e^{\beta_i x}\sin\beta_i x = e_4(\beta_i) \, ,$$

$$i = 1, 2, 3 \ldots$$

Deflections have been numbered as per the convention of Fig.5.1.

Stage (4):

$$v_{14} = a_1 + C_{41}\, e_1(\alpha) + C_{42}\, e_2(\alpha)$$

$$v_{15} = a_2 x^4 + C_{43} x^3 + C_{44} x^2 + C_{45} x + C_{46}$$

$$v_{16} = (v_{10})_{x \to (x-\ell)} + C_{47}\, e_1(\beta_3) + C_{48}\, e_2(\beta_3) + C_{49}\, e_3(\beta_3) + C_{50}\, e_4(\beta_3)$$

$$v_{17} = (v_{11})_{x \to (x-\ell)} + C_{51}\, e_1(\beta_2) + C_{52}\, e_2(\beta_2) + C_{53}\, e_3(\beta_2) + C_{54}\, e_4(\beta_2)$$

$$v_{18} = (v_{12})_{x \to (x-\ell)} + C_{55}\, e_1(\beta_1) + C_{56}\, e_2(\beta_1) + C_{57}\, e_3(\beta_1) + C_{58}\, e_4(\beta_1)$$

$$v_{19} = a_2 x^4 + C_{59} x^3 + C_{60} x^2 + C_{61} x + C_{62}$$

$$v_{20} = a_1 + C_{63}\, e_3(\alpha) + C_{64}\, e_4(\alpha)$$

The equations in further stages have a certain repetitive pattern and can be written more concisely if the notations are further shortened. The above equations can be written again as

$$v_{14} = a_1 + (C_{41,42})[e_{1,2}(\alpha)]$$

$$v_{15} = a_2 x^4 + (C_{43,46})(x^{3,0})$$

$$v_{16} = (v_{10})_{x \to (x-\ell)} + (C_{47,50})[e_{1,4}(\beta_3)]. \quad \text{etc}$$

Similarly stages 5 to 7 will have the forms of equations below.

Stage (5):

$$v_{21} = a_1 + (C_{65,66})[e_{1,2}(\alpha)]$$

$$v_{22} = a_2 x^4 + (C_{67,70})(x^{3,0})$$

$$v_{23} = (v_{16})_{x \to (x-l)} + (C_{71,74})[e_{1,4}(\beta_4)]$$

$$v_{24} = (v_{17})_{x \to (x-l)} + (C_{75,78})[e_{1,4}(\beta_3)]$$

$$v_{25} = (v_{18})_{x \to (x-l)} + (C_{79,82})[e_{1,4}(\beta_2)]$$

$$v_{26} = (v_{19})_{x \to (x-l)} + (C_{83,86})[e_{1,4}(\beta_1)]$$

$$v_{27} = a_2 x^4 + (C_{87,90})(x^{3,0})$$

$$v_{28} = a_1 + (C_{91,92})[e_{3,4}(\alpha)]$$

Stage (6):

$$v_{29} = a_1 + (C_{93,94})[e_{1,2}(\alpha)]$$

$$v_{30} = a_2 x^4 + (C_{95,98})(x^{3,0})$$

$$v_{31} = (v_{23})_{x \to (x-l)} + (C_{99,102})[e_{1,4}(\beta_5)]$$

$$v_{32} = (v_{24})_{x \to (x-\ell)} (C_{103,106}) [e_{1,4}(\beta_4)]$$

$$v_{33} = (v_{25})_{x \to (x-\ell)} (C_{107,110}) [e_{1,4}(\beta_3)]$$

$$v_{34} = (v_{26})_{x \to (x-\ell)} (C_{111,114}) [e_{1,4}(\beta_2)]$$

$$v_{35} = (v_{27})_{x \to (x-\ell)} (C_{115,118}) [e_{1,4}(\beta_1)]$$

$$v_{36} = a_2 x^4 + (C_{119,122})(x^{3,0})$$

$$v_{37} = a_1 + (C_{123,124}) [e_{3,4}(\alpha)]$$

Stage (7):

$$v_{38} = a_1 + (C_{125,126}) [e_{1,2}(\alpha)]$$

$$v_{39} = a_2 x^4 + (C_{127,130})(x^{3,0})$$

$$v_{40} = (v_{31})_{x \to (x-\ell)} + (C_{131,134}) [e_{1,4}(\beta_6)]$$

$$v_{41} = (v_{32})_{x \to (x-\ell)} + (C_{135,138}) [e_{1,4}(\beta_5)]$$

$$v_{42} = (v_{33})_{x \to (x-\ell)} + (C_{139,142}) [e_{1,4}(\beta_4)]$$

$$v_{43} = (v_{34})_{x \to (x-l)} + (C_{143,146})[e_{1,4}(\beta_3)]$$

$$v_{44} = (v_{35})_{x \to (x-l)} + (C_{147,150})[e_{1,4}(\beta_2)]$$

$$v_{45} = (v_{36})_{x \to (x-l)} + (C_{151,154})[e_{1,4}(\beta_1)]$$

$$v_{46} = a_2 x^4 + (C_{155,158})(x^{3,0})$$

$$v_{47} = a_1 + (C_{159,160})[e_{3,4}(\alpha)]$$

* * *

APPENDIX II

```
ORTRAN IV G COMPILER        MAIN            07-30-76        12:43:59

      C***SHORT FACE ADVANCING WITH ANH. CENTRE PACKS
      C***PROG FOR DEFLNS & PACK LOADS AT POINTS A,B
      C***BY LONGL. CONSIDERATIONS
      C***INVOLVING APPLICATION OF CONTINUITY CONDITIONS TO
      C***DEFLN FCNS OF STAGE 7 & SOLVING RESULTING SIMULTANEOUS EQNS
      C***TO OBTAIN 36 INTEGRATION CONSTS,C125--C160,OF STAGE 7.
      C***
0001        SUBROUTINE P(N,X,Y,A,H)
      C***Y(1) IS THE FUNCTION A*(X-H)**N
      C***Y(2),Y(3),Y(4) ARE THE DERIVATIVES
0002        DOUBLE PRECISION X,Y(4),Z,A,H
0003        Z=X-H
0004        Y(1)=A*Z**N
0005        Y(2)=A*N*Z**(N-1)
0006        Y(3)=A*N*(N-1)*Z**(N-2)
0007        Y(4)=A*N*(N-1)*(N-2)*Z**(N-3)
0008        RETURN
0009        END

TOTAL MEMORY REQUIREMENTS 000308 BYTES
0001        SUBROUTINE ECOS(A,B,X,Y,C,H)
      C***Y(1) IS THE FUNCTION   C*EXP(A*(X-H))*COS(B*(X-H))
      C***Y(2),Y(3),Y(4) ARE THE DERIVATIVES
0002        DOUBLE PRECISION A,B,C,X,Y(4),Z,Z1,Z2,H,DEXP,DCOS,DSIN
0003        Z1=A*(X-H)
0004        Z2=B*(X-H)
0005        Y(1)=C*DEXP(Z1)*DCOS(Z2)
0006        Z=C*DEXP(Z1)*DSIN(Z2)
0007        Y(2)=A*Y(1)-B*Z
0008        Y(3)=(A*A-B*B)*Y(1)-2.*A*B*Z
0009        Y(4)=(A*A-3.*B*B)*A*Y(1)-(3.*A*A-B*B)*B*Z
0010        RETURN
0011        END

TOTAL MEMORY REQUIREMENTS 0002DC BYTES
0001        SUBROUTINE ESIN(A,B,X,Y,C,H)
      C***Y(1) IS THE FUNCTION   C*EXP(A*(X-H))*SIN(B*(X-H))
      C***Y(2),Y(3),Y(4) ARE THE DERIVATIVES
0002        DOUBLE PRECISION A,B,C,X,Y(4),Z,Z1,Z2,H,DEXP,DCOS,DSIN
0003        Z1=A*(X-H)
0004        Z2=B*(X-H)
0005        Y(1)=C*DEXP(Z1)*DSIN(Z2)
0006        Z=C*DEXP(Z1)*DCOS(Z2)
0007        Y(2)=A*Y(1)+B*Z
0008        Y(3)=(A*A-B*B)*Y(1)+2.*A*B*Z
0009        Y(4)=(A*A-3.*B*B)*A*Y(1)+(3.*A*A-B*B)*B*Z
0010        RETURN
0011        END

TOTAL MEMORY REQUIREMENTS 0002DA BYTES
      C***MEANINGS OF SYMBOLS USED IN PROG
      C***E=ALPHA,F1,F2,...=BETA1,BETA2,...,D3,D4=C3,C4
```

```
G COMPILER        MAIN              07-30-76        12:44:03

C***T1,T2,...=K11,K12,..., Q=Q2/24D2,QQ=(Q1+Q2)/K2,
C***H1,H2,...=L,2L,..., HH=6L+(L1+W)/2, R=INT.CONSTS FROM
C***PREVIOUS STAGES OCCURRING IN DEFLN EQNS OF ST 7
C***ADEL1,...=DELTA1 AT A,...,  BDEL1,...=DELTA1 AT B,...,
C***LA1,...=PACK LOADS AT A, LB1,...=PACK LOADS AT B.
C***
      DOUBLE PRECISION E,Q,QQ,D3,D4,HH,H1,H2,H3,H4,H5,X1,X2,X3,
     *X4,X5,X6,X7,X8,X9,S,Z,F1,F2,F3,F4,F5,F6,T1,T2,T3,T4,T5,T6,
     *R(80,3),A(36,36),B(36),C(36),
     *K(4),L(4),KK(4),LL(4),KKK(4),LLL(4),MM(4),NN(4),MMM(4),NNN(4),
     *G(4),V(4),GG(4),VV(4),MA(4),MB(4),MC(4),MD(4),ME(4),MF(4),
     *MG(4),MH(4),NA(4),NB(4),NC(4),ND(4),NE(4),NF(4),NG(4),NH(4),
     *NI(4),NJ(4),NK(4),NL(4),NM(4),NP(4),NQ(4),NR(4),NS(4),NT(4),NU(4),
     *AA(36,36),WKS1(36),WKS2(36),
     *LA1,LA2,LA3,LA4,LB1,LB2,LB3,LB4,LB5,
     *Y1,Y2,Y3,Y4,Y5,Y6,EX11,EX12,EX21,EX22,EX31,EX32,EX41,EX42,
     *EX51,EX52,CO1,CO2,CO3,CO4,CO5,SI1,SI2,SI3,SI4,SI5,
     *ADEL1,ADEL2,ADEL3,ADEL4,ADEL5,AS1,AS2,AS3,AS4,BDEL1,BDEL2,
     *BDEL3,BDEL4,BDEL5,BDEL6,BS1,BS2,BS3,BS4,BS5,RA
C***DEFINE THE CONSTS INVOLVED
      E=0.39
      Q=7.986D-7
      QQ=7.4D-3
      D3=-1.0053D-4
      D4=1.0891D-2
      HH=23.5
      H1=3.0
      H2=6.0
      H3=9.0
      H4=12.0
      H5=15.0
      X1=29.0
      X2=23.0
      X3=20.0
      X4=17.0
      X5=14.0
      X6=11.0
      X7=8.0
      X8=5.0
      X9=0.0
C***ASSIN INITIAL ZERO VALUES TO ALL MATRIX & R.H.S. ELEMENTS
      DO 3 I=1,36
      DO 2 J=1,36
    2 A(J,I)=0.0
    3 CONTINUE
      DO 4 I=1,36
      B(I)=0.0
    4 CONTINUE
      DO 1 J=1,3
      RA=18./(J+1)
      WRITE(6,20)RA
C***DEFINE K11 ETC, BETA1 ETC
      S=4.8D+7
      Z=4.4295D+6
      M1=J+1
```

```
0035                T1=(M1/6.)/(3.65+M1/6.)*Z
0036                F1=(T1/S)**0.25
0037                M2=M1*2
0038                T2=(M2/6.)/(3.65+M2/6.)*Z
0039                F2=(T2/S)**0.25
0040                M3=M1*3
0041                T3=(M3/6.)/(3.65+M3/6.)*Z
0042                F3=(T3/S)**0.25
0043                M4=M1*4
0044                T4=(M4/6.)/(3.65+M4/6.)*Z
0045                F4=(T4/S)**0.25
0046                M5=M1*5
0047                T5=(M5/6.)/(3.65+M5/6.)*Z
0048                F5=(T5/S)**0.25
0049                M6=M1*6
0050                T6=(M6/6.)/(3.65+M6/6.)*Z
0051                F6=(T6/S)**0.25
          C***LIST THE KNOWN INTEGR CONSTS OF THE LAST 5 SETS
0052                R(1,1)=-4.6280D-4
0053                R(1,2)=-8.082D-4
0054                R(1,3)=-1.085D-3
0055                R(2,1)=5.343D-3
0056                R(2,2)=5.1294D-3
0057                R(2,3)=5.0161D-3
0058                R(3,1)=4.0156D-6
0059                R(3,2)=1.396D-6
0060                R(3,3)=4.281D-7
0061                R(4,1)=1.088D-5
0062                R(4,2)=3.646D-6
0063                R(4,3)=1.3569D-6
0064                R(5,1)=-1.5106D-5
0065                R(5,2)=-1.447D-5
0066                R(5,3)=-1.4075D-5
0067                R(6,1)=4.8246D-5
0068                R(6,2)=4.4974D-5
0069                R(6,3)=4.2951D-5
0070                R(7,1)=5.4536D-4
0071                R(7,2)=5.1547D-4
0072                R(7,3)=4.9787D-4
0073                R(8,1)=8.4811D-3
0074                R(8,2)=8.4267D-3
0075                R(8,3)=8.3942D-3
0076                R(9,1)=-3.07406D-3
0077                R(9,2)=-3.4583D-3
0078                R(9,3)=-3.67592D-3
0079                R(10,1)=5.3731D-3
0080                R(10,2)=4.76802D-3
0081                R(10,3)=4.363866D-3
0082                R(11,1)=1.08606D-6
0083                R(11,2)=6.776D-7
0084                R(11,3)=3.346D-7
0085                R(12,1)=-7.782D-7
0086                R(12,2)=3.226D-7
0087                R(12,3)=6.8726D-7
0088                R(13,1)=-3.958970-4
```

```
      R(13,2)=-7.00308D-4
      R(13,3)=-9.34495D-4
      R(14,1)=4.84009D-3
      R(14,2)=4.53769D-3
      R(14,3)=4.362212D-3
      R(15,1)=3.3275D-6
      R(15,2)=2.0902D-6
      R(15,3)=1.1154D-6
      R(16,1)=-3.7328D-6
      R(16,2)=-7.9106D-7
      R(16,3)=1.148D-7
      R(17,1)=-1.3635D-5
      R(17,2)=-1.28034D-5
      R(17,3)=-1.22644D-5
      R(18,1)=4.369D-5
      R(18,2)=3.88272D-5
      R(18,3)=3.59584D-5
      R(19,1)=4.92996D-4
      R(19,2)=4.51647D-4
      R(19,3)=4.26303D-4
      R(20,1)=8.37685D-3
      R(20,2)=8.30279D-3
      R(20,3)=8.256671D-3
      R(21,1)=-5.23068D-3
      R(21,2)=-5.159248D-3
      R(21,3)=-5.08069D-3
      R(22,1)=4.25363D-3
      R(22,2)=3.589039D-3
      R(22,3)=3.232307D-3
      R(23,1)=5.0469D-8
      R(23,2)=3.70526D-8
      R(23,3)=2.011757D-8
      R(24,1)=1.4249D-7
      R(24,2)=4.0657D-8
      R(24,3)=1.34335D-8
      R(25,1)=-2.909974D-3
      R(25,2)=-3.169327D-3
      R(25,3)=-3.296346D-3
      R(26,1)=4.987145D-3
      R(26,2)=4.334143D-3
      R(26,3)=3.91994D-3
      R(27,1)=1.3576D-7
      R(27,2)=9.9486D-8
      R(27,3)=5.64637D-8
      R(28,1)=1.5846D-7
      R(28,2)=1.7045D-8
      R(28,3)=-1.6561D-8
      R(29,1)=-3.600823D-4
      R(29,2)=-6.278407D-4
      R(29,3)=-8.292188D-4
      R(30,1)=4.488396D-3
      R(30,2)=4.133935D-3
      R(30,3)=3.926838D-3
      R(31,1)=1.1597D-7
      R(31,2)=1.02616D-7
```

```
0144                R(31,3)=3.297984D-8
0145                R(32,1)=-3.442690-6
0146                R(32,2)=-1.488385D-6
0147                R(32,3)=-7.96073D-7
0148                R(33,1)=-1.285786D-5
0149                R(33,2)=-1.20165D-5
0150                R(33,3)=-1.148329D-5
0151                R(34,1)=3.887568D-5
0152                R(34,2)=3.311845D-5
0153                R(34,3)=2.969D-5
0154                R(35,1)=4.529692D-4
0155                R(35,2)=4.0685D-4
0156                R(35,3)=3.787515D-4
0157                R(36,1)=8.305867D-3
0158                R(36,2)=8.225464D-3
0159                R(36,3)=8.175957D-3
0160                R(37,1)=-7.370432D-3
0161                R(37,2)=-7.242291D-3
0162                R(37,3)=-6.959424D-3
0163                R(38,1)=3.3474D-3
0164                R(38,2)=2.585594D-3
0165                R(38,3)=2.155705D-3
0166                R(39,1)=3.210767D-9
0167                R(39,2)=5.880384D-10
0168                R(39,3)=6.970262D-10
0169                R(40,1)=-2.022599D-8
0170                R(40,2)=-1.325778D-8
0171                R(40,3)=-6.32054D-9
0172                R(41,1)=-4.954501D-3
0173                R(41,2)=-4.86027D-3
0174                R(41,3)=-4.773911D-3
0175                R(42,1)=4.028142D-3
0176                R(42,2)=3.38522D-3
0177                R(42,3)=3.044490-3
0178                R(43,1)=1.91682D-9
0179                R(43,2)=4.611323D-9
0180                R(43,3)=3.441623D-9
0181                R(44,1)=-6.448671D-8
0182                R(44,2)=-3.838702D-8
0183                R(44,3)=-1.934658D-8
0184                R(45,1)=-2.755122D-3
0185                R(45,2)=-2.988714D-3
0186                R(45,3)=-3.101184D-3
0187                R(46,1)=4.747351D-3
0188                R(46,2)=4.106691D-3
0189                R(46,3)=3.703713D-3
0190                R(47,1)=9.76306D-8
0191                R(47,2)=4.245291D-8
0192                R(47,3)=2.251157D-8
0193                R(48,1)=-7.658295D-8
0194                R(48,2)=-5.219236D-8
0195                R(48,3)=-3.784153D-8
0196                R(49,1)=-3.371495D-4
0197                R(49,2)=-5.885794D-4
0198                R(49,3)=-7.76586D-4
```

```
R(50,1)=4.272338D-3
R(50,2)=3.914308D-3
R(50,3)=3.706822D-3
R(51,1)=3.471120-8
R(51,2)=1.226626D-7
R(51,3)=6.097622D-8
R(52,1)=-3.723395D-6
R(52,2)=-1.572905D-6
R(52,3)=-8.044916D-7
R(53,1)=-1.256796D-5
R(53,2)=-1.178596D-5
R(53,3)=-1.129653D-5
R(54,1)=3.526172D-5
R(54,2)=2.923887D-5
R(54,3)=2.566436D-5
R(55,1)=4.287181D-4
R(55,2)=3.824077D-4
R(55,3)=3.544234D-4
R(56,1)=8.267445D-3
R(56,2)=8.188298D-3
R(56,3)=8.140044D-3
R(57,1)=-9.866526D-3
R(57,2)=-9.041299D-3
R(57,3)=-8.384885D-3
R(58,1)=1.305449D-3
R(58,2)=6.222418D-4
R(58,3)=4.604161D-4
R(59,1)=2.299224D-10
R(59,2)=1.433592D-10
R(59,3)=7.297279D-11
R(60,1)=-7.250476D-10
R(60,2)=1.342535D-10
R(60,3)=3.392519D-11
R(61,1)=-7.197619D-3
R(61,2)=-6.991142D-3
R(61,3)=-6.725797D-3
R(62,1)=3.284251D-3
R(62,2)=2.529874D-3
R(62,3)=2.126369D-3
R(63,1)=2.38228D-10
R(63,2)=1.474679D-10
R(63,3)=9.387325D-11
R(64,1)=6.227345D-11
R(64,2)=1.901323D-10
R(64,3)=3.671686D-11
R(65,1)=-4.829611D-3
R(65,2)=-4.743215D-3
R(65,3)=-4.663324D-3
R(66,1)=3.938532D-3
R(66,2)=3.315592D-3
R(66,3)=2.98422D-3
R(67,1)=2.713205D-10
R(67,2)=1.531191D-9
R(67,3)=1.11849D-9
R(68,1)=-4.958264D-8
```

```
0254                R(68,2)=-1.86279D-8
0255                R(68,3)=-9.051889D-9
0256                R(69,1)=-2.68424D-3
0257                R(69,2)=-2.914089D-3
0258                R(69,3)=-3.025945D-3
0259                R(70,1)=4.632481D-3
0260                R(70,2)=4.00978D-3
0261                R(70,3)=3.619491D-3
0262                R(71,1)=1.027625D-7
0263                R(71,2)=5.216058D-8
0264                R(71,3)=2.789525D-8
0265                R(72,1)=-9.208398D-8
0266                R(72,2)=-5.535073D-8
0267                R(72,3)=-4.086423D-8
0268                R(73,1)=-3.257126D-4
0269                R(73,2)=-5.711408D-4
0270                R(73,3)=-7.551823D-4
0271                R(74,1)=4.168143D-3
0272                R(74,2)=3.820987D-3
0273                R(74,3)=3.621435D-3
0274                R(75,1)=4.312751D-8
0275                R(75,2)=9.845397D-8
0276                R(75,3)=4.645394D-8
0277                R(76,1)=-3.634394D-6
0278                R(76,2)=-1.533191D-6
0279                R(76,3)=-7.867891D-7
0280                R(77,1)=-1.252415D-5
0281                R(77,2)=-1.179641D-5
0282                R(77,3)=-1.134372D-5
0283                R(78,1)=3.314766D-5
0284                R(78,2)=2.717079D-5
0285                R(78,3)=2.364061D-5
0286                R(79,1)=4.170126D-4
0287                R(79,2)=3.720083D-4
0288                R(79,3)=3.44976D-4
0289                R(80,1)=8.25133D-3
0290                R(80,2)=8.17523D-3
0291                R(80,3)=8.129126D-3
          C***FORM THE MATRIX
0292                CALL ECOS(-E,E,X1,A(1,1),1.,0.)
0293                CALL ESIN(-E,E,X1,A(1,2),1.,0.)
0294                CALL P(3,X1,A(1,3),-1.,0.)
0295                CALL P(2,X1,A(1,4),-1.,0.)
0296                CALL P(1,X1,A(1,5),-1.,0.)
0297                CALL P(0,X1,A(1,6),-1.,0.)
0298                CALL P(3,X2,A(5,3),1.,0.)
0299                CALL P(2,X2,A(5,4),1.,0.)
0300                CALL P(1,X2,A(5,5),1.,0.)
0301                CALL P(0,X2,A(5,6),1.,0.)
0302                CALL ECOS(-F6,F6,X2,A(5,7),-1.,0.)
0303                CALL ESIN(-F6,F6,X2,A(5,8),-1.,0.)
0304                CALL ECOS(F6,F6,X2,A(5,9),-1.,0.)
0305                CALL ESIN(F6,F6,X2,A(5,10),-1.,0.)
0306                CALL ECOS(-F6,F6,X3,A(9,7),1.,0.)
0307                CALL ESIN(-F6,F6,X3,A(9,8),1.,0.)
```

```
      CALL ECOS(F6,F6,X3,A(9,9),1.,0.)
      CALL ESIN(F6,F6,X3,A(9,10),1.,0.)
      CALL ECOS(-F5,F5,X3,A(9,11),-1.,0.)
      CALL ESIN(-F5,F5,X3,A(9,12),-1.,0.)
      CALL ECOS(F5,F5,X3,A(9,13),-1.,0.)
      CALL ESIN(F5,F5,X3,A(9,14),-1.,0.)
      CALL ECOS(-F5,F5,X4,A(13,11),1.,0.)
      CALL ESIN(-F5,F5,X4,A(13,12),1.,0.)
      CALL ECOS(F5,F5,X4,A(13,13),1.,0.)
      CALL ESIN(F5,F5,X4,A(13,14),1.,0.)
      CALL ECOS(-F4,F4,X4,A(13,15),-1.,0.)
      CALL ESIN(-F4,F4,X4,A(13,16),-1.,0.)
      CALL ECOS(F4,F4,X4,A(13,17),-1.,0.)
      CALL ESIN(F4,F4,X4,A(13,18),-1.,0.)
      CALL ECOS(-F4,F4,X5,A(17,15),1.,0.)
      CALL ESIN(-F4,F4,X5,A(17,16),1.,0.)
      CALL ECOS(F4,F4,X5,A(17,17),1.,0.)
      CALL ESIN(F4,F4,X5,A(17,18),1.,0.)
      CALL ECOS(-F3,F3,X5,A(17,19),-1.,0.)
      CALL ESIN(-F3,F3,X5,A(17,20),-1.,0.)
      CALL ECOS(F3,F3,X5,A(17,21),-1.,0.)
      CALL ESIN(F3,F3,X5,A(17,22),-1.,0.)
      CALL ECOS(-F3,F3,X6,A(21,19),1.,0.)
      CALL ESIN(-F3,F3,X6,A(21,20),1.,0.)
      CALL ECOS(F3,F3,X6,A(21,21),1.,0.)
      CALL ESIN(F3,F3,X6,A(21,22),1.,0.)
      CALL ECOS(-F2,F2,X6,A(21,23),-1.,0.)
      CALL ESIN(-F2,F2,X6,A(21,24),-1.,0.)
      CALL ECOS(F2,F2,X6,A(21,25),-1.,0.)
      CALL ESIN(F2,F2,X6,A(21,26),-1.,0.)
      CALL ECOS(-F2,F2,X7,A(25,23),1.,0.)
      CALL ESIN(-F2,F2,X7,A(25,24),1.,0.)
      CALL ECOS(F2,F2,X7,A(25,25),1.,0.)
      CALL ESIN(F2,F2,X7,A(25,26),1.,0.)
      CALL ECOS(-F1,F1,X7,A(25,27),-1.,0.)
      CALL ESIN(-F1,F1,X7,A(25,28),-1.,0.)
      CALL ECOS(F1,F1,X7,A(25,29),-1.,0.)
      CALL ESIN(F1,F1,X7,A(25,30),-1.,0.)
      CALL ECOS(-F1,F1,X8,A(29,27),1.,0.)
      CALL ESIN(-F1,F1,X8,A(29,28),1.,0.)
      CALL ECOS(F1,F1,X8,A(29,29),1.,0.)
      CALL ESIN(F1,F1,X8,A(29,30),1.,0.)
      CALL P(3,X8,A(29,31),-1.,0.)
      CALL P(2,X8,A(29,32),-1.,0.)
      CALL P(1,X8,A(29,33),-1.,0.)
      CALL P(0,X8,A(29,34),-1.,0.)
      A(33,34)=1.0
      A(34,33)=1.0
      A(35,32)=2.0
      A(36,31)=6.0
      CALL ECOS(E,E,X9,A(33,35),-1.,0.)
      CALL ESIN(E,E,X9,A(33,36),-1.,0.)
C***FORM THE R.H.S.
      CALL P(4,X1,B(1),Q,0.)
      B(1)=B(1)-QQ
```

```
0362                CALL P(4,X2,K(1),Q,HH)
0363                CALL P(2,X2,L(1),D3,HH)
0364                CALL ECOS(-F1,F1,X2,KK(1),R(1,J),H5)
0365                CALL ESIN(-F1,F1,X2,LL(1),R(2,J),H5)
0366                CALL ECOS(F1,F1,X2,KKK(1),R(3,J),H5)
0367                CALL ESIN(F1,F1,X2,LLL(1),R(4,J),H5)
0368                CALL ECOS(-F2,F2,X2,MM(1),R(9,J),H4)
0369                CALL ESIN(-F2,F2,X2,NN(1),R(10,J),H4)
0370                CALL ECOS(F2,F2,X2,MMM(1),R(11,J),H4)
0371                CALL ESIN(F2,F2,X2,NNN(1),R(12,J),H4)
0372                CALL ECOS(-F3,F3,X2,G(1),R(21,J),H3)
0373                CALL ESIN(-F3,F3,X2,V(1),R(22,J),H3)
0374                CALL ECOS(F3,F3,X2,GG(1),R(23,J),H3)
0375                CALL ESIN(F3,F3,X2,VV(1),R(24,J),H3)
0376                CALL ECOS(-F4,F4,X2,MA(1),R(37,J),H2)
0377                CALL ESIN(-F4,F4,X2,MB(1),R(38,J),H2)
0378                CALL ECOS(F4,F4,X2,MC(1),R(39,J),H2)
0379                CALL ESIN(F4,F4,X2,MD(1),R(40,J),H2)
0380                CALL ECOS(-F5,F5,X2,NA(1),R(57,J),H1)
0381                CALL ESIN(-F5,F5,X2,NB(1),R(58,J),H1)
0382                CALL ECOS(F5,F5,X2,NC(1),R(59,J),H1)
0383                CALL ESIN(F5,F5,X2,ND(1),R(60,J),H1)
0384                CALL P(4,X2,B(5),-Q,0.)
0385                DO 6 I=1,4
0386                II=I+4
0387                IF(I.NE.1)GO TO 5
0388                B(5)=B(5)+D4
0389              5 CONTINUE
0390              6 B(II)=B(II)+K(I)+L(I)+KK(I)+LL(I)+KKK(I)+LLL(I)+
                   *MM(I)+NN(I)+MMM(I)+NNN(I)+G(I)+V(I)+GG(I)+VV(I)+
                   *MA(I)+MB(I)+MC(I)+MD(I)+NA(I)+NB(I)+NC(I)+ND(I)
0391                CALL P(4,X3,K(1),-Q,HH)
0392                CALL P(2,X3,L(1),-D3,HH)
0393                CALL ECOS(-F1,F1,X3,KK(1),-R(1,J),H5)
0394                CALL ESIN(-F1,F1,X3,LL(1),-R(2,J),H5)
0395                CALL ECOS(F1,F1,X3,KKK(1),-R(3,J),H5)
0396                CALL ESIN(F1,F1,X3,LLL(1),-R(4,J),H5)
0397                CALL ECOS(-F2,F2,X3,MM(1),-R(9,J),H4)
0398                CALL ESIN(-F2,F2,X3,NN(1),-R(10,J),H4)
0399                CALL ECOS(F2,F2,X3,MMM(1),-R(11,J),H4)
0400                CALL ESIN(F2,F2,X3,NNN(1),-R(12,J),H4)
0401                CALL ECOS(-F3,F3,X3,G(1),-R(21,J),H3)
0402                CALL ESIN(-F3,F3,X3,V(1),-R(22,J),H3)
0403                CALL ECOS(F3,F3,X3,GG(1),-R(23,J),H3)
0404                CALL ESIN(F3,F3,X3,VV(1),-R(24,J),H3)
0405                CALL ECOS(-F4,F4,X3,MA(1),-R(37,J),H2)
0406                CALL ESIN(-F4,F4,X3,MB(1),-R(38,J),H2)
0407                CALL ECOS(F4,F4,X3,MC(1),-R(39,J),H2)
0408                CALL ESIN(F4,F4,X3,MD(1),-R(40,J),H2)
0409                CALL ECOS(-F5,F5,X3,ME(1),-R(57,J),H1)
0410                CALL ESIN(-F5,F5,X3,MF(1),-R(58,J),H1)
0411                CALL ECOS(F5,F5,X3,MG(1),-R(59,J),H1)
0412                CALL ESIN(F5,F5,X3,MH(1),-R(60,J),H1)
0413                CALL P(4,X3,B(9),Q,H5)
0414                CALL P(3,X3,NA(1),R(5,J),H5)
```

```
      CALL P(2,X3,NB(1),R(6,J),H5)
      CALL P(1,X3,NC(1),R(7,J),H5)
      CALL ECOS(-F1,F1,X3,ND(1),R(13,J),H4)
      CALL ESIN(-F1,F1,X3,NE(1),R(14,J),H4)
      CALL ECOS(F1,F1,X3,NF(1),R(15,J),H4)
      CALL ESIN(F1,F1,X3,NG(1),R(16,J),H4)
      CALL ECOS(-F2,F2,X3,NH(1),R(25,J),H3)
      CALL ESIN(-F2,F2,X3,NI(1),R(26,J),H3)
      CALL ECOS(F2,F2,X3,NJ(1),R(27,J),H3)
      CALL ESIN(F2,F2,X3,NK(1),R(28,J),H3)
      CALL ECOS(-F3,F3,X3,NL(1),R(41,J),H2)
      CALL ESIN(-F3,F3,X3,NM(1),R(42,J),H2)
      CALL ECOS(F3,F3,X3,NP(1),R(43,J),H2)
      CALL ESIN(F3,F3,X3,NQ(1),R(44,J),H2)
      CALL ECOS(-F4,F4,X3,NR(1),R(61,J),H1)
      CALL ESIN(-F4,F4,X3,NS(1),R(62,J),H1)
      CALL ECOS(F4,F4,X3,NT(1),R(63,J),H1)
      CALL ESIN(F4,F4,X3,NU(1),R(64,J),H1)
      DO 8 I=1,4
      II=I+8
      IF(I.NE.1)GO TO 7
      B(9)=B(9)-D4+R(8,J)
    7 CONTINUE
    8 B(II)=B(II)+K(I)+L(I)+KK(I)+LL(I)+KKK(I)+LLL(I)+
     *MM(I)+NN(I)+MMM(I)+NNN(I)+G(I)+V(I)+GG(I)+VV(I)+
     *MA(I)+MB(I)+MC(I)+MD(I)+NA(I)+NB(I)+NC(I)+ND(I)+
     *NE(I)+NF(I)+NG(I)+NH(I)+NI(I)+NJ(I)+NK(I)+NL(I)+
     *NM(I)+NP(I)+NQ(I)+NR(I)+NS(I)+NT(I)+NU(I)+ME(I)+
     *MF(I)+MG(I)+MH(I)
      CALL P(4,X4,K(1),-Q,H5)
      CALL P(3,X4,L(1),-R(5,J),H5)
      CALL P(2,X4,KK(1),-R(6,J),H5)
      CALL P(1,X4,LL(1),-R(7,J),H5)
      CALL ECOS(-F1,F1,X4,G(1),-R(13,J),H4)
      CALL ESIN(-F1,F1,X4,V(1),-R(14,J),H4)
      CALL ECOS(F1,F1,X4,GG(1),-R(15,J),H4)
      CALL ESIN(F1,F1,X4,VV(1),-R(16,J),H4)
      CALL ECOS(-F2,F2,X4,MM(1),-R(25,J),H3)
      CALL ESIN(-F2,F2,X4,NN(1),-R(26,J),H3)
      CALL ECOS(F2,F2,X4,MMM(1),-R(27,J),H3)
      CALL ESIN(F2,F2,X4,NNN(1),-R(28,J),H3)
      CALL ECOS(-F3,F3,X4,MA(1),-R(41,J),H2)
      CALL ESIN(-F3,F3,X4,MB(1),-R(42,J),H2)
      CALL ECOS(F3,F3,X4,MC(1),-R(43,J),H2)
      CALL ESIN(F3,F3,X4,MD(1),-R(44,J),H2)
      CALL ECOS(-F4,F4,X4,ME(1),-R(61,J),H1)
      CALL ESIN(-F4,F4,X4,MF(1),-R(62,J),H1)
      CALL ECOS(F4,F4,X4,MG(1),-R(63,J),H1)
      CALL ESIN(F4,F4,X4,MH(1),-R(64,J),H1)
      CALL P(4,X4,B(13),Q,H4)
      CALL P(3,X4,NA(1),R(17,J),H4)
      CALL P(2,X4,NB(1),R(18,J),H4)
      CALL P(1,X4,NC(1),R(19,J),H4)
      CALL ECOS(-F1,F1,X4,ND(1),R(29,J),H3)
      CALL ESIN(-F1,F1,X4,NE(1),R(30,J),H3)
```

```
ORTRAN IV G COMPILER        MAIN            07-30-76        12:44:03

0465                CALL ECOS(F1,F1,X4,NF(1),R(31,J),H3)
0466                CALL ESIN(F1,F1,X4,NG(1),R(32,J),H3)
0467                CALL ECOS(-F2,F2,X4,NH(1),R(45,J),H2)
0468                CALL ESIN(-F2,F2,X4,NI(1),R(46,J),H2)
0469                CALL ECOS(F2,F2,X4,NJ(1),R(47,J),H2)
0470                CALL ESIN(F2,F2,X4,NK(1),R(48,J),H2)
0471                CALL ECOS(-F3,F3,X4,NL(1),R(65,J),H1)
0472                CALL ESIN(-F3,F3,X4,NM(1),R(66,J),H1)
0473                CALL ECOS(F3,F3,X4,NP(1),R(67,J),H1)
0474                CALL ESIN(F3,F3,X4,NQ(1),R(68,J),H1)
0475                DO 10 I=1,4
0476                II=I+12
0477                IF(I.NE.1)GO TO 9
0478                B(13)=B(13)-R(8,J)+R(20,J)
0479              9 CONTINUE
0480             10 B(II)=B(II)+K(I)+L(I)+KK(I)+LL(I)+G(I)+V(I)+GG(I)+VV(I)+
                  *MM(I)+NN(I)+MMM(I)+NNN(I)+MA(I)+MB(I)+MC(I)+MD(I)+
                  *NA(I)+NB(I)+NC(I)+ND(I)+NE(I)+NF(I)+NG(I)+NH(I)+
                  *NI(I)+NJ(I)+NK(I)+NL(I)+NM(I)+NP(I)+NQ(I)+
                  *ME(I)+MF(I)+MG(I)+MH(I)
0481                CALL P(4,X5,K(1),-Q,H4)
0482                CALL P(3,X5,L(1),-R(17,J),H4)
0483                CALL P(2,X5,KK(1),-R(18,J),H4)
0484                CALL P(1,X5,LL(1),-R(19,J),H4)
0485                CALL ECOS(-F1,F1,X5,G(1),-R(29,J),H3)
0486                CALL ESIN(-F1,F1,X5,V(1),-R(30,J),H3)
0487                CALL ECOS(F1,F1,X5,GG(1),-R(31,J),H3)
0488                CALL ESIN(F1,F1,X5,VV(1),-R(32,J),H3)
0489                CALL ECOS(-F2,F2,X5,MM(1),-R(45,J),H2)
0490                CALL ESIN(-F2,F2,X5,NN(1),-R(46,J),H2)
0491                CALL ECOS(F2,F2,X5,MMM(1),-R(47,J),H2)
0492                CALL ESIN(F2,F2,X5,NNN(1),-R(48,J),H2)
0493                CALL ECOS(-F3,F3,X5,MA(1),-R(65,J),H1)
0494                CALL ESIN(-F3,F3,X5,MB(1),-R(66,J),H1)
0495                CALL ECOS(F3,F3,X5,MC(1),-R(67,J),H1)
0496                CALL ESIN(F3,F3,X5,MD(1),-R(68,J),H1)
0497                CALL P(4,X5,B(17),Q,H3)
0498                CALL P(3,X5,NA(1),R(33,J),H3)
0499                CALL P(2,X5,NB(1),R(34,J),H3)
0500                CALL P(1,X5,NC(1),R(35,J),H3)
0501                CALL ECOS(-F1,F1,X5,ND(1),R(49,J),H2)
0502                CALL ESIN(-F1,F1,X5,NE(1),R(50,J),H2)
0503                CALL ECOS(F1,F1,X5,NF(1),R(51,J),H2)
0504                CALL ESIN(F1,F1,X5,NG(1),R(52,J),H2)
0505                CALL ECOS(-F2,F2,X5,NH(1),R(69,J),H1)
0506                CALL ESIN(-F2,F2,X5,NI(1),R(70,J),H1)
0507                CALL ECOS(F2,F2,X5,NJ(1),R(71,J),H1)
0508                CALL ESIN(F2,F2,X5,NK(1),R(72,J),H1)
0509                DO 12 I=1,4
0510                II=I+16
0511                IF(I.NE.1)GO TO 11
0512                B(17)=B(17)-R(20,J)+R(36,J)
0513             11 CONTINUE
0514             12 B(II)=B(II)+K(I)+L(I)+KK(I)+LL(I)+G(I)+V(I)+GG(I)+VV(I)+
                  *MM(I)+NN(I)+MMM(I)+NNN(I)+MA(I)+MB(I)+MC(I)+MD(I)+
```

```
     *NA(I)+NB(I)+NC(I)+ND(I)+NE(I)+NF(I)+NG(I)+NH(I)+
     *NI(I)+NJ(I)+NK(I)
      CALL P(4,X6,K(1),-Q,H3)
      CALL P(3,X6,L(1),-R(33,J),H3)
      CALL P(2,X6,KK(1),-R(34,J),H3)
      CALL P(1,X6,LL(1),-R(35,J),H3)
      CALL ECOS(-F1,F1,X6,G(1),-R(49,J),H2)
      CALL ESIN(-F1,F1,X6,V(1),-R(50,J),H2)
      CALL ECOS(F1,F1,X6,GG(1),-R(51,J),H2)
      CALL ESIN(F1,F1,X6,VV(1),-R(52,J),H2)
      CALL ECOS(-F2,F2,X6,MM(1),-R(69,J),H1)
      CALL ESIN(-F2,F2,X6,NN(1),-R(70,J),H1)
      CALL ECOS(F2,F2,X6,MMM(1),-R(71,J),H1)
      CALL ESIN(F2,F2,X6,NNN(1),-R(72,J),H1)
      CALL P(4,X6,B(21),Q,H2)
      CALL P(3,X6,NA(1),R(53,J),H2)
      CALL P(2,X6,NB(1),R(54,J),H2)
      CALL P(1,X6,NC(1),R(55,J),H2)
      CALL ECOS(-F1,F1,X6,ND(1),R(73,J),H1)
      CALL ESIN(-F1,F1,X6,NE(1),R(74,J),H1)
      CALL ECOS(F1,F1,X6,NF(1),R(75,J),H1)
      CALL ESIN(F1,F1,X6,NG(1),R(76,J),H1)
      DO 14 I=1,4
      II=I+20
      IF(I.NE.1)GO TO 13
      B(21)=B(21)-R(36,J)+R(56,J)
   13 CONTINUE
   14 B(II)=B(II)+K(I)+L(I)+KK(I)+LL(I)+G(I)+V(I)+GG(I)+VV(I)+
     *MM(I)+NN(I)+MMM(I)+NNN(I)+NA(I)+NB(I)+NC(I)+ND(I)+
     *NE(I)+NF(I)+NG(I)
      CALL P(4,X7,K(1),-Q,H2)
      CALL P(3,X7,L(1),-R(53,J),H2)
      CALL P(2,X7,KK(1),-R(54,J),H2)
      CALL P(1,X7,LL(1),-R(55,J),H2)
      CALL ECOS(-F1,F1,X7,G(1),-R(73,J),H1)
      CALL ESIN(-F1,F1,X7,V(1),-R(74,J),H1)
      CALL ECOS(F1,F1,X7,GG(1),-R(75,J),H1)
      CALL ESIN(F1,F1,X7,VV(1),-R(76,J),H1)
      CALL P(4,X7,B(25),Q,H1)
      CALL P(3,X7,NA(1),R(77,J),H1)
      CALL P(2,X7,NB(1),R(78,J),H1)
      CALL P(1,X7,NC(1),R(79,J),H1)
      DO 16 I=1,4
      II=I+24
      IF(I.NE.1)GO TO 15
      B(25)=B(25)-R(56,J)+R(80,J)
   15 CONTINUE
   16 B(II)=B(II)+K(I)+L(I)+KK(I)+LL(I)+G(I)+V(I)+GG(I)+VV(I)+
     *NA(I)+NB(I)+NC(I)
      CALL P(4,X8,K(1),-Q,H1)
      CALL P(3,X8,L(1),-R(77,J),H1)
      CALL P(2,X8,KK(1),-R(78,J),H1)
      CALL P(1,X8,LL(1),-R(79,J),H1)
      CALL P(4,X8,B(29),Q,0.)
      DO 18 I=1,4
```

```
      II=I+28
      IF(I.NE.1)GO TO 17
      B(29)=B(29)-R(80,J)
   17 CONTINUE
   18 B(II)=B(II)+K(I)+L(I)+KK(I)+LL(I)
      B(33)=QQ
C***SOLVE THESE EQNS BY NAG F04ATF
      IFAIL=0
      CALL F04ATF(A,36,B,36,C,AA,36,WKS1,WKS2,IFAIL)
      WRITE(6,30)(C(I),I=1,36)
C***CALCULATE DEFLECTIONS AT A,B
      Y1=3.5
      Y2=6.5
      Y3=9.5
      Y4=12.5
      Y5=15.5
      Y6=18.5
      F1=F1*Y2
      F2=F2*Y3
      F3=F3*Y4
      F4=F4*Y5
      F5=F5*Y6
      EX11=DEXP(-F1)
      EX12=DEXP(F1)
      CO1=DCOS(F1)
      SI1=DSIN(F1)
      EX21=DEXP(-F2)
      EX22=DEXP(F2)
      CO2=DCOS(F2)
      SI2=DSIN(F2)
      EX31=DEXP(-F3)
      EX32=DEXP(F3)
      CO3=DCOS(F3)
      SI3=DSIN(F3)
      EX41=DEXP(-F4)
      EX42=DEXP(F4)
      CO4=DCOS(F4)
      SI4=DSIN(F4)
      EX51=DEXP(-F5)
      EX52=DEXP(F5)
      CO5=DCOS(F5)
      SI5=DSIN(F5)
      ADEL1=Q*Y1**4+R(17,J)*Y1**3+R(18,J)*Y1**2+R(19,J)*Y1+R(20,J)
      AS1=EX11*(R(29,J)*CO1+R(30,J)*SI1)+EX12*(R(31,J)*CO1+R(32,J)*SI1
      ADEL2=ADEL1+AS1
      AS2=EX21*(R(45,J)*CO2+R(46,J)*SI2)+EX22*(R(47,J)*CO2+R(48,J)*SI2
      ADEL3=ADEL2+AS2
      AS3=EX31*(R(65,J)*CO3+R(66,J)*SI3)+EX32*(R(67,J)*CO3+R(68,J)*SI3
      ADEL4=ADEL3+AS3
      AS4=EX41*(C(15)*CO4+C(16)*SI4)+EX42*(C(17)*CO4+C(18)*SI4)
      ADEL5=ADEL4+AS4
      WRITE(6,40)ADEL1,ADEL2,ADEL3,ADEL4,ADEL5
      BDEL1=Q*Y1**4+R(5,J)*Y1**3+R(6,J)*Y1**2+R(7,J)*Y1+R(8,J)
      BS1=EX11*(R(13,J)*CO1+R(14,J)*SI1)+EX12*(R(15,J)*CO1+R(16,J)*SI1
      BDEL2=BDEL1+BS1
```

```
G COMPILER        MAIN              07-30-76          12:44:03

      BS2=EX21*(R(25,J)*CO2+R(26,J)*SI2)+EX22*(R(27,J)*CO2+R(28,J)*SI2)
      BDEL3=BDEL2+BS2
      BS3=EX31*(R(41,J)*CO3+R(42,J)*SI3)+EX32*(R(43,J)*CO3+R(44,J)*SI3)
      BDEL4=BDEL3+BS3
      BS4=EX41*(R(61,J)*CO4+R(62,J)*SI4)+EX42*(R(63,J)*CO4+R(64,J)*SI4)
      BDEL5=BDEL4+BS4
      BS5=EX51*(C(11)*CO5+C(12)*SI5)+EX52*(C(13)*CO5+C(14)*SI5)
      BDEL6=BDEL5+BS5
      WRITE(6,50)BDEL1,BDEL2,BDEL3,BDEL4,BDEL5,BDEL6
C***CALCULATE PACK LOADS AT A,B
      LA1=(ADEL2-ADEL1)*T1
      LA2=LA1+(ADEL3-ADEL2)*T2
      LA3=LA2+(ADEL4-ADEL3)*T3
      LA4=LA3+(ADEL5-ADEL4)*T4
      WRITE(6,60)LA1,LA2,LA3,LA4
      LB1=(BDEL2-BDEL1)*T1
      LB2=LB1+(BDEL3-BDEL2)*T2
      LB3=LB2+(BDEL4-BDEL3)*T3
      LB4=LB3+(BDEL5-BDEL4)*T4
      LB5=LB4+(BDEL6-BDEL5)*T5
      WRITE(6,70)LB1,LB2,LB3,LB4,LB5
   20 FORMAT('1RATE OF ADVANCE ',1PD8.1)
   30 FORMAT('0     ',4(1PD13.6,2X))
   40 FORMAT('ODEFLN AT A ',5(1PD11.4,2X))
   50 FORMAT('ODEFLN AT B ',6(1PD11.4,2X))
   60 FORMAT('OLOAD AT A ',4(1PD10.3,2X))
   70 FORMAT('OLOAD AT B ',5(1PD10.3,2X))
    1 CONTINUE
      STOP
      END

IORY REQUIREMENTS 00D142 BYTES
.MINATED


.G
;INS
```

RATE OF ADVANCE 9.0D 00

3.240855D 00 -9.238245D 01 -7.728925D-05 2.741920D-03

4.248510D-02 2.547743D-01 -1.176313D-02 -1.417640D-03

2.923730D-11 -9.862840D-11 -9.779902D-03 1.314062D-03

2.821561D-11 -1.385305D-11 -7.139884D-03 3.260866D-03
1.087985D-10 -1.994970D-10 -4.784007D-03 3.904049D-03

1.173973D-09 -5.284885D-08 -2.658090D-03 4.591206D-03

1.035914D-07 -9.589483D-08 -3.210094D-04 4.130507D-03

4.570045D-08 -3.601384D-06 -1.257031D-05 3.215098D-05
4.128119D-04 8.247112D-03 8.471116D-04 2.113805D-04

DEFLN AT A 1.0173D-02 1.0781D-02 1.0956D-02 1.0826D-02 1.0810D-02

DEFLN AT B 1.0453D-02 1.1102D-02 1.1179D-02 1.1150D-02 1.1134D-02 1.1134D-02

LOAD AT A 2.255D 02 2.769D 02 2.485D 02 2.294D 02

LOAD AT B 2.404D 02 2.936D 02 2.660D 02 2.468D 02 2.462D 02

RATE OF ADVANCE 6.0D 00

4.045803D 00 -9.062811D 01 -7.731622D-05 2.741829D-03

4.239876D-02 2.529871D-01 -1.078525D-02 -1.597402D-03

1.399090D-13 -5.711119D-11 -9.005138D-03 6.093590D-04
5.579756D-12 -6.215519D-11 -6.968591D-03 2.516320D-03
1.156968D-11 -3.472198D-11 -4.708751D-03 3.292753D-03
1.617396D-09 -2.254569D-08 -2.892579D-03 3.983344D-03

5.086457D-08 -5.478568D-08 -5.656389D-04 3.795223D-03
9.853753D-08 -1.521904D-06 -1.187542D-05 2.631074D-05
3.691561D-04 8.173571D-03 7.735710D-04 1.729832D-04

DEFLN AT A 9.9301D-03 1.0388D-02 1.0416D-02 1.0389D-02 1.0381D-02

DEFLN AT B 1.0280D-02 1.0781D-02 1.0809D-02 1.0784D-02 1.0776D-02 1.0776D-02

LOAD AT A 2.443D 02 2.716D 02 2.365D 02 2.238D 02

LOAD AT B 2.672D 02 2.937D 02 2.618D 02 2.493D 02 2.505D 02

```
RATE OF ADVANCE  4.5D 00

      4.488819D 00  -9.0019170 01  -7.7275630-05   2.7371630-03


4.222546D-02   2.508909D-01  -9.984248D-03  -1.436168D-03
1.824648D-12  -2.665997D-11  -8.356939D-03   4.479628D-04
5.729189D-12  -3.478978D-11  -6.708825D-03   2.114894D-03


6.695124D-13  -2.520550D-11  -4.637507D-03   2.969295D-03
1.250842D-09  -1.105300D-08  -3.009055D-03   3.602068D-03


2.733248D-08  -4.043642D-08  -7.498589D-04   3.603402D-03
4.636645D-08  -7.820317D-07  -1.144286D-05   2.287210D-05
3.429902D-04   8.129087D-03   7.290867D-04   1.503754D-04

DEFLN AT A  9.7832D-03   1.0157D-02   1.0165D-02   1.0141D-02   1.0137D-02

DEFLN AT B  1.0179D-02   1.0596D-02   1.0603D-02   1.0581D-02   1.0577D-02   1.0578D-02

LOAD AT A  2.554D 02   2.652D 02   2.284D 02   2.202D 02

LOAD AT B  2.849D 02   2.936D 02   2.591D 02   2.510D 02   2.530D 02

 STOP     0
EXECUTION TERMINATED


$SIG
```

APPENDIX III

AN IV G COMPILER MAIN 07-30-76 10:12:18

```
      C***SHORT FACE ADVANCING WITH CONVL. CENTRE PACKS
      C***PROG FOR DEFLNS & PACK LOADS AT PT A BY LONGL. CONSIDERATIONS
      C***INVOLVING APPLICATION OF CONTINUITY CONDITIONS TO
      C***DEFLN. EQNS. UP TO STAGE 9
      C***& SOLVING RESULTING SIMULTANEOUS EQNS.
      C***TO OBTAIN 244INTEGRATION CONSTS.
      C***
            SUBROUTINE ECOS(A,B,X,Y,C)
      C***Y(1) IS THE FUNCTION C*EXP(AX)*COS(BX)
      C***Y(2),Y(3),Y(4) ARE THE DERIVATIVES
            DOUBLE PRECISION A,B,C,X,Y(4),Z,Z1,Z2,DEXP,DCOS,DSIN
            Z1=A*X
            Z2=B*X
            Y(1)=C*DEXP(Z1)*DCOS(Z2)
            Z=C*DEXP(Z1)*DSIN(Z2)
            Y(2)=A*Y(1)-B*Z
            Y(3)=(A*A-B*B)*Y(1)-2.*A*B*Z
            Y(4)=(A*A-3.*B*B)*A*Y(1)-(3.*A*A-B*B)*B*Z
            RETURN
            END
```

AL MEMORY REQUIREMENTS 0002B6 BYTES

```
            SUBROUTINE ESIN(A,B,X,Y,C)
      C***Y(1) IS THE FUNCTION C*EXP(AX)*SIN(BX)
      C***Y(2),Y(3),Y(4) ARE THE DERIVATIVES
            DOUBLE PRECISION A,B,C,X,Y(4),Z,Z1,Z2,DEXP,DCOS,DSIN
            Z1=A*X
            Z2=B*X
            Y(1)=C*DEXP(Z1)*DSIN(Z2)
            Z=C*DEXP(Z1)*DCOS(Z2)
            Y(2)=A*Y(1)+B*Z
            Y(3)=(A*A-B*B)*Y(1)+2.*A*B*Z
            Y(4)=(A*A-3.*B*B)*A*Y(1)+(3.*A*A-B*B)*B*Z
            RETURN
            END
```

AL MEMORY REQUIREMENTS 0002B4 BYTES

```
            SUBROUTINE P(N,X,Y,A,H)
      C***Y(1) IS THE FUNCTION A*(X-H)**N
      C***Y(2),Y(3),Y(4) ARE THE DERIVATIVES
            DOUBLE PRECISION X,Y(4),Z,A,H
            Z=X-H
            Y(1)=A*Z**N
            Y(2)=A*N*Z**(N-1)
            Y(3)=A*N*(N-1)*Z**(N-2)
            Y(4)=A*N*(N-1)*(N-2)*Z**(N-3)
            RETURN
            END
```

AL MEMORY REQUIREMENTS 000308 BYTES

```
      C***MEANINGS OF SYMBOLS USED IN PROG.
      C***E=ALPHA,F=BETA,D3=C3,D4=C4,EP=E(PACK),
```

```
G COMPILER       MAIN            07-30-76        10:12:21

C***Q=Q2/24D2,QQ=(Q1+Q2)/K2,H=(L1+W)/2,PL1,PL2,...=PACK LOADS AT PT A
C***A,B,C IN EACH STAGE ARE THE ELEMENTS OF THE MATRIX EQN A*C=B,
C***C BEING THE UNKNOWNS.
C***
      DOUBLE PRECISION E,Q,QQ,K,H,D3,D4,F,A1(16,16),A2(20,20),
     *A3(24,24),A4(28,28),A5(32,32),A6(36,36),B1(16),B2(20),
     *B3(24),B4(28),B5(32),B6(36),C1(16),C2(20),C3(24),C4(28),C5(32),
     *C6(36),AA1(16,16),AA2(20,20),AA3(24,24),AA4(28,28),AA5(32,32),
     *AA6(36,36),WKS11(16),WKS21(16),WKS12(20),WKS22(20),WKS13(24),
     *WKS23(24),WKS14(28),WKS24(28),WKS15(32),WKS25(32),WKS16(36),
     *WKS26(36),KK(4),LL(4),MM(4),NN(4),VV(4),X3,X4,X5,X6,
     *A7(40,40),B7(40),C7(40),AA7(40,40),WKS17(40),WKS27(40),
     *A8(44,44),B8(44),C8(44),AA8(44,44),WKS18(44),WKS28(44),
     *PL5,PL6,V54,V66,EP,
     *V9,V16,V24,V33,V43,V54,PL1,PL2,PL3,PL4,PL5,DEXP,DCOS,DSIN
C***LIST THE KNOWN CONSTS.
      E=0.39
      Q=7.986D-7
      QQ=7.4D-3
      H=5.5
      D3=-1.0053D-4
      D4=1.0891D-2
      DO 101 L=1,5
      K=3.5D+4*L/1.9
      EP=K*1.9
      WRITE(6,1000)EP
      F=(K/4.8D+7)**0.25
C***ASSIGN INITIAL ZERO VALUES TO ALL MATRIX & R.H.S. ELEMENTS
      DO 1 I=1,16
      DO 1 J=1,16
      A1(J,I)=0.
      B1(I)=0.
    1 CONTINUE
      DO 2 I=1,20
      DO 2 J=1,20
      A2(J,I)=0.
    2 B2(I)=0.
      DO 3 I=1,24
      DO 3 J=1,24
      A3(J,I)=0.
    3 B3(I)=0.
      DO 4 I=1,28
      DO 4 J=1,28
      A4(J,I)=0.
    4 B4(I)=0.
      DO 5 I=1,32
      DO 5 J=1,32
      A5(J,I)=0.
    5 B5(I)=0.
      DO 6 I=1,36
      DO 6 J=1,36
      A6(J,I)=0.
    6 B6(I)=0.
      DO 70 I=1,40
      DO 70 J=1,40
```

```
0              A7(J,I)=0.
1           70 B7(I)=0.
2              DO 80 I=1,44
3              DO 80 J=1,44
4              A8(J,I)=0.
5           80 B8(I)=0.
          C***STAGE 2--FORM & SOLVE EQNS FOR C5 TO C20
6              CALL ECOS(-E,E,14.,A1(1,1),1.)
7              CALL ESIN(-E,E,14.,A1(1,2),1.)
8              CALL P(3,14.,A1(1,3),-1.,0.)
9              CALL P(2,14.,A1(1,4),-1.,0.)
0              CALL P(1,14.,A1(1,5),-1.,0.)
1              CALL P(0,14.,A1(1,6),-1.,0.)
2              CALL P(3,9.,A1(5,3),1.,0.)
3              CALL P(2,9.,A1(5,4),1.,0.)
4              CALL P(1,9.,A1(5,5),1.,0.)
5              CALL P(0,9.,A1(5,6),1.,0.)
               CALL ECOS(-F,F,9.,A1(5,7),-1.)
               CALL ESIN(-F,F,9.,A1(5,8),-1.)
               CALL ECOS(F,F,9.,A1(5,9),-1.)
               CALL ESIN(F,F,9.,A1(5,10),-1.)
               CALL ECOS(-F,F,6.,A1(9,7),1.)
               CALL ESIN(-F,F,6.,A1(9,8),1.)
               CALL ECOS(F,F,6.,A1(9,9),1.)
               CALL ESIN(F,F,6.,A1(9,10),1.)
               CALL P(3,6.,A1(9,11),-1.,0.)
               CALL P(2,6.,A1(9,12),-1.,0.)
               CALL P(1,6.,A1(9,13),-1.,0.)
               CALL P(0,6.,A1(9,14),-1.,0.)
               A1(13,14)=1.
               A1(14,13)=1.
               A1(15,12)=2.
               A1(16,11)=6.
               CALL ECOS(E,E,0.,A1(13,15),-1.)
               CALL ESIN(E,E,0.,A1(13,16),-1.)
               CALL P(4,14.,B1(1),Q,0.)
               B1(1)=B1(1)-QQ
               CALL P(4,9.,KK(1),Q,H)
               CALL P(2,9.,LL(1),D3,H)
               CALL P(4,9.,B1(5),-Q,0.)
               DO 8 I=1,4
               II=I+4
               IF(I.NE.1)GO TO 7
               B1(5)=B1(5)+D4
             7 CONTINUE
             8 B1(II)=B1(II)+KK(I)+LL(I)
               CALL P(4,6.,KK(1),-Q,H)
               CALL P(2,6.,LL(1),-D3,H)
               CALL P(4,6.,B1(9),Q,0.)
               DO 10 I=1,4
               II=I+8
               IF(I.NE.1)GO TO 9
               B1(9)=B1(9)-D4
             9 CONTINUE
            10 B1(II)=B1(II)+KK(I)+LL(I)
```

```
      B1(13)=QQ
      IFAIL1=0
      CALL F04ATF(A1,16,B1,16,C1,AA1,16,WKS11,WKS21,IFAIL1)
C***STAGE 3-C21 TO C40
      CALL ECOS(-E,E,17.,A2(1,1),1.)
      CALL ESIN(-E,E,17.,A2(1,2),1.)
      CALL P(3,17.,A2(1,3),-1.,0.)
      CALL P(2,17.,A2(1,4),-1.,0.)
      CALL P(1,17.,A2(1,5),-1.,0.)
      CALL P(0,17.,A2(1,6),-1.,0.)
      CALL P(3,12.,A2(5,3),1.,0.)
      CALL P(2,12.,A2(5,4),1.,0.)
      CALL P(1,12.,A2(5,5),1.,0.)
      CALL P(0,12.,A2(5,6),1.,0.)
      CALL ECOS(-F,F,12.,A2(5,7),-1.)
      CALL ESIN(-F,F,12.,A2(5,8),-1.)
      CALL ECOS(F,F,12.,A2(5,9),-1.)
      CALL ESIN(F,F,12.,A2(5,10),-1.)
      CALL ECOS(-F,F,9.,A2(9,7),1.)
      CALL ESIN(-F,F,9.,A2(9,8),1.)
      CALL ECOS(F,F,9.,A2(9,9),1.)
      CALL ESIN(F,F,9.,A2(9,10),1.)
      DO 12 J=11,20
      JJ=J-4
      DO 12 I=9,20
      II=I-4
      A2(I,J)=A1(II,JJ)
   12 CONTINUE
      CALL P(4,17.,B2(1),Q,0.)
      B2(1)=B2(1)-QQ
      CALL P(3,12.,B2(5),C1(3),0.)
      CALL P(2,12.,KK(1),C1(4),0.)
      CALL P(1,12.,LL(1),C1(5),0.)
      DO 14 I=1,4
      II=I+4
      IF(I.NE.1)GO TO 13
      B2(5)=B2(5)+C1(6)
   13 CONTINUE
   14 B2(II)=B2(II)+KK(I)+LL(I)
      CALL P(4,9.,B2(9),Q,H)
      CALL P(2,9.,KK(1),D3,H)
      CALL P(4,9.,LL(1),-Q,0.)
      CALL P(3,9.,MM(1),-C1(3),0.)
      CALL P(2,9.,NN(1),-C1(4),0.)
      CALL P(1,9.,VV(1),-C1(5),0.)
      DO 16 I=1,4
      II=I+8
      IF(I.NE.1)GO TO 15
      B2(9)=B2(9)+D4-C1(6)
   15 CONTINUE
   16 B2(II)=B2(II)+KK(I)+LL(I)+MM(I)+NN(I)+VV(I)
      DO 18 I=13,20
      II=I-4
      B2(I)=B1(II)
   18 CONTINUE
```

```
      IFAIL2=0
      CALL F04ATF(A2,20,B2,20,C2,AA2,20,WKS12,WKS22,IFAIL2)
C***STAGE 4--C41 TO C64
      CALL ECOS(-E,E,20.,A3(1,1),1.)
      CALL ESIN(-E,E,20.,A3(1,2),1.)
      CALL P(3,20.,A3(1,3),-1.,0.)
      CALL P(2,20.,A3(1,4),-1.,0.)
      CALL P(1,20.,A3(1,5),-1.,0.)
      CALL P(0,20.,A3(1,6),-1.,0.)
      CALL P(3,15.,A3(5,3),1.,0.)
      CALL P(2,15.,A3(5,4),1.,0.)
      CALL P(1,15.,A3(5,5),1.,0.)
      CALL P(0,15.,A3(5,6),1.,0.)
      CALL ECOS(-F,F,15.,A3(5,7),-1.)
      CALL ESIN(-F,F,15.,A3(5,8),-1.)
      CALL ECOS(F,F,15.,A3(5,9),-1.)
      CALL ESIN(F,F,15.,A3(5,10),-1.)
      CALL ECOS(-F,F,12.,A3(9,7),1.)
      CALL ESIN(-F,F,12.,A3(9,8),1.)
      CALL ECOS(F,F,12.,A3(9,9),1.)
      CALL ESIN(F,F,12.,A3(9,10),1.)
      DO 20 J=11,24
      JJ=J-4
      DO 20 I=9,24
      II=I-4
   20 A3(I,J)=A2(II,JJ)
      CALL P(4,20.,B3(1),Q,0.)
      B3(1)=B3(1)-QQ
      CALL P(3,15.,B3(5),C2(3),0.)
      CALL P(2,15.,KK(1),C2(4),0.)
      CALL P(1,15.,LL(1),C2(5),0.)
      DO 22 I=1,4
      II=I+4
      IF(I.NE.1)GO TO 21
      B3(5)=B3(5)+C2(6)
   21 CONTINUE
   22 B3(II)=B3(II)+KK(I)+LL(I)
      CALL P(3,12.,B3(9),C1(3),0.)
      CALL P(2,12.,KK(1),C1(4),0.)
      CALL P(1,12.,LL(1),C1(5),0.)
      CALL P(3,12.,MM(1),-C2(3),0.)
      CALL P(2,12.,NN(1),-C2(4),0.)
      CALL P(1,12.,VV(1),-C2(5),0.)
      DO 24 I=1,4
      II=I+8
      IF(I.NE.1)GO TO 23
      B3(9)=B3(9)+C1(6)-C2(6)
   23 CONTINUE
   24 B3(II)=B3(II)+KK(I)+LL(I)+MM(I)+NN(I)+VV(I)
      DO 26 I=13,24
      II=I-4
      B3(I)=B2(II)
   26 CONTINUE
      IFAIL3=0
      CALL F04ATF(A3,24,B3,24,C3,AA3,24,WKS13,WKS23,IFAIL3)
```

```
C***STAGE 5--C65 TO C92
      CALL ECOS(-E,E,23.,A4(1,1),1.)
      CALL ESIN(-E,E,23.,A4(1,2),1.)
      CALL P(3,23.,A4(1,3),-1.,0.)
      CALL P(2,23.,A4(1,4),-1.,0.)
      CALL P(1,23.,A4(1,5),-1.,0.)
      CALL P(0,23.,A4(1,6),-1.,0.)
      CALL P(3,18.,A4(5,3),1.,0.)
      CALL P(2,18.,A4(5,4),1.,0.)
      CALL P(1,18.,A4(5,5),1.,0.)
      CALL P(0,18.,A4(5,6),1.,0.)
      CALL ECOS(-F,F,18.,A4(5,7),-1.)
      CALL ESIN(-F,F,18.,A4(5,8),-1.)
      CALL ECOS(F,F,18.,A4(5,9),-1.)
      CALL ESIN(F,F,18.,A4(5,10),-1.)
      CALL ECOS(-F,F,15.,A4(9,7),1.)
      CALL ESIN(-F,F,15.,A4(9,8),1.)
      CALL ECOS(F,F,15.,A4(9,9),1.)
      CALL ESIN(F,F,15.,A4(9,10),1.)
      DO 30 J=11,28
      JJ=J-4
      DO 30 I=9,28
      II=I-4
   30 A4(I,J)=A3(II,JJ)
      CALL P(4,23.,B4(1),Q,0.)
      B4(1)=B4(1)-CQ
      CALL P(3,18.,B4(5),C3(3),0.)
      CALL P(2,18.,KK(1),C3(4),0.)
      CALL P(1,18.,LL(1),C3(5),0.)
      DO 32 I=1,4
      II=I+4
      IF(I.NE.1)GO TO 31
      B4(5)=B4(5)+C3(6)
   31 CONTINUE
   32 B4(II)=B4(II)+KK(I)+LL(I)
      CALL P(3,15.,B4(9),C2(3),0.)
      CALL P(2,15.,KK(1),C2(4),0.)
      CALL P(1,15.,LL(1),C2(5),0.)
      CALL P(3,15.,MM(1),-C3(3),0.)
      CALL P(2,15.,NN(1),-C3(4),0.)
      CALL P(1,15.,VV(1),-C3(5),0.)
      DO 34 I=1,4
      II=I+8
      IF(I.NE.1)GO TO 33
      B4(9)=B4(9)+C2(6)-C3(6)
   33 CONTINUE
   34 B4(II)=B4(II)+KK(I)+LL(I)+MM(I)+NN(I)+VV(I)
      DO 36 I=13,28
      II=I-4
      B4(I)=B3(II)
   36 CONTINUE
      IFAIL4=0
      CALL F04ATF(A4,28,B4,28,C4,AA4,28,WKS14,WKS24,IFAIL4)
C***STAGE 6--C93 TO C124
      CALL ECOS(-E,E,26.,A5(1,1),1.)
```

```
      CALL ESIN(-E,E,26.,A5(1,2),1.)
      CALL P(3,26.,A5(1,3),-1.,0.)
      CALL P(2,26.,A5(1,4),-1.,0.)
      CALL P(1,26.,A5(1,5),-1.,0.)
      CALL P(0,26.,A5(1,6),-1.,0.)
      CALL P(3,21.,A5(5,3),1.,0.)
      CALL P(2,21.,A5(5,4),1.,0.)
      CALL P(1,21.,A5(5,5),1.,0.)
      CALL P(0,21.,A5(5,6),1.,0.)
      CALL ECOS(-F,F,21.,A5(5,7),-1.)
      CALL ESIN(-F,F,21.,A5(5,8),-1.)
      CALL ECOS(F,F,21.,A5(5,9),-1.)
      CALL ESIN(F,F,21.,A5(5,10),-1.)
      CALL ECOS(-F,F,18.,A5(9,7),1.)
      CALL ESIN(-F,F,18.,A5(9,8),1.)
      CALL ECOS(F,F,18.,A5(9,9),1.)
      CALL ESIN(F,F,18.,A5(9,10),1.)
      DO 38 J=11,32
      JJ=J-4
      DO 38 I=9,32
      II=I-4
   38 A5(I,J)=A4(II,JJ)
      CALL P(4,26.,B5(1),Q,0.)
      B5(1)=B5(1)-QQ
      CALL P(3,21.,B5(5),C4(3),0.)
      CALL P(2,21.,KK(1),C4(4),0.)
      CALL P(1,21.,LL(1),C4(5),0.)
      DO 40 I=1,4
      II=I+4
      IF(I.NE.1)GO TO 39
      B5(5)=B5(5)+C4(6)
   39 CONTINUE
   40 B5(II)=B5(II)+KK(I)+LL(I)
      CALL P(3,18.,B5(9),C3(3),0.)
      CALL P(2,18.,KK(1),C3(4),0.)
      CALL P(1,18.,LL(1),C3(5),0.)
      CALL P(3,18.,MM(1),-C4(3),0.)
      CALL P(2,18.,NN(1),-C4(4),0.)
      CALL P(1,18.,VV(1),-C4(5),0.)
      DO 42 I=1,4
      II=I+8
      IF(I.NE.1)GO TO 41
      B5(9)=B5(9)+C3(6)-C4(6)
   41 CONTINUE
   42 B5(II)=B5(II)+KK(I)+LL(I)+MM(I)+NN(I)+VV(I)
      DO 44 I=13,32
      II=I-4
      B5(I)=B4(II)
   44 CONTINUE
      IFAIL5=0
      CALL F04ATF(A5,32,B5,32,C5,AA5,32,WKS15,WKS25,IFAIL5)
C***STAGE 7--C125 TO C160
      CALL ECOS(-E,E,29.,A6(1,1),1.)
      CALL ESIN(-E,E,29.,A6(1,2),1.)
      CALL P(3,29.,A6(1,3),-1.,0.)
```

```
      CALL P(2,29.,A6(1,4),-1.,0.)
      CALL P(1,29.,A6(1,5),-1.,0.)
      CALL P(0,29.,A6(1,6),-1.,0.)
      CALL P(3,24.,A6(5,3),1.,0.)
      CALL P(2,24.,A6(5,4),1.,0.)
      CALL P(1,24.,A6(5,5),1.,0.)
      CALL P(0,24.,A6(5,6),1.,0.)
      CALL ECOS(-F,F,24.,A6(5,7),-1.)
      CALL ESIN(-F,F,24.,A6(5,8),-1.)
      CALL ECOS(F,F,24.,A6(5,9),-1.)
      CALL ESIN(F,F,24.,A6(5,10),-1.)
      CALL ECOS(-F,F,21.,A6(9,7),1.)
      CALL ESIN(-F,F,21.,A6(9,8),1.)
      CALL ECOS(F,F,21.,A6(9,9),1.)
      CALL ESIN(F,F,21.,A6(9,10),1.)
      DO 46 J=11,36
      JJ=J-4
      DO 46 I=9,36
      II=I-4
   46 A6(I,J)=A5(II,JJ)
      CALL P(4,29.,B6(1),Q,0.)
      B6(1)=B6(1)-QQ
      CALL P(3,24.,B6(5),C5(3),0.)
      CALL P(2,24.,KK(1),C5(4),0.)
      CALL P(1,24.,LL(1),C5(5),0.)
      DO 48 I=1,4
      II=I+4
      IF(I.NE.1)GO TO 47
      B6(5)=B6(5)+C5(6)
   47 CONTINUE
   48 B6(II)=B6(II)+KK(I)+LL(I)
      CALL P(3,21.,B6(9),C4(3),0.)
      CALL P(2,21.,KK(1),C4(4),0.)
      CALL P(1,21.,LL(1),C4(5),0.)
      CALL P(3,21.,MM(1),-C5(3),0.)
      CALL P(2,21.,NN(1),-C5(4),0.)
      CALL P(1,21.,VV(1),-C5(5),0.)
      DO 50 I=1,4
      II=I+8
      IF(I.NE.1)GO TO 49
      B6(9)=B6(9)+C4(6)-C5(6)
   49 CONTINUE
   50 B6(II)=B6(II)+KK(I)+LL(I)+MM(I)+NN(I)+VV(I)
      DO 52 I=13,36
      II=I-4
      B6(I)=B5(II)
   52 CONTINUE
      IFAIL6=0
      CALL F04ATF(A6,36,B6,36,C6,AA6,36,WKS16,WKS26,IFAIL6)
C***STAGE 8--C161 TO C200
      CALL ECOS(-E,E,32.,A7(1,1),1.)
      CALL ESIN(-E,E,32.,A7(1,2),1.)
      CALL P(3,32.,A7(1,3),-1.,0.)
      CALL P(2,32.,A7(1,4),-1.,0.)
      CALL P(1,32.,A7(1,5),-1.,0.)
```

```
      CALL P(0,32.,A7(1,6),-1.,0.)
      CALL P(3,27.,A7(5,3),1.,0.)
      CALL P(2,27.,A7(5,4),1.,0.)
      CALL P(1,27.,A7(5,5),1.,0.)
      CALL P(0,27.,A7(5,6),1.,0.)
      CALL ECOS(-F,F,27.,A7(5,7),-1.)
      CALL ESIN(-F,F,27.,A7(5,8),-1.)
      CALL ECOS(F,F,27.,A7(5,9),-1.)
      CALL ESIN(F,F,27.,A7(5,10),-1.)
      CALL ECOS(-F,F,24.,A7(9,7),1.)
      CALL ESIN(-F,F,24.,A7(9,8),1.)
      CALL ECOS(F,F,24.,A7(9,9),1.)
      CALL ESIN(F,F,24.,A7(9,10),1.)
      DO 54 J=11,40
      JJ=J-4
      DO 54 I=9,40
      II=I-4
   54 A7(I,J)=A6(II,JJ)
      CALL P(4,32.,B7(1),Q,0.)
      B7(1)=B7(1)-QQ
      CALL P(3,27.,B7(5),C6(3),0.)
      CALL P(2,27.,KK(1),C6(4),0.)
      CALL P(1,27.,LL(1),C6(5),0.)
      DO 56 I=1,4
      II=I+4
      IF(I.NE.1)GO TO 55
      B7(5)=B7(5)+C6(6)
   55 CONTINUE
   56 B7(II)=B7(II)+KK(I)+LL(I)
      CALL P(3,24.,B7(9),C5(3),0.)
      CALL P(2,24.,KK(1),C5(4),0.)
      CALL P(1,24.,LL(1),C5(5),0.)
      CALL P(3,24.,MM(1),-C6(3),0.)
      CALL P(2,24.,NN(1),-C6(4),0.)
      CALL P(1,24.,VV(1),-C6(5),0.)
      DO 58 I=1,4
      II=I+8
      IF(I.NE.1)GO TO 57
      B7(9)=B7(9)+C5(6)-C6(6)
   57 CONTINUE
   58 B7(II)=B7(II)+KK(I)+LL(I)+MM(I)+NN(I)+VV(I)
      DO 60 I=13,40
      II=I-4
      B7(I)=B6(II)
   60 CONTINUE
      IFAIL7=0
      CALL F04ATF(A7,40,B7,40,C7,AA7,40,WKS17,WKS27,IFAIL7)
C***STAGE 9--C201 TO C244
      CALL ECOS(-E,E,35.,A8(1,1),1.)
      CALL ESIN(-E,E,35.,A8(1,2),1.)
      CALL P(3,35.,A8(1,3),-1.,0.)
      CALL P(2,35.,A8(1,4),-1.,0.)
      CALL P(1,35.,A8(1,5),-1.,0.)
      CALL P(0,35.,A8(1,6),-1.,0.)
      CALL P(3,30.,A8(5,3),1.,0.)
```

```
      CALL P(2,30.,A8(5,4),1.,0.)
      CALL P(1,30.,A8(5,5),1.,0.)
      CALL P(0,30.,A8(5,6),1.,0.)
      CALL ECOS(-F,F,30.,A8(5,7),-1.)
      CALL ESIN(-F,F,30.,A8(5,8),-1.)
      CALL ECOS(F,F,30.,A8(5,9),-1.)
      CALL ESIN(F,F,30.,A8(5,10),-1.)
      CALL ECOS(-F,F,27.,A8(9,7),1.)
      CALL ESIN(-F,F,27.,A8(9,8),1.)
      CALL ECOS(F,F,27.,A8(9,9),1.)
      CALL ESIN(F,F,27.,A8(9,10),1.)
      DO 62 J=11,44
      JJ=J-4
      DO 62 I=9,44
      II=I-4
   62 A8(I,J)=A7(II,JJ)
      CALL P(4,35.,B8(1),Q,0.)
      B8(1)=B8(1)-QQ
      CALL P(3,30.,B8(5),C7(3),0.)
      CALL P(2,30.,KK(1),C7(4),0.)
      CALL P(1,30.,LL(1),C7(5),0.)
      DO 64 I=1,4
      II=I+4
      IF(I.NE.1)GO TO 63
      B8(5)=B8(5)+C7(6)
   63 CONTINUE
   64 B8(II)=B8(II)+KK(I)+LL(I)
      CALL P(3,27.,B8(9),C6(3),0.)
      CALL P(2,27.,KK(1),C6(4),0.)
      CALL P(1,27.,LL(1),C6(5),0.)
      CALL P(3,27.,MM(1),-C7(3),0.)
      CALL P(2,27.,NN(1),-C7(4),0.)
      CALL P(1,27.,VV(1),-C7(5),0.)
      DO 66 I=1,4
      II=I+8
      IF(I.NE.1)GO TO 65
      B8(9)=B8(9)+C6(6)-C7(6)
   65 CONTINUE
   66 B8(II)=B8(II)+KK(I)+LL(I)+MM(I)+NN(I)+VV(I)
      DO 68 I=13,44
      II=I-4
      B8(I)=B7(II)
   68 CONTINUE
      IFAIL8=0
      CALL F04ATF(A8,44,B8,44,C8,AA8,44,WKS18,WKS28,IFAIL8)
C***CALCULATE DEFLN,PACK LOAD
      V9=Q*13.5**4+C2(3)*13.5**3+C2(4)*13.5**2+C2(5)*13.5+C2(6)
      X3=DEXP(-F*13.5)*DCOS(F*13.5)
      X4=DEXP(-F*13.5)*DSIN(F*13.5)
      X5=DEXP(F*13.5)*DCOS(F*13.5)
      X6=DEXP(F*13.5)*DSIN(F*13.5)
      V16=V9+C3(7)*X3+C3(8)*X4+C3(9)*X5+C3(10)*X6
      V24=V9+C4(11)*X3+C4(12)*X4+C4(13)*X5+C4(14)*X6
      V33=V9+C5(15)*X3+C5(16)*X4+C5(17)*X5+C5(18)*X6
      V43=V9+C6(19)*X3+C6(20)*X4+C6(21)*X5+C6(22)*X6
```

```
0471              V54=V9+C7(23)*X3+C7(24)*X4+C7(25)*X5+C7(26)*X6
0472              V66=V9+C8(27)*X3+C8(28)*X4+C8(29)*X5+C8(30)*X6
0473              WRITE(6,2000)V9,V16,V24,V33,V43,V54,V66
0474              PL1=(V16-V9)*K
0475              PL2=(V24-V9)*K
0476              PL3=(V33-V9)*K
0477              PL4=(V43-V9)*K
0478              PL5=(V54-V9)*K
0479              PL6=(V66-V9)*K
0480              WRITE(6,3000)PL1,PL2,PL3,PL4,PL5,PL6
0481         1000 FORMAT('0PACK MODULUS ',1PD9.2)
0482         2000 FORMAT('0DEFLECTIONS ',7(1PD11.4,2X))
0483         3000 FORMAT('0PACK LOAD ',6(1PD10.3,2X))
0484          101 CONTINUE
0485              STOP
0486              END

  TOTAL MEMORY REQUIREMENTS 02633E BYTES
EXECUTION TERMINATED
```

```
$R -LOAD#+*NAG
EXECUTION BEGINS

PACK MODULUS  3.50D 04

DEFLECTIONS  1.3656D-02   1.8416D-02   2.2324D-02   2.4890D-02   2.6243D-02   2.6747D-02   2.6768D-02

PACK LOAD  8.769D 01   1.597D 02   2.069D 02   2.319D 02   2.412D 02   2.415D 02

PACK MODULUS  7.00D 04

DEFLECTIONS  1.2799D-02   1.6065D-02   1.8227D-02   1.9304D-02   1.9651D-02   1.9626D-02   1.9474D-02

PACK LOAD  1.203D 02   1.999D 02   2.396D 02   2.524D 02   2.515D 02   2.459D 02

PACK MODULUS  1.05D 05

DEFLECTIONS  1.2252D-02   1.4780D-02   1.6234D-02   1.6814D-02   1.6904D-02   1.6802D-02   1.6673D-02

PACK LOAD  1.397D 02   2.200D 02   2.521D 02   2.570D 02   2.514D 02   2.443D 02

PACK MODULUS  1.40D 05

DEFLECTIONS  1.1868D-02   1.3954D-02   1.5027D-02   1.5374D-02   1.5368D-02   1.5259D-02   1.5161D-02

PACK LOAD  1.537D 02   2.328D 02   2.583D 02   2.579D 02   2.498D 02   2.427D 02

PACK MODULUS  1.75D 05

DEFLECTIONS  1.1581D-02   1.3371D-02   1.4207D-02   1.4423D-02   1.4376D-02   1.4275D-02   1.4202D-02

PACK LOAD  1.648D 02   2.419D 02   2.618D 02   2.575D 02   2.482D 02   2.414D 02

 STOP     0
EXECUTION TERMINATED
```

APPENDIX IV

APPENDIX IV

Modification of the face element source program to include the failure criterion, obtaining τ_1 at each bench mark

1. Orange job card
2. £H MTS945
3. £SIGNON ID
4. Password
5. £CRE Filename

   (Creates a file for face element data cards)
6. £EMP Filename
7. £COPY *SOURCE* Filename

Data cards for face element run
8. £ENDFILE
9. £R *GETDISK PAR=MTS945

   (Instructs the operator to mount the disc)
10. £CRE - A TYPE=SEQ SIZE=nP
11. £CRE - B TYPE=SEQ SIZE=nP

12. £CRE -C TYPE=SEQ SIZE=nP

13. £CRE -D TYPE=SEQ SIZE=nP

14. £CRE -F TYPE=SEQ SIZE=nP

(Creates sequential temporary files - A to -F for buffer space)

15. £COPY MNB6 : FACEL2D TO -ABC

(Copies face element source program to scratch file -ABC)

16. £GET -ABC

17. £R *ED

(Begins editing the source program in -ABC)

18. 587I 8

```
SC= 3.2E+04

ST= 4.0E+03

TC= 0.5*(SC*ST)**0.5

TA= (SC-ST)/4./TC

DO 7 I=1,NBM

TC1=(PRINP(3*I-2)-PRINP(3*I-1))*TC/SC+PRINP(3*I-2)*TA
```

```
      7  WRITE (6,110) I, TC1

    110  FORMAT ("  ",I4,1PE10.3)
```

(FORTRAN program cards for writing τ_1 for each b.m.as per failure criterion)

19. Q

20. £CRE FHPW1.5

21. £EMP FHPW1.5

22. £R *FORTRAN SCARDS = -ABC SPUNCH=FHPW1.5

(Creates an object program FHPW1.5 from editing on -ABC)

23. £R FHPW1.5 1= -A 2= -B 3 = -C 4 = -D 5 = Filename 7 = -E 8= -F

(Runs the new object program to give τ_1-values in addition to the usual face element output)

24. £R *FREEDISK PAR = MT5945

25. £L Filename

26. £SIG

* * *